BioMedical Engineering and Imaging Institute 10th Annual

BMEII SYMPOSIUM

Advancing Healthcare Through Biomedical Engineering, A.I., Imaging, and Nanomedicine

April 27-28, 2022

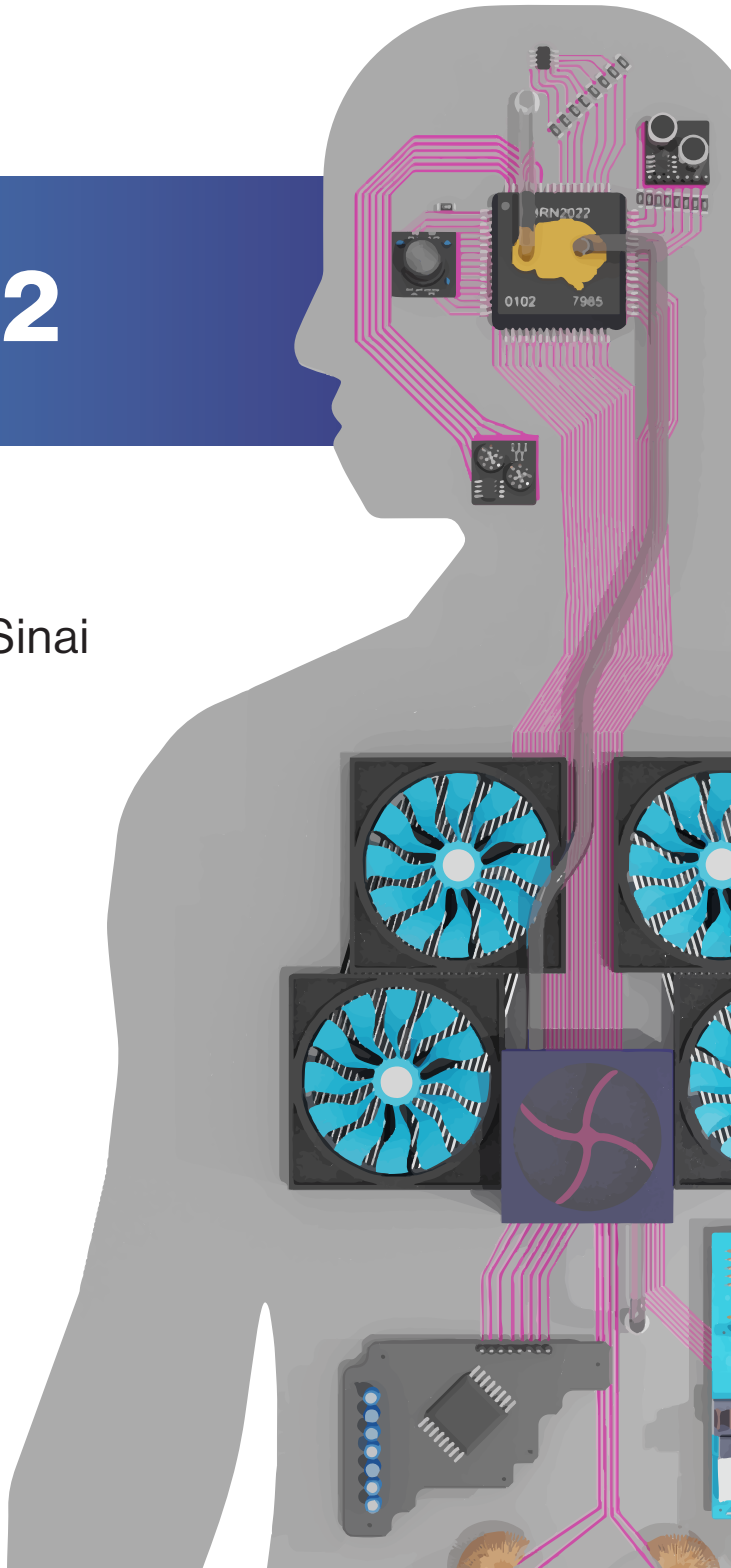

Davis Conference Center

Icahn School of Medicine at Mount Sinai

New York, NY

Icahn School of Medicine at Mount Sinai

BioMedical Engineering and Imaging Institute

10^{th} Annual BMEII Symposium April 27^{th}-28^{th}, 2022

The organizing committee members: Akbar Alipour, Octavia Bane, Christopher Cannistraci, Li Feng, Georgios Soultanidis, Mallory Stellato, Xiang Xu

The Editors of this program: Akbar Alipour, Christopher Cannistraci, Georgios Soultanidis, Mallory Stellato

Contents

Timetable

Wednesday, April 27th, 2022	
5:00 – 5:30 PM	First Day Registration
5:30 – 6:30 PM	Poster Presentations
6:30 – 8:00 PM	*Windows To Our Body* Art Exhibit
Thursday, April 28th, 2022	
8:00 AM - 8:30 AM	Second Day Registration
8:30 AM - 9:00 AM	**Dennis S. Charney, MD** Anne and Joel Ehrenkranz Dean, Icahn School of Medicine at Mount Sinai **Zahi Fayad, PhD** Director, BioMedical Engineering and Imaging Institute (BMEII)
9:00 AM - 9:45 AM	*Fireside Chat:* “Entrepreneurship & The Future of Healthcare” **Toby Cosgrove, MD** Executive Advisor, Former President and CEO, Cleveland Clinic *Moderated by* **William H. Morris, MD, MBA** Healthcare and Life Sciences, Google Cloud

9:45 AM - 10:15 AM	**Selected oral presentations** **Akbar Alipour, PhD** **Octavia Bane, PhD** **Xueyan Mei, PhD**
10:15 AM - 10:45 AM	Coffee Break
10:45 AM - 11:30 AM	“Population Neuroimaging in UK Biobank: How to Scan 100,000 People” **Karla Miller, PhD** Professor of Biomedical Engineering University of Oxford
11:30 AM - 12:00 PM	**Ana Devesa Arbiol, MD, PhD** **Isabella Morgan** **Lior Zangi , PhD**
12:00 PM - 12:45 PM	“DNA Barcoded Nanoparticles: Thousands of Experiments at Once” **James Dahlman, PhD** Associate Professor of Biomedical Engineering, Emory Medical School
12:45 PM - 1:45 PM	Lunch
1:45 PM - 2:30 PM	“Universal Digital High Resolution Melting for Fast and Broad Pathogen Screening” **Stephanie Fraley, PhD** Associate Professor of Bioengineering University of California, San Diego
2:30 PM - 3:15 PM	“The Body in Action” **Penny Gowland, PhD** Professor of Physics, Faculty of Science, University of Nottingham

3:15 PM - 3:45 PM	Afternoon Break
3:45 PM - 4:30 PM	"Machine to Brain Interface – Integrating Sensory Perception with Cognition" **Nitish V. Thakor, PhD** Professor of Biomedical Engineering, Electrical Engineering, Neurology, Johns Hopkins University
4:30 PM - 5:15 PM	"Artificial Intelligence in Medicine: Moral and Practical Questions" **Tessa Sundaram Cook, MD, PhD, CIIP, FSIIM** Assistant Professor, Radiology Perelman School of Medicine at the University of Pennsylvania **Tim Leiner, MD, PhD** Professor of Radiology Mayo Clinic **Robbie Freeman, RN, MSN** Vice President of Clinical Innovation & Chief Nursing Informatics Officer, Mount Sinai Health System
5:15 PM - 5:30 PM	Closing Remarks **Burton P. Drayer, MD** Charles M. and Marilyn Newman Professor and System Chair Diagnostic, Molecular and Interventional Radiology, Icahn School of Medicine at Mount Sinai
5:30 PM	Event Ends

Message from the Director

On behalf of the BioMedical Engineering and Imaging Institute and the Icahn School of Medicine at Mount Sinai, I would like to welcome you to the 10th Annual BMEII Symposium, the first under our new name. We are excited to host this important event once again, bringing together the leaders and rising stars across the imaging, nanomedicine, AI and biomedical engineering fields to share our vision of advancing healthcare through innovation and rigorous research.

The program for this year reflects our commitment to promoting the best biomedical engineering discoveries, destined to improve healthcare and the overall quality of service. We are happy to host renowned speakers on topics ranging from nanomedicine to cancer imaging to healthcare leadership. In addition to the invited speakers, six abstract submissions, out of more than fifty submissions, to give oral presentations. Those abstracts have been chosen as exemplars of advances in the field and the embodiment of our vision.

We hope you will take this opportunity to attend all the talks and the poster session, interact with the participants, and explore new areas of collaboration.

Zahi A. Fayad, PhD
Director, BioMedical Engineering and Imaging Institute

BMEII

Our mission is centered around development, validation, translation and education of innovative technology in biomedical imaging to address both basic and clinical research problems and therefore improve human health.

The BioMedical Engineering and Imaging Institute (BMEII) is a state of the art research facility housed in 20,000 square feet in the Hess Center of Science and Medicine (CSM). BMEII (Director, Zahi A. Fayad, PhD) is comprised of faculty, staff and trainees responsible for coordinating and executing all research projects performed in these facilities. Currently BMEII has over 65 members with expertise in all aspects of translational imaging research. The faculty consists of Biomedical and Electrical Engineers and Radiologists who are leading experts in neuroimaging, cardiovascular imaging, body/cancer imaging, and nanomedicine. Highly skilled staff provides a full suite of support services for image acquisition, image analysis, scheduling and performance of the proposed experiments.

Access to the BMEII facility is based on a fee for service schedule (for more info, visit our website). These user fees are calculated to cover the operating and maintenance costs of the instruments and related Core expenses. These rates are determined and periodically reviewed by the Dean's Office and adjusted to reflect the actual costs. User fees include technical support for operation of imaging equipment.

For internal Mount Sinai users, resource usage time is compiled from the web-based scheduling system and charged directly to your account on a monthly basis. Any questions on the charges should be addressed to the BMEII Director.

Human Imaging Core

MR/PET (3T) Siemens mMR

The 3T MR/PET is a fully integrated and capable of simultaneous whole body PET and MRI scanning. This allows more precisely coregistered functional and structural acquisition while reducing the radiation dose in PET imaging by replacing the CT scans with an MRI scan. True simultaneous acquisition of MR and PET data by the hybrid system merges the highly sensitive PET metabolic information with the highly specific MR anatomical and functional information. The 3T MRI system is a whole body imaging system, capable of routine as well as advanced imaging of all body regions. The PET scanner will be fully integrated into the MR, utilizing state of the art solid-state technology for simultaneous PET imaging during MR image or spectrum acquisition. The 3T MR-PET is designed for the purposes of oncological and neurological diagnostic imaging. The highly integrated nature of these systems provides the capability for full spatial and temporal correlation between both modalities. The maximum gradient amplitude will be approximately 40 mT/m per axis, with a maximum gradient slew rate of about 200 T/m/s per axis. The system's magnet has an integrated cooling system and active shielding. The shimming capabilities include: Active (with 3 electric and 5 electric nonlinear linear shim channels) and Passive shims for maintaining very high homogeneity and excellent image quality over a wide range of applications. Online shimming is performed in less than 20 seconds in order to optimize homogeneity. The RF transmit and receive system include: compact, air cooled tube RF amplifier providing 35 kW peak power; integrated electronics with cabinet water cooling; integrated circularly polarized whole body RF coil; up to 32 receive channels. The PET system include: adaptation to a work environment within high magnetic fields including APD and LSO based detector technology; adaptation and optimization of numerous MR components to an integrated PET imaging unit; high-resolution, high-count rate, positron emission tomography (PET) imaging of metabolic and physiologic processes; high quality metabolic and anatomic image registration and fusion for optimal lesion detection and identification within the body; state-of-the-art 3D PET data acquisition and analysis tools; state-of-the-art 3D PET reconstruction, attenuation and scatter correction software. Expected PET performance specifications: spatial resolution: $<$6.5mm; timing resolution: $<$ 4.5 ns; sensitivity: $>$ 0.5%; axial FOV: > 19 cm ; transaxial FOV: up to 45 cm. The system also supports MR and PET gated scan acquisition; support for list mode acquisition, offline histogramming and reconstruction; special calibration. Alignment and quality control sources including shielding; multimodality workplace; 3D iterative reconstruction.

7T Siemens MR whole body scanner

This is an ultrahigh field 7.0 Tesla actively shielded whole body MRI scanner. The super-conducting magnet is self-shielded, reducing its overall footprint and making it compact and lightweight by 7T standards, weighing 24-tons. The (warm) inner bore of the magnet is 82 cm, which houses the 60 CM inner patient bore. The dimensions of the magnet without covers is approximately 2.5 m in length, 2.6 m in width, and 2.65 m in height. The 5-Gauss line extends slightly further than for a 3T scanner with 5.6 m radial and 7.8 m axial dimension. A whole-body gradient system provides gradient amplitude of up to 70 mT/m per axis, and a maximum slew rate of up to 200 T/m/s. The RF transmit system comes with 8 parallel transmit channels; 8 individually shaped RF pulses can be prescribed simultaneously and independently in amplitude and phase. The multi-nuclei package allows for imaging and spectroscopy at non-proton frequencies, i.e. detection of e.g. ^{19}F, ^{31}P, ^{7}Li, ^{23}Na, ^{13}C, ^{17}O. Our 7T/820AS is configured to accommodate an 8-channel Tx-array and 48-channel Rx receivers. Several coils are currently available such as the 1- channel Tx and 32-channel Rx head coil and the 8-channel Tx and 8-channel Rx head coil.

3T Siemens MAGNETOM Skyra

This is an FDA approved 3 Tesla human MRI scanner. Its wide bore design (173 cm system length with 70 cm) can accommodate subjects with larger body compositions compared to the 60 cm bore of a typical clinical 1.5T & 3T. A newly deigned RF system and coil architecture integrates (Tim 4G) with all digital-in/digital-out technology. The scanner has an actively shielded water-cooled gradient system and zero helium boil-off. Specialized RF distribution increases uniformity in all body regions. Onboard software is available for: neuro, angio, cardiac, body, onco applications. A variety of coils for all body parts and configuration is available.

PET/CT Siemens Biograph Vision

Biograph Vision™ is next generation, high-precision combined positron emission tomography (PET) / computed tomography (CT) system developed by Siemens Healthineers. The PET device in the system features 3.2mm lutetium oxyorthosilicate (LSO) crystals and digital silicon photomultiplier (SiPM) sensors making it the fastest time-of-flight system, with temporal resolution of 214 picoseconds and sensitivity 100 counts per second (cps) / kBq. This leads to improved spatial resolution with reduced partial volume effects, enabling faster scans and/or lowering the administered dose to the patient. The exceptional sensitivity of

the detectors gives the necessary range of count rate from 90Y to 82Rb studies. The CT component has features of the SOMATOM Definition line of scanners. The system features Sinogram Affirmed Iterative Reconstruction (SAFIRE) algorithm for iterative reconstruction to improve the image quality and Iterative Metal Artifact Reduction to reduce metal artifacts. The CT can be utilized also as a low dose screening tool of lung cancer in high-risk patients. With its exceptional features and resolution, this system is used for the whole-body examination of patients to diagnose cancer, as well as cardiac and nervous disorders.

Multidetector CT (MDCT) Siemens Somatom Definition Flash

This Dual Source CT, uses two Xray sources and two detectors simultaneously, to cover the entire thorax in less than a second. A 2 meter scan requires only 5 seconds, enhancing the efficiency of perfusion or dynamic vascular imaging and reduction the dose for all scans, resulting, e.g. in dose down to sub-mSv for cardiac imaging. Dual Energy automatically provides a second contrast for without any extra dose. Advance software efficiently manages the reduction in dose allowing for: limited exposure to radiation-sensitive organs and increases tissue contrast with no sacrifice to image quality.

Two 1.5T Siemens MR MAGNETOM Aera

Short and open appearance (145 cm system length with 70 cm Open Bore Design) can accommodate subjects with larger body compositions compared to the 60 cm bore of a typical clinical 1.5T & 3T. Newly deigned RF system and coil architecture integrates with all digitalin/digital-out technology, one system use standard gradients (33 mT/m @125 T/m/s) and the second system has advanced gradients (45 mT/m @ 200 T/m/s). Actively shielded water-cooled gradient system with zero helium boil-off. Inline software is specially designed for: neuro, angio, cardiac, body, onco, breast, ortho, pediatric and scientific specialties such as Magnetic Resonance Elastography; a technique that measures the stiffness of tissues by introducing shear waves and imaging their propagation.

Siemens ACUSAN S3000 ARFI Ultrasound

The ultrasound system automatically produces an acoustic ‘push’ pulse that generates shear-waves, which propagate into the tissue. Using image-based localization and a proprietary implementation of acoustic radiation force impulse (ARFI) technology, shear wave speed may be quantified, in a precise anatomical region, focused on a region of interest, with a predefined size, provided by the system. Measurement value and depth are also reported, and the results of the elasticity are expressed in m/s. This system provides new method for the evaluation of the elastic properties of tissues is now available in the Cancer/Body Core. Clinical applications of ARFI imaging include: liver fibrosis quantification, breast, colorectal and prostate tumor imaging.

Dual Source-Dual Detector Siemens Force CT

The Force is the third iteration of Siemens’ dualsource CT design which features two sets of x-ray tubes and detectors for enhanced imaging of all patients, including young children, patients with renal insufficiency, and those who cannot hold their breath. Due to its low-kV imaging technique, Force broadens CT’s application for patients with renal insufficiency and

offers an acquisition speed of 737 mm/sec, so an entire adult chest, abdomen, and pelvis study can be done in one second with no breath-holds. In cardiac imaging, Force can obtain an entire study within one-quarter of a heart beat at a temporal resolution of 66 msec, which is the speed required to freeze the fastest-moving anatomy, such as the right coronary artery.

”Mock” MR PSTNet

The MRI simulator allows researchers to acclimatize the subjects to the ‘enclosed’ and loud MRI environment before they actually go into a real scanner. This is especially important for studies involving children.

fMRI peripherals

All the MRI scanners are equipped with the latest state of the art peripherals for functional imaging including LCD goggles, integrated eyetracking, fiber optic subject response gloves, pneumatic computerized headphones with microphones as well as a full spectrum of physiological recording probes for ECG, GSR, pulse-Ox etc. There is also a specialized MRI compatible computerized olfacto-meter.

Neuro Testing room

A sound proofed and independent temperature-controlled neuro testing room is located near the 3T MRI for physiological testing such as EEG, ERP and other modalities. This room is also equipped with large monitors for paradigm training and testing.

Small Animal Imaging Core

9.4T MRI Bruker

This is a high-resolution MRI scanner used for in-vivo imaging of mice and smaller specimens. It is 9.4 Tesla 89-mm bore MRI system operating at a proton frequency of 400 MHz (Bruker, Billerica, MA). The 9.4T is equipped with a mouse respiratory and cardiac sensor connected to a monitoring and gating system (SA Instruments, Inc., Stony Brook, NY). Sedation is administered by an Isoflurane/O2 gas mixture delivered through a nose cone and placed in a 30 mm birdcage coil with an animal handling system. Additionally, a temperature controller is available in the bore of the magnet, to maintain the animal in the RF coil at a selected temperature. Recent upgrades (Bruker Paravision 4) have enabled the use of navigator pulses to allow for cardiac and/or respiratory gating without the use of electrodes.

7.0T MRI Bruker Biospec 70/30

This is a high-resolution MR scanner for small animals. The maximum bore diameter for imaging is 15.4cm. This system is equipped with two gradient choices, a large built-in gradient system with up to 200 mt/m and a slew rate of 640 T/m/s. This gradient in combination with a large circular polarized coil will allow imaging of animals up to 15.4cm in diameter. The system is also equipped with a high performance gradient insert with 440mT/m and slew rate of 3,440 T/m/s for high-resolution imaging. The system has 2 transmit and 4 receive channels. There is a 35mm ID circular polarized coil for in-vivo mouse imaging as well as a 4-channel phased array for mouse brain and a 4-channel phased array for mouse cardiac imaging. There are also 3 other dual tuned 20mm surface coils for 31P, 13C and 19F. The 7T Bruker is equipped with the Autopac system, a fully integrated animal handling, laser guided po-

sitioning system. Animal warming holders are available for rats and mice as well as a full spectrum of monitoring peripherals for ECG, triggering and respiratory monitoring etc.

Mediso nanoScan Micro PET/CT

The newest acquisition to the Small Animal Imaging Center, nanoScan Micro PET/CT has the highest PET resolution using the industry's most advanced pixelated modular LYSO detectors. It has an exceptionally high-count rate tolerance supporting high activity studies of multiple animals or short half-life isotopes. The system has easy access to the animal from both the front and the back of the PET/CT gantry and state-of-the-art Tera-TomoTM 3D PET image reconstruction engine. High imaging throughput can be obtained by large bore size and large field-of-view in both axial and transaxial directions in addition to multiCell imaging chambers for mice, rats and rabbits and a PrepaCell Preparation station.

Biophotonic IVIS-Spectrum

The IVIS Spectrum in vivo imaging system uses a novel patented optical imaging technology to facilitate non-invasive longitudinal monitoring of disease progression, cell trafficking and gene expression patterns in living animals. The IVIS Spectrum is a versatile and advanced in vivo imaging system. An optimized set of high efficiency filters and spectral un-mixing algorithms lets you take full advantage of bioluminescent and fluorescent reporters across the blue to near infrared wavelength region. It also offers single-view 3D tomography for both fluorescent and bioluminescent reporters that can be analyzed in an anatomical context us-

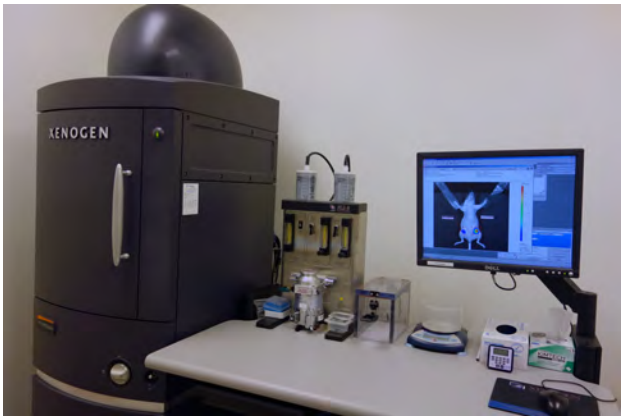

ing our Digital Mouse Atlasor. For advanced fluorescence pre-clinical imaging, the IVIS Spectrum has the capability to use either trans-illumination (from the bottom) or epi-illumination (from the top) to illuminate in vivo fluorescent sources. 3D diffuse fluorescence tomography can be performed to determine source localization and concentration using the combination of structured light and trans illumination fluorescent images. The instrument is equipped with 10 narrow band excitation filters (30nm bandwidth) and 18 narrow band emission filters (20nm bandwidth) that assist in significantly reducing autofluorescence by the spectral scanning of filters and the use of spectral unmixing algorithms. In addition, the spectral unmixing tools allow the researcher to separate signals from multiple fluorescent reporters within the same animal.

Micro Ultrasound Vevo 2100 VisualSonics

This is dedicated Ultrasound system for small animal models (mice to rabbits) of disease. This scanner is capable of all imaging modes found in clinical US scanners such as color Doppler, M-mode, 3D imaging and volume analysis but at much higher spatial resolution. It allows for rapid animal screening of tumor and other models. The higher resolution of this system will also allow for image-guided injection. B-Mode (2D) imaging for anatomical visualization and quantification, with enhanced temporal resolution with frame rates up to 740 fps (in 2D for a 4x4 mm FOV) , and enhanced image uniformity with multiple focal zones. M-Mode is for visualization and quantification of wall motion in cardiovascular research, single line acquisition allows for the very high-temporal (1000 fps) resolution necessary for analysis of LV function. Anatomical M-Mode is for adjustable anatomical orientation in reconstructed M-Mode imaging; software automatically optimizes field of view for maximum frame rate. Pulsed-Wave Doppler Mode (PW) is for quantification of blood flow. Color Doppler Mode is used for detection of blood vessels including flow directional information and mean velocities; as well as for identification of small vessels not visible in B-Mode. Power Doppler Mode is for detection and quantification of blood flow in small vessels not visible in B-Mode; increased frame rates allow for significantly faster data acquisition. Tissue Doppler Mode for quantification of myocardial tissue movement; for example in assessing diastolic dysfunction. Vevo MicroMarker® Nonlinear Contrast Agent Imaging can be used for quantification of relative perfusion & molecular expression of endothelial cell surface markers; enhanced sensitivity to Vevo MicroMarker contrast agents as linear tissue signal is suppressed. 3D-Mode Imaging is for anatomical and vascular visualization, when combined with either B-Mode, Power Doppler Mode or Nonlinear Contrast Imaging; allows for quantification of volume and vascularity within a defined anatomical structure. Digital RF-Mode is for the acquisition and expor-

tation of radio frequency (RF) data in digital format for further analysis; full screen acquisition provides a complete data set for more comprehensive analysis and tissue characterization. ECG and Respiration Gating is used to suppress imaging artifacts due to respiration and cardiac movements. Both are important in cardiac and abdominal imaging for both 2D and 3D data sets. Transducers: * MS-200 12.5 or 21 MHz, Depth from 2mm to 36mm *MS-250 16 or 21 MHz, Depth from 2mm to 30mm *MS-400 24 or 30 MHz, Depth from 2mm to 20mm *MS-550D 32 or 40 MHz, Depth from 1mm to 15mm http://www.visualsonics.com/vevo2100 .

Near IR Frangioni imager

This rodent scanner is designed to visualize cellular probes that fluoresce in the Near IR region which provides much better tissue penetration than traditional Green Fluorescent Proteins.

BMEII Research Laboratories

RF Coil Laboratory

The RF Coil Laboratory in BMEII was initially established in 2010. This fully equipped electronics lab is available for RF coil building and troubleshooting. The lab is equipped with vector network analyzers, oscilloscopes, a circuit board printer, 3D printers, a signal generators, DC power supplies, as well as other standard electronics equipment. BMEII core staff, trainees, and faculty have produced numerous custom RF coils and components for basic and translational research projects. These include coils for high resolution imaging at 7T of the human cervical spine cord, brainstem, carotid arteries, and body, as well as a dedicated coil for rabbit cardiac imaging. Recently, a passive wireless RF array for enhancement of RF fields in the central nervous system was designed, prototyped, and tested in the facility. In addition to RF hardware, users have also developed mechanical and electronic accessories that are utilized for specific experiments in the high magnet field environment of the MRI scanners.

Nanomedicine Laboratory

The Nanomedicine laboratory has 2 modules: the synthetic lab and the analytical / biochemistry / biology lab. We are able to synthesize established imaging reagents for supply and distribution. In the synthetic lab, there are 2 large synthetic chemistry hoods that can accommodate 4 synthetic chemists working simultaneously. Each scientist has individual bench space for work-up and for storing samples, reagents, buffers and the like. The analytical/biochemistry/biology lab has 2 smaller hoods for doing wet chemistry work. Both facilities have been equipped with state-of-the-art instruments to support the work. The synthetic lab is well equipped for investigators to perform small-scale syntheses of organic, inorganic and organometallic compounds for use in a multitude of imaging modalities as well as drug delivery nanoparticles. In addition, we are also capable of labeling peptides and antibodies with commercially available optical dyes, CT, or MR contrast agents.

Radiochemistry Laboratory

With the establishment of the Biomedical Engineering and Imaging Institute, the nanomedicine program has expanded its facilities to include a radiochemistry suite on SC-1 in the dose preparation room. This has been a long-desired vision and goal for the team and facility, as now nano-platform design, synthesis, radioactive labelling, imaging, and biodistribution studies can all take place within the institute. This greatly reduces reliance on other institutions in the creation of new radioactive tracers and immunotherapeutic nanoscale platforms. Newly purchased equipment, such as an Shimadzu HPLC system (with UV and Radiodetectors), and a radioTLC system, were placed within the newly shielded bio-safety cabinet. Other new additions include vortexes, thermomixers, microfluidics pumps and chips, a microcentrifuge, and a new computer. These additions complement the dose calibration room, which already included two dose calibrators, a large centrifuge, storage for radioactive isotopes, and a computer dedicated for dose tracking, which will soon be the main hub for NMIS. SC-1 continues

to be a full-stop shop for in vivo imaging and biodistribution studies, and with the addition of the radiochemistry suite, our abilities to create novel therapies and diagnostic tools have been significantly bolstered. For more information on the radiochemistry suite, please reach out to a member of the nanomedicine team led by Assistant Professor Mandy Van Leent and Assistant Professor Abraham J. P. Teunissen. The Radiochemistry laboratory is also equipped with gamma counters and a dose calibrator.

Bioinformatics and Data Processing

One of the main functions of BMEII is to provide the infrastructure for access to research imaging. A comprehensive set of imaging modalities are supported for both human as well as animal work. Scheduling support for access to the different scanners consists of web-based online calendars as well as live telephone scheduling support. BMEII also provides a central hub for image distribution and archival. There are 32TB of online storage where all imaging data is pushed to and distributed from. The capacity will be expanded annually as needed.

Image Analysis Support

BMEII provides image analysis for cardiovascular, body/oncological and neuro imaging. The image analysis for specific projects needs to be discussed directly with the BMEII core (contact BMEII Director Dr. Zahi Fayad.) This core consists of IT personnel, software engineers, imaging physicists, research assistants and other support personnel. Expert consultation for research projects including protocol design, specialized pulse sequences, special image acquisition hardware (coils), custom made functional MRI stimulus hardware are all supported. Comprehensive project based image analysis support is also provided. Modalities supported include PET, MRI, fMRI, DTI and its variants, resting state fMRI. Image analysis training is also supported for those researchers who want to learn more about image analysis in general. Training ranges from regular classroom based graduate course taught by BMEII faculty to hands on training on the use of specific software packages such as FSL, SPM, Brainvoyager and BMEII's own in house developed software packages in all areas (neuro, body, oncology and cardiovascular). The data center has a dedicated servers room which houses a larger Mac Server Cluster with 2 x 16TB of initial online storage with direct connectivity to all the imaging modalities in CSM. In addition, there is also an image analysis room equipped with large viewing display and high performance workstations open for the researcher to learn or perform image analysis.

BMEII XNAT

BMEII XNAT serves as the central point for research data transfer, archive, and sharing. BMEII XNAT is built upon a secure database, supports automated pipelines for processing managed data, and provides tools for exploring the data. Only users authorized by the study investigators can access their data. BMEII XNAT is fully HIPAA compliant. The BMEII XNAT team provides support for data migration between various DICOM repositories, HIPAA de-identification, image preprocessing, image quality control, and other customized services. Currently BMEII XNAT runs on two mirrored Linux servers with 60TB storage space on each. It can host more than 15,000 image sessions with backups. BMEII XNAT user training, documentation, and imaging data management consultations are available by request (https://BMEII.mssm.edu/xnat). A yearly service sup-

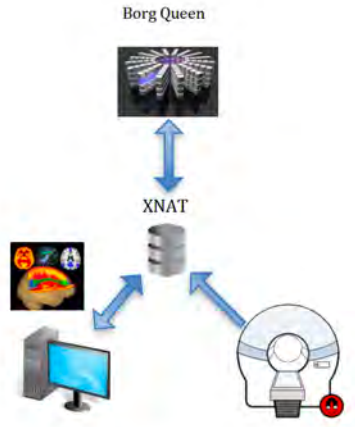

port contract has been established with the XNAT developer group from Radiologics Inc.

Flywheel

MRI data pre-processing, denoising and processing will be performed using custom-built and publicly available pipelines supported by the HIPAA and GDPR compliant web platform, Flywheel (https://flywheel.io). Flywheel is a cloud-based research data platform that streamlines data ingest, curates data to common standards, automates processing and supports secure collaboration. Flywheel supports core research facilities by improving productivity for research management including tools for data deidentification and machine learning workflow automation. In addition, a rule-based framework is used to automate quality assurance using configurable data validation tools. The analysis software tools found in XNAT Borg Queen, Flywheel provide reproducible calculations on all data within the system, enabling high-quality, reproducible research and accurate recording of all completed analysis. The recording of all pipelines, results, and workflows are documented on the web-interface. All data go in and out of the platform through a single, secure, permissions-based model. Data is encrypted while in transit using SSL certificates and can also be encrypted at rest. All data is managed in a secure project context with access controls integrated with institutional authentication protocols.

CPU/GPU Servers

BMEII-HPC-1: Server capable of deep-learning, intensive image and data analysis, the BMEII-HPC-1 server is a NVIDIA DGX-1, comprising of a dual 20 core Intel Xeon 2.2GHz CPU, 512GB of RAM, 7TB of storage, eight NVIDIA Tesla V100 GPUs with a total 256GB of GPU RAM, 5,120 NVIDIA Tensor Cores and 40,960 NVIDIA CUDA Cores. BMEII-HPC-1 provides BMEII with the performance of 1 petaFLOPS. The server runs Ubuntu 18.04 and can support other OS through either Linux containers or virtual machines.

Borg ESXi Cluster: There are 2 VMware ESXI v7 servers each containing a total of 32 cores of AMD 2.35GHz CPU, 512GB of RAM (DDR4-2666), 1TB of storage, and a total of 2 NVIDIA GTX 2080 Ti GPUs with 11GB memory as of early 2021. This cluster also contains a JBOD server expanding the total available storage to 382TB. The VMware servers can support other OS through either Linux and Windows virtual machines. The Borg ESXi cluster will enable advanced compute nodes for Flywheel and XNAT implementations.

DGX-A100: As BMEII continues to increase our AI and deep-learning capabilities, the NVIDIA DGXA100 delivering up to 6x the training performance of the DGX-1. Comprising of dual 64 core AMD Rome 7742 2.25GHz CPUs, 1TB of RAM, 15TB of Gen 4 NVME SSD storage, eight NVIDIA A100 GPUs with a total 320GB of GPU RAM, 5,120 NVIDIA Tensor Cores and 40,960 NVIDIA CUDA Cores as of early 2021. DGX-A100 provides BMEII with the performance of 5 petaFLOPS AI and 10 petaFLOPS INT8. The server runs Ubuntu 18.04 and can support other OS through either Linux containers or virtual machines.

Image reconstruction tools for PET and fast MR imaging

BMEII is equipped with a dedicated workstation for PET images reconstructions, such as the Siemens e7-tools and the open-source package STIR (http://stir.sourceforge.net/). The e7-tools are a collection of Microsoft Windows command line programs that allow the processing and reconstruction of Siemens PET emission data both using iterative and analytical algorithms. The software is capable of generating of other correction factors including attenuation, scatter and normalization. The software also allows for listmode histogramming and rebinning. The software is installed on an external computer to reconstruct PET images away from the scanners. STIR software on the other hand is an open source toolbox that offers the same functionalities as the e7tools, but is not limited to the analysis of Siemens PET emission data. Also available is a dedicated workstation housing PET-SORTEO (Simulation Of Realistic Tridimensional Emitting Objects), a simulation tool that uses Monte Carlo techniques to generate realistic PET data from voxelized descriptions of tracer distributions, in accordance with the scanner geometry and physical characteristics.

Mount Sinai Imaging Research Warehouse (IRW)

The IRW is a platform intended to facilitate research by allowing researchers to gain open access to imaging data in the Mount Sinai Data Warehouse (MSDW). HIPAA compliance is handled by providing a mirror of the Mount Sinai PACS in a de-identified/ pseudoanonymized state. Exams that are archived in Mount Sinai PACS, arising from an ORG that populates other data types to the MSDW, are sent to the IRW. All data in the IRW will use an alternative HIPAA-compliant identifier that could be cleanly referenced to its associated data in the MSDW. IRW images are archived on a NAS storage server with 250TB RAID6 space, which can host approximately more than 2 million exams. There are two servers that receive and de-identify images from PACS, followed by the forwarding of these images to three servers for archiving. There is a F5 load balancer that evenly distributes the archiving and querying loads among the archive servers. For the archive servers, VioArchive (by Vital Images) is used as the storage repository software for research images. De-identified DICOM files transferred to the VioArchive archive servers will be inspected by IRW personnel for quality assurance. Researchers can use a DICOM client like OsiriX to query and retrieve images from the IRW to their local workstation. Researchers can also use VitreaView (http://vitrea.mssm.edu/vitrea-view/auth/login or http://view.mssm.edu/vitrea-

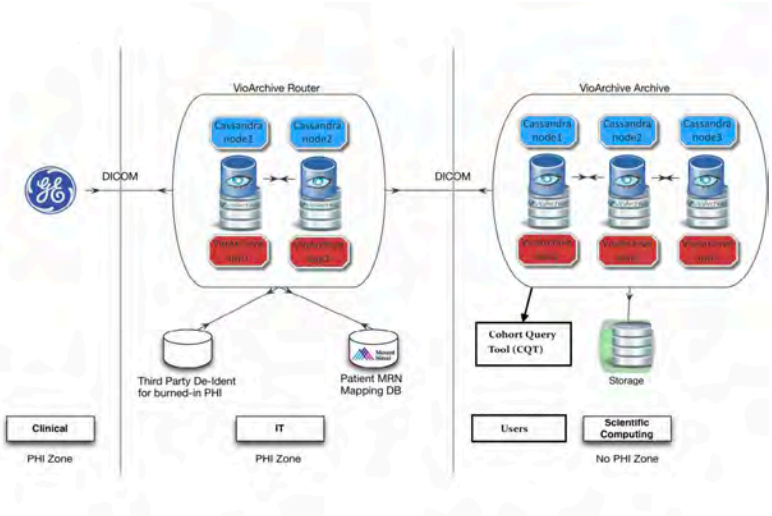

view/auth/login) to view de-identified images. IRB approval is not required for Mount Sinai internal data usage. As end of 2019, the IRW has accumulated more than 500,000 studies including CT, MR, DX, PET, CR, MG, NM, and other modalities. Currently, the IRW team is providing datasets for several deep learning applications and projects. More information is also available online@ http://BMEII.mssm.edu

Contact:
Zahi A. Fayad, PhD – Director, BMEII
Zahi.fayad@mssm.edu
(212) 824-8452

Christopher J. Cannistraci, MS – Director, Research Operations
Christopher.cannistraci@mssm.edu
(212) 824-8466

Biographies of the Hosts

Zahi A. Fayad, PhD, FAHA, FACC, FISMRM

Director, BioMedical Engineering and Imaging Institute
Director, Cardiovascular Imaging Research
Lucy G. Moses Professor in Medical Imaging and Bioengineering
Vice-Chair for Research, Department of Radiology
Professor of Radiology and Medicine (Cardiology), and AI & Human Health
Icahn School of Medicine at Mount Sinai

Dr. Fayad's research has been dedicated to the detection and prevention of cardiovascular disease with many seminal contributions in the field of multimodality biomedical imaging and nanomedicine. Recent collaborative work has been in the study of psychosocial stress exposure in the brain, the cardiovascular system and the immune system; the development of platform nanotechnology to produce nanobiologics for immunotherapy in multiple disease conditions; the development of the Mount Sinai Imaging Research Warehouse (de-identified, pseudo-anonymized images and metadata) as a unique repository of radiological imaging/reports for focused imaging and general healthcare research; COVID-19 data and data science research by cofounding the Mount Sinai COVID Informatics Center now known as the Mount Sinai Clinical Intelligence Center; the use of mobile health (wearables and apps) for the study of disease and the deployment of digital therapies like the Warrior Watch and Warrior Shield programs.

Dr. Fayad serves in editorial roles for the *Journal of the American College of Cardiology Imaging*, the *Journal of Cardiovascular Magnetic Resonance*, the *Journal of the American College of Cardiology*, *Arteriosclerosis Thrombosis and Vascular Biology*, the *Journal of Cardiovascular Magnetic Resonance* and is former Associate Editor of *Magnetic Resonance in Medicine*. In 2015, he chaired the Scientific Advisory Board of the Institut National de la Santé et de la Recherche Médicale (INSERM) PARCC program at the HEGP in Paris.

Dr. Fayad is the recipient of multiple prestigious awards, has authored more than 400 peer-

reviewed publications, 50 book chapters, and over 500 meeting presentations. He has trained over 100 post doctoral fellows, clinical fellows, and students, many of whom went on to receive major awards, fellowships, and positions in academia and industry.

Dr. Fayad is currently the Principal Investigator of multiple federal, foundation and industry grants, and in 2021, ranked in the top 10 in NIH research overall funding in the field of Radiology. His work on stress, the immune system and cardiovascular disease published in the Lancet was featured in the Altmetric Top 100 (2017), Highly Cited Researchers by Clarivate Analytics (2018, 2019, 2020, 2021), Mount Sinai Jacobi Medallion Award (2019).

Dr. Fayad received his B.S. in electrical engineering from Bradley University, his M.S. in biomedical engineering from Johns Hopkins University, and Ph.D. in bioengineering from the University of Pennsylvania.

Dennis S. Charney, MD

Anne and Joel Ehrenkranz Dean
Icahn School of Medicine at Mount Sinai
Executive Vice President for Academic Affairs
The Mount Sinai Medical Center
New York, NY

Dennis S. Charney, MD, is Anne and Joel Ehrenkranz Dean of the Icahn School of Medicine at Mount Sinai and President for Academic Affairs for the Mount Sinai Health System. An internationally acclaimed expert in the neurobiology and treatment of mood and anxiety disorders, Dr. Charney has made fundamental contributions to the understanding of the causes of human anxiety, fear, and depression, and to the discovery of new treatments for mood and anxiety disorders.

Under Dean Charney's leadership, the Icahn School of Medicine at Mount Sinai has risen to, and maintained, its strength among the top 15 U.S. medical schools in National Institutes of Health (NIH) funding, and currently ranks second in funding per faculty member from all sponsored projects. With an emphasis on innovation and discovery and a track record of strategic recruitments across the biomedical sciences and in genomics, computational biology, and information technology, the School has cultivated a supercharged, Silicon Valley-like atmosphere in the academic setting. As the sole medical school partnering with the seven hospitals of the Mount Sinai Health System, the Icahn School of Medicine at Mount Sinai has one of the most expansive educational, research and clinical footprints in the nation.

Early in his tenure as Dean, Dr. Charney unveiled Mount Sinai's $2.25 billion strategic plan, which laid the foundation for establishing multidisciplinary research institutes as hubs for scientific and clinical collaboration. Within and across the institutes, faculty investigators and physicians work together to push the boundaries of science and medicine in order to address the most pressing biomedical challenges of our time. Dr. Charney is now overseeing the creation of complementary clinical institutes for the entire Mount Sinai Health System. These new institutes are Centers of Excellence for disease-specific areas such as cancer, heart disease, diabetes, HIV, and pulmonary diseases. Together the research and clinical institutes are generating game-changing models in translational research, clinical excellence

and standards of care.

Recent affiliations with Rensselaer Polytechnic Institute, Google, IBM and Apple further enhance the landscape for discovery at Icahn School of Medicine at Mount Sinai. These unique relationships have expanded opportunities for cross-fertilization of ideas and programs, and present exciting educational, scientific and clinical possibilities for our students and faculty alike.

Dean Charney's career began in 1981 at Yale University School of Medicine, where, within nine years, he rose from Assistant Professor to tenured Professor of Psychiatry. While at Yale, he chaired the National Institute of Mental Health (NIMH) Board of Scientific Counselors, which advises the institute's director on intramural research programs. In 2000, the NIMH recruited Dr. Charney to lead their Mood and Anxiety Disorder Research Program — one of the largest programs of its kind in the world — and the Experimental Therapeutics and Pathophysiology Branch. That year, Dr. Charney was elected to the National Academies of Medicine.

In 2004, Dr. Charney was recruited to Icahn School of Medicine at Mount Sinai as Dean of Research. In 2007, he was appointed Dean of the School and Executive Vice President for Academic Affairs of the Medical Center. In 2013, Dr. Charney was named President for Academic Affairs for the Health System. He is currently one of the longest-serving Deans of any American medical school.

Dr. Charney's own robust research program has garnered recognition through virtually every major award in his field. His investigations of the causes and treatment of depression have generated new hypotheses regarding the mechanisms of antidepressant drugs and have resulted in novel therapies, including Lithium and Ketamine for treatment-resistant depression. The work of his research team demonstrating that Ketamine as a rapidly acting antidepressant has been hailed as one of the most exciting developments in antidepressant therapy in more than half a century.

Dr. Charney is a committed educator and role model who lectures within Mount Sinai, nationally and internationally. He has mentored and taught scores of junior faculty, postdoctoral fellows, medical students and graduate students throughout his career.

Recently, Dr. Charney's pioneering research has expanded to include the psychobiological mechanisms of human resilience to stress, and has led to the identification of ten key resilience factors for building the strength to weather and recover from stress and trauma. This work is in the basis for his inspiring book for lay audiences, Resilience: The Science of Mastering Life's Greatest Challenges, co-authored by Steven Southwick and published by Cambridge University Press in 2012.

A prolific author, Dr. Charney has written more than 600 publications, including groundbreaking scientific papers, chapters, and books. His many books include: Neurobiology of Mental Illness (Oxford University Press, USA, Fourth Edition, 2013); The Peace of Mind Prescription: An Authoritative Guide to Finding the Most Effective Treatment for Anxiety and Depression (Houghton Mifflin Harcourt, 2004); The Physician's Guide to Depression and Bipolar Disorders(McGraw-Hill Professional, 2006), Resilience and Mental Health: Challenges Across the Lifespan (Cambridge University Press, 2011).

Burton Drayer, MD

Dean for Clinical Affairs
Professor and System Chair - Diagnostic, Molecular and Interventional Radiology
Icahn School of Medicine at Mount Sinai
New York, NY

Burton Paul Drayer, MD, is the Charles M. and Marilyn Newman Professor and System Chair of the Department of Diagnostic, Molecular, and Interventional Radiology for The Mount Sinai Health System and the Icahn School of Medicine at Mount Sinai. He previously served as the President of The Mount Sinai Hospital from November 2003 to September 2008 and CEO of the Mount Sinai Doctors Faculty Practice and Dean for Clinical Affairs from November 2014 to January 2021.

Dr. Drayer's academic appointments began in 1977 as Associate Professor of Radiology at the University of Pittsburgh Health Center. From 1979 to 1986, Dr. Drayer was faculty at Duke University Medical Center where he became Professor of Radiology and Assistant Professor of Medicine (Neurology). He is Board Certified in both Radiology/Neuroradiology and Neurology. In 1986, he was appointed Chair of the Division of Neuroimaging Research-Education at the Barrow Neurological Institute in Phoenix Arizona where he remained until 1995 and became Chair of Radiology at St. Joseph's Hospital. In 1995, Dr. Drayer moved to his present Radiology position at the Mount Sinai Medical Center.

Internationally known for his research using anatomic, physiologic, and functional imaging of the aging brain, brain iron (the first to define the normal and abnormal presence of iron using MRI), neurodegenerative disorders, brain infarction, xenon enhanced CT for measuring regional cerebral blood flow (first described its potential, feasibility, and application), MR angiography, multiple sclerosis, and intrathecal contrast media toxicity, Dr. Drayer has over 200 publications in major journals as well as multiple book chapters. He has been on many editorial boards and was Editor of Neuroimaging Clinics of North America from 1990 to 2005. He is also well recognized as an expert in the development of outpatient imaging facilities, imaging center design, and advanced imaging equipment. Dr. Drayer also served on the Board of Directors of Hospitals Insurance Company (HIC), a malpractice liability insurance captive from 2003 to 2018 and the Proton Beam Center from 2014 to present.

Dr. Drayer has been a leader in the major national and international Radiology societies. He was on the Board of Directors of the American Society of Neuroradiology (ASNR) from 1990 to 2000 and was ASNR President (1996-1997). He was also a founding member and the inaugural Chairman of the Research Foundation of the ASNR (1995-2001). He was on the Board of Directors of the Radiological Society of North America (RSNA) as the Liaison for the Annual Meeting and IT from 2003 to 2008, Chairman of the Board in 2009, and President Elect and President in 2010 and 2011. He was Chairman of the RSNA Research and Education Foundation from 2015-2016. Additionally, Dr. Drayer was on the Board of Chancellors of the American College of Radiology (ACR) from 2009-2015 and Chaired the ACR Panel on Neurologic Imaging

Appropriateness Criteria from 1994-2003. He also served on the Board of Directors of the Academy of Radiology Research (ARR) from 1995 to 2000 and 2009 to 2012.

Among the honors presented to Dr. Drayer were the ASNR Cornelius Dyke (1977) and Outstanding Paper (1978, 1981) awards, the Jacobi Medallion of the Mount Sinai Medical Center (2009), honorary fellowship in the Royal College of Surgeons, Ireland (2011), honorary member of the European Society of Radiology (2012), and the Gold Medal of the ASNR in 2011 and the RSNA in 2016. Dr. Drayer is a fellow of both the American Academy of Neurology and the American College of Radiology. His career has been dedicated to enhancing the educational, clinical, research and administrative platform for his associates at Mount Sinai as well as the national and international community of radiologists and imaging scientists.

Biographies of Invited Speakers

Tessa Sundaram Cook, MD, PhD

University of Pennsylvania

Dr. Cook is an Assistant Professor of Radiology at the Perelman School of Medicine at the University of Pennsylvania in Philadelphia. She has a strong background in imaging informatics, having completed her doctoral work in quantitative image processing in the Penn Image Computing and Science Laboratory (PICSL). During her residency, Dr. Cook developed RADIANCE, only the second open-source radiation exposure monitoring tool used worldwide. She is an active member of multiple radiology societies, including the SIIM, ACR, AUR, and RSNA. She received one of the 2011 E. Stephen Amis, Jr. Fellowships in Quality and Safety from the ACR. She was one of the four AUR GERRAF fellows for 2013-2015. Dr. Cook currently enjoys an academic appointment in radiology that enables her to continue her clinical work in cardiovascular imaging and research in imaging informatics. She is the director of the Imaging Informatics Fellowship in the Department of Radiology, as well as the clinical director of the 3-D and Advanced Imaging Laboratory. She also co-directs the Center for Practice Transformation in Radiology. In 2020, Dr. Cook was inducted into the College of SIIM Fellows and received the inaugural Dr. Ruth Dayhoff Award for the Advancement of Women in Medical Imaging Informatics. She is currently the Chair-Elect of SIIM. Dr. Cook's current research sits squarely at the intersection of imaging informatics and health services. In her various roles, she is pursuing innovative methods to enhance the delivery of longitudinal patient care in radiology and improve radiologists' workflow.

Toby Cosgrove, MD

Cleveland Clinic

Toby Cosgrove, MD, is former CEO and current Executive Advisor of Cleveland Clinic. He is Strategic Advisor to Care Centrix, Senior Advisor of Innova Health Partners, and is Member of the Board of Directors of Cleveland Clinic Abu Dhabi, American Well, and Hims & Hers. As an expert on health issues, he is a frequent commentator in national and international media.

As CEO and President of Cleveland Clinic from 2004 through 2017, he led the $8 billion organization to new heights of achievement and efficiency, seeing it ranked the #2 hospital in America (U.S. News). In his role as Executive Advisor, he is working with Cleveland Clinic leadership on strategies for national and international growth.

Dr. Cosgrove graduated from Williams College and the University of Virginia School of Medicine. He trained at Massachusetts General Hospital and Brook General Hospital in London. In 1967, he was a surgeon in the U.S. Air Force, earning a Bronze Star.

Dr. Cosgrove joined Cleveland Clinic in 1975, and chaired the Department of Thoracic and Cardiovascular surgery from 1989 to 2004. He performed over 22,000 operations and earned an international reputation in valve repair. He holds 30 patents for medical innovations. As CEO from 2004 to 2017, he reorganized services, improved outcomes and patient experience, and strengthened the organization's finances.

He is a member of the National Academy of Medicine, and a Fellow of the National Academy of Inventors. In 2016, he was a Fortune Businessperson of the Year (No. 14). Three successive presidents of the United States have consulted him on healthcare issues.

Stephanie I. Fraley, PhD

University of California, San Diego

Dr. Stephanie I. Fraley is an Associate Professor of Bioengineering at the University of California, San Diego. She earned her B.S. in Chemical Engineering in 2006 from The University of Tennessee, Chattanooga and her Ph.D. in Chemical and Biomolecular Engineering in 2011 from The Johns Hopkins University. She has contributed fundamental knowledge in the fields of 3D cell migration and molecular detection technology, for which she received a Burroughs Wellcome Fund Career Award at the Scientific Interface and was named a SAGE Bionetworks Scholar, Kavli Frontiers of Science Fellow, NSF CAREER awardee, Biomedical Engineering Society Rising Star in Cellular and Molecular Bioengineering, and Biomaterials Science Emerging Investigator.

A primary focus of the Fraley lab is to develop molecular detection technologies that address critical unmet needs for infectious disease diagnosis and surveillance. In light of the current pandemic, it is not difficult to see why such research is critical for effective patient treatment, prevention of disease spread, and the detection and tracing of novel variants. The Fraley lab is working to bring a new age of rapid, broad-based, quantitative, and inexpensive technology to address these challenges. They have built and characterized a novel platform that is capable of accomplishing rapid and broad pathogen identification, with sensitivity to the single genome level and the ability to characterize mixed infections. These capabilities are achieved by innovating digital PCR with DNA melt analysis concepts with “big data” and machine learning frameworks. Their ongoing work uses this approach to automatically detect both known and novel emerging pathogens with clinically impactful speed, sensitivity, and specificity.

Robbie Freeman, RN, MSN, NE-BC

Mount Sinai Heath System

Robbie Freeman, RN, MSN, NE-BC, is Vice President of Clinical Innovation and Chief Nursing Informatics Officer (CNIO) at the Mount Sinai Health System. In this role, he drives the technology strategy to support nursing practice and patient care across the hospital and ambulatory care settings, leveraging technology such as machine learning, artificial intelligence, and virtual care. He also oversees the clinical data science and digital engagement teams and leads the nursing informatics team. During his time at the Mount Sinai Health System, Mr. Freeman has held a variety of roles. He started on the front lines, providing bedside patient care. He has held several leadership roles focusing on quality, technology, and hospital operations. His most recent role was as Vice President of Clinical Innovations at The Mount Sinai Hospital, where he built machine learning products to improve patient safety and hospital operations. Before that, he served as Senior Director of Clinical Operations for The Mount Sinai Hospital. He also leads a Health System-wide initiative focused on digital engagement to enhance the patient, family, and caregiver experience for hospitalized patients.

Mr. Freeman Chair's the American Nurses Association (ANA) Advisory Board on Data Science and AI. He is pursuing his doctorate in nursing practice at Yale University, where his research interest is the application of artificial intelligence products in clinical workflows. He holds a Master of Science in business analytics from the New York University (NYU) Stern School of Business and a Master of Science in nursing, specializing in clinical systems management. He is also a graduate of the Phillips School of Nursing at Mount Sinai, where he serves on the Board of Trustees. Mr. Freeman is an adjunct assistant professor of health administration at NYU, where he teaches a graduate course on advanced healthcare analytics. He is also the recipient of The New York Times's Tribute to Nurses award for technological innovations and is an Aspen Institute Spotlight Health Scholar. In 2016, Mr. Freeman completed the Clinical Quality Fellowship Program, a program sponsored by Greater New York Hospital Association and the United Hospital Fund that teaches clinicians to lead quality improvement and patient safety initiatives.

James Dahlman, PhD

Georgia Institute of Technology

James Dahlman is the McCamish Early Career Associate Professor in the Department of Biomedical Engineering at Georgia Tech and Emory School of Medicine. His lab works at the interface of chemical engineering, genomics, and gene editing by applying big data approaches to nanomedicine. His trainees have developed DNA barcoded nanoparticles to measure how hundreds of nanoparticles deliver mRNA and siRNA in multiple cell types from a single animal in vivo, and the lab uses these approaches to deliver RNA outside the liver without targeting ligands. James was a co-founder and Board Chairman of Guide Therapeutics, which was acquired by Beam Therapeutics.

James has published in Nature, Nat Nano, Nat Biotech, Nat BME, Nat Metabolism, Nat Rev Cancer, Nat Rev Genetics, Science, Science Translational Medicine, Cell, Scientific American, and other high-impact journals. He has won awards including the BMES Rita Schaffer Award, ASGCT Outstanding New Investigator Award, Georgia Tech Outstanding Achievement in Early Career Research Award, Tech Review TR35, Controlled Release Society GDGE Award, and had his barcoding work described as a Top 10 Emerging Technology by the World Economic Forum. James received a B.S. in Biomedical Engineering from Wright State in 2009, a Ph.D. in 2015 from the Harvard-MIT HST Program, where he studied with Robert Langer, and as an LSRF post-doc, studied CRISPR-Cas9 with Feng Zhang.

Penny Gowland, PhD

University of Nottingham

I work on developing and applying quantitative MRI to solve biomedical questions. I exploit the capabilities of ultra-high field MRI in neuroscience, developing methods for studying neurodegeneration, and using the increased contrast to noise ratio available at ultra-high field to study 'single trial' fMRI of changing brain function, and to develop techniques to probe the origin of the BOLD effect which is responsible for fMRI. I am the physics lead on a unique interdisciplinary project which has developed MRI methods to study many features of gastrointestinal (GI) function using standard clinical MR scanners; this could revolutionize the diagnostic pathway for patients with GI problems. I have used MRI to develop new understanding about the function of the human placenta and I have a strong interest in applying quantitative imaging methods to studying human development particularly in the fetus. The GI and placental work will both benefit for upright scanning and I am now undertaking a project aimed at maximizing the capability of low field, open MRI. Finally I have a long term interest in studying the safety of MRI.

Tim Leiner, MD, PhD

Mayo Clinic and Utrecht University Medical Center

Prof. Tim Leiner is a cardiovascular radiologist at Mayo Clinic, Rochester, MN and a Professor of Radiology at Utrecht University Medical Center, Utrecht, The Netherlands. He received his M.D. in 2000 from Maastricht University Medical School. In 2002 he obtained his Ph.D. from the same University. Following his Ph.D. he spent 18 months as a postdoctoral research fellow at the Cardiac MR Center at the Beth Israel Deaconess Medical Center / Harvard Medical School in Boston under Dr. Warren Manning. He then completed his Radiology residency at Maastricht University Medical Center, during which he spent 3 months at the Vascular Imaging Laboratory at the University of Washington, Seattle, WA under Professors Jeffrey H. Maki and Chun Yuan.

His research interests center around the development and implementation of new cardiovascular MR and CT techniques. Dr. Leiner has served as faculty member and member of the organizing committees at the annual meetings of the International Society for Magnetic Resonance in Medicine (ISMRM), European Society for Magnetic Resonance in Medicine and Biology (ESMRMB), Society for Cardiovascular Magnetic Resonance (SCMR), European Society for Cardiovascular Radiology (ESCR), Society for cardiovascular Computed Tomography (SCCT), European Congress of Radiology (ECR), Radiological Society of North America (RSNA), and at annual meetings of the Dutch Radiological Society. He has chaired the Scientific Program Committee of the ESMRMB in 2017. Dr. Leiner has served on the Editorial Boards of European Radiology, the Dutch Medical Journal and the Journal of Cardiovascular Magnetic Resonance (JCMR). He currently is Associate Editor of the Journal of Magnetic Resonance Imaging (JMRI) and Radiology – Cardiothoracic. Dr. Leiner has served on the Board of Trustees of the ISMRM from 2006-2009 and the Board of Trustees of the Society for Cardiovascular Magnetic Resonance (SCMR) from 2016-2019. He is the author of over 350 original papers, review articles and book chapters as well as editor of several electronic radiology textbooks. He is the immediate past president of the ISMRM.

Karla Miller, PhD

University of Oxford

Dr. Miller works on developing and applying quantitative MRI to solve biomedical questions. She exploits the capabilities of ultra-high field MRI in neuroscience, developing methods for studying neurodegeneration, and using the increased contrast to noise ratio available at ultra-high field to study 'single trial' fMRI of changing brain function, and to develop techniques to probe the origin of the BOLD effect which is responsible for fMRI. Dr. Miller is the physics lead on a unique interdisciplinary project which has developed MRI methods to study many features of gastrointestinal (GI) function using standard clinical MR scanners; this could revolutionize the diagnostic pathway for patients with GI problems. Additionally, she has used MRI to develop new understanding about the function of the human placenta and has a strong interest in applying quantitative imaging methods to studying human development, particularly in the fetus. She is currently working on a project aimed at maximizing the capability of low field, open MRI, and has a long term interest in studying the safety of MRI.

William H. Morris, MD, MBA, FACP

Health Care and Life Science Executive, Google Cloud

Dr. William Morris is a Healthcare and Life Science customer executive at Google Cloud. He is focused on enabling HCLS partners to successfully adopt, deploy and scale transformative digital solutions. He was previously the Executive of Cleveland Clinic Innovations and Ventures at Cleveland Clinic and the Associate Chief Information Officer. He had oversight of design, development, and deployment of all clinical IT systems and health IT innovations, as well as all commercialization and business development functions.

Dr. Morris earned his medical degree from Case Western Reserve University School of Medicine and completed training in Internal Medicine at Beth Israel Deaconess Medical Center, Harvard Medical School. He also received his MBA in 2017 from Case Western Reserve University Weatherhead School of Management. Dr. Morris also continues to practice medicine.

Nitish V. Thakor, PhD

Johns Hopkins University and National University of Singapore

Nitish V. Thakor is a Professor of Biomedical Engineering, Electrical and Computer Engineering and at Johns Hopkins University since 1983. He also joined the National University of Singapore in 2012 and served as the Founding Director of Singapore Institute for Neurotechnology (SINAPSE). Prof. Thakor's technical expertise is in the fields of Medical Instrumentation and Neuroengineering, where he has carried out research on many technologies for brain monitoring, implantable neurotechnologies, neuroprosthesis and brain-machine interface. He has published over 430 refereed journal papers (GH Index 86), obtained 16 US and international patents and co-founded 3 active companies. He was previously the Editor in Chief of IEEE Transactions on Neural Systems and Rehabilitation Engineering, and currently the EIC of Medical and Biological Engineering and Computing (Springer/Nature). He is the Editor of an upcoming authoritative reference Handbook of Neuroengineering. Prof. Thakor is a recipient of the Technical Achievement Award (Neuroengineering) as well as the Academic Career Award from the IEEE Engineering in Medicine and Biology Society. He received a Research Career Development Award from the National Institutes of Health and a Presidential Young Investigator Award from the National Science Foundation, and is a Fellow of the American Institute of Medical and Biological Engineering, Life Fellow of IEEE, Biomedical Engineering Society, and International Federation of Medical and Biological Engineering. He is a recipient of a Distinguished Alumnus Award from Indian Institute of Technology, Bombay, India, and a Centennial Medal from the University of Wisconsin School of Engineering. He was elected to the National Academy of Inventors in 2021.

Selected for oral presentations

Chief Editor: Octavia Bane, PhD

Review Committee:

- Akbar Alipour, PhD
- Emre Altinmakas, MD, PhD
- Valentin Fauveau, MSc
- Li Feng, PhD
- Yael Jacob, PhD
- Xueyan Mei, PhD
- Judit Morla-Folch, PhD
- Alan Seifert, PhD
- Georgios Soultanidis, PhD
- Bram Teunissen, PhD
- Mandy Van Leent, MD, PhD
- Xiang Xu, PhD
- Yang Yang, PhD

Development of a Metasurface to Improve MRI at Ultra-High Fields

Akbar Alipour[1], Alan C Seifert[1], Bradley N Delman[2], and Priti Balchandani[1]

[1] ABioMedical Engineering and Imaging Institute, Icahn School of Medicine at Mount Sinai, New York
[2] Department of Diagnostic, Molecular and Interventional Radiology, Icahn School of Medicine at Mount Sinai, New York

Introduction: Ultra-high field (UHF) MRI systems (7T+) leverage increased SNR over conventional field strengths for anatomical and functional MRI of human brain. However, challenges associated with wavelength effects at UHF, such as transmit radiofrequency (RF) magnetic field (B1+) inhomogeneity, limit broad application of UHF MRI [1]. One area of weakness is the posterior fossa, where reduction in coil transmit efficiency significantly reduces SNR compared with other brain regions. Approaches to resolving this issue of B1+ inhomogeneity include parallel transmit systems, and passive RF shimming devices such as high permittivity materials (HPM), metasurfaces, or passive RF arrays. However, these methods have some drawbacks including unstable material parameters of dielectric pads, high-cost and complexity of PTx systems. We developed a simple device named the broadside-coupled split-ring-resonator (BC-SRR)-based metasurface [2]. Placed against the posterior caudal head inside a head coil, this device improves transmit efficiency and signal sensitivity in this challenging region.

Materials and Methods: The proposed metasurface is formed of a periodic set of BC-SRRs patterned on top of a 5 mm thick HPM. Each circular BC-SRR element consists of two open conducting rings, 3.5 cm in diameter, which are etched on both sides of a flexible dielectric (Kapton) substrate, with gaps oriented in opposite positions, as shown in Figure 1. Phantom and in-vivo images of a healthy volunteer were acquired on a 7T MRI scanner (Siemens, Magnetom) using a commercially available 1Tx/32Rx head RF coil (Nova Medical, Wilmington, MA, USA). To assess the metasurface's performance, B1+ and SNR maps were calculated in a phantom with/without the metasurface. B1+ maps were measured using the presaturation-prepared turbo-FLASH based method [3]. In-vivo images were acquired in a human subject using 2D GRE and 2D TSE sequences both with and without the metasurface.

Results: Measured B1+ and SNR maps in the phantom with/without the metasurface show placement of the metasurface inside the coil is associated with 2.1-fold and 1.4-fold increase in the transmit efficiency and SNR in the ROI encircled with dashed red (Fig. 2). In-vivo images obtained using the metasurface improve structural visualization by locally enhancing SNR, leading to notably improved tissue contrast (Fig. 3). In both sequences, acceptable signal homogeneity was achieved.

Conclusions: The increase in SNR can be leveraged to obtain a higher resolution image over the same scanning time or faster acquisition at the same resolution. This device could improve the performance of existing commercial coils at 7T for whole brain and other applications.

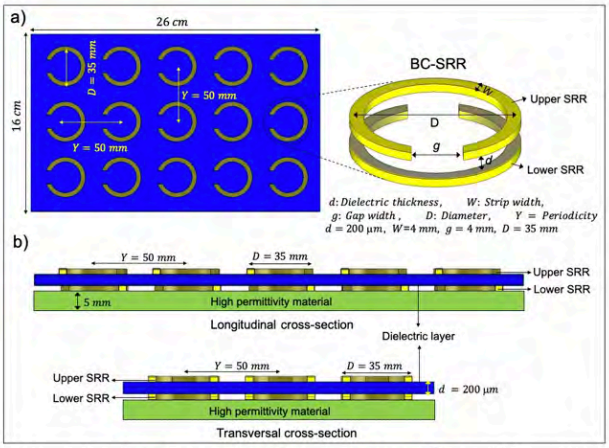

Figure 1: A schematic of the metasurface ($26\ cm \times 16\ cm \times 5\ mm$), which consists of a 3×5 matrix of BC-SRRs and a dielectric pad.

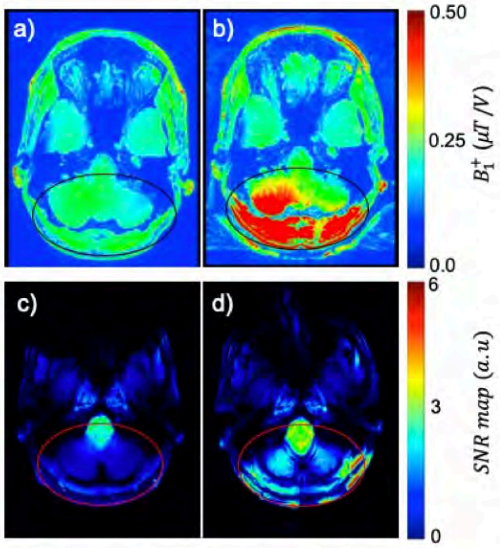

Figure 2: Experimental B_1^+ (top row) and SNR (bottom row) maps without (left) and with (right) the metasurface show an improvement in the inferior regions of the brain in the presence of the metasurface.

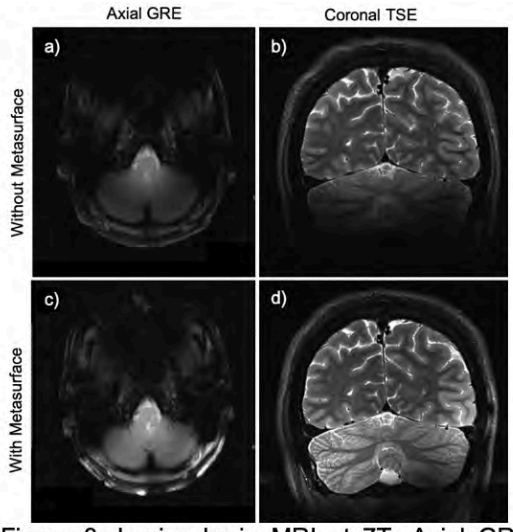

Figure 3: In-vivo brain MRI at 7T. Axial GRE and coronal TSE images obtained without (top row) and with (bottom row) the metasurface show significant SNR improvement in the inferior regions in the presence of the metasurface, particularly in the cerebellum and brainstem.

Advanced diffusion-weighted MRI and proteomic analysis as potential predictors of renal tumor histopathology

Octavia Bane[1,2], Jorge Daza[3], Berengere Salome[4], John P. Sfakianos[3], Andrew Charap[4], Kirolos Meilika[3], Kennedy Okhawere[3], Amir Horowitz[4], Bachir Taouli[1,2], Ketan Badani[3], Sara Lewis[1,2]

[1] 1Department of Radiology, Icahn School of Medicine at Mount Sinai
[2] BioMedical Engineering and Imaging Institute, Icahn School of Medicine at Mount Sinai
[3] Department of Urology, Icahn School of Medicine at Mount Sinai
[4] Division of Oncological Sciences, Icahn School of Medicine at Mount Sinai

Introduction: Due to heterogeneity of small renal masses (SRM), and to limited diagnostic accuracy of biopsies, pre-operative distinction of benign lesions from renal cell carcinoma (RCC), and particularly from clear cell (cc)RCC, the subtype with the greatest risk of recurrence and poorest survival, is an unmet need. The purpose of our study was to establish feasibility of a novel approach composed of intravoxel incoherent motion model of diffusion (IVIM-DWI) and high-throughput urine proteome analysis from patients with SRM for histologic classification and characterization.

Materials and Methods: Thirty prospectively enrolled patients (M/F:22/8, 60 ± 11.3 years) with SRMs scheduled for partial nephrectomy surgery underwent advanced IVIM-DWI MRI at 1.5T (2D SS EPI, TR/TE: 4700/81 ms, 20 6-mm coronal slices, in-plane resolution 2.09x2.4 mm^2) with 9 b-values (0,10,30,50,80,120,200,400,800 s/mm^2)(1). A radiologist with 10 years of experience traced ROIs covering all visible slices of the tumor. Tumor IVIM parameters (true diffusion D, pseudo-diffusion Ds, and perfusion fraction PF) were calculated using a biexponential, pixel-by-pixel Bayesian fit, and ADC was calculated using a monoexponential fit over all b-values>100 s/mm^2. A subset of 10 patients (M/F:5/5, 58 ± 12 years) also underwent a high-throughput analysis of urine collected on the day of surgery, using a panel of 92 Olink proteomics inflammation-related markers (2).

Results: We examined 30 lesions (ccRCC/non-ccRCC/benign: 18/6/6) in 30 patients. Examples of patients with clear-cell renal carcinoma (ccRCC) are shown in Fig.1. In the subset of patients with proteomics and DWI, pathology of SRMs revealed 7 ccRCC, 1 non-ccRCCs (chromophobe RCC), and 2 benign masses. Mean (p=0.008) and median (p=0.018) ADC, and mean (p=0.006) and median (p=0.015) D were significantly elevated in ccRCC vs. other RCC subtypes (Fig.2), and distinguished ccRCCs from other RCCs with good diagnostic performance (AUC$>$0.8). Clustering analysis of urinary protein markers showed a predominant upregulation of the urine inflammation markers in ccRCC cases ($p<0.045$). We observed strong false-discovery-rate-adjusted correlations (Fig.3) between the urine inflammatory protein EN-RAGE and mean ADC (r=0.9, p=0.0003), mean PF (r=0.79, p=0.0003), and D (r=0.9 p=0.003), and the chemokine CCL23 and PF (r=0.63, p=0.048).

Conclusions: SRMs may produce a local inflammatory response in the kidney that is reflected in changes in expression of inflammatory proteins in the urine. IVIM parameters correlated with urine protein expression, which suggests that a combined non-invasive approach of imaging and proteomics would be beneficial in stratifying patients with renal masses for treatment. Validation of this approach is needed in a larger number of cases.

Figure 1. Correlative analysis of DWI and urine Olink proteomics reveals a ccRCC signature associated with inflammation and DWI parameters. Side by side comparison of representative maps from DWI parameters evaluated (D, PF and ADC). ccRCC (in a male patient, 71 years) and non-ccRCC (chromophobe RCC in a female patient, 60 years) representative pictures of cases with higher PF, D and ADC coefficients in ccRCC compared to non-ccRCC. Tumor location is shown on T2w and T1w at 3 minutes post-contrast anatomical images. Maps are shown for illustrative purpose only.

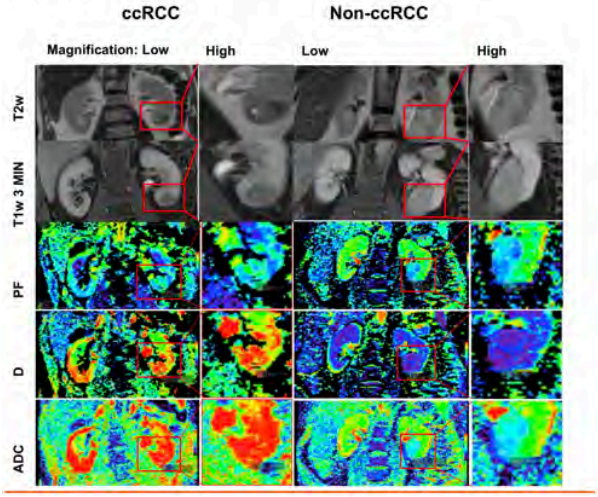

Figure 2. Group comparison of DWI parameters that were significant for distinguishing ccRCC from other RCC.

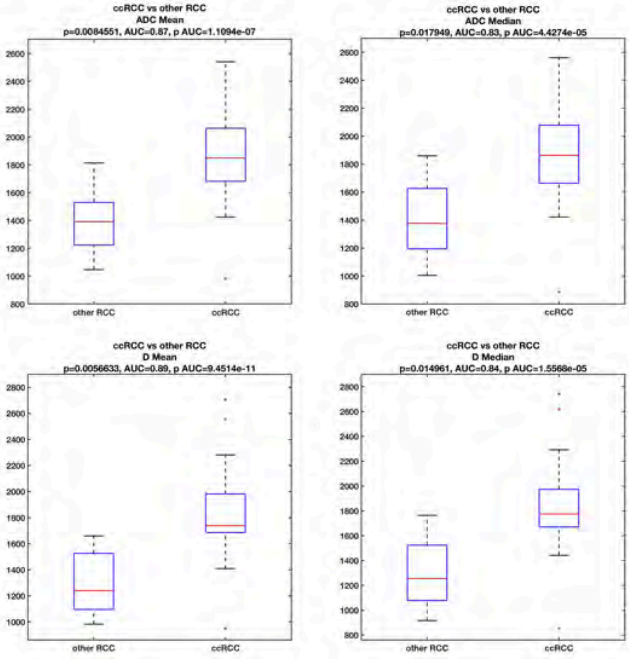

Figure 3. Scatterplots from Spearman correlation analysis on differentially expressed urine proteins between ccRCC and non-ccRCC and IVIM-DWI parameters.

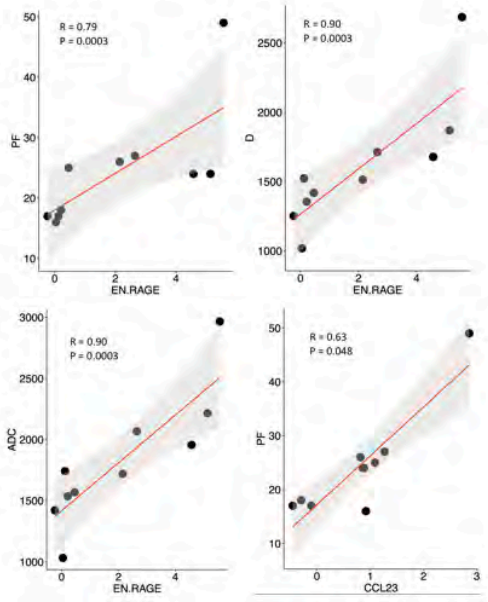

Long-COVID cardiopulmonary sequelae: characterization by 18F-FDG PET/MR and DECT imaging

Ana Devesa[1]; Philip Robson[1]; Sonali Bose[1], Valentin Faveau[1], Steve Liao[1]; Munir Ghesani[2], Renata Pyzik[1] Zahi Fayad[1]; Maria Trivieri[1,3]

[1] BioMedical Engineering and Imaging Institute, Icahn School of Medicine at Mount Sinai, New York, NY, United States
[2] Division of Nuclear Medicine; Department of Radiology, Icahn School of Medicine at Mount Sinai, New York, NY, United States
[3] Cardiovascular Institute, Icahn School of Medicine at Mount Sinai, New York, NY, United States

Introduction: Long-COVID is emerging as a new syndrome with pleiotropic clinical manifestations and debilitating symptoms affecting millions of COVID survivors. Little is known about the underlying pathogenesis and its propensity for developing into longer-term complications, especially cardiopulmonary. As such, there is an urgent need to characterize these long-term sequelae better. Our objective was to conduct an observational study of patients experiencing persistent cardiopulmonary symptoms between 9 and 12 months after initial infection and to describe the prevalence of inflammatory cardiovascular findings using ^{18}F-FDG PET/MR imaging. In addition, we sought to understand any potential correlations between cardiovascular and pulmonary abnormalities by comparing results in patients undergoing both ^{18}F-FDG PET/MR and dual-energy computed tomography (DECT).

Materials and Methods: Adult subjects (> 20 years of age) with a self-reported history of COVID-19 infection, long-COVID syndrome, and predominant cardiopulmonary symptoms were recruited in our study to undergo cardiopulmonary ^{18}F-FDG PET/MR and/or iodinated contrast-enhanced DECT of the lungs.

Results: A total of 98 patients were enrolled in the study. 47% were male, and the mean age was 48 years. The median time between COVID-19 infection and imaging was 303 [141] months. The most common long-COVID symptom was shortness of breath (80%), followed by palpitations (48%) and chest pain (42%). 27% reported being admitted during the Acute COVID phase, and 26% required ICU-level care. Of the enrolled patients, 91 underwent ^{18}F-FDG PET/MR imaging, and 71 underwent DECT. PET/MR was abnormal in 57% of subjects, with 24% having evidence of myocarditis, 22% pericarditis, 11% periannular, and 30% vascular uptake (aortic, pulmonary, or both) as shown in Figure 1. On DECT, there were abnormalities in 90% of subjects, with 67.1% and 58.6% participants demonstrating pulmonary infiltrates and abnormal perfusion, respectively (Figure 2). Of the subjects that had abnormal PET/MR, an abnormal DECT was found in 100% of the participants with myocarditis and periannular uptake, and in 78.6% and 76.5% of the subjects with pericarditis and vascular uptake.

Conclusions: This is the largest cohort of long-COVID subjects being evaluated with advanced cardiopulmonary imaging, with the longest follow-up after COVID-19 infection. Our results indicate a high prevalence of abnormalities on both ^{18}F-FDG PET/MR and DECT and as well as confirming the occurrence of myocarditis and pericarditis, identify previously unrecognized sequelae such as periannular and vascular inflammation, which might warrant further monitoring to exclude the development of complications such as Pulmonary Hypertension and Valvular Heart Disease.

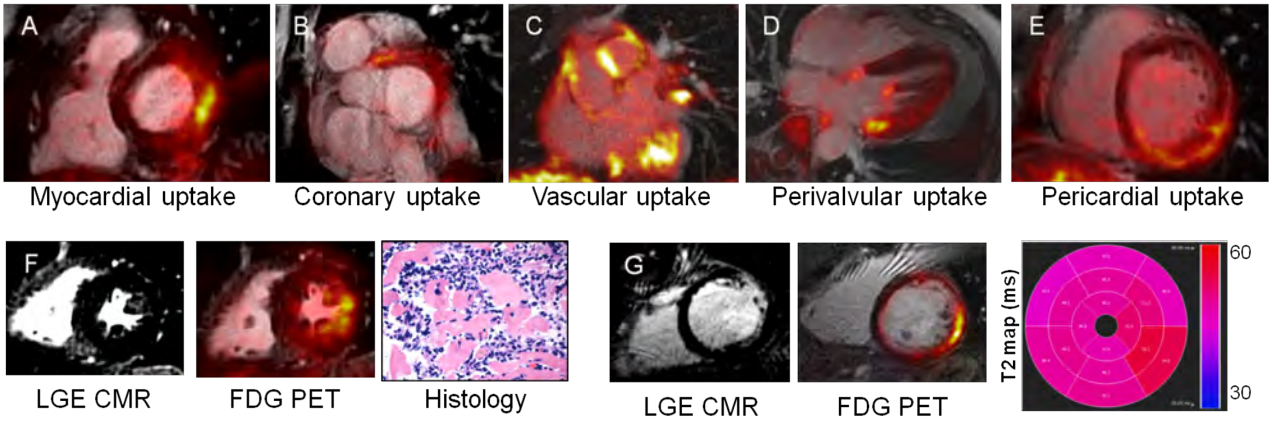

Figure 0.1: A-G: Four patterns of ^{18}F-FDG PET/MR have emerged (A-E) indicating 1) myocardial **(A)**, 2) vascular (including coronary **(B)** and the pulmonary artery and ascending aorta **(C)**), perivannular/perivavular **(D)** and pericardial inflammation **(E)**. ^{18}F-FDG uptake appears in conjunction with scarring as shown on late gadolinium enhanced (LGE) CMR, with histological confirmation of lymphocytic myocarditis **(F)** and T2 enhancement on CMR **(G)**.

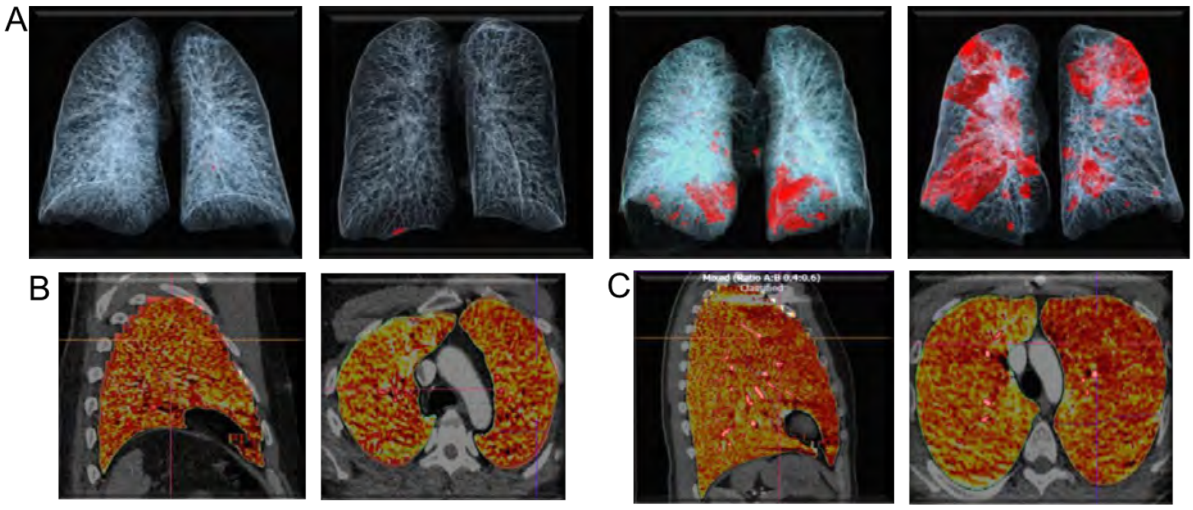

Figure 0.2: Prevalence of abnormal DECT finding by PET/MR imaging categories. **(A)** DECT images showing varying amount of lung opacities (in red). **(B)** Representative DECT perfusion images with homogenous distribution of contrast agent. **(C)** Representative DECT perfusion showing abnormal perfusion.

Therapeutic potential of specific modified mRNA translational system 2.0 (SMRTs 2.0) with minimally invasive delivery to cardiomyocytes in the heart

Keerat Kaur[1,2,3], Magdalena M. Zak[1,2,3], Jimeen Yoo[1,2,3], Ann Anu Kurian[1,2,3] , Jeffrey Downey[1], Filip K Swirski[1], Anthony Fargnoli[4], Seonghun Yoon[1,2,3], Lior Zangi[1,2,3]

[1] Cardiovascular Research Institute, Icahn School of Medicine at Mount Sinai, New York, NY 10029, USA
[2] Department of Genetics and Genomic Sciences, Icahn School of Medicine at Mount Sinai, New York, NY 10029, USA.
[3] Black Family Stem Cell Institute, Icahn School of Medicine at Mount Sinai, New York, NY 10029, USA.
[4] The Janssen Pharmaceutical Companies of Johnson & Johnson, NJ, 08560

Introduction: Ischemic heart failure (HF) secondary to myocardial infraction (MI) is a leading cause of mortality, mainly due to permanent loss of functional cardiomyocytes (CM) that are replaced by non-CMs post MI. This urgent unresolved medical need led scientists to evaluate whether induction of cardiac protection post cardiac ischemic injury can attenuate CM loss after ischemic injury. We recently have used acid ceramidase (AC) modRNA to alter sphingolipid metabolism and induce cardiac protection (Circulation, March 2020), however, our AC modRNA delivery required an open chest surgery follow by direct intramyocardial injection of the modRNA, moreover, delivery of AC modRNA can be done only once in this setting. In the same year, we were able to construct the first Specific modRNA Translation system (SMRTs) that allows modRNA translation specifically in CM (Circulation, April 2020, Circulation, Dec 2020). Here, we describe a minimal invasive method to deliver therapeutic modRNA directly to cardiomyocytes in the heart post ischemic reperfusion (I/R).

Materials and Methods: We used modRNA design, CRISPR technology, formulation of nanoparticles to prepare CM specific modified mRNA translational system 2.0 (CM-SMRTs-2.0), which allow specific translation of modRNA in CMs in the heart. We evaluate organ and cell specificity, pharmacokinetics, and the therapeutic potential of intervenes (I.V) delivery of CM-SMRTs-2.0 in I/R model.

Results: We showed using Luc and nuclear mCherry CM-SMRTs-2.0 translate specifically in CMs in the heart and not in other organs or cell types. We showed that modRNA translation in the heart of Luc CM-SMRTs-2.0 start 10 minutes post I.V injection and last for up to 2-3 days with the ability to replenish the modRNA by repeatedly I.V injection every 3 days. Mechanistically, we show that I.V delivery of AC CM-SMRTs-2.0 immediately post ischemic injury allows AC expression in the heart, reduce cell death and inflammation two days post I/R model. We also show that four I.V injections of AC-CM-SMRTs-2.0 in intervals of 3 days apart post I/R, reduce cardiac remodeling, and improve contractility 28 days post injury. Importantly, these 4 I.V injections did not lead to any significant tissue toxicity with comparison to untreated controls.

Conclusions: We describe here a novel platform, called CM-SMRTs 2.0, that enable us to deliver modRNA specifically to CM in the heart via I.V injection, without to limitation of open chest surgery. This new platform can be used to identify novel therapeutic targets, evaluate gene function and for gene correction.

Therapeutic potential of specific modified mRNA translational system 2.0 (SMRTs 2.0) with minimally invasive delivery to cardiomyocytes in the heart

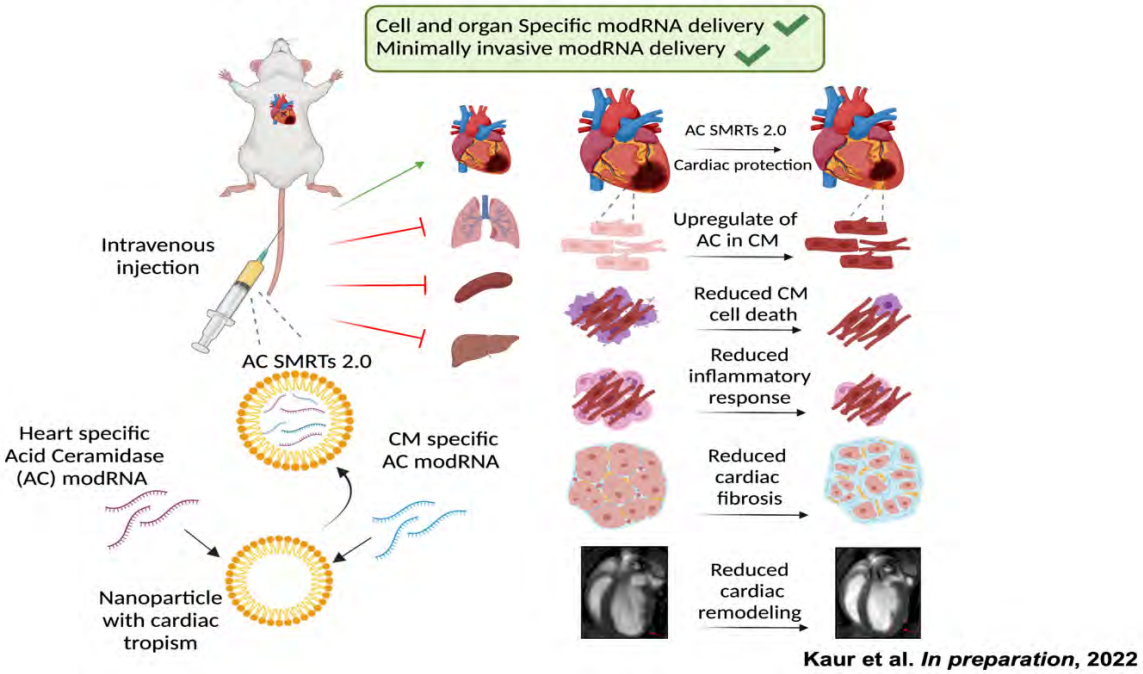

Kaur et al. *In preparation*, 2022

RadImageNet: A Large-scale Radiologic Dataset for Deep Learning Research

Xueyan Mei[1], Zelong Liu[1], Philip M. Robson[1,2], Brett Marinelli[2], Mingqian Huang[2], Amish Doshi,[2], Adam Jacobi[2], Chendi Cao[1], Katherine E. Link[1], Thomas Yang[1], Ying Wang[3], Hayit Greenspan[1], Timothy Deyer[4,5], Zahi A. Fayad[1,2], Yang Yang[1,2]

[1] BioMedical Engineering and Imaging Institute, Icahn School of Medicine at Mount Sinai, 1470 Madison Ave, New York, New York, 10029
[2] Department of Diagnostic, Interventional and Molecular Radiology, Icahn School of Medicine at Mount Sinai, 1468 Madison Ave, New York, New York, 10029
[3] Department of Mathematics, The University of Oklahoma, 660 Parrington Oval, Norman, Oklahoma, 73019
[4] Department of Radiology, Cornell Medicine, 525 E 68th Street, New York, New York, 10065
[5] Department of Radiology, East River Medical Imaging, 519 E 72nd Street, New York, New York, 10065

Introduction: Imaging artificial intelligence algorithms often rely on transfer learning by applying ImageNet pretrained models to radiologic datasets. Pretrained models composed of radiologic features trained on large medical imaging datasets are scarce. In this study, we created a large dataset of pre-annotated images and to show the models developed based on this dataset outperformed ImageNet models when utilizing transfer learning.

Materials and Methods: This retrospective study included patients who had a radiologic study between 2005 and 2020 at an outpatient imaging facility. Key images from the studies were annotated by board-certified radiologists. These images were used for RadImageNet model training from scratch. The RadImageNet models were compared to ImageNet models using the Area Under Receiver Operating Characteristic Curve (AUROC) for eight downstream classification tasks and using dice scores for two segmentation problems. The DeLong test and paired t-test were performed to compare the AUROC and segmentation scores, respectively.

Results: The RadImageNet database consists of 1.35 million annotated medical images from 131,872 patients who underwent CT, MRI, and ultrasound for musculoskeletal, neurologic, oncologic, gastrointestinal, endocrine, abdominal, and pulmonary pathologies. For transfer learning tasks on small datasets - thyroid nodule (US), breast masses (US), ACL injuries (MRI) and meniscal tears (MRI) - the RadImageNet models demonstrated significant advantage ($p<0.001$) to ImageNet models (9.4 percent, 4.0 percent, 4.8 percent, and 4.5 percent AUROC improvements, respectively). For larger datasets - pneumonia (CXR), COVID-19 (CT) and intracranial hemorrhage (CT) - the RadImageNet models also illustrated improvements of AUROC ($p<0.001$) by 1.9 percent, 6.1 percent, 1.7 percent, and 0.9 percent, respectively. In addition, lesion localizations of the RadImageNet models were improved by 64.6 percent and 16.4 percent on thyroid and breast ultrasound datasets.

Conclusions: The results indicate that RadImageNet pre-trained models could be a better starting point for transfer learning in radiologic imaging AI applications with better interpretability, especially for smaller radiologic datasets.

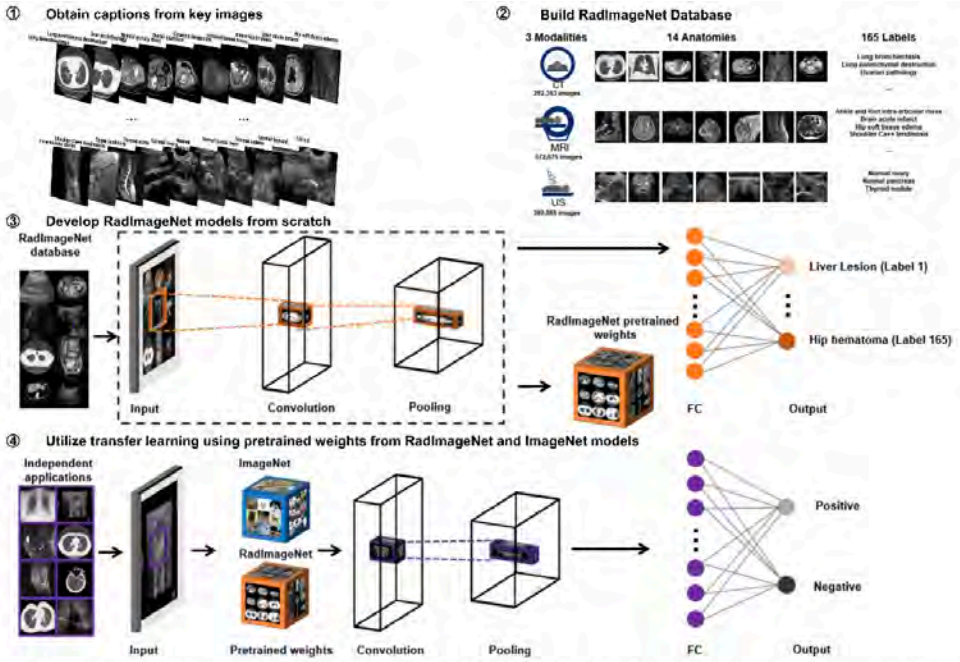

Curation of a medical imaging database RadImageNet, development of pre-trained convolutional neural networks over RadImageNet, and comparison of RadImageNet pre-trained models and ImageNet pre-trained models on multiple medical imaging applications. This study was designed in four phases. First, key images and associated diagnoses were annotated by radiologists. Second, the images and diagnoses were further grouped by modalities, anatomies, and labels according to their imaging patterns to construct the medical imaging only database RadImageNet. Third, four neural networks as pre-trained models were trained from scratch on the basis of RadImageNet. Finally, the pre-trained models from RadImageNet and ImageNet were utilized and compared on eight medical imaging applications in AUROCs and dice scores if ground truth segmentation masks are available.

A Novel Phantom Model for Chronic Subdural Hematoma Evacuation

Isabella Morgan[1,2], John Durbin[1,2], Joseph Borrello[1,2], Tyree Williams[1,2], Benjamin Rodriguez[1,2], Joshua Bederson[1,2], Benjamin Rapoport[1,2], Turner S. Baker[1,2]

[1] Sinai Biodesign, Department of Neurosurgery, Mount Sinai Hospital, New York, USA
[2] Department of Neurosurgery, Mount Sinai Hospital, New York, USA

Introduction: Training neurosurgeons is a challenging task due to the complex, time-consuming, and case-specific procedures that they must master. Cadaver models often lack the physiological characteristics necessary to replicate a procedure and animal models are not always accurate, nor available. The development of case-specific phantom models is necessary to increase the number of procedures each trainee is exposed to and, as a result, improve the quality of education. These models are especially relevant in minimally invasive procedures, such as burr-hole chronic subdural hematoma (CSDH) evacuation, which doesn't have a suitable cadaver or animal model.

Materials and Methods: A novel phantom model was created, incorporating powder-based 3D printing technology with hydrogel tissue modeling to accurately recreate a 60mL chronic subdural hematoma case. The skull model was constructed utilizing 3D-powder-based printing and a 3D silicone brain mold was built with a 10% polyvinyl alcohol mixture. Similarly, dura measuring 1mm(H) x 10 cm(W) x 8 cm(L) was cast with the same polyvinyl alcohol formulation. The hematoma was created by encasing, in a thin plastic sack, a 4:2 water and gelatin mixture totaling 60mL. Simulated CSDH evacuation surgery consisted of visualizing the hematoma with an endoscope and removing it with an active evacuator. Following the evacuation, participating biomedical engineers were asked to rate the model's accuracy on a five-point scale, from "highly accurate" to "poorly accurate," while focusing on four major elements: (1) Skull composition, (2) Dura composition, (3) Hematoma composition, and (4) Overall Model.

Results: The model was able to recreate a CSDH, enabling the successful evacuation of subdural hemorrhage with neuroendoscopy. The evacuation from initiation of aspiration to completion was conducted in 228 seconds, resulting in the evacuation of 84.58% of the hematoma. Skull composition performed best, with all raters rating it as 'highly accurate.' Hematoma composition received the worst score, with the major complaint being the lack of coagulation simulated.

Conclusions: The phantom model was shown to successfully reproduce a CSDH. Hematoma consistency is currently poor; however, incorporation of an improved coagulant simulant is currently underway. An additional study collecting feedback from residents and practicing neurosurgeons is being designed and will be initiated within 2022. Phantom models are a useful tool for the training of new surgeons and both, refinement, and development of novel techniques. The model shown here demonstrated a subdural hematoma model that is highly customizable, inexpensive and requires no special disposal, unlike animal and cadaver models

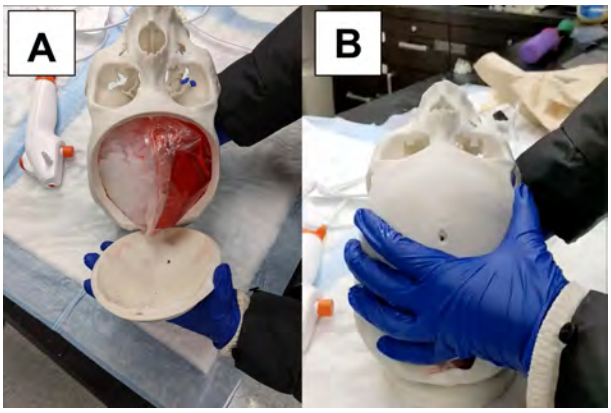

Figure 0.1: Phantom Model for Chronic Subdural Hematoma. (A) Open Cranium; (B) Closed Cranium.

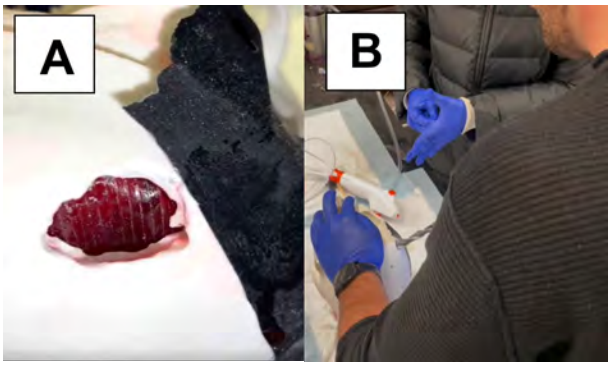

Figure 0.2: Phantom Cranial Access. (A) Burr Hole with Subdural Hematoma in Sight; (B) Drilling of Phantom Cranium.

Figure 0.3: Endoscopic Evacuation of Phantom Subdural Hematoma. (A) Endoscopic View of Subdural Hematoma Sack, With Evacuator in Sight; (B) External View of Engineer Performing the Endoscopic Evacuation

Selected for poster presentations

BioMEMS Sensors to Monitor Orthopaedic Strain and Predict Bone Fracture Healing

Akbar Alipour[1], Jakob G. Wolynski[2], Conor J. Sutherland[2], Emre Unal[3], Christian M. Puttlitz[2], Kirk C. McGilvray[2], Hilmi V. Demir[3]

[1] BioMedical Engineering and Imaging Institute, Icahn School of Medicine at Mount Sinai, New York
[2] Department of Mechanical Engineering and School of Biomedical Engineering, Orthopaedic Bioengineering Research Laboratory, Colorado State University, Fort Collins, Colorado
[3] Departments of Electrical and Electronics Engineering and Physics, Institute of Materials Science and Nanotechnology (UNAM), Bilkent University, Ankara, Turkey

Introduction: Current diagnostic modalities, such as radiographs or computed tomography, exhibit limited ability to predict the outcome of bone fracture healing. Failed fracture healing after orthopaedic surgical treatments are typically treated by secondary surgery; however, the negative correlation of time between primary and secondary surgeries with resultant health outcome and medical cost accumulation drives the need for improved diagnostic tools [1]. This study describes the simultaneous use of multiple (n = 5) implantable flexible substrate wireless microelectromechanical (fsBioMEMS) sensors adhered to an intramedullary nail (IMN) to quantify the biomechanical environment along the length of fracture fixation hardware during simulated healing in ex vivo ovine tibiae.

Materials and Methods: The system is composed of a multi-sensor fsBioMEMS sensor-implant construct and an external excitation/receiving apparatus consisting of a multi-antenna array and a network analyzer (Fig. 1). The multi-antenna array is designed with five evenly spaced antennae, allowing for simultaneous excitation/receiving of resonance response frequency (RRF) signals from five independent fsBioMEMS sensors [2]. We performed a series of experimental and analytical investigations of increasing complexity upon MEMS-based telemetric measurements [3] of local fracture mechanics by observing shifts in the sensor's RRF using computational models, prototype fabrication, ex-vivo simulations, and in-vivo animal models (Fig. 2).

Results: Signal attenuation experiments demonstrated that RRF signal changes could be measured through as much as 90 of muscle, 50 of fat, or 30 of skin. Measurements of signal through an unobstructed air gap established a loss of measurable RRF signal change after 10 . The ex-vivo data (Fig. 3) indicated significant differences associated with sensor location on the IMN ($p < 0.01$) and fracture state ($p < 0.01$). These data indicate that the fsBioMEMS sensor can serve as a tool to diagnose the current state of fracture healing, and further supports the use of the fsBioMEMS as a means to predict fracture healing due to the known existence of latency between changes in fracture site material properties and radiographic changes.

Conclusions: The use of fsBioMEMS sensors present clinical potential due to a number of advantageous features, including: their small and flexible nature which allows for efficacious placement on orthopaedic hardware, inductive power allowing for long-term use without the need for power source implantation, and wireless transmission allowing for non-invasive measurements.

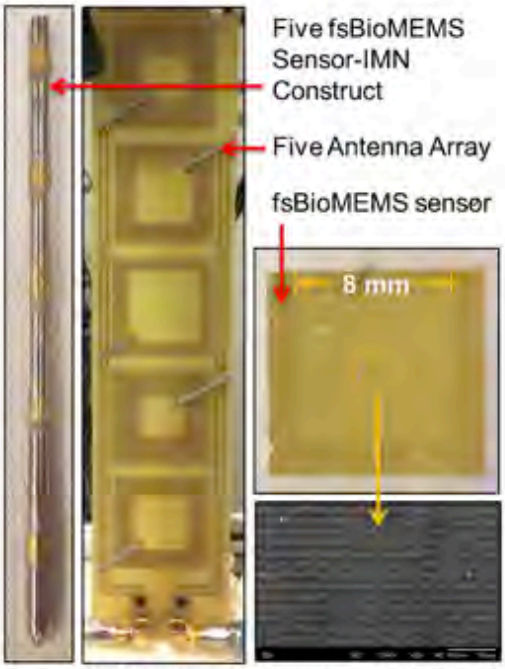

Figure 1: Macro and scanning electron microscopy digital images of a single fsBioMEMS sensor, digital image of the sensor-intramedullary nail (IMN) construct containing five evenly space fsBioMEMS sensors, and a digital image of the five-antenna array used for measuring resonant radio frequency (RRF) of the fsBioMEMS sensors.

Figure 2: A) Dissected ovine tibia, fixed via fsBioMEMS sensor construct. B) Radiographs demonstrating the five fsBioMEMS sensor locations and osteotomy states used to simulate the temporally increasing bone stiffness of a healing fracture.

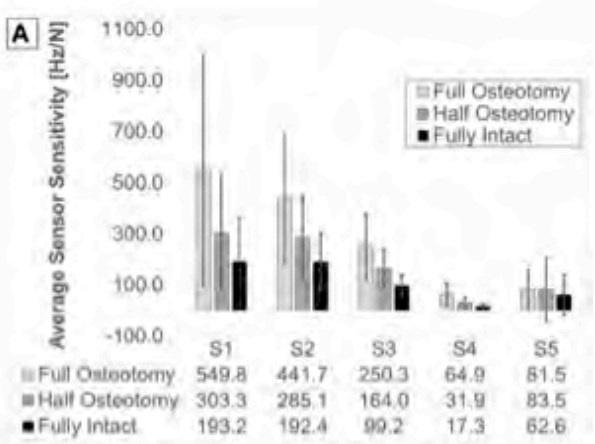

Figure 3: Average compiled (n = 9) sensor sensitivities for a five fsBioMEMS sensor construct during ex-vivo simulated bone healing of ovine tibia.

MRI-based radiomics quantification for characterization of small renal masses: Data quality control and preliminary results

Haitham Al-mubarak[1], Octavia Bane[1], Nicolas Gillingham[2], Christopher Kyriakakos[3], Ghadi Abboud1, Jordan Cuevas[1], Janette Rodgriguez[1], Kirolos Meilika[4], Amir Horowitz[5], Jorge Daza [4,5], Ketan Badani[5], Bachir Taouli [1,3], Sara Lewis[1,3]

[1] 1 BioMedical Engineering and Imaging Institute, Icahn School of Medicine at Mount Sinai, New York, NY, USA
[2] Department of Diagnostic, Molecular and Interventional Radiology, Icahn School of Medicine at Mount Sinai, Mount Sinai West, New York, NY 10019, USA
[3] Department of Diagnostic, Molecular and Interventional Radiology, Icahn School of Medicine at Mount Sinai, Mount Sinai Hospital, New York, NY, USA
[4] Department of Urology, Icahn School of Medicine at Mount Sinai, New York, NY
[5] Precision Immunology Institute / Tisch Cancer Institute, Icahn School of Medicine at Mount Sinai, New York, NY

Introduction: Renal cell carcinoma (RCC) is the third most common genitourinary cancer in the US (1). Increased use of magnetic resonance imaging (MRI) has allowed for earlier tumor detection and improved characterization. Radiomics is motivated by the hypothesis that medical imaging informs tissue biology by quantifying tumor heterogeneity mathematically by analyzing the spatial distribution and relationships of gray levels. The introduction of radiomics into clinical practice is hindered by challenges in reproducibly extracting radiomic features, addressing sources of variability and model validation. The purpose of our study is to employ machine learning (ML) statistical models to differentiate RCC from benign renal masses and to evaluate radiomic features' stability using inter-observer and inter-package measurement analysis based on clinical MRI sequences.

Materials and Methods: In this IRB approved prospective study, we included 26 patients (19M,7F; age 60$\pm$10.3 y) with small renal masses undergoing partial nephrectomy (PN). All patients were scanned on a 1.5T MRI system, using a protocol comprised of T2-WI,DWI/ADC and T1-WI pre- and contrast enhanced sequences obtained at 1 and 3 minutes post-injection of gadolinium (Gadavist). Tumor volume of interest delineated by Observers 1 and 2 using two software packages with extraction of radiomics features [Olea Medical (108 features); 3D-Slicer (540 features)]. Histopathology of the resected renal masses identified tumor diagnosis, TNM stage, and WHO grade. ML model (RUSBoosted) was used to discriminate benign from malignant renal masses (see Fig.1, cluster analysis). Inter-observer and inter-package comparison of radiomics measurements was performed using intra-class correlation coefficient (ICC).

Results: After exclusion of redundant features by principal component analysis, RUSBoosted model differentiated RCC from benign lesions, using a combination of qualitative and quantitative radiomics features, with an AUC=0.71 and accuracy=73 percent on the training set (70 percent), and AUC=0.67 and accuracy=85.7 percent on the validation set (30 percent). Inter-observer comparison of radiomics measurements found that T1-W pre-contrast, T1-W post-contrast, and T2-W yielded the greatest proportion of features with good/moderate ICC, while ADC measurements yielded low/moderate ICCs. Inter-package comparisons demonstrated that most features had moderate/poor ICC, with greatest stability found for measurements extracted from T1-W post-contrast (Table 1).

Conclusions: MRI-based radiomics features demonstrate a good accuracy in distinguishing RCC from benign renal tumors with a greater stability across observers and software packages. Knowledge of radiomic feature stability and model selection will aid in the validation of the combined radiomics-qualitative models in clinical practice. Further work is required in a larger number of patients.

Inter-Observer (3D Slicer)

	ADC	T2W	T1W pre	T1 post 1 min	T1 post 3 min
Good	12(12%)	83(80%)	30(28.8%)	79 (76%)	72 (76%)
Moderate	34(32%)	21(20.1%)	64 (61.5%)	27 (25.9%)	28 (27%)
Poor	61(58.6%)	3(2.9%)	13(12.5%)	1(0.96%)	7(6.7%)

Inter-Observer (Olea)

	ADC	T2W	T1W pre	T1 post 1 min	T1 post 3 min
Good	4(3.8%)	73(70%)	38(36.5%)	75(72%)	78 (76%)
Moderate	25(24%)	21(20.2%)	52(50%)	27(26%)	23 (22%)
Poor	78(75%)	10(10%)	17(%16.3%)	5(4.8%)	5(5%)

Inter-package (Observer 1)

	ADC	T2W	T1W pre	T1 post 1 min	T1 post 3 min
Good	8 (7.7%)	24 (23%)	26 (24.9%)	36(34.56%)	43(41.32%)
Moderate	19 (18.3%)	13 (12.5%)	22 (21.1%)	25(24%)	16(15.4%)
Poor	77 (74%)	67 (64.4%)	56(53.8%)	43(41.3%)	45(43.2%)

Inter-package (Observer 2)

	ADC	T2W	T1W pre	T1 post 1 min	T1 post 3 min
Good	0 (0%)	23 (22.1%)	15 (14.4%)	34(32.7%)	38(36.5%)
Moderate	3 (2.9%)	19 (18.3%)	24 (23%)	23(22.1%)	16(15.4%)
Poor	101 (97%)	62 (60%)	65(62.5%)	47(45.2%)	50(48%)

*(good: ICC>0.8; moderate: ICC=0.5-0.8; poor: ICC<0.5).

Table 1. Inter-observer and inter-package assessment of radiomic measurement stability in small renal masses using interclass correlation coefficient.

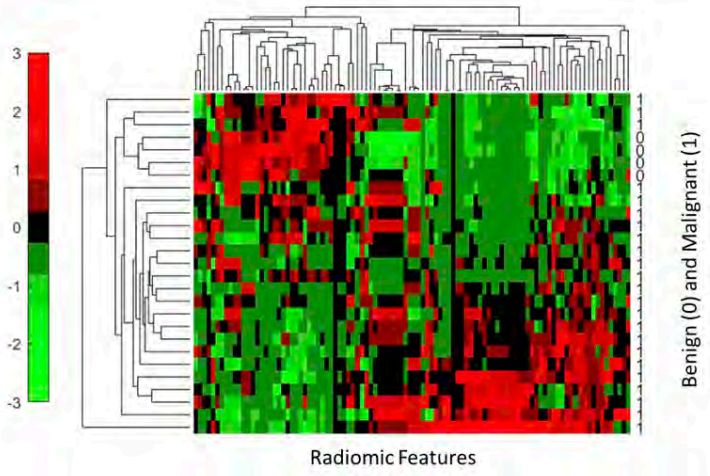

Figure-1- Cluster analysis of radiomics features and tumor type.

Application of high-resolution 7-Tesla MRI to investigate sex-dependent differences in limbic structures in trigeminal neuralgia

Judy Alper M.S.[1,2], Alan C Seifert PhD[1], Gaurav Verma PhD[1], Yael Jacob PhD[1], Ameen Al Qadi B.S.[1], Joshua Bederson M.D.[3], Raj K Shrivastava M.D.[3], Bradley N Delman M.D., M.S.[4], Priti Balchandani PhD[1]

[1] BioMedical Engineering and Imaging Institute, Icahn School of Medicine at Mount Sinai, New York, NY, United States
[2] Biomedical Engineering, City College of New York, New York, NY, United States
[3] Neurosurgery and Otolaryngology, Mount Sinai Medical Center, New York, NY, United States
[4] Diagnostic, Molecular, and Interventional Radiology, Mount Sinai Medical Center, New York, NY, United States

Introduction: Trigeminal Neuralgia (TN) is a chronic neurological condition which is twice as common in women as in men (NINDS). While there are studies which have investigated the pathophysiology of TN, its etiology is still poorly understood, and it has become important to investigate the entire pain network for regions that may be involved in TN pain, beyond the trigeminal nerve itself. There is strong evidence for the existence of sex differences in the prevalence and neurobiology of chronic pain as well, making it important to consider sex in studies investigating pain pathophysiology, including studies of TN. The objective of this pilot study was to leverage ultra-high field MRI to examine quantitative differences in limbic structures involved in the pain network, including the hippocampus, amygdala, thalamus, and their subnuclei, in male and female TN patient cohorts as compared to age and gender matched healthy controls.

Materials and Methods: Thirteen TN patients (mean age 42.9 years, standard deviation 12.2 years, 5 males and 8 females) and thirteen matched controls (mean age 42.5 years, standard deviation 10.2 years) were scanned at 7-Tesla MRI with high resolution, T1-weighted imaging. An automated algorithm, Freesurfer image analysis suite version 6.0, was used to segment the limbic structures and their subnuclei. The subnuclei volumes were normalized to total brain volume, which was also provided by Freesurfer 6.0. Two-tailed, independent Student's t-tests were used to compare subnuclei volumes between TN patients and controls for males and females separately, with the symptomatic side in patients compared to the same side in matched healthy controls.

Results: Segmentation results in a single TN subject, which provide the basis of the volumetric analysis, are shown in Figure 1. In female TN patients, the paralaminar subnucleus volume (0.04 mm3) of the amygdala was reduced on the symptomatic side compared with controls (0.05 mm^3, p = 0.03, d = -1.2). No significant differences were found in male TN patients compared to controls and no significant differences were found in the other regions in the male and female subsets.

Conclusions: This early finding, generated through a highly sensitive 7T MRI protocol, may suggest a potential difference between volumetric changes in male and female TN patients in chronic pain. We observed reduced paralaminar nucleus volume in female TN patients. Given the small sample size in this pilot study, a larger study is warranted to further explore these differences.

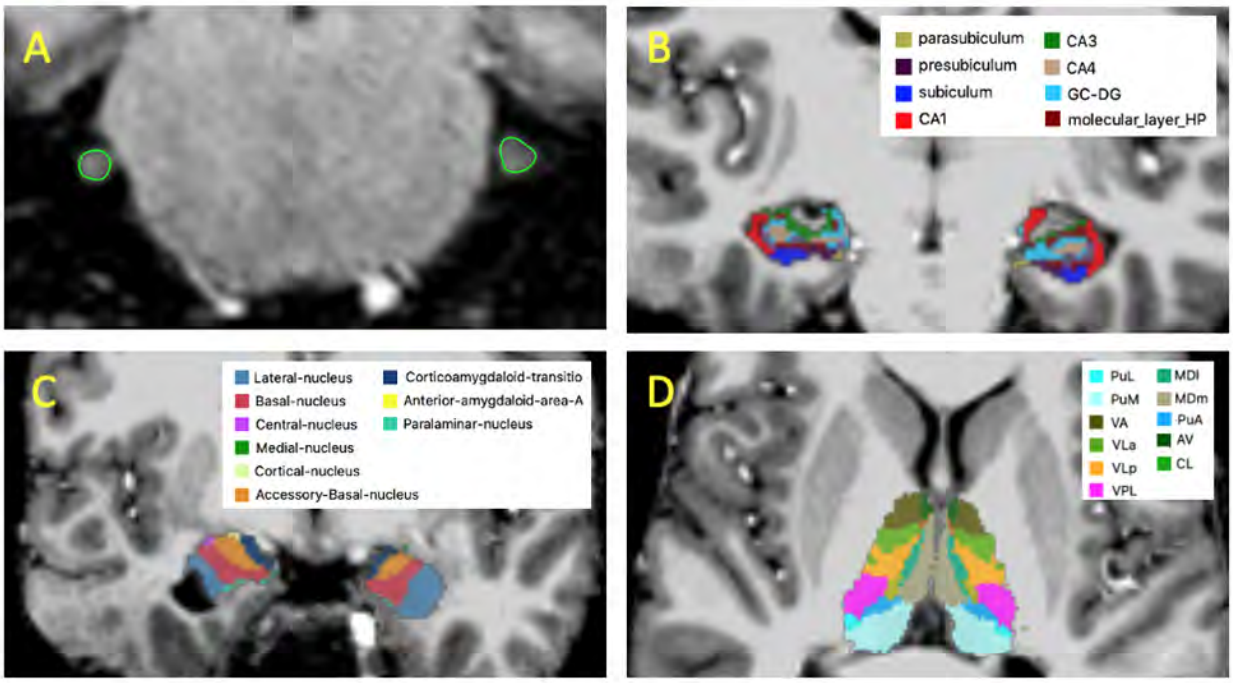

Figure 0.1: Segmentation of trigeminal nerve and limbic structures on a coronal slice in a TN subject.

Diffusion and perfusion MRI for prediction of HCC response to neoadjuvant immunotherapy

Enamul Bhuiyan[1,2] , Paul Kennedy[1,2], Octavia Bane[1,2], Elizabeth Miller[3], Stefanie Hectors[3], Hung Kam Cheung [3], Muhammed Shareef[3], M. Isabel Fiel[4], Stephen Ward[4], Myron Schwartz[5], Miriam Merad[6], Thomas Marron[7], Bachir Taouli[1,2]

[1] BioMedical Engineering and Imaging Institute (BMEII), Icahn School of Medicine at Mount Sinai, New York, NY USA
[2] Department of Diagnostic, Molecular and Interventional Radiology, Icahn School of Medicine at Mount Sinai, New York, NY USA
[3] Regeneron Pharmaceuticals Inc. Tarrytown, NY, United States
[4] Department of Pathology, Molecular and Cell Based Medicine, Icahn School of Medicine at Mount Sinai, New York, NY USA
[5] Recanati/Miller Transplantation Institute, Icahn School of Medicine at Mount Sinai, New York, NY USA
[6] Precision Immunology Institute, Icahn School of Medicine at Mount Sinai, New York, NY USA
[7] The Tisch Cancer Institute, Icahn School of Medicine at Mount Sinai, New York, NY USA

Introduction: Neoadjuvant immunotherapy has the potential to decrease the risk of hepatocellular carcinoma (HCC) recurrence post resection. The objectives of this study were to assess the value of pre-treatment MRI parameters for prediction of HCC immunophenotype and response in a cohort of patients undergoing neoadjuvant immunotherapy prior to liver resection. We hypothesize that diffusion and perfusion MRI measured at baseline can predict HCC response to neoadjuvant immunotherapy. We observed that ADC was lower in tumors with high tumor infiltraeting lymophocytes, and uptake rate measured with DCE-MRI was higher in responding tumors.

Materials and Methods: In this prospective study, 17 patients (10M/7F, mean age 64$\pm$12y) underwent MRI at baseline and following completion of neoadjuvant immunotherapy (cemiplimab: anti-PD1) prior to liver resection (post treatment MRI to resection interval:4$\pm$2 days). Multi b-value DWI was performed using SSEPI and 11 b-values (range:50-800s/mm^2). DCE-MRI was performed using gadoxetate contrast. Freehand ROIs were drawn on the DCE-MRI images in the tumor, liver, aorta and portal vein (Figure), in tumor on the IVIM-DWI images. A dual-input dual-compartment model was used to quantify DCE-MRI parameters (Fa,Fp,Ft,MTT,Ve,fi,ki,ART) in tumors. Model-free parameters (TTP,Upslope) were also calculated. A Bayesian fitting algorithm was used to perform pixelwise mapping of diffusion parameters (ADC,D,Ds) and perfusion fraction (PF) in the ROIs. ADC values were extracted from a separate monoexponential fit through the signal data (b$>$100s/mm2). Resected samples were assessed by a pathologist who measured degree of necrosis and the grade of tumor infiltrating lymphocytes (TILs), presence of tertiary lymphoid structure (TLS). Tumor response was assessed using RECIST 1.1 and degree of tumor necrosis at histopathology (significant tumors necrosis: STN $\geq$70 percent).

Results: Only baseline MRI findings are discussed. 17 tumors were assessed (mean size 7.0$\pm$4.5cm). 3/17(17.6 percent) patients had STN, and 3/17(17.6 percent) had partial response based on RECIST. TILs were present in 12/14 tumors at histopathology. The significant results from DWI and DCE-MRI are summarized in Table. Tumor ki was significantly increased in patients with STN compared to nonresponders (4.15$\pm$2.70 vs 1.68$\pm$1.14, AUC=0.90, p=0.032). Uptake fraction fi was significantly higher with patients with partial response based on RECIST (PR/NR:5.79$\pm$3.31/2.05$\pm$1.59, AUC=0.92, p=0.23) (Table). ADC was significantly lower in the patients with abundant TILS (grade 3):(1.28$\pm$0.24 vs 1.52$\pm$0.27, AUC=0.79, p=0.046). Diffusion coefficient D(TILs grade 3/TILs grade 0-2:1.10$\pm$0.17/1.33$\pm$0.29, AUC=0.80, p=0.007) were significantly lowe in patients with abundant of TILs.

Conclusions: Our initial results demonstrate the potential utility of diffusion and perfusion parameters for prediction of HCC immunophenotype and for predicting response to neoadjuvant immunotherapy.

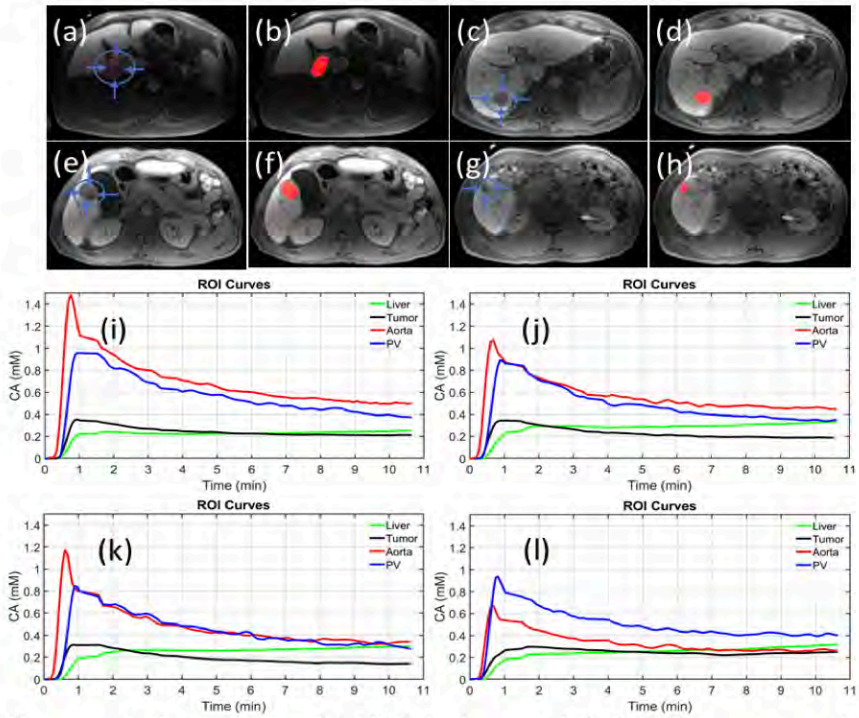

Figure: Representative images of 4 HCC lesions and their ROIs curves and the corresponding ROIs in 4 different patients. Lesion and ROI of a 54-year-old male (a, b, i), 57-year-old male (c, d, j), 52-year-old male (e, f, k) and a 72-year-old male (g, h, i). The lesions are indicated by the blue arrows and the ROIs are red regions. Data (i-l) represents signal intensity-time curves. Aorta is in red, PV in blue, HCC (tumor) in black, and liver in green.

Parameters	**TILs (grade 3, n=8)**	**No TILs (grade 0-2, n=9)**	**AUC**	**p-value**
ADC (10^{-3} mm^2/s)	1.28±0.24	1.52±0.27	0.79	0.046
D (10^{-3} mm^2/s)	1.10±0.17	1.33±0.29	0.80	0.007
Parameters	**STN (n=3)**	**Non-STN (n=14)**	**AUC**	**p-value**
ki (min^{-1})	4.15 (2.70)	1.68 (1.14)	0.90	0.032
Parameters	**PR (RECIST, n=3)**	**NR (RECIST, n=14)**	**AUC**	**p-value**
fi (%)	5.79±3.31	2.05±1.59	0.91	0.023

Table: Significant diffusion and perfusion parameters and corresponding AUCs for prediction of tumor immunphenoypes and tumor response. STN: significant tumor necrosis >70%.

Enabling Long-Duration FRESH 3D Printing

Joseph Borrello[1,2,3,4], Zirui Zheng[2,5], Kevin D. Costa[2]

[1] Graduate School of Biomedical Sciences, Icahn School of Medicine at Mount Sinai
[2] Cardiovascular Research Institute, Icahn School of Medicine at Mount Sinai
[3] Biomedical Engineering and Imaging Institute, Icahn School of Medicine at Mount Sinai
[4] Sinai BioDesign, Department of Neurosurgery, The Mount Sinai Hospital
[5] The Cooper Union for the Advancement of Science and Art

Introduction: Additive manufacturing (AM), or 3D printing, has transformed fields including tissue engineering, biofabrication, and surgical training. One of the most unique and versatile AM techniques for the biomedical sciences is Freeform Reversible Embedding of Suspended Hydrogels (FRESH), which involves extruding soft biological materials within a thermoreversable gelatin microparticle support bath that counteracts gravity to allow freeform printing of delicate structures that would otherwise collapse.[1,2] However, the semi-aqueous support bath loses water through evaporation over time.[3] As the support bath dehydrates, its unique rheological properties and functionality are compromised, limiting the size and complexity of models that can be printed. Therefore, we proposed using a thin layer of mineral oil to create a hydrophobic film on top of the support bath, blocking the gradual evaporation of water from the emulsion without impeding the print head or requiring operator intervention (Figure 1).

Materials and Methods: Gelatin support baths were produced from lyophilized gelatin powder (LifeSupport, FluidForm, Sudbury, MA) according to manufacturer instructions. Briefly, the gelatin powder was re-hydrated with calcium chloride solution, vortexed for 2 minutes, and centrifuged to create a gelatin slurry with the rheological properties of a Bingham plastic[2]. This slurry was then scooped into a dish and a thin layer ($\sim$2mm) of mineral oil was deposited on top. 3D printed models were made from sodium alginate solution (4% wt), crosslinked by calcium ions in the support bath. Several 3D models were printed to evaluate the stability of the oil layer and confirm it would not interfere with production of the 3D construct over the course of very long prints (16+ hour duration).

Results: The mineral oil layer effectively prevented evaporative water loss for up to 72 hours. Under several challenging motion patterns, including a large spiral pattern and a dense mechanical metamaterial lattice (Figure 2), it was found that the support bath maintained its rheological properties for the entire duration of the print, and the mineral oil layer did not bleed into the gelatin or otherwise impact the final results of the printed constructs (Figure 3).

Conclusions: The need to run large and/or complex multi-day prints has become increasingly common. We have demonstrated that with the simple yet effective addition of a protective, hydrophobic surface layer, 3D FRESH printing of models with increased complexity and size becomes much more feasible and requires minimal modification to the existing AM workflow.

References:

1. Hinton, T. J. *et al*. Three-dimensional printing of complex biological structures by freeform reversible embedding of suspended hydrogels. Sci. Adv. 1, e1500758 (2015)

2. Lee, A. *et al*. 3D bioprinting of collagen to rebuild components of the human heart. Science 365, 482–487 (2019).

3. Mirdamadi, E. *et al* FRESH 3D Bioprinting a Full-Size Model of the Human Heart. ACS Biomater. Sci. Eng. 6, 6453–6459 (2020).

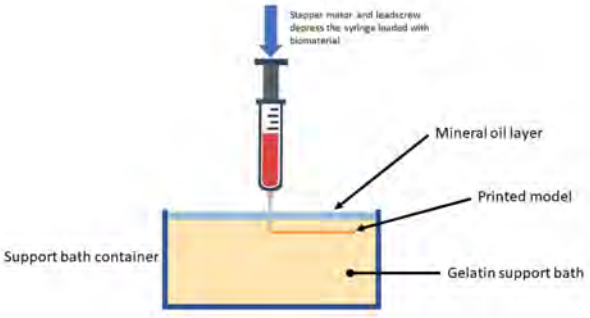

Figure 0.1: Schematic representation of mineral oil-modified FRESH 3D printing.

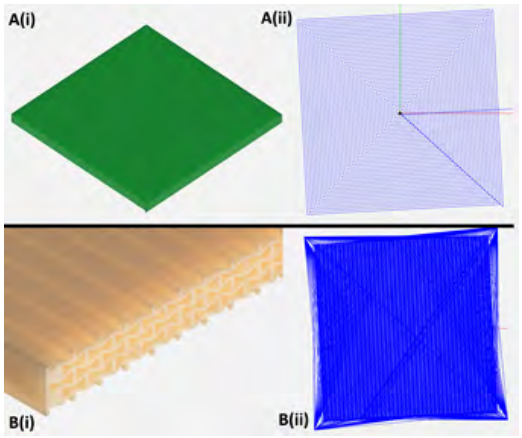

(a) Figure 2: Renders and corresponding Gcode travel paths for test models. **(A)** A large, rectilinear spiral (i) intended to approximate a regular "mixing" motion (ii). **(B)** A mechanical metamaterial lattice (i), which involves numerous rapid movements within the support bath, approximating a more random agitation pattern (ii).

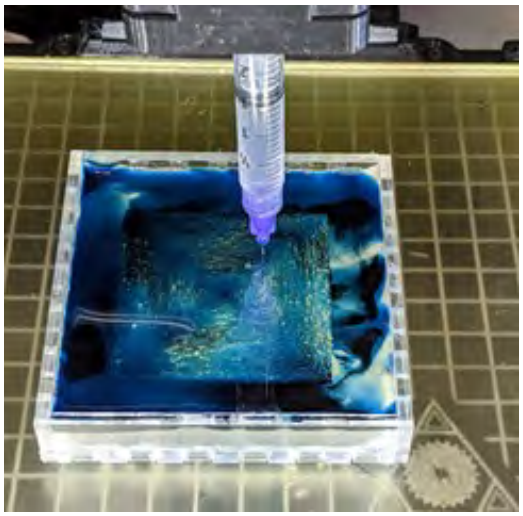

(b) Figure 3: Final result of a 40x40x2-mm rectilinear spiral model after 72 hours of mineral oil-modified FRESH 3D printing.

In silico evaluation of head immobilization pins

Joseph Borrello[1,2,3,4], Khristian Lang[4,5], Turner Baker[4,6], Joshua Bederson[4], Benjamin Rapoport[4],

[1] Graduate School of Biomedical Sciences, Icahn School of Medicine at Mount Sinai
[2] Cardiovascular Research Institute, Icahn School of Medicine at Mount Sinai
[3] Biomedical Engineering and Imaging Institute, Icahn School of Medicine at Mount Sinai
[4] Mount Sinai BioDesign, Department of Neurosurgery, The Mount Sinai Hospital
[5] Masters in Translational Medicine Program, The City College of New York
[6] Department of Population Health Science and Policy, Icahn School of Medicine at Mount Sinai

Introduction: Head immobilization is frequently employed during neurosurgical procedures to ensure consistent cranial positioning and minimize motion during surgery. Despite employment in over 50% of all neurosurgery cases[1], however, there is incomplete consensus around the detailed practices for head fixation, which leads to surgical complications[2,3]. These complications generally fall into two categories: slippage and traction loss (too little pressure), or fractures and tissue damage (too much pressure), reflecting the difficulties associated with optimal pressure application. While previous research has focused on the optimal positioning of head clamp pins[4], very little work has examined the design of the pins themselves. In this study we aimed to determine if existing pins are optimized to maximize traction while minimizing excessive clamping pressures. **Materials and Methods:** Pin models were generated using Fusion 360 computer-aided design (CAD) software (Autodesk, San Rafael, CA). Pins from a Mayfield head clamp were provided for measurement and reverse-engineering to produce a 3D CAD model, in addition to a three-pronged design variant of our own creation (referred to as the "tripod" model, Figure 1). Both models were subsequently meshed for finite element modeling to simulate the pressures and forces experienced during standard intraoperative head immobilization.

Results: The initial batch of simulations aimed to determine if the tripod design would reduce localized pressure on the skull. For many design variants, the model succeeded in significantly reducing the forces experienced at each of the three contact points. Furthermore, these designs also reduced overall stress values on the skull, effectively distributing the clamping forces over a wider area (Figure 2). While these results were generally encouraging, we failed to observe any consistent trends around the design variants (Figure 3). A second batch of simulations were also performed to determine the traction force of each tip design, however, these results also failed to indicate a specific design variant that consistently outperformed the Mayfield pin.

Conclusions: Complications from head fixation remain persistent in many neurosurgical settings, with competing interests of maintaining traction and reducing injury. While our design concept of distributing the pin forces across three tips rather than just one did generally improve stresses on the skull, we were not able to consistently match improved force distribution with an improvement in traction. For now, while the current pin designs may not be perfect, we believe they represent the best design compromises, and encourage future investigations into both head clamping approaches and fixation pin designs.

1. Berry, C., Sandberg, D. I., Hoh, D. J., Krieger, M. D. & McComb, J. G. Use of cranial fixation pins in pediatric neurosurgery. Neurosurgery 62, 913–918; discussion 918-919 (2008).

2. Sakakura, K. et al. Estimation of Risk Factors for Head Slippage Using a Head Clamp System. A Retrospective Study. Ther. Clin. Risk Manag. 16, 189–194 (2020).

3. Cheng, G. et al. Potential risk analysis and experience summarization of unstable factors of cranial fixation devices in neurosurgical operations: three-case reports and systematic review. Chin. Neurosurg. J. 7, 25 (2021).

4. Thijs, D. & Menovsky, T. The Mayfield Skull Clamp: A Literature Review of Its Complications and Technical Nuances for Application. World Neurosurg. 151, 102–109 (2021).

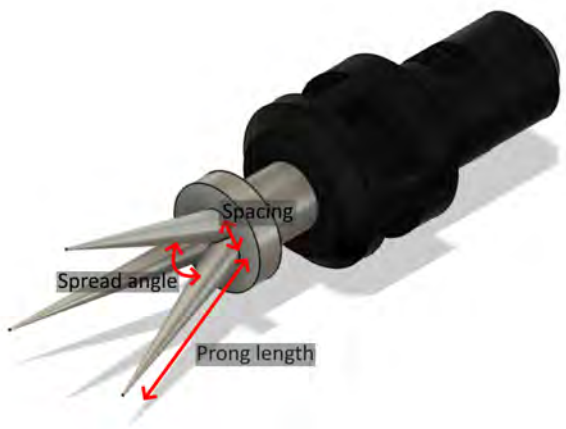

Figure 0.1: Model of our “tripod” pin design.

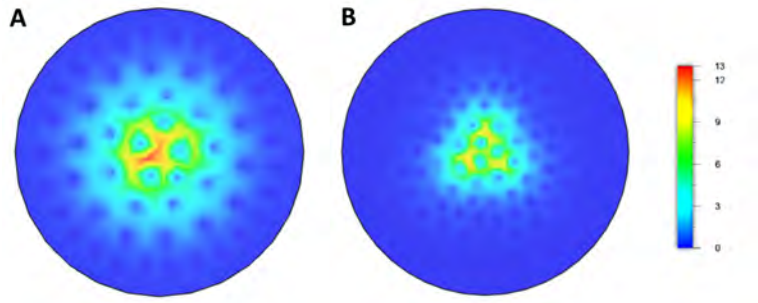

Figure 0.2: Heatmaps plotting clamping force distribution on a section of the skull for a conventional Mayfield head pin (A) and our “tripod” design (B).

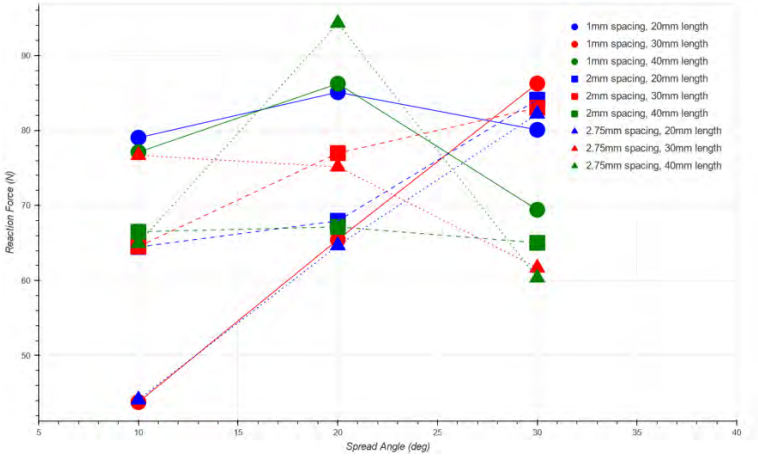

Figure 0.3: Plot of clamping reaction force on the skull versus spreading angle of the three “tripod” prongs, for a variety of design combinations for prong length and spacing.

Lung Inflammation before and after CPAP therapy in OSA patients: A PET/MRI Study

Bora Cengiz[1], Oren Cohen[2] , Adam Jacobi[1], Venkatesh Mani[1], Mayte Suarez-Farinas[3], Arif Sheikh[1], Neomi Shah[2]

[1] Department of Diagnostic, Molecular, and Interventional Radiology, Icahn School of Medicine at Mount Sinai, New York, NY
[2] Division of Pulmonary, Critical Care and Sleep Medicine, Icahn School of Medicine at Mount Sinai, New York NY
[3] Center for Biostatistics, Department of Population Health Sciences and Policy, Icahn School of Medicine at Mount Sinai, New York, NY

Introduction: The association of obstructive sleep apnea (OSA) and lung inflammation is unclear. We utilized positron-emission tomography/magnetic resonance imaging (PET/MRI) to investigate the patterns of 18F-fluorodeoxyglucose (FDG) uptake in patients with OSA before and after continuous positive airway pressure (CPAP) therapy.

Materials and Methods: Patients 21-80 years-old and newly diagnosed with OSA, using home sleep testing (Respiratory Disturbance Index $\geq$ 5, 3 percent desaturation), underwent consecutive FDG PET/MRIs of the chest and neck before and 3-4 months after CPAP. The FDG uptake was qualitatively and quantitatively analyzed via mean standardized uptake values (SUV). Each lung was non-anatomically segmented as upper (RUL, LUL), middle (RML, LML), and lower (RLL, LLL) zones respectively, and then was compared to its post-CPAP counterpart. Compliance to CPAP was defined as utilization of CPAP for more than 4 hours for at least 70 percent of treatment period.

Results: Our analytical sample consisted of 48 patients with 85 percent men. Mean age was 50 ±12 years and body mass index was 31.5$\pm$5 kg/m2. 40 percent of the patients were smokers; 46 percent had hypertension, 6 percent had diabetes and 42 percent had dyslipidemia. On qualitative analysis, upper lung zones were relatively spared with FDG uptake compared to mid and lower lung zones where FDG uptake was more prominent post-CPAP [RML (30 percent to 3 percent), RLL (60 percent to 62 percent) and LLL (30 percent to 40percent)] compared to pre- and post-CPAP, respectively (all p $>$0.05). 48 percent of the patients were compliant to CPAP. Compared to pre-CPAP, 42 percent of post-CPAP scans demonstrated an increase of FDG uptake with 25 percent increase in the left lung and 34 percent in the right lung. There was an 8 percent increase in the Mean Blood Pool and 4 percent increase in liver SUV mean. The SUV mean of each lung segment was not statistically different before and after CPAP (Table 1) and SUV means of right and left lungs were also not statistically different.

Conclusions: While there was no statistically significant difference in FDG uptake pre- and post-CPAP on lung PET/MRI, on qualitative analysis, FDG uptake was more prominent in the lower lung segments post-CPAP. Future larger studies are needed to investigate whether CPAP is associated with lung inflammation and whether it influences severity and distribution of lung inflammation.

Table 1. Quantitative analysis of lung uptake				
Lung Zone SUV mean (SD)	**Pre-CPAP**	**Post-CPAP**	**Change**	**P value**
Right upper zone	0.62 (0.15)	0.66 (0.19)	0.04 (0.18)	0.13
Right middle zone	0.67 (0.21)	0.72 (0.23)	0.05 (0.20)	0.06
Right lower zone	0.86 (0.28)	0.89 (0.26)	0.03 (0.22)	0.29
Right Lung	0.73 (0.21)	0.77 (0.22)	0.04 (0.18)	0.09
Left upper zone	0.63 (0.14)	0.64 (0.10)	0.01 (0.10)	0.67
Left middle zone	0.64 (0.22)	0.65 (0.16)	0.01 (0.20)	0.68
Left lower zone	0.64 (0.22)	0.62 (0.14)	-0.02 (0.20)	0.60
Left Lung	0.63 (0.17)	0.64 (0.13)	0.01 (0.15)	0.85
Liver	1.95 (0.37)	2.0 (0.37)	0.05 (0.25)	0.17
Mediastinal Blood Pool	1.50 (0.27)	1.52 (0.32)	0.02 (0.23)	0.56
SUV, Standardized uptake value; SD, standard deviation; CPAP, continuous positive airway pressure				

18F-FDG PET/CT evaluation in left ventricular assist device infections

Ana Devesa[1]; Eman Rashed[1], Philip Robson[1], Renata Pyzik[1], Munir Ghesani[2], Julie Roldan[1], Noah Moss[1], Kim Ashley[1], Ana Young[1], Zahi Fayad[1]; Maria Trivieri[1,3]

[1] BioMedical Engineering and Imaging Institute, Icahn School of Medicine at Mount Sinai, New York, NY, United States
[2] Division of Nuclear Medicine; Department of Radiology, Icahn School of Medicine at Mount Sinai, New York, NY, United States
[3] Cardiovascular Institute, Icahn School of Medicine at Mount Sinai, New York, NY, United States

Introduction: The clinical use of left ventricular assist devices (LVAD) is on the rise. Device-related infections are a common complication that associates worse clinical outcomes; however, clinical diagnosis of LVAD infections remains challenging. The aim of the study was to evaluate the role of ^{18}F-FDG PET/CT imaging on the diagnosis of this entity and on the clinical management.

Materials and Methods: 37 patients with clinical suspicion of LVAD infection underwent ^{18}F-FDG PET/CT. Clinical categories were (1) positive wound and blood culture, (2) positive wound and negative blood culture and (3) no positive cultures. Imaging categories were classified in driveline infection, pump pocket infection and device infection.

Results: Mean age was 55.7 ± 14.8 years and 35.5% were female. Infection (increased ^{18}F-FDG uptake) of the driveline and pump pocket was evidenced in 95% of the cases; a device infection was observed in 84% of patients (Figure 1). The highest SUVmax values were observed in the driveline (SUVmax 8.07) and the pump pocket (SUVmax 8.38), compared to lower values evidenced in the device (SUVmax 5.17), suggesting that the intensity of the infection decreases as it gets far from the origin. The most frequent clinical category was 2 (54%). ^{18}F-FDG uptake was the highest in those patients with clinical category 1 (SUVmax 10.7), suggesting a more severe infection, and decreases in categories 2 (SUVmax 10.2) and 3 (SUVmax 9.0). The most frequently detected microorganism was Pseudomonas, followed by methicillin-susceptible Staphylococcus aureus (MSSA), Serratia and methicillin-resistant Staphylococcus aureus. The highest SUVmax was evidenced in patients with MSSA infection (SUVmax 12) followed by those with Pseudomonas (SUVmax 10.4).

Conclusions: ^{18}F-FDG PET/CT allows to characterize the location and extent of LVAD infections, providing information on the affected components. In addition, it allows confirmation of the presence of device infection in patients with clinical suspicion and negative cultures. Characterization by PET/CT could have an impact on the clinical management of these patients.

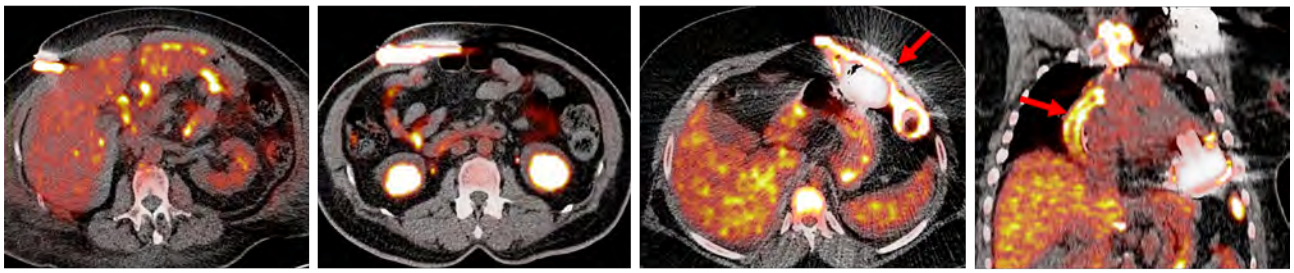

Driveline entry | Driveline subcutaneous pathway | Pump pocket | Outflow tract

Figure 0.4: Representative example of fused ^{18}F-FDG PET/CT showing the different sites of infection as evidenced by increased ^{18}F-FDG uptake.

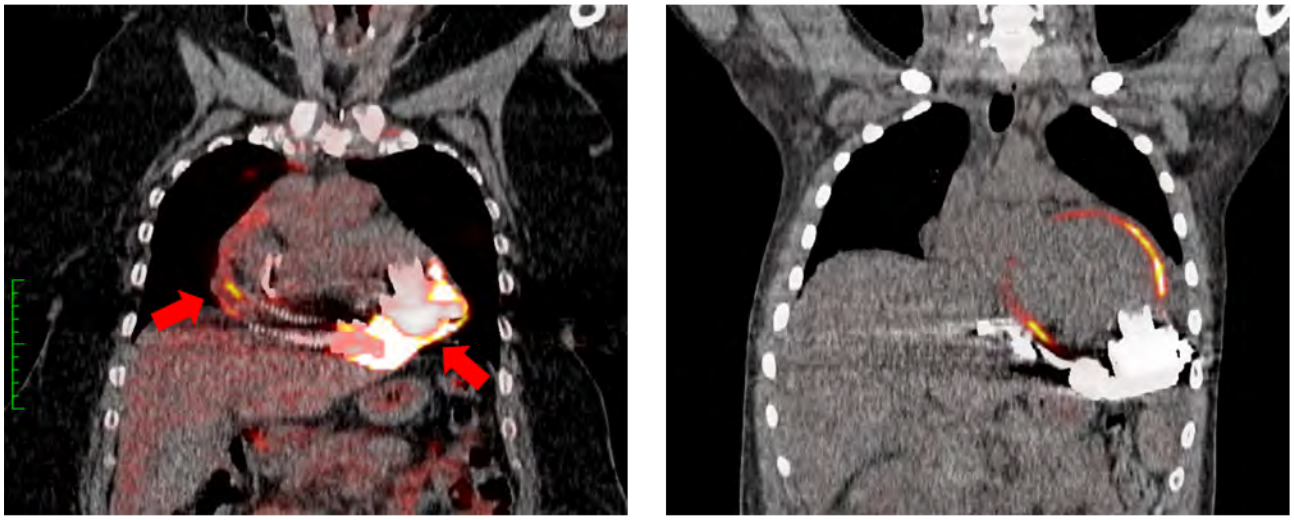

Figure 0.5: . Left panel shows fused ^{18}F-FDG PET/CT imaging with increased FDG uptake corresponding to the LVAD pump and cannula (red arrows). Right panel shows fused ^{18}F-FDG PET/CT imaging with no FDG uptake around the LVAD pump or cannula; diffuse (non-specific) myocardial uptake is observed.

PET/MRI characterization of Arrhythmic Mitral Valve Prolapse with Only Mild or Moderate Mitral Regurgitation

Ana Devesa[1,2]; Sonika Patel1; Marc A. Miller[1]; Steve Liao1; Philip Robson[1,2]; Renata Pyzik[1,2]; Adam Jacobi[1]; David H Adams[1]; Ahmed El- Eshmawi[1]; Percy Boateng[1]; Dimosthenis Pandis[1]; Daniel N. Pugliese[1]; Jonathan Gandhi[1]; Emmanuel Ekanem[1]; Daniel Ross Musikantow[1]; Jacob S. Koruth[1]; William Wang[1]; Mohit Turagam[1]; Srinivas R. Dukkipati[1]; Vivek Y. Reddy[1]; Zahi Fayad[1,2]; Maria Trivieri[1,2]

[1] Icahn School of Medicine at Mount Sinai, New York, NY
[2] BioMedical Engineering and Imaging Institute

Introduction: Mitral valve prolapse (MVP) has been associated with ventricular arrhythmias (VA) and sudden cardiac death (SCD). The association between the degree of mitral regurgitation (MR) and MVP-related SCD is controversial. Replacement fibrosis, which is known to occur in the absence of severe MR, may be preceded and accompanied by an inflammatory response.

Materials and Methods: 12 patients with degenerative MVP and mild or moderate MR by transthoracic echocardiography underwent ^{18}F-FDG PET/MRI ("Hybrid" PET/MRI). Focal ^{18}F-FDG uptake and LGE were evaluated as a surrogate of inflammation and fibrosis, respectively. Ambulatory extended ECG monitoring was performed to assess VA burden and severity.

Results: Mean age was 57 ± 10.7 years, 66.7 percent were female. Mean LVEF and indexed LV end-diastolic volume were 58.6 ± 5.8 percent and 85.2 ± 13.6 ml/m^2. Inflammation (^{18}F-FDG uptake) was present in 83.3 percent of patients (n=10). Focal ^{18}F-FDG uptake and LGE (PET+/MRI+) were present in 75.0 percent (n=9); there were matching areas of FDG and LGE in all cases. 1 patient had focal ^{18}F-FDG uptake and no LGE (PET+/MR-). 2 patients did not have inflammation; one did not present fibrosis (PET-MR-) and one did not undergo LGE (PET-). Abnormal T1 values (a surrogate of microscopic fibrosis) were present in 87.5 percent. Complex ventricular ectopy was detected in 83.3 percent (n=10).

Conclusions: In this cohort of patients with only mild or moderate MR, of which a majority had complex ventricular ectopy, 75 percent had evidence of myocardial inflammation and fibrosis. These findings might explain the reported prevalence of SCD in patients with MVP that have less than severe MR, as inflammation and fibrosis are both known to be pro-arrhythmic. Future studies are needed to determine whether the presence of myocardial inflammation impacts the natural history of degenerative MVP and confers a higher risk of adverse outcome.

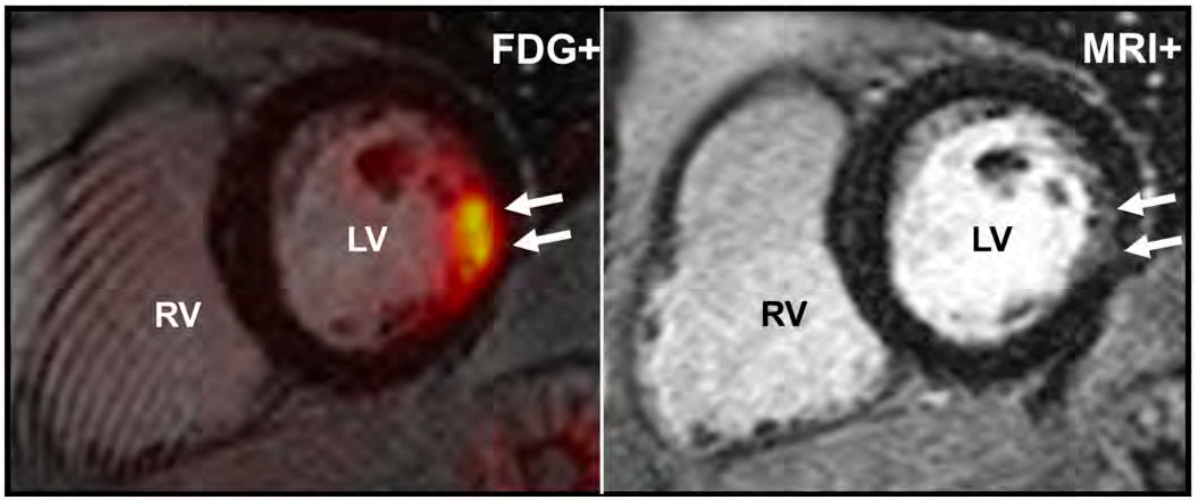

Table 1

Baseline characteristics	**n=12**
Age, y	57±10.72
Female	8 (66.7)
Transthoracic echocardiography	
LVEDD, mm	48.3±6.23
LVESD, mm	30.3±5.92
LVEF, %	61.8±5.59
Lateral TDI, cm/s	14.12±5.22
Mitral regurgitation severity	
• Mild	7 (58.3)
• Moderate	5 (41.7)
Bileaflet MV prolapse	6 (50.0)
Posterior leaflet prolapse	6 (50.0)
Mitral annular disjunction	9 (75.0)
Pickelhaube sign	4 (33.3)
Cardiac PET/MR	
• PET+/MR+	9 (75.0)
• PET+/MR-	1 (8.3)
• PET-/MR-	1 (8.3)
• PET-/noncontrast MR	1 (8.3)
FDG uptake (n=10)	
Mean SUVmax, SUV	4.75±3.12
Matching FDG and LGE	9 (90.0)
CMR characteristics	
T1, ms (n=8)	1109.70±45.97
Abnormal T1*	7 (87.5)
ECV, % (n=7)	28.21±5.70
Abnormal ECV*	2 (28.6)
T2, ms (n=8)	48.35±3.44
Abnormal T2*	3 (37.5)

*7 normal controls underwent CMR to define normal myocardial tissue values: 1045.1±63.6 ms (native T1); 25.0±7.8 % (ECV); 44.0 ± 10.6 ms (T2).

Influenza A Virus aggravates myocardial infarction through a type I interferon-dependent mechanism

Jeffrey Downey[1], Mandy M T van Leent[2], Jazz Munitz[2], Wolfram C. Poller[1], Zahi A. Fayad[2], Filip K. Swirski[1]

[1] Cardiovascular Research Institute and Department of Medicine, Icahn School of Medicine at Mount Sinai, New York, NY, USA
[2] BioMedical Engineering and Imaging Institute, Icahn School of Medicine at Mount Sinai, New York, NY, USA

Introduction: Respiratory infections caused by viruses like influenza A virus (IAV) are the source of substantial morbidity and mortality through direct pathogen virulence and/or subsequent pulmonary immunopathology. Additionally, there is growing appreciation that certain infections can cause multi-organ inflammation and damage, including in the heart. Indeed, IAV infection has been associated with heightened myocardial infarction (MI) risk. Type I interferons (IFN-I) are a pleotropic family of cytokines produced in the lung following IAV infection that are critical in antiviral immunity. However, their prolonged or systemic production is associated with poorer MI prognosis. We, therefore, investigated a potential role of IAV-induced IFN-I in the worsening of MI.

Materials and Methods: C57BL/6J (WT) and *Ifnar1*$^{-/-}$ (those lacking IFN-I signaling) mice were infected with a sublethal dose of IAV (35 PFU) or vehicle control. At 6 days post-infection, mice were subjected to a type II MI using isoproterenol (ISO; 160mg/kg i.p.), a non-selective β-adrenoreceptor agonist. The effects of the MI on cardiac function were assessed by cardiac magnetic resonance imaging, echocardiogram or electrocardiograph, while inflammation and cardiac damage were elucidated via flow cytometry and plasma troponin levels, respectively. **Results:** IAV-infected WT mice subjected to MI exhibited synergistically enhanced cardiac damage and dysfunction, as evidenced by increased plasma troponin levels (Figure 1), as well as a decline in left ventricular ejection fraction, fraction shortening and increased cardiac fibrosis. MI alone promoted myelopoiesis (Figure 2A-B) and accumulation of recruited inflammatory CCR2+ macrophages (Figure 3A) and neutrophils (Figure 3B) in the heart. On the other hand, in WT mice, MI following IAV infection caused hematopoietic collapse, as evidenced by a near complete loss of myeloid progenitors (Figure 4A), as well as a reduction in recruited cardiac macrophages (Figure 4B). In stark contrast, *Ifnar1*$^{-/-}$ mice were completely protected from the effects of MI during IAV infection, confirming a dependence of IFN-I in this susceptibility. Interestingly, MI and IAV infection led to an enrichment of IFN-I-producing CX3CR1^{+} Ly6C^{lo} monocytes within the heart of WT mice (Figure 5), suggesting this may be the responsible cell type.

Conclusions: Herein, we outline a novel axis of IAV-induced susceptibility to MI via IFN-I signaling. While IFN-I is essential in antiviral immunity, our results suggest a dichotomous role in cardiac inflammation, providing experimental evidence for why respiratory infections are known to accelerate cardiovascular disease, while proposing care must be taken in potential IFN-based viral therapies.

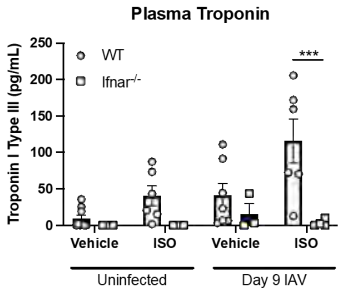

Figure 1: Plasma troponin levels following infection and/or infarction. WT and *Ifnar1*$^{-/-}$ mice were infected with IAV or not for 6 days and then injected with 160 mg/kg of ISO i.p to induce a type II MI for 3 days (9 days post-IAV). Plasma was collected and troponin quantified by ELISA.

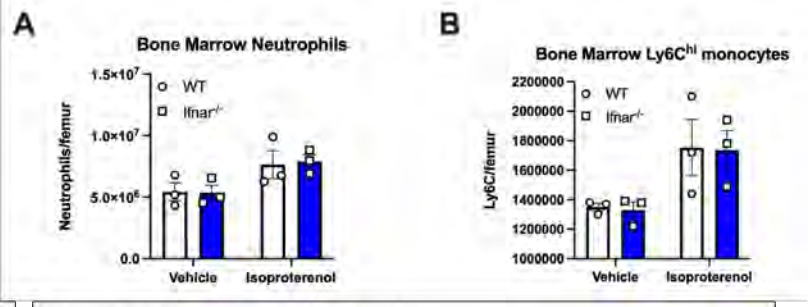

Figure 2: MI increases myeloid cell production.
WT and *Ifnar1*$^{-/-}$ mice were injected with ISO and 3 days later bone marrow was analyzed for the levels of neutrophils (A) and Ly6C^{hi} monocytes (B) by flow cytometry.

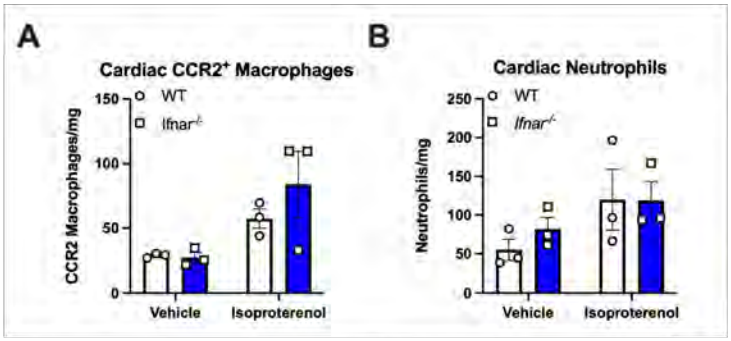

Figure 3: MI promotes myeloid cell infiltration into the heart.
WT and *Ifnar1*$^{-/-}$ mice were injected with ISO and 3 days later the heart was analyzed for levels of recruited cardiac CCR2^{+} macrophages (A) and neutrophils (B) by flow cytometry.

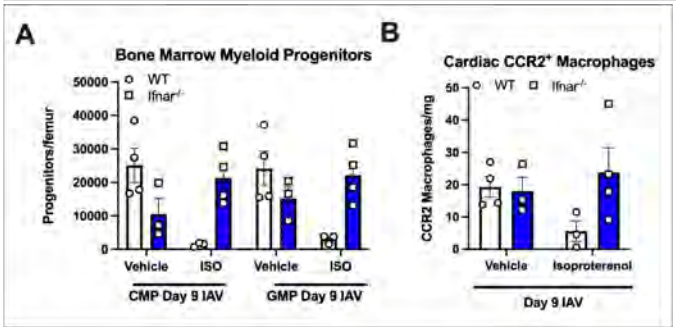

Figure 4: IAV and MI causes bone marrow exhaustion and loss of recruited cardiac macrophages in a IFN-I-dependent manner
WT and *Ifnar1*$^{-/-}$ mice were injected were infected with IAV for 6 days and then injected with ISO. 3 days later the BM was scrutinized via flow cytometry for levels of CMPs and GMPs (A) and the heart for recruited cardiac CCR2^{+} macrophages (B).

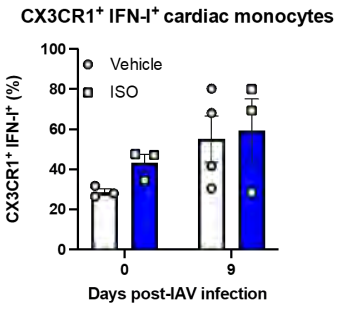

Figure 5: IAV and MI enriches a monocyte subset producing IFN-I
WT mice were infected with IAV or vehicle control for 6 days and then injected with ISO. 3 days later (9 days post-IAV) levels of CX3CR1^{+} Ly6C^{lo} monocytes producing IFN-I were assessed via flow cytometry.

Figure 0.1

Quantifying the efficacy of meningioma preoperative embolization through volumetric analysis: an observational study

Denzel E. Faulkner[1,2], Rui Feng[3], Alexis Bruhat[2,3] , Fred Kwon[2,3] , Turner S. Baker[2,3,4]
Christopher Kellner[3], J Mocco[3], Johanna Fifi[3], Tomoyoshi Shigematsu[3], Shahram Majidi[3],
Raj Shrivastava[3], Joshua Bederson[3], Benjamin I. Rapoport[2,3]

[1] Biomedical Engineering, Rensselaer Polytechnic Institute, 110 Eighth Street, Troy, NY, USA
[2] Mount Sinai BioDesign, Icahn School of Medicine at Mount Sinai, Mount Sinai Hospital, New York, USA
[3] Department of Neurosurgery, Icahn School of Medicine at Mount Sinai, Mount Sinai Hospital, New York, USA
[4] Department of Health Science & Policy, Icahn School of Medicine at Mount Sinai, Mount Sinai Hospital, New York, USA

Introduction: Endovascular embolization is an adjunct to surgical treatment of meningiomas.1–4 Serving to reduce blood loss during resection, embolization has been shown to induce tumor necrosis, tumor volume reduction, and improvement of postoperative symptoms.2,5,6 A recent meta-analysis indicated endovascular embolization does not significantly improve patient outcomes, suggesting that further investigation into methodologies and associated outcomes following tumor embolization is required.5 Here we present results from a unique set of 20 consecutive meningioma resection cases for which magnetic resonance imaging (MRI) data was collected both before ('pre-embolization') and after ('post-embolization') the tumor embolization preoperatively.

Materials and Methods: Twenty patients underwent an additional MRI after tumor embolization, prior to resection. MRI images were acquired on a 1.5T or a 3.0T scanner. Contrast-enhanced T1-weighted axial volumetric simulation images were used for analysis. Manual image segmentation was conducted with Slicer software (slicer.org). Embolization was quantified as the ratio of residual contrast-enhancing volume to post-procedure tumor volume. Percent embolization was computed as a voxel-based ratio obtained through digital volumetric analysis of the appropriate image sequences.

Results: Six patients showed low embolization efficacy ($<$ 25%), seven showed medium embolization efficacy (25% - 75%), and six patients showed high embolization efficacy ($>$ 75%). Average embolization efficacy was 45.28% (se 7.39). A paired student t-test failed to show statistically significant differences in tumor volumes before and after treatment. Average tumor reduction was 3.48 cm^3 (se 2.58) which resulted in an average relative reduction of 5.58% (se 2.88). A paired student t-test showed statistically significant differences between the pre-embolization tumor volumes and the residual contrast-enhanced volumes after treatment. Average initial tumor volume was 60.36 cm^3 (se 12.35), average residual contrast-enhanced volume was 29.22 cm^3 (se 7.00), and the total tumor volume after treatment was 56.88 cm^3 (se 11.07).

Conclusions: This study suggests a benefit of additional MRI imaging prior to the resection of embolized tumors, enabling precise quantification of embolization efficiency prior to tumor removal. Embolization efficacy may play a role in determining the surgical utility of preoperative embolization, and may have an impact on parameters such as embolization-induced tumor necrosis (and other factors related to resectability), as well as tumor-related intraoperative blood loss. Imaging and quantitative analysis may also lead to improved embolization techniques. Further studies are underway to both automate this process of embolization quantification and to enable the quantification of embolized tumors through other imaging modalities, such as angiography.

Table 0.1

Statistical Analysis			
	Pre-Embolization Tumor Volume (cm^3)	**Residual Contrast-Enhanced Volume (cm^3)**	**Post-Embolization Total Tumor Volumes (cm^3)**
Minimum Volume (cm^3)	9.85	0.72	9.26
Average Volume ±SEM (cm^3)	60.36	29.22	56.88
Maximum Volume (cm^3)	252.77	117.44	213.30
Average Embolization Ratio		45.28%	
Average Absolute Difference in Tumor Size (cm^3)		-3.48	
Average Relative Difference in Tumor Size		-5.58%	

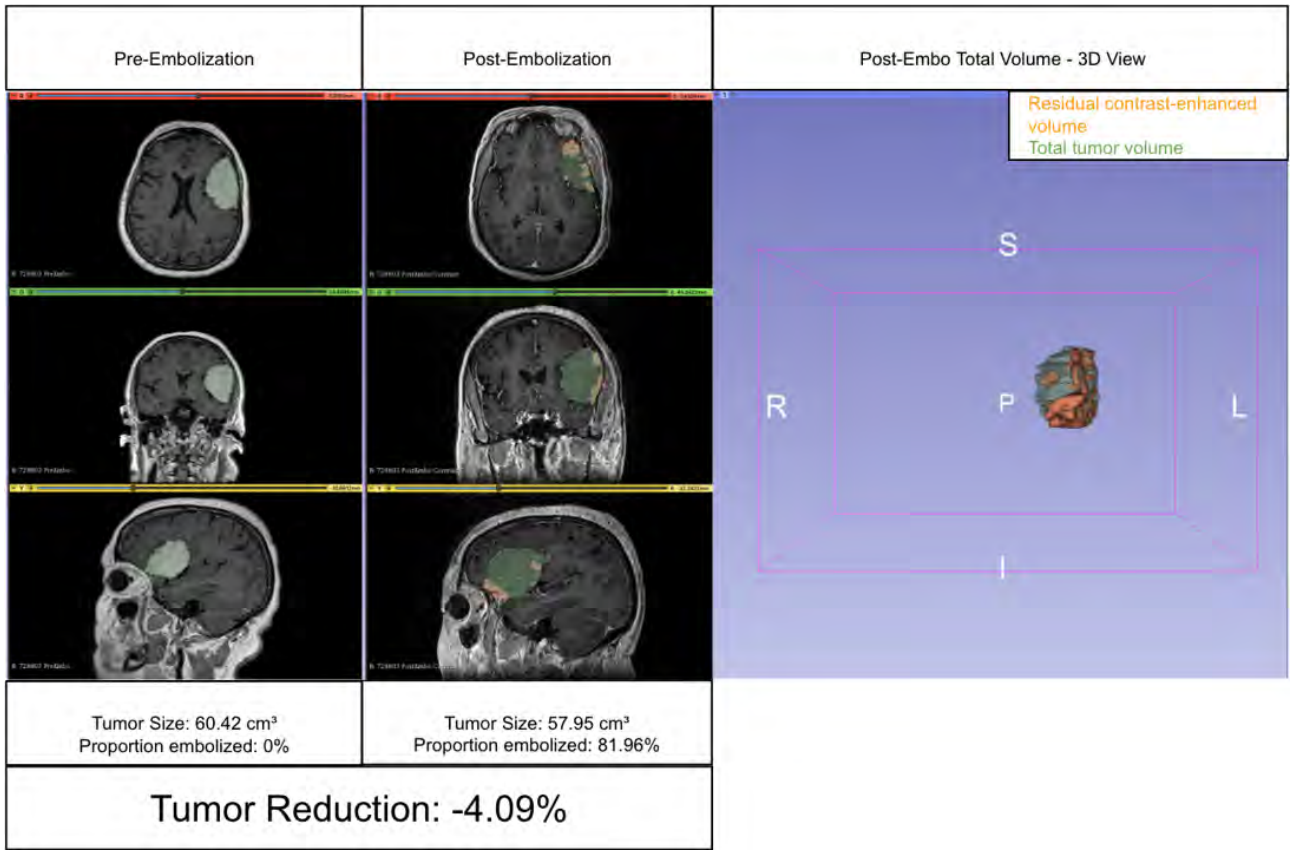

Figure 0.1: 1 MRI hand-segmented analysis of patient (A) before treatment and (B) after treatment. (C) 3D rendering of residual contrast-enhanced volume within the total tumor volume after treatment embolization efficacy.

Spiral VIBE UTE-MRI for Lung Imaging in Post-COVID patients

Valentin Fauveau[1], Adam Jacobi[2], Adam Bernheim[2], Michael Chung[2], Renata Pyzik[1], Marco Pereanez[1], Yang Yang[1,2], Thomas Benkert[3], Zahi A Fayad[1,2], Li Feng[1,2]

[1] BioMedical Engineering and Imaging Institute, Icahn School of Medicine at Mount Sinai, New York, USA
[2] Department of Radiology, Icahn School of Medicine at Mount Sinai, New York, USA
[3] MR Application Development, Siemens Healthcare GmbH, Erlangen, Germany

Introduction: Spiral VIBE UTE-MRI is a relatively new MRI technique that combines ultra-short echo time acquisitions with a stack-of-spirals trajectory. Compared to the computed tomography (CT), the Spiral VIBE UTE-MRI is a radiation-free imaging technique that coud be used for longitudinal lung studies, for example, recurrent controls of COVID-recovered patients (post-COVID patients). In this study, we aimed to analyze the motion sensitivity of different reordering schemes and breath holding positions in Spiral UTE MRI to determine the optimized protocol for lung imaging. The diagnostic quality for the optimized Spiral UTE-MRI protocol was then compared to CT for a group of post-COVID patients.

Materials and Methods: Spiral VIBE UTE-MRI was performed in a total of 31 subjects (15 males, 16 females, mean age= 44.6$\pm$14.6 years). For each subject, four 3D spiral UTE datasets were acquired, two scans with the line-in-partition ordering and two with the partition-in-line; both reordering schemes were collected during the inspiratory and expiratory breath-hold positions. A blind assessment was performed by three experienced chest radiologists to assess lung image quality on a 5-1 scale, from best to worst. Among the 31 patients studied to assess the motion sensitivity for pulmonary Spiral-UTE-MRI, a total of 24 post-COVID patients (11 males, 13 females, mean age= 46.58$\pm$14.8 years) underwent also a routine chest CT. The diagnostic quality of all MR images was compared with CT based on a 3-point scale (1: non-diagnostic quality, 2: adequate quality but worse than CT, 3: similar to CT).

Results: Spiral VIBE UTE images acquired during the inspiratory breath-hold position are significantly better ($P<0.05$) . The partition-in-line reordering is more sensitive to motion than the line-in-partition scheme The Spiral UTE with line-in-partition reordering performed during the inspiration phase was considered the best protocol in our study. Among the 24 post-COVID patients who underwent the routine chest CT, only 3 showed post-COVID lesions. Two cases presenting lesions were observable through the MR images. Overall, 15 cases (62.5 percent) were considered to have a diagnostic quality similar to CT, 5 cases (21 percent) were considered acceptable but worse than CT and 4 cases (16.5 percent) were considered not useful.

Conclusions: Spiral VIBE UTE-MRI is a radiation-free method that takes advantage of the ultrashort echo time and the stack-of-spiral trajectories to achieve good image quality. This novel MRI method could be used for longitudinal studies of lung structure change which might be important for certain patient population such as post-COVID patients.

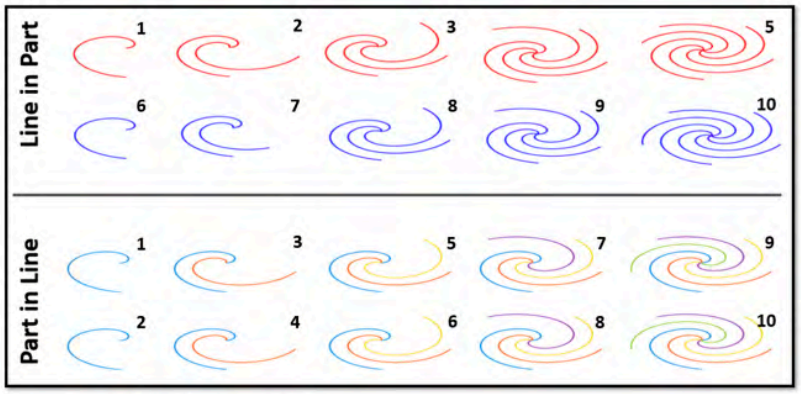

Figure 1. Line-in-Part vs Part-in-Line Reordering.
Line-in-Part: Collects all interleaves of the same partition (slice) before moving to the next one.
Part-in-Line: Collects the same interleave for all partitions (slices) before moving to the next one.

	Spiral Inspiration	Spiral Expiration	Spiral FS Inspiration	Spiral FS Expiration	Cartesian Inspiration	Cartesian Expiration
Large Arteries Score	3.63 ± 0.42	3.25 ± 0.65	3.21 ± 0.47	3.04 ± 0.68	3.66 ± 0.6	3.32 ± 0.67
Large Airways Score	3.55 ± 0.46	2.94 ± 0.7	3.6 ± 0.46	2.9 ± 0.64	3.34 ± 0.83	2.83 ± 0.71
Segmental Arteries Score	2.98 ± 0.49	2.46 ± 0.59	2.66 ± 0.49	2.25 ± 0.52	2.89 ± 0.61	2.44 ± 0.54
Segmental Broncho vascular Structures Score	2.47 ± 0.51	1.95 ± 0.54	2.31 ±0.59	1.84 ± 0.54	2.36 ± 0.58	1.84 ± 0.48
Subsegmental Vessels Score	2.11 ± 0.38	1.72 ± 0.42	1.97 ± 0.46	1.63 ± 0.41	2.05 ± 0.52	1.67 ± 0.37
Artifact Level Score	2.57 ± 0.46	3.12 ± 0.61	2.95 ± 0.47	3.35 ± 0.66	2.8 ± 0.75	3.24 ± 0.59

Figure 2. Results: Average scores for all three reviewers.

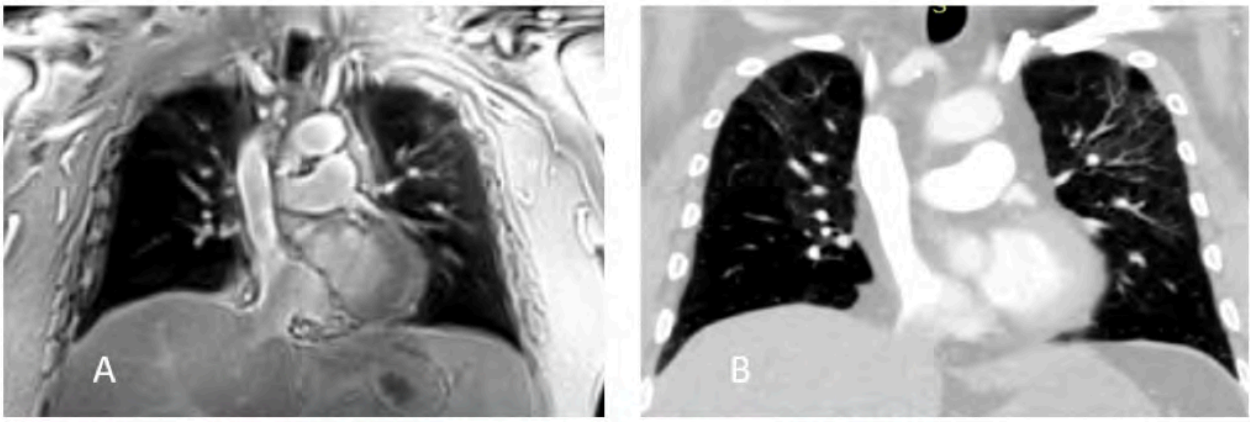

Figure 3. Example of Spiral UTE MRI (A) with good diagnostic quality compared to CT (B).
A. Acquired on 5/20/2021
B. Acquired on 1/25/2021

Figure 0.2

Comparing FreeSurfer estimates and reliability of volume and cortical thickness measures

Carolina Ferreira-Atuesta MD MSc[1], Sarah Binder[1], Lydia Piendel[1,2], Jacqueline Emerson[1,3], Jonathan Sutkowski[1], Nancy Andrew-Jaja[1], Trey Hedden, PhD[1]

[1] Department of Neurology, Icahn School of Medicine at Mount Sinai, New York, USA
[2] Department of Neurology, 2nd Faculty of Medicine, Charles University, University Hospital Motol, Prague, Czech Republic
[3] Faculty of Medicine, Duke University, North Carolina, USA

Introduction: Anatomical volume and cortical thickness are measures of neurodegeneration to track disease progression and evaluation of treatment efficacy. FreeSurfer software provides automatic structural parcellation and segmentation to estimate volume and thickness. T1-weighted inputs are commonly used, but T2 or T2*FLAIR images can be added. This study compared FreeSurfer estimates for T1 only vs T1+T2 or T1+T2*FLAIR inputs with regard to reliability and its relation to amyloidosis.

Materials and Methods: 3-Tesla MRI data were included for 379 scans (T1: 35%, T1+T2: 35%, T1+T2*FLAIR: 31% - session 1: 39%, 2: 34%, 3: 27%) from 60 healthy older adults (mean age 71, 67% female). FreeSurfer-derived estimates of volume and cortical thickness were obtained for T1, T1+T2, and T1+T2*FLAIR inputs. Kruskal Wallis tests followed by Dunn post hoc test were used to identify estimates that were significantly different across sequences. Two-way mixed model analyses were performed on each estimate, including subject and session as grouping factors. Interclass correlation coefficients measured similarity and reliability. A secondary analysis was performed using FreeSurfer's longitudinal pipeline. Amyloid-PET SUVR levels were available for 54% of subjects. Bonferroni correction and estimated marginal means were used to correct for multiple comparisons.

Results: For volume estimates, 17% of pairwise combinations (7% T1+T2vsT1+T2*Flair, 6% T1vs T1+T2, and 4% T1vsT1+T2*FLAIR) showed significant differences between sequences adjusting for multiple comparisons. The cross-sectional similarity between sequences had median ICC=0.87. Test-retest reliability within sequences had median ICC=0.88 for T1, 0.87 for T1+T2 and 0.78 for T1+T2*FLAIR. For thickness estimates, 73% of pairwise combinations (27% T1+T2vsT1+T2*FLAIR, 23% T1vsT1+T2*FLAIR, and 22% T1vsT1+T2) showed significant differences between sequences after adjusting for multiple comparisons. The cross-sectional similarity between sequences had median ICC=0.43. Test-retest reliability within sequences had median ICC=0.78 for T1, 0.74 for T1+T2 and 0.30 for T1+T2*FLAIR. When using the longitudinal pipeline, test-retest reliability within sequences improved considerably for all input methods.. Amyloid SUVRs had non-significant correlations with all ICC measures..

Conclusions: Overall, volumes had high similarity across sequence inputs and high test-retest reliability. Thickness showed less reliability across sequences and sessions driven by low similarity and low reliability for T1+T2*FLAIR. The longitudinal pipeline resulted in more reliable estimates across sessions. Amyloid deposition did not impact reliability estimates. These results suggest that T1 only or T1+T2 inputs have high reliability across sessions and should be considered in clinical trials designs that measure change in volume or thickness.

A. Test-retest reliabiity within sequences for each ROI volume estimates

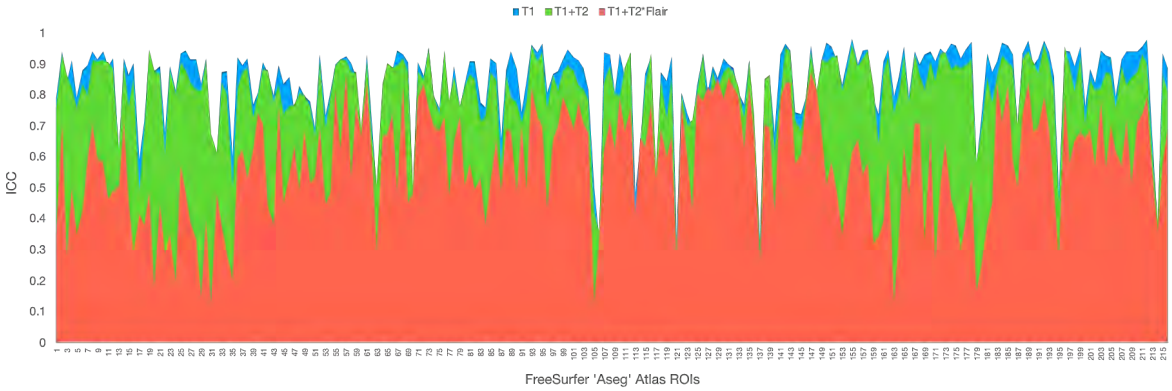

B. Test-retest reliabiity within sequences for each ROI thickness estimates

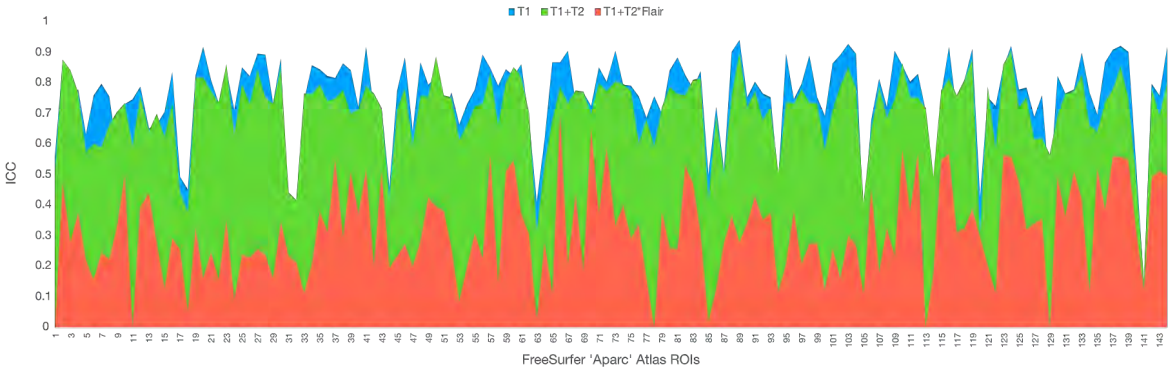

C. Median intraclass correlation coefficients for each analysis

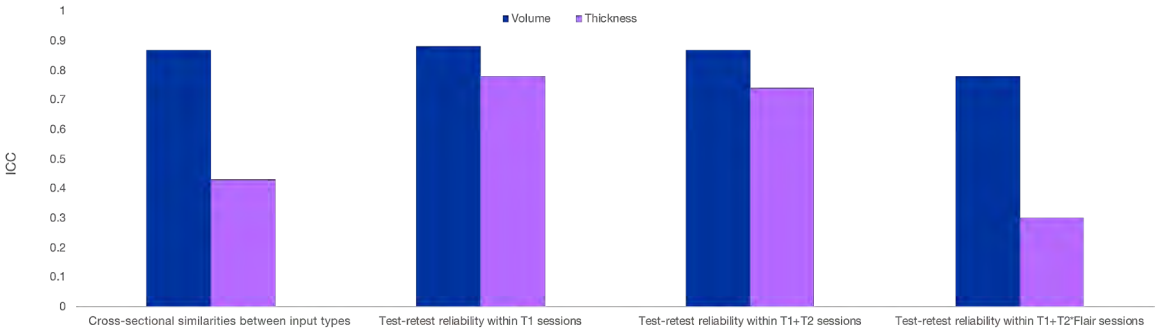

Figure 0.1

Copper liver deposits modify tissue T1 in toxic-milk mouse model of Wilson's disease

Lazar Fleysher[1], Ming Yin Lun[1], Johnny Ng[1], Venkatesh Mani[1], Cheuk Tang[1], Zahi Fayad[1], Thomas Schiano[2], Roman Fleysher[3]

[1] Biomedical Engineering and Imaging Institute. Department of Radiology, Mount Sinai Medical Center, NY, NY 10029
[2] Recanati/Miller Transplantation Institute Mount Sinai Medical Center, NY, NY 10029
[3] Albert Einstein School of Medicine Bronx, NY 10461

Introduction: In Wilson's disease patients, the impaired copper metabolism and excretion lead to a deposition of copper in various tissues and cause organ damage. The toxic-milk mouse mutants develop chronic hepatitis which resembles that seen in WD patients. In this work, we measure T1 values in the liver of toxic-milk and wild-type mice. Such methodology could provide a method for non-invasive monitoring of de-coppering treatment in patients with Wilson's disease.

Materials and Methods: Wilson's disease (WD), aka progressive hepatolenticular degeneration is a rare autosomal recessive condition caused by a defect in the ATP7B gene1 (1) which normally encodes for a copper-transporting ATPase that facilitates the combination of copper and α2-globulin into ceruloplasmin in liver. This process is responsible for the elimination of the majority of copper in healthy individuals. In WD patients, the impaired copper metabolism and excretion lead to deposition of redundant free copper in the brain, liver, cornea and other locations, and cause organ damage (2). As de-coppering treatment is typically employed, it may be important to quantify the effectiveness of this therapy using imaging. Since accumulation of copper in tissue causes shorting of MRI signal T1 relaxation time, we hypothesize that accurate T1-mapping could be one such approach to infer effectiveness of the treatment. The toxic-milk mouse has a naturally occurring mutation in the murine ATP7B homologue and causes a development of chronic hepatitis which resembles that seen in WD patients. By 6 months of age, the copper concentration could be 100 times higher than that in the wild type (3). In this work, we compare T1 values measured from the liver of toxic-milk (TX) and wild-type (WT) mice.

Results: Five six-month-old toxic-milk mice and five six-month-old wild-type mice were imaged ex-vivo on a Bruker 7T BioSpec scanner using a TRITONE(4) T1-mapping protocol optimized for T1=500 (ms): FA(^{o})/TR(ms)/NEX=90/3195/1:36/367/3:26/13/54 covering $60 \times 32 \times 32$ (mm^3) volume at $0.4 \times 0.4 \times 0.4$ (mm^3) resolution. TRITONE minimizes T1 measurement error for the specified imaging time while removing B1-related systematic error. Anatomical images were acquired using FLASH sequence covering $50 \times 50 \times 10$ (mm^3) volume at $0.2 \times 0.2 \times 0.5$ (mm^3) resolution with FA(o)/TR(ms)/TE(ms) /NEX=30/500/10/28.

Conclusions: It is expected that the accumulation of diamagnetic Cu(I) will cause a shorting of tissue T1 relaxation times. Indeed, average liver tissue T1-value (mean and standard error on the mean) for TX-mice (559 SEM 51 ms) is lower than that of WT mice (585 SEM 35 ms). The Cu(I) concentration in TX was between 1.0-2.5 (mg/g) of wet weight.

Acknowledgments: Funding for this research was provided by Alexion, AstraZeneca Rare Disease.

References:

1. Ala et. al. Lancet. 2007;369(9559):397-408. 2. Patil et. al. J Clin Exp Hepatol. 2013;3(4):321-36. 3. Hadrian at al. Mol Biol Rep 48, 1903–1914 (2021). 4. Fleysher et al. MRI 2008 Jul;26(6):781-9.

Table 0.1

Sample type	TX1	TX2	TX3	TX4	TX5	WT1	WT2	WT3	WT4	WT5
T1 (ms)	587	588	596	554	472	472	705	602	525	625

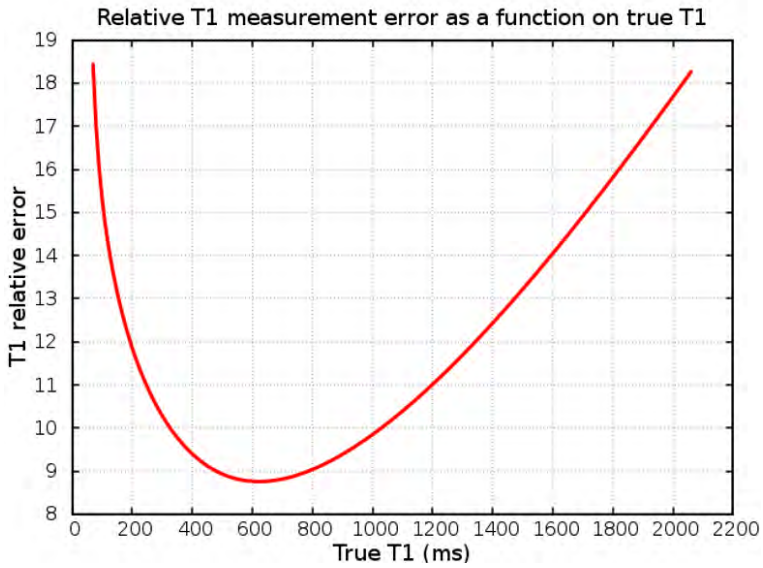

Figure 0.1: TRITONE relative error around the tuning point T1ref=500(ms) (see reference 4).

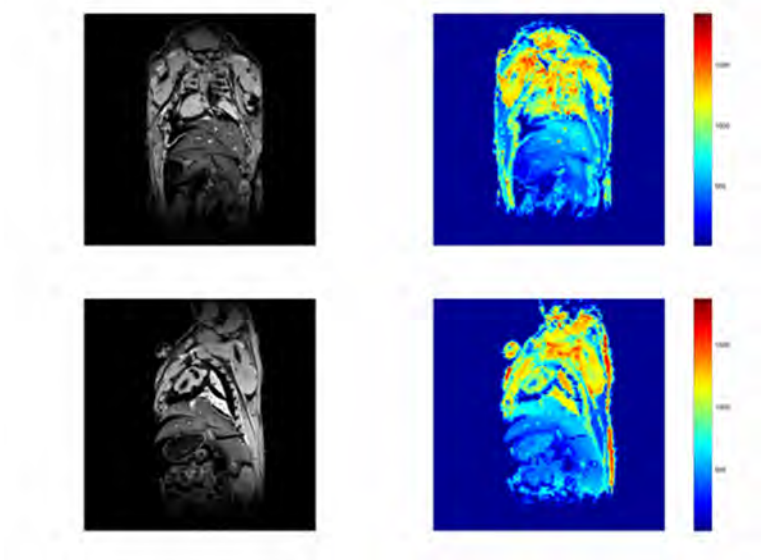

Figure 0.2: T1-weighted and T1 map images for a toxic mouse (top row) and wild type mouse (bottom row).Anatomical images clearly show wide-spread liver tissue damage.

Noise-Fill Interpolation Improves Statistical Power of Lesion Detection in Voxel-Wise Analyses

Roman Fleysher[1], Lazar Fleysher[2], Namhee Kim[3], Michael L Lipton[1], and Craig A Branch[1]

[1] Gruss Magnetic Resonance Research Center, Department of Radiology, Albert Einstein College of Medicine, Bronx, NY, United States,
[2] Biomedical Engineering and Imaging Institute, Department of Radiology, Mount Sinai Medical Center, New York, NY, United States
[3] Department of Neurological Sciences, Rush Medical College, Chicago, IL, United States

Introduction: Image interpolation is inextricable in many image analysis steps including registration of low resolution images to a standard high resolution template. Interpolated images are often smoothed and their voxel intensities are not statistically independent which severely complicates subsequent statistical analysis at the group level. Difficult to account correlations lead to higher than expected false-positive rates. We propose a new, noise-fill, image interpolation method which avoids both spatial blurring and loss of statistical independence of the voxel intensities.

Materials and Methods: This study was approved by IRB and includes one diffusion data set from a healthy individual which was used as a seed for subsequent simulations. Imaging was performed using a 3.0T Philips Achieva TX scanner (Philips Medical Systems, Best, the Netherlands) utilizing its 32 channel head coil with the following protocol: TR/TE=10000/65msec, 32 diffusion directions, b-value=800sec/mm^2, 2mm^3 isotropic resolution, $128 \times 128 \times 70$ matrix. DTI data was processed to produce maps of eigenvalues and eigenvectors to be used in the simulations.

Results: Intact eigenvalues and eigenvectors were used to generate DTI data for controls according to the original b-value/b-vector configuration (Fig 1). Both minor eigenvalues were increased in a single voxel to create small low FA lesion (ΔFA=-0.01) in the simulated patient DTI data (Fig 1). We emulate voxel-wise analysis of a patient against 29 controls over a 1mm^3 isotropic resolution template ($256 \times 256 \times 140$ matrix) using t-test retaining voxels with $p<0.01$ (two-tailed). Performance of lesion detection was evaluated using receiver operating curve (ROC) by varying size threshold of low FA clusters. Lesion was considered detected when a low FA cluster survived size threshold anywhere in the brain. Null and alternative hypotheses were simulated 1200 times each. Noise-fil interpolation from 2 to 1mm is achieved by filling K-space to the desired spatial resolution with noise, at the level of that of the scanner hardware. Results are compared to commonly used tri-linear interpolation with and without blur as well as zero-fill.

Conclusions: We show that noise-fill interpolation improves sensitivity of lesion detection in simulated examples of patient-specific voxel-wise cluster analyses where fractional anisotropy (FA) derived from a low resolution brain diffusion scan of a patient is compared to those of a healthy cohort over a high resolution template using a voxel-wise t-test.

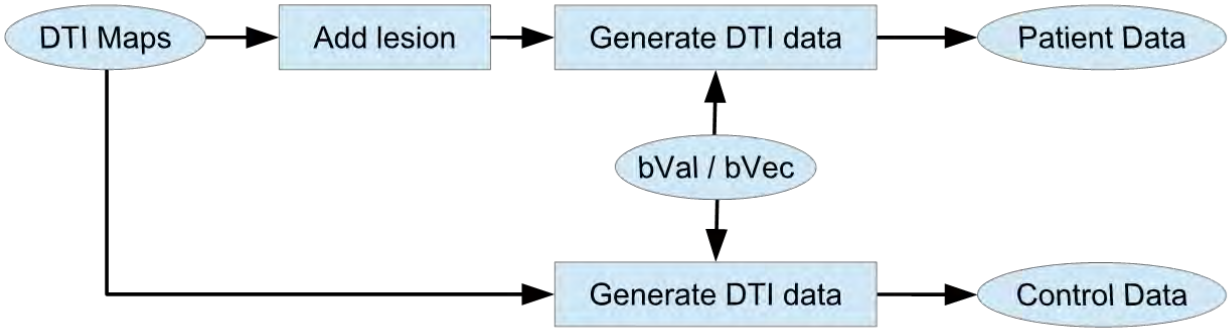

Figure 0.1: Generation of simulated patient and control DTI data to be used in the study.

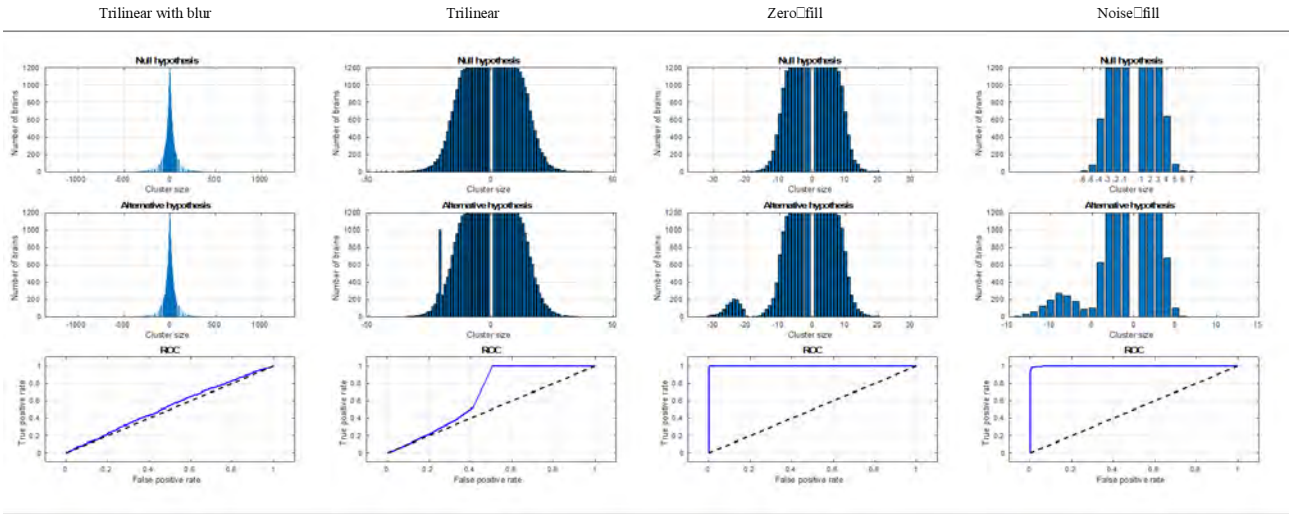

Figure 0.2: Distribution of cluster sizes and corresponding receiver operating curves for several interpolation schemes. Cluster sizes for low FA are negative, high FA are positive. Top: no lesion. Middle: small 8mm^3 low FA lesion is inserted and is evident as a bump on the left. Bottom: ROC for lesion detection. Note that top right distribution, noise-fill interpolation under the null hypothesis, is the only one from the top row identical to the gold standard.

Resting-state fMRI-based screening of deschloroclozapine in rhesus macaques predicts dosage-dependent behavioral effects

Atsushi Fujimoto[1*], Catherine Elorette[1*], J. Megan Fredericks[1], Satoka H. Fujimoto[1], Lazar Fleysher[4], Peter H. Rudebeck[1+], and Brian E. Russ[1,2,3,+]

[1] Nash Family Department of Neuroscience and Friedman Brain Institute, Icahn School of Medicine at Mount Sinai, One Gustave L. Levy Place, New York, NY 10029
[2] Center for Biomedical Imaging and Neuromodulation, Nathan Kline Institute, 140 Old Orangeburg Road, Orangeburg, NY 10962
[3] Department of Psychiatry, New York University at Langone, One, 8, Park Ave, New York, NY 10016
[4] BioMedical Engineering and Imaging Institute, Icahn School of Medicine at Mount Sinai, One Gustave L. Levy Place, New York, NY 10029
[*] These authors contributed equally to this work
[+] Joint last author

Introduction: Virally-mediated chemogenetic techniques hold the promise of circuit-specific neuromodulation for human brain disorders. Their protracted development in primates and issues related to the specificity of the actuator drugs has significantly slowed their implementation. Here we took a multi-disciplinary approach to assessing the translational appropriateness of a newly identified actuator drug, deschloroclozapine (DCZ).

Materials and Methods: Resting-state functional MRI (rs-fMRI) data was acquired from seven rhesus macaques (6 males and 1 female) after administration of either vehicle, 0.1 or 0.3 mg/kg DCZ, the latter of which produce 80% and near 100% chemogenetic receptor occupancy, respectively. Seed-based comparative-connectome analysis and independent component analysis assessed dose dependent neural impact. Two subsets of subjects were tested on socio-emotional tasks (N = 4), and a probabilistic learning task (N = 3), assessing DCZ's impact on unconditioned and conditioned affective responses, respectively.

Results: Neither vehicle nor 0.1 mg/kg DCZ changed overall functional connectivity, affective responses, or reaction times in the learning task. 0.3 mg/kg DCZ increased functional connectivity, particularly in frontal regions, and increased reaction times in the learning task. Notably, there was a positive correlation between changes in overall functional connectivity and reaction time.

Conclusions: These experiments show the utility of rs-fMRI for in-vivo drug screening and benchmarking. We found that low dose DCZ does not alter brain function or affective behavior. However, higher doses of DCZ impacts frontal connectivity and is associated with deficits in task execution. Implementation of these methods will accelerate the development of chemogenetic in primates for research and therapeutic approaches.

Modeling the brain wide effects of subcallosal ACC deep brain stimulation in macaques

Satoka H. Fujimoto[1], Brian E. Russ[1,2,3], Ki Sueng Choi[5], Lazar Fleysher[4], Gaurav Verma[4,5], Catherine Elorette[1], Atsushi Fujimoto[1], Davide Folloni[1], Helen S. Mayberg[5], Peter H. Rudebeck[1]

[1] Nash Family Department of Neuroscience and Friedman Brain Institute, Icahn School of Medicine at Mount Sinai, One Gustave L. Levy Place, New York, NY 10029
[2] Center for Biomedical Imaging and Neuromodulation, Nathan Kline Institute, 140 Old Orangeburg Road, Orangeburg, NY 10962
[3] Department of Psychiatry, New York University at Langone, One, 8, Park Ave, New York, NY 10016
[4]BioMedical Engineering and Imaging Institute, Icahn School of Medicine at Mount Sinai, One Gustave L. Levy Place, New York, NY 10029
[5]Nash Family Center for Advanced Circuit Therapeutics, Mount Sinai West Hospital, 1000 10th Ave, New York, NY 10019

Introduction: Deep brain stimulation targeting subcallosal anterior cingulate cortex (scACC-DBS) is a promising therapy for treatment resistant depression. However, despite its potential for treating depression, little is known about the brain-wide mechanisms through which scACC-DBS works. Prior work has reported that in people who recover from depression following scACC-DBS there are alterations in brain-wide resting-state networks such as the default mode network (DMN). Here we tested the hypothesis that scACC DBS specifically alters connectivity within the default mode network using a translationally relevant vivo neuroimaging approach in non-human primates.

Materials and Methods: We implanted two rhesus macaque monkeys with a single scACC-DBS electrode to establish the brain-wide effects of continuous stimulation following the paradigm successfully used in patients. Specifically, we stimulated for 6 weeks (parameters: 5mA, 90 μsec, 130Hz, DBS system; ActivaSC, Medtronic). Electrodes were targeted to the confluence of 3 white matter tracts which are targeted in human patients: the cingulum bundle, forceps minor, and uncinate fasciculs. These three tracts were visualized using presurgery diffusion tractography. Whole brain resting-state functional MRIs (rs-fMRIs) were acquired before surgery and following 6 weeks of stimulation. The data were analyzed using a seed-based comparative-connectome analysis.

Results: Six weeks of scACC-DBS stimulation specifically decreased functional connectivity (FCs) between scACC and a number of different areas including, bilateral medial and dorsolateral frontal lobe, bilateral superior temporal lobe and ipsilateral hippocampus. Notably, the biggest change in scACC FC was with posterior cingulate cortex (PCC), a major node in the DMN. In contrast, the FC between scACC and anterior insular cortex was increased. Additionally, there was no obvious global change in brain-wide FC.

Conclusions: Chronic scACC-DBS can change specific brain network which are connecting with scACC, especially the DMN. Our data reveal the specific effects of scACC-DBS on brain-wide functional connectivity, information essential for optimizing this treatment for depression patients as well as establishing the brain mechanisms that become pathological in depression.

Cognitive subgroups of early psychosis differ in global and local brain aging

Shalaila S. Haas[1], Ruiyang Ge[2], Nicole Sanford[2], Amirhossein Modabbernia[1], Abraham Reichenberg[1], Heather Whalley[3], Rene S. Kahn[1], Sophia Frangou[1,2]

[1] Department of Psychiatry, Icahn School of Medicine at Mount Sinai, New York City, New York, USA
[2] Department of Psychiatry, Djavad Mowafaghian Centre for Brain Health, University of British Columbia, Vancouver, Canada
[3] Division of Psychiatry, University of Edinburgh, Edinburgh, United Kingdom

Introduction: Previous studies have implicated accelerated aging in the pathophysiology of schizophrenia. Global brain aging predictions, have shown accelerated aging in patients with early psychosis (EP), but are not informative about regional differences. Additionally, the link between brain-aging and cognition in EP has not been addressed. Here, we used machine learning algorithms to identify cognitive subgroups of EP and then applied a deep learning algorithm to assess regional and global patterns of brain-aging in each subgroup compared to healthy individuals.

Materials and Methods: Global and local brain-age-gap-estimates (G-brainAGE and L-brainAGE) measuring deviation between neuroimaging-predicted and actual age, were computed from T1-weighted structural neuroimaging data from 84 patients with early-stage schizophrenia (illness duration < 5 years) and 1169 healthy individuals using machine learning algorithms. Multi-domain cognitive data from the same sample were submitted to Heterogeneity through Discriminative Analysis (HYDRA) to identify cognitive clusters in patients.

Results: HYDRA identified a cognitively impaired cluster (n=69) and a cognitively spared subgroup (n=15) of patients (Fig.1). Compared to healthy individuals, G-brainAGE was significantly higher in the cognitively impaired subgroup (mean [SD] = 11.08 [7.16]; T [P] = 4.72 [< 0.001]) compared to healthy individuals (mean [SD] = 4.54 [4.73]), and also showed widespread elevation in L-brainAGE, with the highest deviances observed in frontal and temporal regions (Fig. 2A). G-brainAGE was elevated but not statistically different from healthy individuals in the cognitively spared cluster (mean [SD] = 8.94 [4.69], T [P] = 0.27 [0.79]), but showed a moderate increase in L-brainAGE localized to the anterior cingulate (Fig. 2B).

Conclusions: These findings suggest that cognitive impairment and accelerated brain aging in patients with early psychosis are linked and highlight the importance of parsing cognitive heterogeneity in early psychosis and the value of spatially fine-grained estimates of brain-aging.

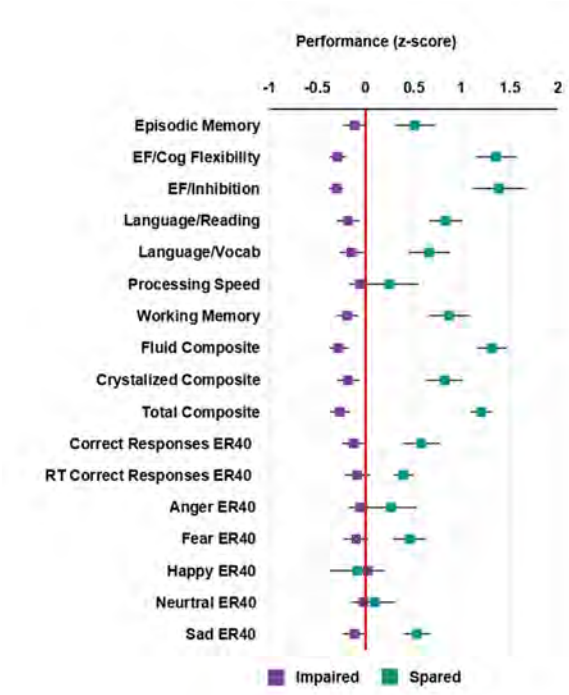

Figure 0.1: **Cognitive profiles of the impaired and spared clusters.** Average standardized cognitive performance profiles in the impaired and spared cognitive subgroups identified using HYDRA clustering. Error bars represent standard error.

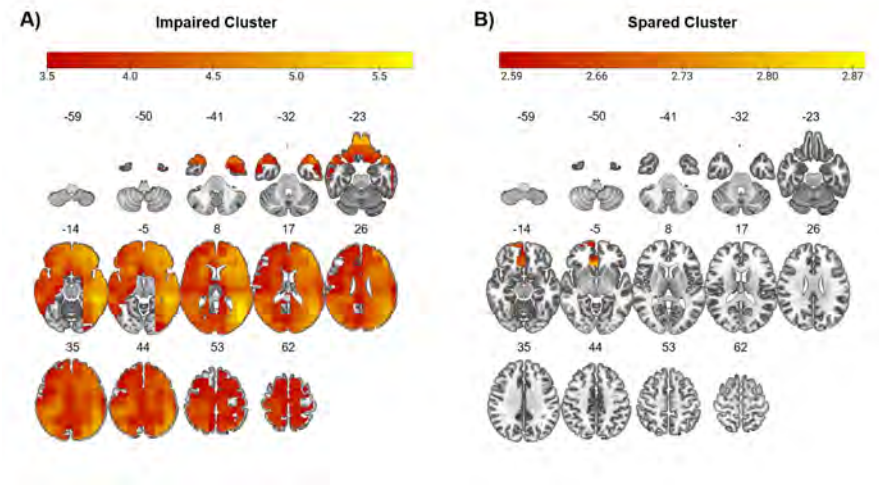

Figure 0.2: **Differences in L-brainAGE between healthy individuals and the cognitive clusters of early psychosis patients.** T-value overlay of statistically significant differences in L-brainAGE between healthy individuals and A) the impaired subgroup (PFWE < 0.05 with familywise error-correction) and B) the spared subgroup (Punc < 0.005). Red/yellow: early psychosis patients $>$ healthy individuals. Images are displayed in neurological orientation with MNI coordinates.

Validation of an Artificial Intelligence-based Software for Assessing Right Ventricular Function by Transthoracic Echocardiography

Brian C Hsia, MD[1], Ashton Lai, MD, PhD[1], Rajeev Samtani, MD[1], Solomon Bienstock, MD[1], Supreet Singh, MD[1], Steve Liao, MD[1], Eric Stern, MD[1], Gina LaRocca, MD, MHSc[1], Javier Sanz, MD[1], Stamatios Lerakis, MD, PhD[1], Lori Croft, MD[1], Gregg W Stone, MD[1], Martin Goldman, MD[1]

[1] The Zena and Michael A. Wiener Cardiovascular Institute, Icahn School of Medicine at Mount Sinai, New York City, NY, USA.

Introduction: Transthoracic echocardiographic (TTE) assessment of right ventricular (RV) function is challenging since the RV is not fully imaged in a single plane. Cardiac magnetic resonance imaging (CMR) is the gold standard to assess RV function. TTE-derived measures including RV fractional area change (FAC), free wall strain (FWS), and tricuspid annular planar systolic excursion (TAPSE) have been shown to correlate with CMR-measured RV ejection fraction (RVEF) but require technical expertise to acquire and measure. We evaluated the sensitivity and specificity of FAC, FWS, and TAPSE derived by a rapid artificial intelligence (AI) software from a single-plane TTE apical 4-chamber (A4C) view for detecting abnormal RV function compared with CMR-derived RVEF.

Materials and Methods: LVivoRV® is a novel AI software that instantaneously quantifies FAC, FWS, and TAPSE from a single A4C TTE view without ultrasound-enhancing agents. We assessed the sensitivity, specificity, positive and negative predictive values, and accuracies of these AI-derived parameters for detecting RV dysfunction as defined by RVEF< 50% and < 40% by CMR. The quality of the echocardiograms to adequately visualize the RV for analysis were graded and stratified. Additionally, we created receiver operating curves for each variable and their respective C-statistics to ascertain how well each variable predicts RV dysfunction.

Results: TTE and CMR were performed within a median of 10 [IQR: 2-32] days of each other in 225 consecutive eligible patients. When RV dysfunction was defined as CMR-derived RVEF< 50%, the sensitivities were 79%, 75%, and 74% for FAC, FWS, and TAPSE respectively; 78% using any 2 criteria; and 62% using all 3 criteria. Specificities were 62%, 62%, and 53% for FAC, FWS, and TAPSE respectively; 61% using any 2 criteria; and 73% using all 3 criteria. Using CMR-derived RVEF< 40%, sensitivities increased to 89%-93% for the 3 parameters while specificities decreased. Specificities improved with better RV image quality. For all patients, the C-statistics for FAC, FWS and TAPSE for prediction of CMR-derived RVEF < 50% were 0.743, 0.699 and 0.637 respectively, and for CMR-derived RVEF < 40% were 0.800, 0.774, 0.684 respectively.

Conclusions: : Using a novel software, the automated AI-derived measurements of RV FAC, FWS, and TAPSE had very good sensitivity and acceptable specificity for detecting RV dysfunction compared with CMR-derived RVEF.

Table 0.1

Abnormal RV function by:								
CMR RVEF<50%	n	Sens	95%Ci	Spec	95%Ci	PPV	NPV	Acc
FAC<28%	124	79	[69, 86]	62	[53, 69]	59	81	69
FAC only	11	4	[1, 10]	95	[89, 97]	36	59	58
FWS>-17%	120	75	[65, 82]	62	[53, 69]	58	78	67
FWS only	3	0	[0, 4]	98	[93, 99]	0	59	58
TAPSE<1.3 cm	131	74	[64, 81]	53	[44, 60]	52	74	61
TAPSE only	20	5	[2, 12]	89	[82, 93]	25	58	55
Any 2 criteria abnormal	124	78	[68, 85]	61	[52, 68]	58	80	68
FAC & FWS	106	72	[61, 79]	70	[61, 77]	62	78	71
FAC & FWS only	13	10	[5, 17]	97	[92, 98]	69	61	61
FAC & TAPSE	104	65	[55, 74]	67	[58, 74]	58	74	66
FAC & TAPSE only	7	3	[1, 9]	97	[92, 98]	43	59	59
FWS & TAPSE	100	65	[55, 74]	70	[61, 77]	60	74	68
FWS & TAPSE only	11	3	[1, 9]	94	[88, 96]	27	58	57
All 3 criteria abnormal	93	62	[51, 71]	73	[64, 79]	61	73	68
Physician Read, Echo Report	222	64	[53, 73]	88	[81, 92]	78	79	78
Echo With Contrast	143	71	[59, 81]	81	[71, 88]	75	78	77
Echo Without Contrast	79	46	[28, 64]	98	[90, 99]	92	79	81
CMR RVEF<40%								
FAC<28%	124	93	[82, 97]	55	[47, 61]	35	97	63
FAC only	11	2	[0, 11]	94	[90, 96]	9	79	76
FWS>-17%	120	89	[76, 95]	56	[48, 62]	34	95	63
FWS only	3	0	[0, 7]	98	[95, 99]	0	79	78
TAPSE<1.3 cm	131	89	[76, 95]	50	[42, 56]	31	95	58
TAPSE only	20	2	[0, 11]	89	[84, 93]	5	78	72
Any 2 criteria abnormal	124	96	[85, 98]	55	[47, 62]	35	98	64
FAC & FWS	106	85	[71, 92]	63	[55, 69]	37	94	67
FAC & FWS only	13	9	[3, 20]	95	[90, 97]	31	80	77
FAC & TAPSE	104	80	[66, 89]	63	[55, 69]	36	93	66
FAC & TAPSE only	7	7	[2, 17]	98	[94, 99]	43	80	79
FWS & TAPSE	100	83	[69, 90]	65	[58, 71]	38	94	69
FWS & TAPSE only	11	4	[1, 14]	95	[90, 97]	18	79	76
All 3 criteria abnormal	93	76	[62, 86]	68	[60, 74]	38	92	69
Physician Read, Echo Report	222	91	[79, 96]	82	[75, 86]	56	97	84
Echo With Contrast	143	92	[78, 97]	75	[65, 82]	55	96	79
Echo Without Contrast	79	89	[56, 98]	93	[84, 96]	62	98	92

Neuroradiologist-Level Performance in Detecting Hydrocephalus Requiring Treatment by Using Deep Learning

Yu Huang[1], Raquel Moreno[1], Rachna Malani[2,3], Alicia Meng[2,3], Nathaniel Swinburne[2,3], Andrei I Holodny[1], Ye Choi[1], Lucas C Parra[4], Robert J Young[2,3]

[1] Department of Radiology, Memorial Sloan Kettering Cancer Center, New York, NY 10065
[2] Department of Neurology, Memorial Sloan Kettering Cancer Center, New York, NY 10065
[3] Brain Tumor Center, Memorial Sloan Kettering Cancer Center, New York, NY 10065
[4] Department of Biomedical Engineering, City College of New York, New York, NY 10031

Introduction: In large clinical centers a small subset of patients present with hydrocephalus that requires surgical treatment. We aimed to develop a screening tool to detect such cases from the head MRI with performance comparable to neuroradiologists.

Materials and Methods: We leveraged 496 clinical MRI exams collected retrospectively at a single clinical site from patients referred for any reason. This diagnostic dataset was enriched to have 259 hydrocephalus cases. A 3D convolutional neural network was trained on 16 manually segmented exams (ten hythocepahlus) and subsequently used to automatically segment the remaining 480 exams and extract volumetric anatomical features. A linear classifier of these features was trained on 240 exams to detect cases of hydrocephalus that required treatment with surgical intervention. Performance was compared to four neuroradiologists on the remaining 240 exams. Performance was also evaluated on a separate screening dataset of 451 exams collected from a routine clinical population to predict the consensus reading from four neuroradiologists using images alone.

Results: The most discriminant features were the Magnetic Resonance Hydrocephalic Index (MRHI), ventricle volume, and the ratio between ventricle and brain volume. At matching sensitivity, the specificity of the machine and the neuroradiologists did not show significant differences for detection of hydrocephalus on either dataset (proportions test, $p > 0.05$). ROC performance compared favorably with the state-of-the-art (AUC 0.90–0.92).

Conclusions: Hydrocephalus cases requiring treatment can be detected automatically from MRI in a heterogeneous patient population based on quantitative characterization of brain anatomy with performance comparable to that of neuroradiologists.

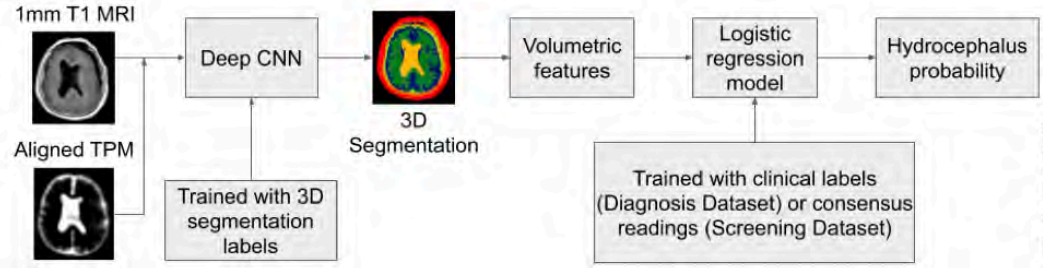

Figure 1: Flowchart of the automated pipeline for machine detection of hydrocephalus.

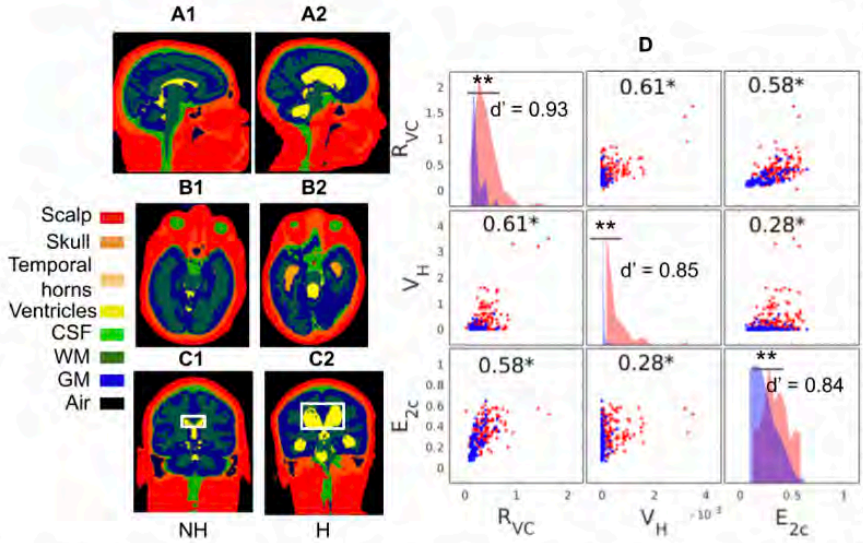

Figure 2: Segmentation for two patients and representative volumetric features for all patients. (A-C) Segmentation for a non-hydrocephalus patient (NH) and hydrocephalus patients (H). (D) Distribution of three representative features extracted from these segmentations. Each point represents a patient (red: hydrocephalus, blue: non-hydrocephalus). Features are ratio of ventricle over extraventricular CSF volume (R_{VC}), volume of the temporal horns (V_H), ratio of ventricle area over area of bounding box averaged over multiple coronal slices (E_{2c}; boxes are white rectangle in panels C1 and C2). Correlation coefficients between each pair of features are noted (*: $p < 0.05$). Histograms of each feature are shown on the diagonal, with red and blue indicating hydrocephalus and non-hydrocephalus, respectively. Separability of each feature measured in Cohen's d' is also noted on the diagonal (**: $p < 0.001$, Wilcoxon rank sum test, N = 240).

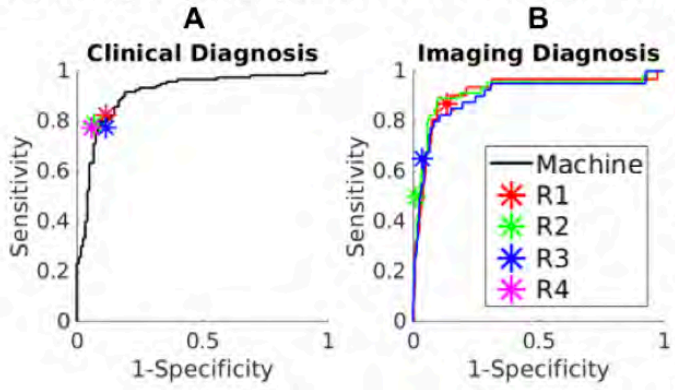

Figure 3: Test-set performances of the machine and neuroradiologists (R1–R4) in detecting hydrocephalus. (A) Prediction of the clinical diagnosis of hydrocephalus requiring treatment in 240 exams (120 positive) in the Diagnosis Dataset; (B) Prediction of the majority readings in the 451 exams in the Screening Dataset; for each radiologist (R1–R3), a slightly different majority diagnosis serves as "ground truth", hence different curves.

Figure 0.1

Shifts in local neuroplasticity in World Trade Center responders with post-traumatic stress disorder

Azzurra Invernizzi[1], Elza Rechtman[1], Paul Curtin[1], Demetrios M. Papazaharias[1], Cheuk Y. Tang[2], Maryam Jalees[1], Alison C. Pellecchia[4], Stephanie Santiago-Michels[4], Melissa A. Carr[4], Evelyn J. Bromet[5], Sean A. Clouston[3], Roberto G. Lucchini[6,7], Benjamin J. Luft[4,8], Megan K. Horton[1]

[1] Department of Environmental Medicine and Public Health, Icahn School of Medicine at Mount Sinai, New York, NY, USA
[2] Department of Radiology and Psychiatry, Icahn School of Medicine at Mount Sinai, New York, NY, USA
[3] Program in Public Health and Department of Family, Population, and Preventive Medicine, Renaissance School of Medicine at Stony Brook University, Stony Brook, NY, USA
[4] World Trade Center Health and Wellness Program, Renaissance School of Medicine at Stony Brook University, Stony Brook, NY, USA
[5] Department of Psychiatry, Renaissance School of Medicine at Stony Brook University, Stony Brook, NY, USA
[6] Department of Environmental Health Sciences, Robert Stemple School of Public Health, Florida International University, Miami, Florida, USA
[7] Department of Medical Surgical Specialties, Radiological Sciences and Public Health, University of Brescia, Italy
[8] Department of Medicine, Renaissance School of Medicine at Stony Brook University, Stony Brook, NY, USA

Introduction: World Trade Center (WTC) responders exposed to a mixture of traumatic and environmental stressors during rescue and recovery efforts have high prevalence (23 percent) of persistent, clinically significant WTC-related post-traumatic stress disorder (PTSD). We applied graph-based network metrics on functional magnetic resonance imaging outcomes and data-driven statistical methods to: (a) identify shifts in network connectivity between WTC-PTSD and non-PTSD responders, (b) investigate the moderating effect of PTSD on the association between WTC-exposure duration and network connectivity, and (c) explore whether shifts in network connectivity are associated with PTSD symptoms.

Materials and Methods: Using graph theory analysis of resting state functional MRI (rs-fMRI) data, we calculated eigenvector centrality (EC) to measure neural connectivity in 111 brain areas (Harvard Oxford Atlas) in WTC responders with PTSD (n = 45) and non-PTSD matched controls (n = 51). Permutation statistics quantified EC differences; partial least squares discriminant analysis (PLS-DA) was used to model divergence in EC values between WTC-PTSD cases and controls. Associations between WTC-exposure duration (months spent on the pile during rescue/recovery efforts) and EC in identified brain areas (i.e., functional hubs) were examined using general linear model (GLM) regression, adjusting for medication usage (psychotropic and opioids) and comorbid depression. Finally, generalized weighted quantile sum (WQS) regression was used to examine associations between an index of PTSD symptom scales (re-experiencing, avoidance, hyperarousal, negative thoughts) and EC in functional hubs.

Results: Utilizing these features in a predictive model enabled effective discrimination (auc: 0.749 (0.651-0.847)) of WTC-PTSD from non-PTSD responders. EC in nine brain regions (right/left anterior inferior temporal gyrus, right superior parietal lobule, right anterior parahippocampal gyrus, right anterior and posterior temporal fusiform cortex, right caudate nucleus, left amygdala and the brainstem) differed significantly and contributed the most to differentiate functional neuro-profiles between WTC-PTSD and non-PTSD responders. The association between exposure duration and EC differed significantly between WTC-PTSD and non-PTSD responders in the right anterior parahippocampal gyrus and left amygdala (p= 0.010 and 0.005, respectively). Within WTC-PTSD, the index of PTSD symptoms was positively associated with EC values in the right anterior parahippocampal gyrus and brainstem.

Conclusions: In the first ever study using rs-fMRI of WTC responders, our data-driven analysis of functional imaging data confirms hypotheses about the key brain areas associated with PTSD and extends our understanding of neural mechanisms linking WTC-exposure with WTC-PTSD. Better understanding of neural mechanisms leading to WTC-PTSD would help intervention and treatment.

Intrasurgical brain monitoring of pain using functional near-infrared spectroscopy

Keerthana Deepti Karunakaran[1] , Ke Peng[2] , Stephen Green[1] , Christine B. Sieberg[1,3,4] , Arielle Mizrahi-Arnaud[1] , Andrea Gomez-Morad[1] , David Zurakowski[5] , Lyle Micheli[6] , Barry Kussman[7] , David Borsook[1,8]

[1] The Center for Pain and the Brain, Department of Anesthesiology, Critical Care and Pain Medicine, Boston Children's Hospital, Harvard Medical School, Boston, USA
[2] Departement en Neuroscience, Centre de Recherche du CHUM, l'Université de Montréal Montreal, QC, CA
[3] Biobehavioral Pediatric Pain Lab; Department of Psychiatry & Behavioral Sciences; Boston Children's Hospital
[4] Department of Psychiatry; Harvard Medical School
[5] Division of Biostatistics, Department of Anesthesiology, Critical Care and Pain Medicine, Boston Children's Hospital, Harvard Medical School, Boston, USA
[6] Department of Sports Medicine, Boston Children's Hospital, Harvard Medical School, Boston, USA
[7] Division of Cardiac Anesthesia, Department of Anesthesiology, Critical Care and Pain Medicine, Boston Children's Hospital, Harvard Medical School
[8] Departments of Psychiatry and Radiology, Massachusetts General Hospital, Hospital, Harvard Medical School, Boston, USA

Introduction: Surgical procedures produces tissue damage through the activation of nociceptor nerve fibers and secondary effects on inflammatory systems. Such ongoing nociceptive afferent signals may produce central sensitization of pain pathways. These may be exacerbated by various factors including the psychological state of the patient (e.g., pain-related worry). Brain-based measures of nociception during the perioperative phase may provide evidence for untreated nociception/pain that could contribute to chronic post-surgical pain. However, surgical monitoring of brain activity under anesthesia is challenging, particularly due to a lack of reliable brain imaging system suitable for a surgical setting. We have previously reported the use of functional near-infrared spectroscopy (fNIRS) to measure evoked nociception in anterior prefrontal cortex and primary somatosensory cortex (S1) in awake, sedated and anesthetized individuals. In this study, we evaluate brain activity during surgery and after surgery in relation to acute postoperative pain levels.

Materials and Methods: We recorded fNIRS cortical activity from PFC and S1 regions during pre-, intra- and post-operative states in 18 patients (18.2 ± 3.3 yrs, 11 females) undergoing knee arthroscopy. Relationship between acute postoperative pain levels and 1) surgery-modulated functional connectivity and 2) acute postoperative functional connectivity was evaluated using a Pearson's r correlation test with 10,000 permutations. The effects of preoperative psychological state (fear of pain and pain catastrophizing) of the patients were mitigated using a partial correlation analysis.

Results: Surgical procedures under anesthesia negatively modulated the connectivity between medial frontopolar cortex (mFPC) and S1, where mFPC activity decreased, and S1 activity increased following a surgical procedure. Greater negative connectivity between, a) left mFPC and right S1 (original r=-.683, ppermutation=0.001), b) right mFPC and right S1 (original r=-.633, ppermutation=0.002), and c) left mFPC and right S1 (original r=-.695, ppermutation=0.0002) during surgery was associated with higher acute postoperative pain levels (potentially suggesting greater nociceptive barrage). Additionally, the functional connectivity of regions within the prefrontal cortex ($p < 0.05$) was reduced during the postoperative state and was found to be negatively associated with postoperative pain level.

Conclusions: Here we provide further support that even under general inhalational anesthesia pain-related pathways are activated by surgically induced nociceptive drive and may contribute to postoperative pain levels. The development of non-invasing imaging systems that are adaptive in the surgical environment and allow real time evaluation of nociceptive events may enable the surgical team to identify patients at high-risk of developing chronic pain and provide patient-tailored preemptive treatment and/or early pain management.

Seeing it to the end-Visualization of the Nervus Terminalis, aka "Cranial Nerve 0" with 7T MRI

Claudia Kirsch MD[1,2,3] , Mackenzie Langan[3] , Akbar Alipour PhD[4] , Gaurav Verma PhD[4] , Daniel Lambert PhD[5] , Ali Khurram PhD[6] , Preet Baldanchani PhD[4,7]

[1] Department Diagnostic, Molecular and Interventional Radiology, Biomedical Engineering and Imaging Institute, Icahn School of Medicine at Mount Sinai
[2] The School of Clinical Dentistry, University of Sheffield
[3] Neuroradiology, Otolaryngology, Department Radiology, Zucker Hofstra School of Medicine at Northwell Health
[4] Molecular and Interventional Radiology, Biomedical Engineering and Imaging Institute, Icahn School of Medicine at Mount Sinai
[5] Molecular Biology, School of Clinical Dentistry, University of Sheffield
[6] Senior Clinical Lecturer, Honorary Consultant Pathologist, School of Clinical Dentistry, University of Sheffield
[7] Molecular and Interventional Radiology, Director Advanced Neuroimaging Research Program, 7 Tesla MRI, Associate Director Biomedical Engineering and Imaging Institute, Icahn School of Medicine at Mount Sinai

Introduction: The "nervus terminalis" (NT), or "tractus olfacto-commissuralis" became officially designated as Cranial Nerve 0, by the Committee on Anatomical Terminology in 1988.[1] The NT are thin neural branches in the subarachnoid space adjacent to olfactory nerve tracts and often disrupted in brain dissections, with Gonadotropin hormone releasing hormone (GnRH) immunoreactivity, and because they synthesize nitrous oxide likely critical roles in immunity and vasomotor dilatation.[2,3] Although NT is highly conserved in vertebrates including whales and dolphins, two species lacking olfactory systems,[4] it is poorly understood due to its absence in the medical and imaging literature. The purpose of this study to review NT's clinical importance and whether it is identifiable on 7 TMRI.

Materials and Methods: After IRB approval, 10 MRIs acquired at Icahn School of Medicine Biomedical Engineering and Imaging Institute (BMEII) using a Siemens 7T Magnetom system scanner (Magnetom, Siemens, Erlangen) with a SC72CD gradient coil, single channel transmitter and 32-channel receive head coil (Nova Medical, Wilmington, MA), were retrospectively reviewed. Heavily T2 weighted sequences were retrospectively reviewed by a board certified neuroradiologist, for olfactory tracts, bulbs, presence or absence of the nervus terminalis.

Results: De-identified 7Tesla, heavily weighted T2 axial, coronal and sagittal images, demonstrated linear neural bundles in the subarachnoid space medial and adjacent to the bilateral olfactory tracts and bulbs consistent with the NT. Axial T2 image below with yellow arrows highlighting NT, light purple vertical and horizonal lines, cross just left of crista galli for reference.

Conclusions: Although highly conserved in vertebrate species, with critical roles in vasodilatation and immune response, the NT, is poorly understood due to its absence in medical texts and the imaging literature. The NT is identifiable in vivo on 7T, T2 weighted images, the ability to identify the nerve may increase awareness of its importance and function.

1. Federal Committee on Anatomical Terminology (1998). Terminologia Anatomica, Thieme, Stuttgart

2. Schober A., Meyer DL, Von Bartheld CS (1994).Central Projections of the Nervus Terminalis and the nervus Praeopticus in the lungfish brain revealed by nitric oxide synthase. J Comp Neuro 340:1-19, PM: 7531722

3. Singru PS, Sakharkar AJ, Subhedar N (2003). Neuronal nitric oxide synthetase in the Olfactory System of an Adult Teleost Fish Oreochromis mossambicus. Brain Res 977: 157-168. PM:12834876

4. Buhl EH, Oelschlager HA(1986). Ontogenetic development of the nervus terminaliss in Toothed Whales. Evidence for its Non-Olfactory Nature. Anat Embryol 173:285-294. PM:3963407

Figure 0.1: Axial T2 image below with yellow arrows highlighting NT, light purple vertical and horizonal lines, cross just left of crista galli for reference

Is curvature a biomarker for major depressive disorder? A morphological study using 7T MRI

Tara Lago[1], Mariella Reynoso[1], Yael Jacob[2], Judy Alper[3], Bradley N Delman[4], James Murrough[2], Priti Balchandani[3], and Gaurav Verma[1]

[1] Staten Island Technical High School, New York, NY, United States
[2] Psychiatry, Icahn School of Medicine at Mount Sinai, New York, NY, United States
[3] Biomedical Engineering and Imaging Institute, Icahn School of Medicine at Mount Sinai, New York, NY, United States
[4] Diagnostic, Molecular and Interventional Radiology, Icahn School of Medicine at Mount Sinai, New York, NY, United States

Introduction: Curvature, measured at centimeter/millimeter scales, quantifies the folds and intrinsic curvature shapes created during the expansion of cortical surfaces. Curvature is a sensitive small-scale biomarker, less affected by confounding variables, such as normalization to other brain regions, and detects subtle changes in brain connectivity. Ultra-high field 7T MRI offers improved spatial resolution, enabling more accurate measurement of mean curvature and better differentiations between subtle morphological features relevant to MDD. By analyzing 7T MRI data, we aim to determine whether curvature measurements are significant differentiators between MDD patients and healthy controls.

Materials and Methods: Forty-two patients diagnosed with major depressive disorder by a practicing psychiatrist, and forty-six healthy controls were scanned using T1-weighted imaging: TE/TR=1.95/3000ms, TI=1050ms, FOV=225×183mm, $320 \times 260 \times 224$ voxels, $0.7 \times 0.7 \times 0.7$ mm3 isotropic resolution, 7 min duration. We performed generalized linear models to analyze the relationship between participants' MDD/control status and measurements for intrinsic curvature index, Gaussian curvature, mean curvature, and folding index derived by FreeSurfer in thirty-four cortical regions per cerebral hemisphere. Age/gender covariation was performed and statistical tests were performed in R and Matlab.

Results: Figure 1 shows each brain region where significant between-group differences were found in curvature. Six regions showed significantly higher curvature measures in MDD patients ($p<0.05$): Inferior temporal, pars triangularis, and supramarginal gyrus showed higher Gaussian curvature, mean curvature, and intrinsic curvature. Lateral orbitofrontal lobe, isthmus cingulate, and entorhinal showed significant differences in one curvature measure. Figure 2 violin plot shows intrinsic curvature in left inferior temporal lobe, showing significant difference between patients and controls, and greater variation among patients. Greater variation in curvature was observed for MDD patients. Figure 3 shows volumetric maps with brain regions showing between-group curvature differences highlighted in red.

Conclusions: We speculate that these regions showed significant curvature differences between MDD patients and HC because of their relevant associations with depression. When the inferior temporal, the pars triangularis, and the lateral orbitofrontal are impaired, MDD patients are less likely to respond to happy facial expressions, more likely to frown, and more likely to use language connected to negative self-thinking and low self-esteem. Changes in the isthmus cingulate are related to difficulties in handling emotional memories. The supramarginal gyrus is activated during periods of lucid dreaming, nightmares, and recurring visions. Lastly, the entorhinal cortex may be linked to rumination, a major symptom of MDD.

P-Values

Regions	Gaussian	Mean	Intrinsic Curvature Index	Folding Index
Pars Triangularis	0.0360	0.0367	0.0357	N/A
Inferior Temporal	0.0287	0.0253	0.00659	0.0329
Supramarginal	0.0037	0.0453	0.0352	N/A
Entorhinal	N/A	N/A	0.0493	N/A
Lateral Orbitofrontal	0.0200	N/A	N/A	N/A
Isthmus Cingulate	0.0362	N/A	N/A	N/A

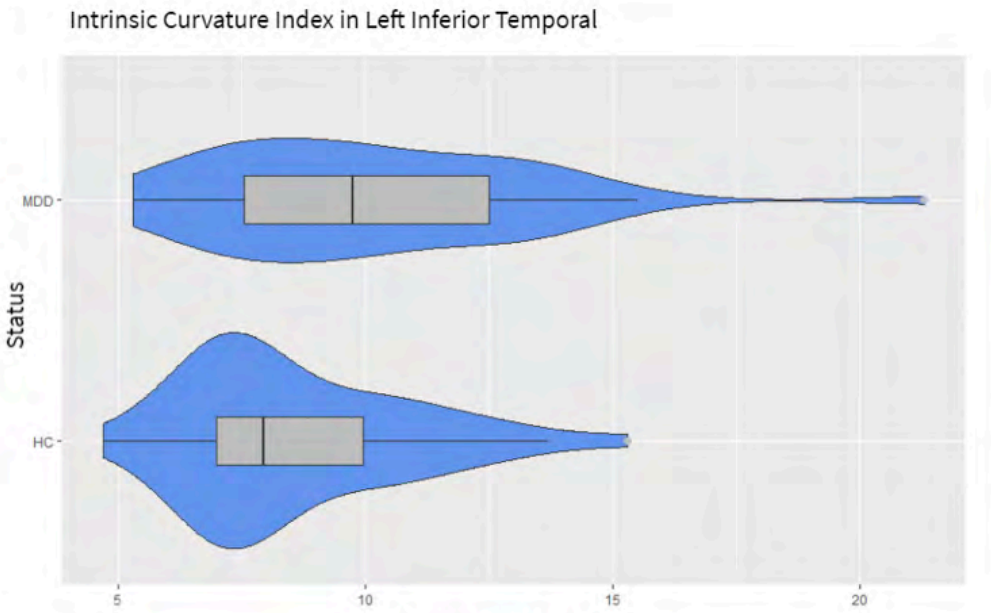

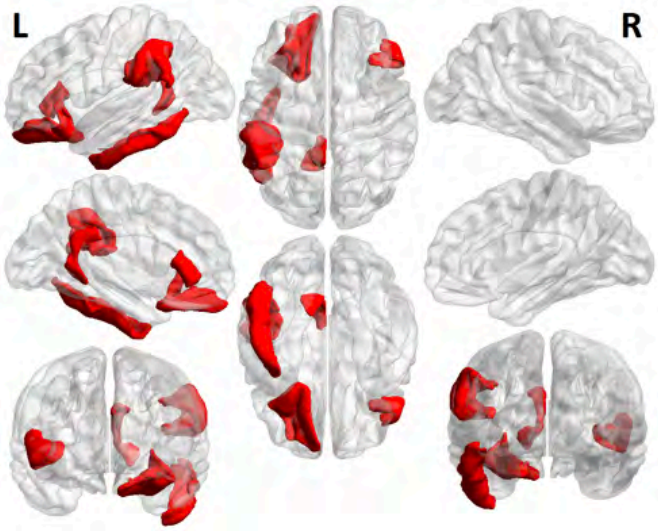

Hypothalamic subnuclei segmentation and diffusion tractography in Major Depressive Disorder at 7T

Mackenzie Langan[1,2], Ameen AlQadi[1], Gaurav Verma[1], Bradley Delman[3], James Murrough[4], Priti Balchandani[*1], and Laurel Morris[*1,4]

[1] Biomedical Engineering and Imaging Institute, Icahn School of Medicine at Mount Sinai, New York, NY, United States
[2] Icahn School of Medicine, Graduate School of Biomedical Sciences, New York, NY, United States
[3] Diagnostic, Molecular and Interventional Radiology, Icahn School of Medicine at Mount Sinai, New York, NY, United States
[4] Department of Psychiatry, Mount Sinai Hospital, New York, NY, United States

Introduction: The hypothalamus is composed of small subnuclei, contributing to regulation of numerous autonomic functions, mood, and stress response. As such, it is an ongoing area of interest in understanding the pathophysiology of Major Depressive Disorder (MDD). The paraventricular nucleus (PVN) may play a significant role in the behavioral manifestations in MDD as an upstream regulator of the Hypothalamus-Pituitary-Adrenal Axis, a regulator of the stress response. Due to its size, proximity to sinuses, inhomogeneity, and signal dropout, visualization, and manual segmentation of the whole hypothalamus and individual subnuclei has been difficult to achieve. Leveraging of increased signal-to-noise ratio and improved soft tissue contrast afforded by ultra-high field (UHF) MRI may provide the increased sensitivity needed to identify subtle structural differences in the hypothalamus in MDD compared to controls. Combined with deep neural network–based segmentation (using FreeSurfer7.2), more accurate and precise segmentation of hypothalamic subnuclei may be achievable, and maybe used with to perform high-resolution diffusion tractographic analysis and investigate tissue properties and microstructural integrity.

Materials and Methods: MRtrix was used to compute volumetric, microstructural and tractograpic metrics from segmented hypothalamic subnuclei (Figure 1) in forty unmedicated patients with MDD and matched controls. We calculated differences in Fractional Anisotropy (FA), tract count (streamline count) and volume for each subnucleus and correlated volumetrics with dimensional measures of anhedonic depression and anxious arousal using the Mood and Anxiety Symptoms Questionnaire (MASQ).

Results: There were no significant volumetric differences between groups. FA values from left anterior superior and left tubular inferior nucleus were higher in MDD, and tract count for right hypothalamus was lower in MDD (Table 1, Figure 2). Within the MDD group there was a significant positive correlation between MASQ anhedonic depression score and volumes of left anterior inferior, left anterior superior and whole right hypothalamus, and a negative correlation between MASQ anxious arousal score and volume of whole right hypothalamus.

Conclusions: We performed the first 7T analysis of volumetric, microstructural and tractographic measures in the hypothalamus in MDD. Differences in FA measures correspond with regions containing the PVN and supraoptic nucleus, two regions linked to regulation of mood, stress responses, and heavily cited as regions of interest in MDD. These regions also correlated with clinical measures of depression and anxiety. By finding significant microstructural differences in regions associated with behavioral manifestations of MDD, we have shown that 7T MRI can be used to segment small structures within the brain and detect differences within an elusive psychiatric group.

Figure 1 Segmentation of hypothalamic subnuclei using FreeSurfer7.2 and

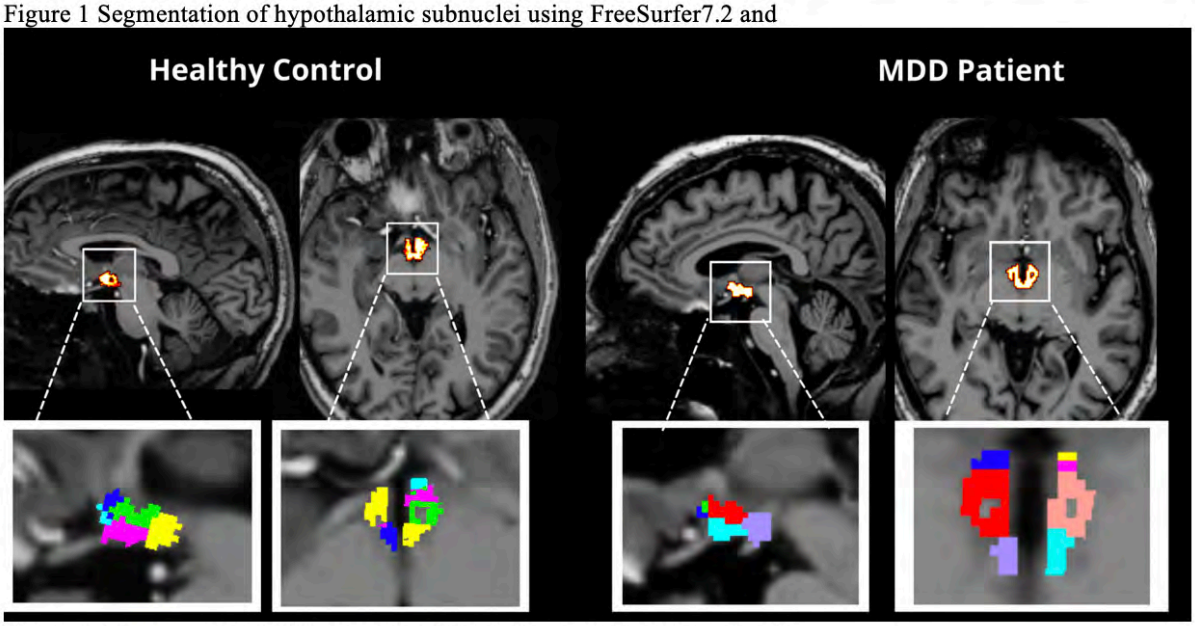

Figure 2. Microstructural differences in MDD patients compared to controls.

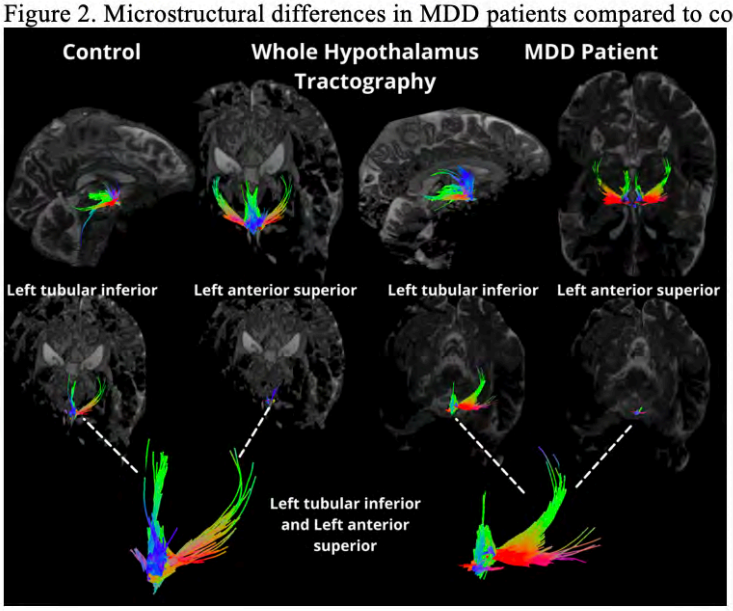

Table 1.

FA Values

Nucleus	MDD Mean	StDev	Control Mean	StDev.	p-value
Left Anterior Inferior	0.281	0.035	0.267	0.052	<0.16
Left Anterior Superior	0.291	0.048	0.264	0.045	**<0.013**
Left Posterior	0.338	0.039	0.326	0.031	<0.166
Left Tubular Inferior	0.349	0.027	0.332	0.028	**<0.011**
Left Tubular Superior	0.328	0.025	0.319	0.029	<0.269
Right Anterior Inferior	0.332	0.038	0.316	0.036	<0.083
Right Anterior Superior	0.278	0.053	0.270	0.039	<0.53
Right Posterior	0.325	0.036	0.321	0.036	<0.666
Right Tubular Inferior	0.318	0.023	0.323	0.041	<0.556
Right Tubular Superior	0.263	0.049	0.268	0.040	<0.664
Whole left FA	1.44	0.309	1.46	0.239	<0.5133
Whole right FA	1.31	0.356	1.42	0.270	<0.285
Whole hypo FA	2.76	0.622	2.85	0.427	<0.7885

Figure 0.2

Segmentation and Quantification of Venous structures and Perivascular Spaces in the Thalamus in Epilepsy Patients at 7T

Mackenzie Langan[1,2], Gaurav Verma[1], Derek Smith[1], Bradley Delman[3], Madeline Fields[4], Rebecca Feldman*[5], and Priti Balchandani*[1]

[1] 1. Biomedical Engineering and Imaging Institute, Icahn School of Medicine at Mount Sinai, New York, NY, United States
[2] Icahn School of Medicine, Graduate School of Biomedical Sciences, New York, NY, United States
[3] Diagnostic, Molecular and Interventional Radiology, Icahn School of Medicine at Mount Sinai, New York, NY, United States
[4] Department of Neurology, Mount Sinai Hospital, New York, NY, United States
[5] University of British Columbia, Vancouver, BC, Canada

Introduction: Epilepsy is a neurological disorder, affecting 50 million people worldwide1. Approximately $1/3$ of epileptic patients do not respond to anti-seizure medications2. Persistent seizures may be correlated with network changes in the brain and the thalamus is thought to be one of the final common pathways for epilepsy, meaning mircostructural or vascular changes could contribute to changes or be a result of focal seizure networks. These changes could be indicative of larger alterations involving neuronal vasculature and neuroinflammatory processes linked to gylmphatic clearance dysfunction, such as perivascular spaces (PVS). These small fluid filled spaces in the brain may be a byproduct of seizure activity or dysfunction in vasculature and glymphatic clearence5. To visualize possible vascular abnormalities within the thalamus, integration of the high sensitivity and enhanced contrast achieved using ultra-high field (UHF) MRI, may be useful to identify abnormalities not detectable at lower field strengths, such as PVS3. Segmentation and quantification of vessels, PVS, and the overlap of PVS and vessels in the thalamus may provide insight into the role of glymphatic drainage, the thalamus and overall networks involved in epilepsy4.

Materials and Methods: An exploratory analysis was performed in ten subjects to explore vascular differences in patients with focal epilepsy relative to controls. Detection of PVS within the thalamus was performed using a frangi-based detection tool called PVSSAS. Figure 1 displays the coregistration and segmentation workflow. Differences in total number of PVS, vessels, overlaps (Figure 2), vessels with more than one PVS, and what percentage of PVS were perivenular, were quantified between groups using a Hessian detection filter linked on an 18-connected network.

Results: We found significant differences in the number of veins in epilepsy patients compared to controls ($P > 0.044$), but no significant differences between groups were detected (Table 1).

Conclusions: In this exploratory analysis, we developed a process for quantification and detection of vessels and PVS within the thalamus that may be important in the pathophysiology of epilepsy. There was a significant difference in the number of thalamic vessels in patients compared to controls. This increase within patients may be explained by increase in branching and may be used to measure integrity of vasculature in this region. We provided a potential tool which leverages UHF neuroimaging to measure detectable differences in vasculature and uncover possible underlying neuroinflammatory processes in epilepsy and may be useful to measure abnormal or disordered vessel growth that could be associated with or be a biproduct of increased seizure activity.

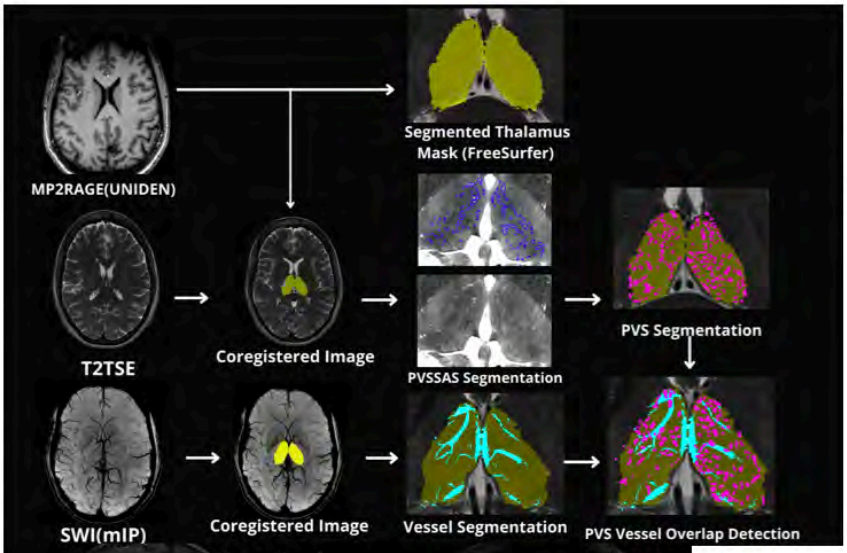

Figure 1. The processing workflow displaying thalamic segmentation, coregistration of thalamic masks, segmented PVS and overlaps between PVS and Vessels.

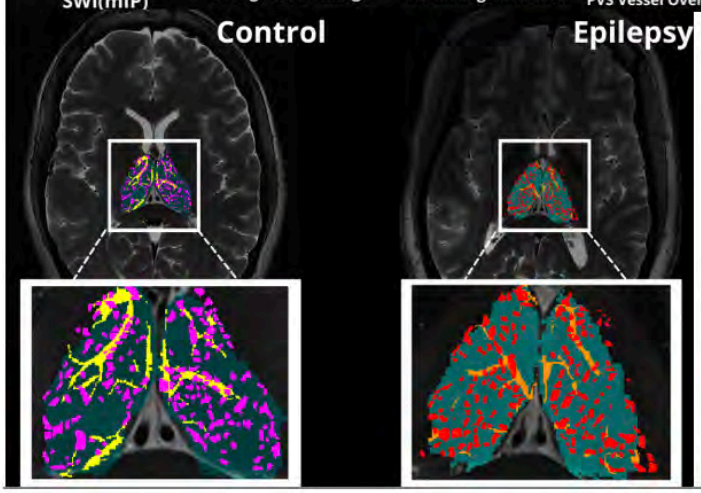

Figure 2. The subsequent overlaps of PVS and vessels in controls compared to epilepsy.

Table 1:

Metric	Control	Epilepsy	*p* value
Average Total Number of PVS	183.8	243.6	<0.386
Average Total Number of Vessels	61	84	**<0.044**
Average Number overlaps	57.4	63.6	<0.612
Percent PVS Perivenular	31.37	29.66	<0.814
Average Number of Vessels with >1 PVS	5.8	5.8	<0.851
Vessel Density	0.005	0.007	<0.106

Figure 0.3

A New Look at Artificial Intelligence and Machine Learning for Computer-aided Diagnosis

Zhengrong Liang[1,2], Marc J. Pomeroy[2], Weiguo Cao[1], Shaojie Chang[1], Jiaxing Tan[3], Ti Bai[4], Yongfeng Gao[1], and Perry J. Pichkardt[5]

[1] Department of Radiology, Stony Brook University, Stony Brook, NY 11794
[2] Department of Biomedical Engineering, Stony Brook University, Stony Brook, NY 11794
[3] Department of Computer Science, City University of New York at CSI, NY 10314, USA
[4] Department of Radiation Oncology, University of Texas Southwestern Medical Centre, Dallas, TX 75390, USA
[5] Department of Radiology, School of Medicine, University of Wisconsin, Madison, WI 53792, USA

Introduction: Computer-aided-diagnosis (CADx) of lesions has been facing the challenge of limited data available because its core technology, machine learning (ML), requires large data. Experts incorporate prior knowledge about lesions into consideration in addition to the available data. This study mimics the experts' performance by modeling prior knowledge in ML for CADx under the condition of limited data, called artificial intelligence (AI)-driven ML-CADx.

Materials and Methods: Computed tomography images of 87 colon polyps (44 malignant and 43 benign) and 67 lung nodules (49 malignant and 18 benign) were extracted from routine patient scans, where the malignant and benign classifications are labeled by the pathological reports of the lesions.

For comparison purposes, two references are set. (1) deep learning (DL)-based CADx, where a mask of rectangular shape is used to crop the lesions' volumes as the inputs. The DL-CADx extracts image features and classifies the features for lesion diagnosis in an end-to-end fashion. (2) traditional learning (TL)-based CADx, where the border of each lesion is manually drawn for a lesion-specific volume. From each volume, a set of image intensity distribution texture features, described by the gray level co-occurrence matrix (GLCM), are computed and classified by the Random Forest (RF) classifier for lesion diagnosis.

One implementation of the presented AI-ML-CADx is based on the TL-CADx pipeline. The lesion modeling is performed on the lesion-specific volume I(x,y,z), where (x,y,z) specifies the coordinates of each image voxel inside the lesion volume. From the image volume I(x,y,z), different mathematical operators are used to compute the quantitative lesion descriptors, which reflect the lesion properties, such as lesion tissue heterogeneity, dynamics, elasticity, and response to X-ray energy. The extracted quantitative lesion descriptors are then inputted to the RF classifier to lesion diagnosis. Another implementation is based on the DL-CADx pipeline, where the GLCMs are the inputs for an end-to-end procedure.

The performances of the four CADx methods are compared using the figure of merit of area under curve of receiver operating characteristics (AUC).

Results: The DL-CADx/TL-CADx/AI-ML-CADx reached AUC scores of 0.84 / 0.87 / 0.98 for the polyp dataset and 0.77 / 0.79 / 0.86 for the nodule dataset. The GLCM-DL-CADx reached AUC of 0.91 for the polyp dataset.

Conclusions: The gains by modeling prior knowledge about lesions into ML for both AI-ML-CADx and GLCM-DL-CADx under the condition of limited data are striking, indicating the great potential of exploring the modeling strategy of human intelligence for AI-driven ML-CADx.

Multiparametric immunoimaging maps inflammatory signatures in murine myocardial infarction models

Alexander Maier[1,2,3], Yohana C. Toner[1,2,4], Jazz Munitz[1,2], Abraham J. P. Teunissen[1,2,5,6], Claudia Calcagno1[1,2], Zahi A. Fayad[1,2], Willem J. M. Mulder[1,2,4,7], Mandy M. T. van Leent[1,2,5]

[1] 1BioMedical Engineering and Imaging Institute, Icahn School of Medicine at Mount Sinai, New York, USA
[2] Diagnostic, Molecular and Interventional Radiology, Icahn School of Medicine at Mount Sinai, New York, NY, USA
[3] Department of Cardiology and Angiology I, Heart Center Freiburg University, Faculty of Medicine, University of Freiburg, Germany
[4] Department of Internal Medicine and Radboud Institute for Molecular Life Sciences, Radboud University Medical Center, 6525 GA Nijmegen, Netherlands
[5] Cardiovascular Research Institute, Icahn School of Medicine at Mount Sinai, New York, USA
[6] Icahn Genomics Institute, Icahn School of Medicine at Mount Sinai, New York, NY, USA.
[7] Department of Chemical Biology, Eindhoven University of Technology, 5612 AZ Eindhoven, Netherlands.

Introduction: The immune response following acute myocardial infarction (MI) encompasses a delicate balance between inflammatory and reparative programs. Our knowledge of these complex mechanisms is mainly derived from studies using a murine model of permanent coronary artery occlusion. In this study we developed, validated and implemented multiparametric imaging methods to investigate cardiac function and the systemic immune response in transient or permanent coronary artery occlusion mouse models.

Materials and Methods: The MI models encompassed either transient (40 min, refered to as ischemia reperfusion, IR) or permanent occlusion (PO) of the left coronary artery, and non-infarcted mice were used as controls. Both models were applied to male C57BL/6 mice. One, two or three days after MI, the animals subjected to systemic immunoimaging of the bone marrow, spleen and myocardium. We performed late gadolinium-enhanced (LGE) and 19F-cardiac magnetic resonance imaging (cMRI), ^{18}F-fluorodeoxyglucose (FDG) positron emission tomography (PET) and ^{18}F-fluorothymidine (FLT) PET. We also performed PET imaging using a 64Cu-labeled tracer targeting chemokine receptor 2 (CCR2) and an ^{89}Zr-labeled nanobody targeting CD11b. Finally, the same MI models were applied to atherosclerosis-prone Apoe-/- mice and systemic inflammation and plaque progression were assessed by flow cytometry and immunohistochemistry four weeks after infarction.

Results: Through LGE cMRI, we observed that IR resulted in a smaller infarct size and better cardiac function compared to PO (Panel a). ^{89}Zr-CD11b nanobody and 64Cu-CCR2 PET demonstrated that mice subjected to IR had less immune cell influx to the ischemic myocardium compared to mice subjected to PO (Panels b and c). This finding was confirmed by flow cytometry analysis of the infarct zone. In contrast, both MI models cause a similar systemic immune response in the bone marrow and spleen as observed with multimodal imaging (Panels d and e). Both IR and PO aggravate atherosclerosis in Apoe-/- mice with higher macrophage and Ly6Chi monocyte numbers in aortas and larger plaque size compared to Apoe-/- mice without MI (Panel f).

Conclusions: We developed and employed multimodal, multiparametric imaging protocols to characterize the immune response in the heart, bone marrow and spleen in two models of myocardial infarction. While cardiac function was superior in the IR model, both types of MI accelerated atherosclerosis.

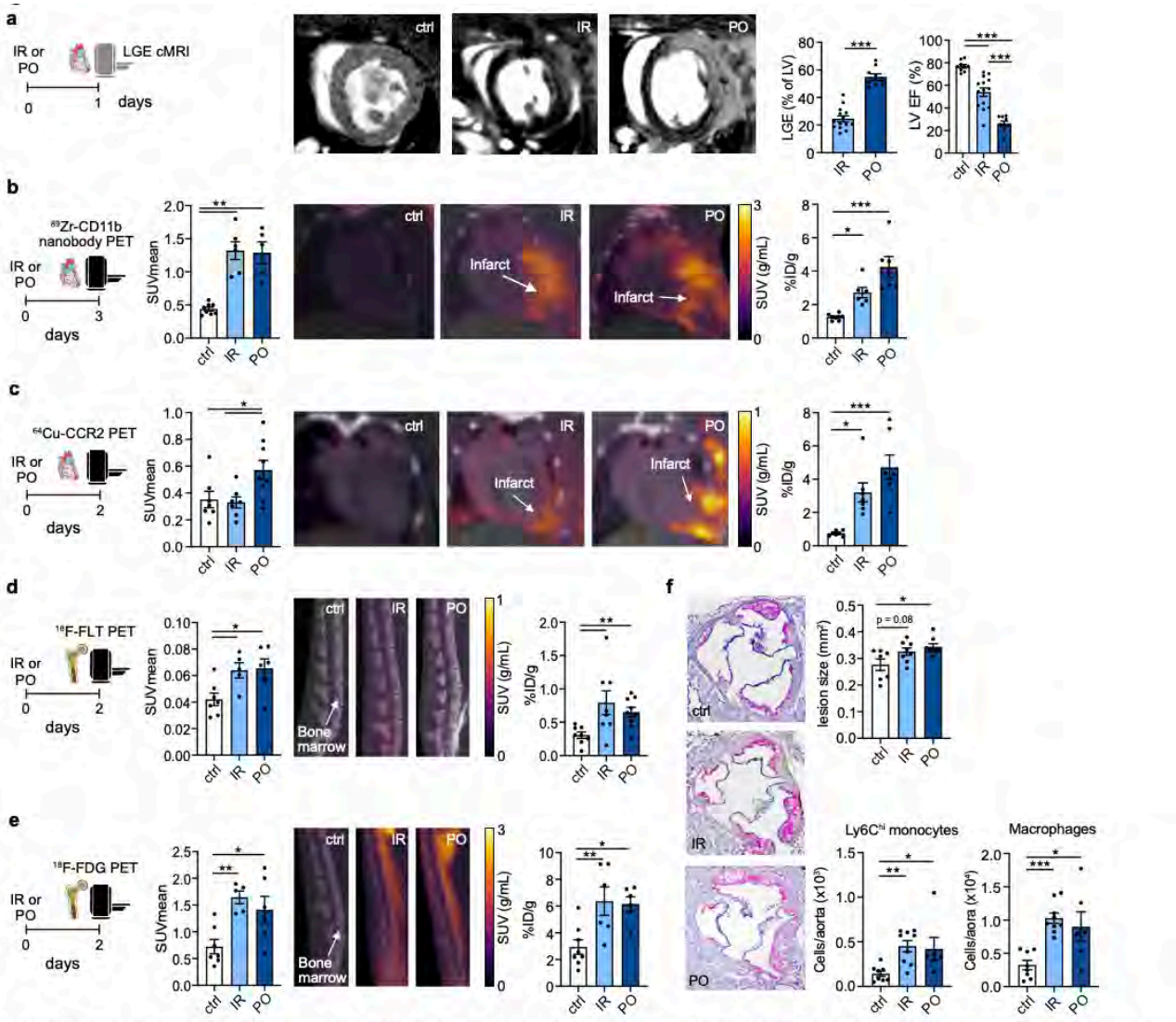

Multiparametric immunoimaging maps inflammatory signatures in murine myocardial infarction models. (a) Necrosis imaging with LGE cMRI. LGE area in % of the left ventricle (n = 9-14, ***p < 0.0001, two-tailed Student's t-test). Left ventricular ejection fraction (LVEF) in % (n = 9-14, ***p < 0.0001 for IR vs. PO, ctrl. vs. IR, and ctrl. vs. PO, one-way ANOVA). (**b**) ^{89}Zr-CD11b nanobody PET was performed three days after IR/PO surgery. Quantification of ^{89}Zr-CD11b nanobody signal in the infarct area (n = 5-8, **p = 0.0021 ctrl. vs. IR and **p = 0.0021 ctrl. vs PO), representative ^{89}Zr-CD11b nanobody PET/CT images and *ex vivo* quantification of ^{89}Zr-CD11b uptake (n = 6-8, *p = 0.0189 ctrl. vs. IR and ***p < 0.0001 ctrl. vs PO). (**c**) ^{64}Cu-CCR2 PET was performed two days after IR/PO surgery. Quantification of ^{64}Cu-CCR2 signal in the infarct zone (n = 7-9, *p = 0.0327 ctrl. vs. IR and *p = 0.0327 ctrl. vs PO), representative ^{64}Cu-CCR2 PET/CT images and *ex vivo* gamma counting of ^{64}Cu-CCR2 uptake (n=7, *p = 0.0110 ctrl. vs. IR and ***p = 0.0002 ctrl. vs PO). (**d**) ^{18}F-FLT PET/CT was performed two days after IR/PO surgery. Quantification of ^{18}F-FLT signal in the lumbar vertebrae (n = 5-7, *p = 0.0317 ctrl. vs. IR and *p = 0.0177 ctrl. vs. PO), representative ^{18}F-FLT PET/CT images and *ex vivo* gamma counting of ^{18}F-FLT uptake in the femoral bone marrow (n = 8-9, **p = 0.0059 ctrl. vs. IR and **p = 0.0064 ctrl. vs. PO). (**e**) ^{18}F-FDG PET was performed two days after IR/PO surgery. Quantification of ^{18}F-FDG signal in the lumbar vertebrae (n = 5-7, **p = 0.0052 ctrl. vs. IR and *p = 0.0253 ctrl. vs. PO), representative images and *ex vivo* gamma counting of ^{18}F-FDG uptake in the femoral bone marrow (n = 6-8, **p = 0.0078 ctrl. vs. IR and *p = 0.0106 ctrl. vs. PO). (**f**) Exemplary images of haematoxylin-stained aortic roots four weeks after IR/PO surgery and quantification of lesion size (n = 6-9, p = 0.0792 ctrl. vs. IR and *p = 0.01 ctrl. vs PO). Ly6C^{hi} monocyte (n = 6-9, **p = 0.0024 ctrl. vs. IR and *p = 0.0209 ctrl. vs PO) and macrophage numbers (n = 6-9, ***p = 0.0004 ctrl. vs. IR and *p = 0.0298 ctrl. vs PO) in aortas four weeks after IR/PO surgery as assessed by flow cytometry. Kruskal-Wallis test were used for all panels unless specified otherwise.

Figure 0.1

Targeted Self-Assembled Protein Micelles for Biomedical Imaging

Heather Mao[1] , Andrew L. Wang[1,2] , Orin Mishkit[3,4], Lakshmi Arivazhagan[4], Maxwell La Forest[4], Casey Donohoe[4], Ann Marie Schmidt[4], Edward A. Fisher[4], Youssef Z. Wadghiri[3,4], Jin Kim Montclare[1,3,5,6]

[1] Department of Chemical and Biomolecular Engineering, New York University Tandon School of Engineering, Brooklyn, NY 11201, United States
[2] Department of Biomedical Engineering, SUNY Downstate Health Sciences University, Brooklyn, NY 11203, United States
[3] Department of Radiology, NYU Langone Health, New York, NY 10016, United States
[4] Department of Medicine, NYU Grossman School of Medicine, New York, NY 10016, United States
[5] Department of Chemistry, New York University, New York, NY 10003, United States
[6] Department of Molecular Pathobiology Biomaterials Division, New York University College of Dentistry, New York, NY, 10010, United States

Introduction: Combined imaging contrast agents and drug carriers may potentially revolutionize prognostic and diagnostic decision making while also improving therapeutic efficiency. Specificity is the key to avoiding off-target binding that can lead to unwanted signals or side effects. Thermoresponsive assembled protein (TRAP) is a synthetic protein construct which is composed of two major domains: a coiled-coil domain derived from cartilage oligomeric matric protein (COMPcc) and an intrinsically disordered elastin-like polypeptide (ELP) domain. TRAP exhibits temperature- and concentration-dependent micellar self-assembly. Because of the multimeric structure of this micelle, there is the potential for strong multivalent binding of targeting peptides. We introduce a targeted variant of TRAPs with the ability to bind to type I collagen (COL1-TRAP), enabling specific and longitudinal imaging of non-alcoholic fatty liver disease (NAFLD) *in vivo*. The physicochemical properties of COL1-TRAP were characterized *in vitro* and the *in vivo* pharmacokinetics and biodistribution were evaluated in a mouse model of NAFLD. COL1-TRAP shows promise as a sensitive and versatile method for monitoring the progression of NAFLD.

Materials and Methods: Circular dichroism was used to confirm the secondary structure of COL1-TRAP and P51-TRAP, while sodium dodecyl sulfate-polyacrylamide gel electrophoresis (SDS-PAGE) and matrix-assisted laser desorption/ionization mass spectrometry (MALDI MS) were used to evaluate the molecular weight of both proteins. The size, concentration and temperature dependence of COL1-TRAP micellar assembly was assessed by using light scattering and fluorescence polarization. Enzyme-linked immunosorbent assay (ELISA) was utilized to measure the binding affinity between protein micelles for collagen type I. Mouse models of NAFLD were injected intracardially with COL1-TRAP conjugated to a near-infrared fluorescent dye, and blood was collected at regular intervals to measure serum half-life. Biodistribution was assessed with *ex vivo* organ fluorescence imaging.

Results: The molecular weight and secondary structure of COL1-TRAP is as expected. COL1-TRAP forms micelles at the temperature of 20 °C and undergoes hydrophobic collapse above 38 °C. Dynamic light scattering shows a sharp increase in size above this higher temperature, consistent with aggregation. The binding affinity (Kd) for collagen type I obtained through indirect ELISA was in the range of 0.558 μM. The *in vivo* experiments showed that the non-alcoholic steatohepatitis (NASH) mice had a higher accumulation signals of COL1-TRAP when comparing to other organs and Chow diet mice groups.

Conclusions: We designed and characterized a new TRAP construct, COL1-TRAP, with the goal of targeted imaging of NAFLD, with the potential for future drug delivery applications.

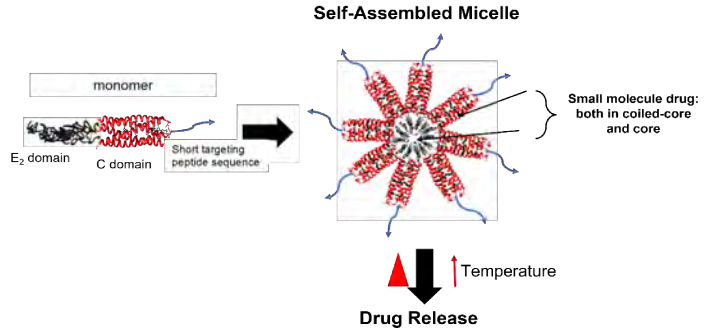

Figure 1:
Design of targeted TRAP variants with proposed micellar assembly. TRAP undergoes temperature responsive hydrophobic collapse, resulting in drug release.

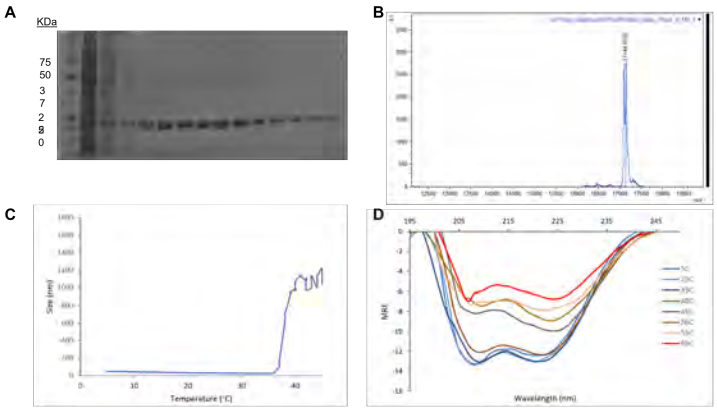

Figure 2. Characterization of COL1-TRAP. **A.** Purification gel showing an expected molecular weight ~17 kDa. **B.** MALDI-TOF verification of molecular weight. **C.** Dynamic light scattering results of temperature dependence of size, showing sharp aggregation above inverse transition temperature of ELP. **D.** Circular dichroism analysis of protein secondary structure showing transition to a more beta-sheet like structure above the same.

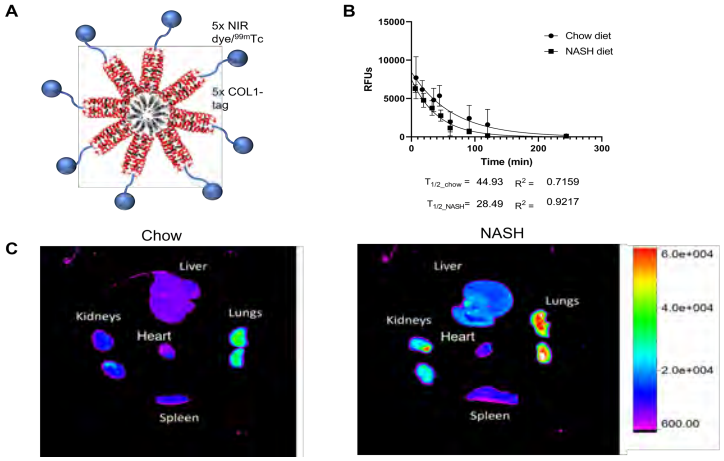

Figure 3. *In vivo* biodistribution and pharmacokinetics of COL1-TRAP. **A.** COL1-TRAP labeled with NIR dye **B.** Serum pharmacokinetics of COL1-TRAP in Chow- and NASH-diet fed mice **C.** *Ex vivo* organ biodistribution of COL1-TRAP in measured by fluorescence imaging.

Evolution of brain circuits supporting spatial navigational memory across sleep

Ankit Parekh[1], Korey Kam[1], Daphne Valencia[1], Amad Fakhoury[1], Lazar Fleysher[1], Bresne Castillo[1], David M. Rapoport[1], Indu Ayappa[1], Andrew W. Varga[1]

[1] Division of Pulmonary, Critical Care and Sleep Medicine, Department of Medicine, Icahn School of Medicine at Mount Sinai

Introduction: Systems consolidation is one of the major theories of sleep's function in memory. Sleep is thought to be important in integrating and distributing hippocampal information to cortical structures such that there is less hippocampal activation, while at the same time increasing striatal activation, upon subsequent experience in the same environment that co-occurs with improved performance. Here we sought to examine the evidence supporting systems consolidation across sleep in spatial navigational memory.

Materials and Methods: 15 healthy subjects (28$\pm$5 yrs., 8 female) with no prior videogame experience and no sleep disorders were recruited to undergo spatial navigational memory testing before and after a night of sleep. Spatial navigational memory was tested across two functional MR (fMRI) sessions (approx. 7PM and 8AM) separated by in-lab nocturnal polysomnography (NPSG) measured sleep using a virtual 3D Maze. Each fMRI session consisted of six runs: three maze trials interleaved with three control trials. During maze trials participants were instructed to reach a prespecified goal as quickly as possible, whereas during the control trials, participants were instructed to navigate a Z-shaped corridor. fMRI data was analyzed in 2-step procedure using Analysis of Functional Neuroimages (AFNI) software package. To estimate hippocampal activity during fMRI, parameter estimates of the change in blood-oxygen-level-dependent (BOLD) signal using the contrast maze-control were used as the primary metric. Regions of interest were limited to the bilateral hippocampus, parahippocampal gyrus, caudate, and putamen using the Eickhoff-Zilles macro labels from the MNI-N27 template.

Results: During in-lab NPSG, participants experienced a total sleep time of 6.1$\pm$1.1 hrs (8.7$\pm$2.9 stage1, 51.2$\pm$7.6 stage2, 21.8$\pm$8.5 stage3, 18.1$\pm$6. REM). Within subjects, compared to pre-sleep, a significantly lower activation of the bilateral hippocampus and parahippocampal gyrus was observed post-sleep (Fig. 1; evening-morning change=0.26$\pm$0.11, $p<0.05$). Compared to pre-sleep, caudate and putamen activity was not significantly different post-sleep (evening-morning change=-0.02$\pm$0.04,p=0.5). Greater evening hippocampal activity was associated with greater change in maze completion times across sleep (rho=0.52, p=0.04).

Conclusions: In young healthy adults, a night of uninterrupted sleep supports redistribution of hippocampal contribution toward spatial navigation. Greater initial pre-sleep hippocampal contribution was associated with improved recall of spatial navigational memory after a night of sleep.

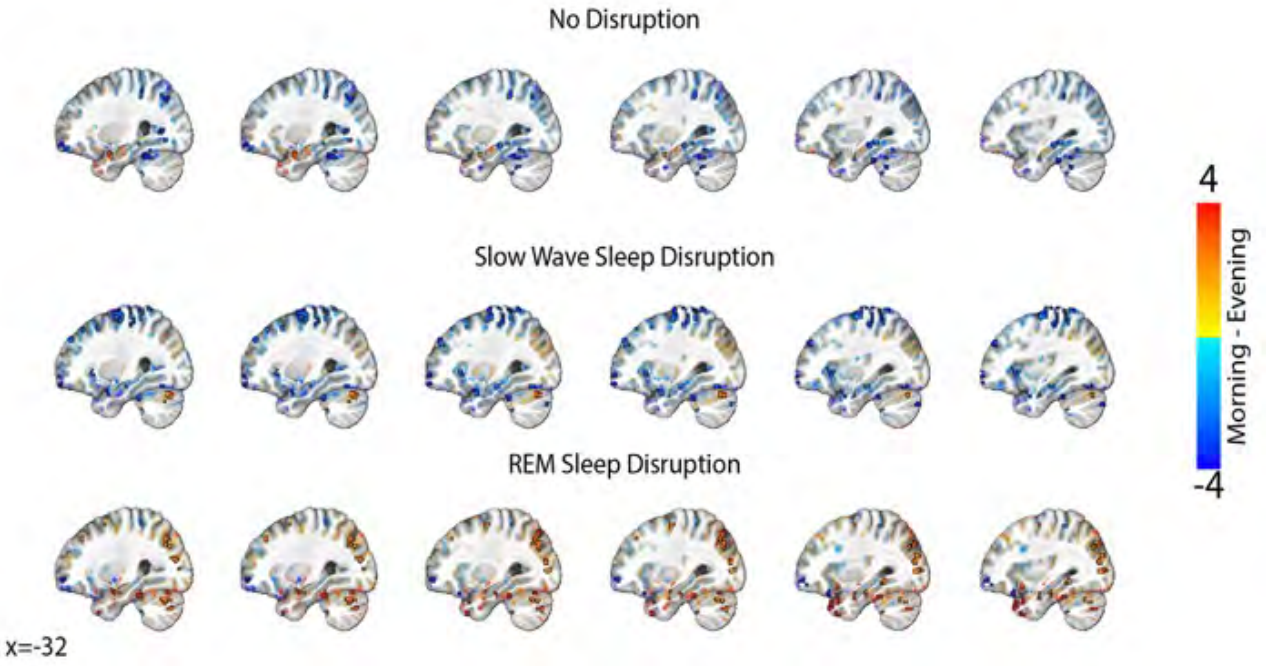
No Disruption
Slow Wave Sleep Disruption
REM Sleep Disruption
x=-32
4
Morning - Evening
-4

Figure 0.1

Development of a graphical tool for measuring coronary artery spatially weighted calcium score from cardiac CT images

Heli J Patel[1], Audrey E Kaufman[1], Marco Pereanez[1], Georgios Soultanidis[1], Sarayu Ramachandran[1], Sonum Naidu[1], Venkatesh Mani[1], Zahi A Fayad[1], Philip Robson[1]

[1] BioMedical Engineering and Imaging Institute, Icahn School of Medicine at Mount Sinai, New York, NY, United States

Introduction: Measuring the amount of calcium within arteries using CT is an established way to assess the severity of coronary atherosclerosis. Current metrics, such as the Agatston score, use thresholding and are not sensitive to low levels of calcification. A previously described metric, called the spatially weighted calcium score (SWCS), was proposed to assess the risk of atherosclerotic plaque in patients with low levels of calcification (Liang et al., BMC Medical Imaging 2012 vol. 12, pg. 7). We are currently developing a semi-automated tool that uses MATLAB to label the path of the coronary artery on CT scans for the purpose of calculating the SWCS. A requirement of the tool will be that the same SWCS should be measured independently of the orientation of the vessel within the imaging volume. In addition, we note that, from the definition of the SWCS (Figure 1), it is apparent that the SWCS depends on the number of points identified as belonging to the vessel path. Moreover, for vessel paths that travel in the plane of the CT image, the number of pixels identified and the resulting SWCS will depend on the aspect ratio of the image pixels. In this work, we sought to develop a phantom containing a fixed quantity of radio-opaque material that could be imaged in any orientation to demonstrate the dependence of SWCS on the number of pixels included in the measurement.

Materials and Methods: A phantom comprised a nasal oxygen cannula filled with iodinated contrast agent (Figure 2). Two scans of the tube were obtained: 1) laid flat (straight) along the length of the scanner perpendicular to the axial image plane, and 2) wrapped once around a hollow, cardboard pipe (curved) with the pipe along the length of the scanner. The image voxel size was 0.3x0.3x1.5 mm^3, giving an aspect ratio of 5. Our tool's graphical user interface was then used to select points on contiguous slices of the scans (Figure 3). For the straight and curved tubes, three measurements were made where a single point was placed on all, every other, and every fourth slice. In addition, the curved tube was assessed again with interpolation of points along the path of the vessel segment that was in the image plane (two points were selected at each end of the segment and intermediate points interpolated by the program). The tool applied the SWCS formula to each point and aggregated the scores to obtain a final SWCS.

Results: Results show a direct, positive correlation between the number of points and the associated SWCS. In addition, the ratio of the number of points for the curved phantom with interpolation and the points for the straight tube was approximately 7. Results are summarized in Table 1.

Conclusions: The SWCS depends on the number of points placed. Also, the number of points included increased for the curved phantom with interpolation of in-plane points as expected. The number of points increased by a factor of 7, which was higher than the expected factor of 5 from considering the aspect ratio of the image voxels. This discrepancy could possibly be rectified by using images with isotropic resolution or by normalizing the data by pixel volume. An additional limitation was that the lumen diameter of the phantom was large compared to the pixel size, possibly introducing spillover between consecutive slices.

Table 1: Results of using our tool on straight versus curved tubes

		No Interpolation			Interpolation			
	Labeled Slice Frequency	Number of points (NoP)	SWCS	Ratio of SWCS relative to NoP	Number of points (NoP)	SWCS	Ratio of SWCS relative to NoP	Ratio of NoP in cuved, interpolated tube to NoP in straight tube
Straight	All	94	376	4	N/A			
	Every other	47	188	4				
	Every fourth	24	96	4				
Curved	All	27	105.231	3.897	655	2193.148	3.348	6.968
	Every other	14	56	4	325	1121.851	3.452	6.915
	Every fourth	7	20	2.857	172	566.297	3.292	7.167

Figure 0.1

$$SWCS = \sum_{j=1}^{m} s_j$$

$$s_i = w(a_i) \times \sum_{k=1, k \neq i}^{m} w(a_k)\delta_{ik}$$

$$w(a_i) = \Phi(a_i; \mu_{100} + 2\sigma_{100}, \sigma^2_{100})$$

Term	Represents
s_i	Voxel's spatially weighted score
$w(a_i)$	Voxel's assigned weight
m	Total number of voxels identified as belonging to the vessel across all CT slices
a_i	Attenuation level of the ith voxel
δ_{ik}	1 if the ith and kth voxel are neighbors; 0 otherwise
$\Phi(x; \mu, \sigma^2)$	Cumulative Normal distribution with mean μ and variance σ^2 evaluated at x
μ_{100}	Sample mean of the Hounsfield Unit (HU) of the reference 100 mg/mL calcium voxels*
σ^2_{100}	Sample variance of the HU of the reference 100 mg/mL calcium voxels*

Figure 1: SWCS equation, along with table listing what each term represents
*To provide image-based signal normalization for estimation of SWCS, a phantom with known concentration of calcium (100 mg/mL) is included in the field of view

Figure 2: Photographs of contrast-filled nasal cannula in straight (left) and curved (right) configuration on CT gantry

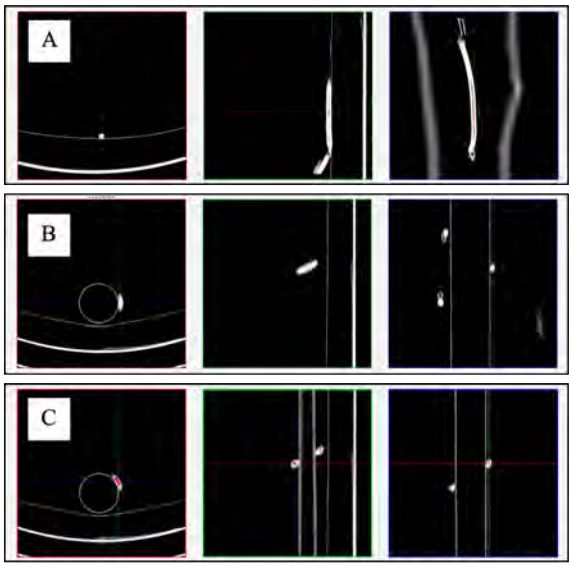

Figure 3: CT scan of contrast-filled phantom in axial, sagittal, and coronal plane (from left to right). Each view shows crosshairs on one labeled point. Points are shown as red dots. A. Straight tube, B. Curved tube without interpolation, C. Curved tube with interpolation

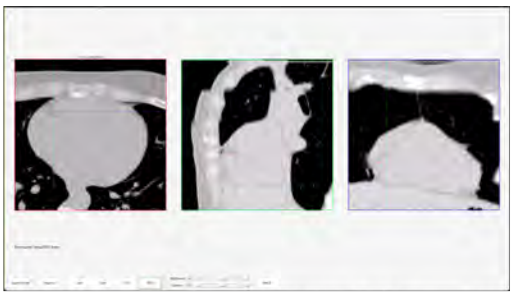

Figure 4: Cardiac CT, with crosshairs marking a single point in the right coronary artery in axial, sagittal, and coronal planes, as viewed in our SWCS tool workstation

^{89}Zr-ApoA1-mimetic peptide as radiotracer for lipoproteins present in macrophages

Geoffrey Prévot[1], Yohana C. Toner[1,2], Mandy M.T. van Leent[1,3], Jazz Munitz[1], Roderick Oosterwijk[1], Anna Vera Verschuur[1], Yuri van Elsas[1], Anne de Dreu[4], Jessica Chimene Fernandes[1], Judit Morla-Folch[1], Nathaniel Sullivan[1], Alexander Maier[1], Christian Mason[1], Thomas Reiner[1], Zahi A. Fayad[1], Willem J.M. Mulder[1,2,4], Abraham J.P. Teunissen[1,3,6], Carlos Pérez-Medina[1,7]

[1] BioMedical Engineering and Imaging Institute, Icahn School of Medicine at Mount Sinai, NY, USA
[2] Department of Internal Medicine and Radboud Center for Infectious Diseases, Radboud University Medical Center, Nijmegen, the Netherlands
[3] Cardiovascular Research Institute, Icahn School of Medicine at Mount Sinai, NY, USA
[4] Laboratory of Chemical Biology, Department of Biochemical Engineering, Eindhoven University of Technology, Eindhoven, The Netherlands
[5] Department of Radiology, Memorial Sloan-Kettering Cancer Center, NY, USA
[6] Icahn Genomics Institute, Icahn School of Medicine at Mount Sinai, NY, USA
[7] Centro Nacional de Investigaciones Cardiovasculares (CNIC), Madrid, Spain

Introduction: Macrophages are involved in physiological and pathophysiological processes, such as myocardial infarct and stroke or cancer, becoming key regulators at the affected tissue. Consequently, macrophages are not just an appealing therapeutic target, but also a valuable diagnostic marker. Several imaging approaches to probe macrophages have been reported in a number of pathological contexts and employing a variety of techniques (i.e, MRI, PET or optical methods), however the lack of specificity towards macrophages it's been the principal limitation. In previous studies it has been demonstrated that high-density lipoprotein (HDL), a natural nanoparticle involved in reverse cholesterol transport, binds to several membrane receptors abundantly expressed on macrophages. The main component on the HDL nanoparticles driving to macrophages membrane receptors is apolipoprotein A1 (apoA1). Capitalizing on this, we designed a tracer that uses mimetic apoA1 (mA1), as opposed to native apoA1 protein, as a potential tool for the study of macrophage burden in mouse models of CVD and cancer.

Materials and Methods: We radiolabeled an apoA1-mimetic peptide (mA1) with zirconium-89 (^{89}Zr) for in vivo macrophage PET imaging. We first characterized ^{89}Zr-mA1's ability to bind to lipoproteins in vitro by size exclusion chromatography, and then corroborated those results in vivo using C57BL/6 and Apoe-/- mice by means of extensive pharmacokinetic. Mouse models of myocardial infarction (MI) and melanoma were used as model of inflammation to study macrophage accumulation through biodistribution and PET imaging studies. Cell specificity was assessed by histology and mass cytometry (CyTOF) using non-radioactive natZr-mA1 at radiotracer relevant doses.

Results: Our data strongly suggests that ^{89}Zr-mA1 bound to lipoproteins both in vitro and in vivo, which resulted in longer circulation times in hypercholesterolemic Apoe-/- mice compared to C57BL/6 controls. ^{89}Zr-mA1 displays a tissue distribution profile similar to apoA1 and high-density lipoprotein, showing strong kidney and liver uptake as well as significant accumulation in bone marrow and spleen. The tracer favorably accumulated in the tumors of melanoma mice and the ischemic myocardium of infarcted animals. In these sites, the tracer was predominantly taken up by macrophages, as determined by mass cytometry (CyTOF).

Conclusions: Our results demonstrate that ^{89}Zr-mA1 has a lipoprotein affinity and thereby favorably accumulates in macrophages in vivo. ^{89}Zr-mA1's high macrophage affinity makes it a promising tool for non-invasively and quantitatively studying diseases characterized by marked changes in macrophage burden.

Quantitative Neuroimaging Findings of Whole Brain DTI Analysis of Long-COVID Patients At 7T

Ameen Al Qadi[1], Oleksandr Khegai[1], Shams Rashid[1], Sera Saju[1], Nathalie Jette[2], Bradley Delman[3], Priti Balchandani[1]

[1] Biomedical Engineering And Imaging Institute, New York NY
[2] Department Of Neurology, Mount Sinai Hospital, New York, NY
[3] Department Of Radiology, Mount Sinai Hospital, New York, NY

Introduction: Coronavirus Disease 2019 (COVID-19) is caused by the severe acute respiratory syndrome coronavirus 2, and causes chronic neurological symptoms that persist after treatment of the main infection, such as brain fog, anosmia, and ageusia[1,2]. Imaging studies have noted tissue microstructure differences in the brains of "Long-COVID" patients, although results conflict[3,4]. Using the superior image resolution and SNR of 7T MRI, we investigated the differences in white matter (WM) integrity by generating DTI tractography for a cohort of Long-COVID patients against healthy controls (HCs).

Materials and Methods: 9 Long-COVID patients and 6 HCs were scanned on a Siemens Magnetom 7T scanner (SiemensHealthcare, Erlangen, Germany) using a SC72CD gradient coil with a single coil transmit and a 32-channel receive elements (Nova Medical, Wilmington, MA, USA). Diffusion-weighted imaging was acquired using reverse phase-encoding in AP & PA directions. Imaging parameters included: b = 1500 s/mm^2, TR = 7200ms, TE = 67.6ms, FOV = 210 mm^2, resolution = 1.05mm^3, and 69 directions. Resulting DWI series were denoised, combined, and corrected for eddy distortions, subject motion, and B1 inhomogeneity using MRtrix[5]. Whole brain tractography, organized into 72 WM tracts, was then generated using TractSeg[6]. Fractional anisotropy (FA) and mean diffusivity (MD) were sampled and used to determine microstructural integrity by testing for group differences between Long-COVID patients and HCs for all tracts. Statistical analyses were performed in R[7].

Results: The left Inferior Cerebellar Peduncle (ICP) ($p < 0.05$), right ICP ($p < 0.05$), and left Parietal-Occipital Pontine (POPT) ($p < 0.05$) were found to have significantly lower MD in the Long-COVID cohort compared to HCs. **Conclusions:** Despite the small cohort, these results demonstrate clear group differences in WM tracts localized to the posterior fossa, occipital, and parietal lobes. These results agree in part with the findings in (3), who found significantly decreased global MD in COVID patients compared to HCs. Furthermore, the specific tracts exhibiting decreased MD were localized to regions responsible for autonomic regulation and sensory information processing. This may help explain the chronic presentation of neurological symptoms, even after treatment for main COVID symptoms.

WM tracts that showed difference when compared with contatraleral structure (such as the right POPT) yielded results close to, but not under the significance threshold. FA results were also not as sensitive as MD results, likely due to the low N. This is consistent with the literature (3), which found no significant differences in regional FA.

Acknowledgments: NCI R01CA202911 R21NS122389

References (DOI):1: 10.1001/jamaneurol.2020.1127 2: 10.1111/ane.13266 3: 10.1016/j.eclinm.2020.100484 4: 10.1007/s00134-020-06241-w 5: 10.1016/j.neuroimage.2019.116137 6: 10.1016/j.neuroimage.2018.07.070 7: https://www.R-project.org/

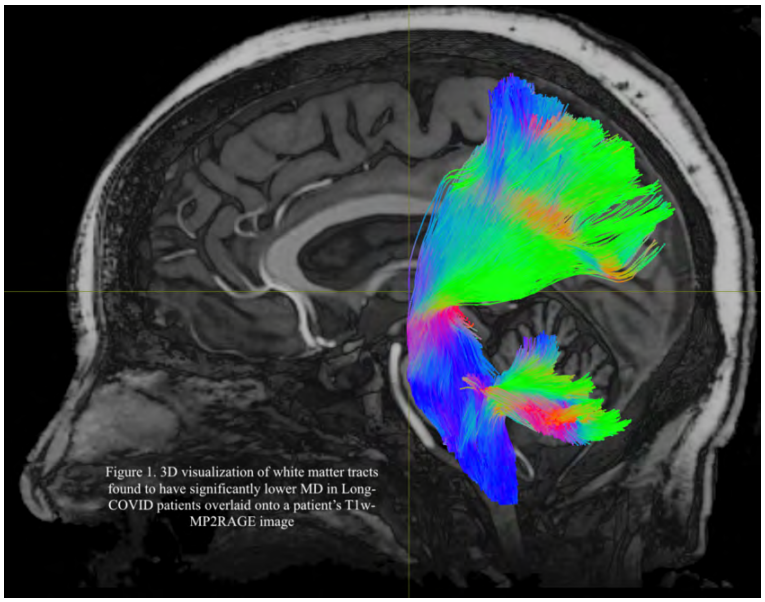

Figure 0.1

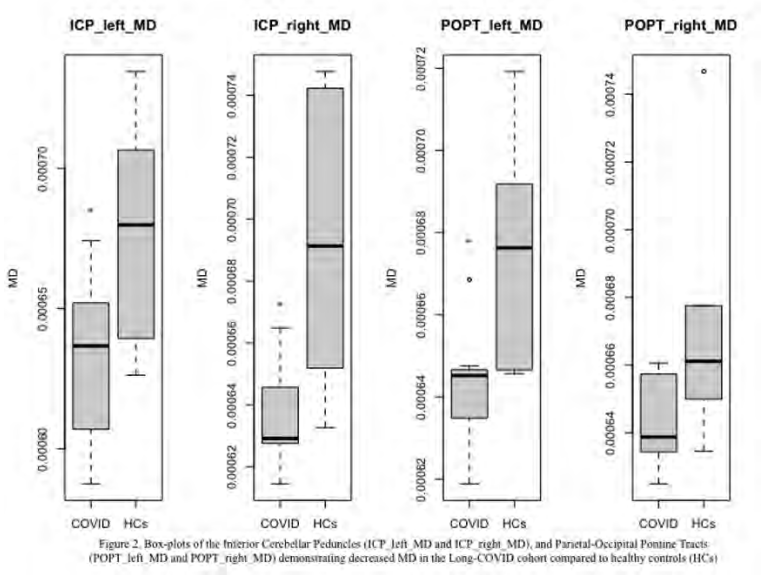

Figure 0.2

Ultrahigh-Field 7T MRI of the Brain of COVID-19 Patients with Neurological Symptoms: An Initial Study

Shams Rashid[1,2], Oleksandr Khegai[1], Nathalie Jette[3], Puneet Belani[1], Puneet Pawha[1], Sera Saju[1], Allison Navis[3], Brian Mathew[3], Jonathan Goldstein[3], Kapil Gururangan[3], Qing Hao[3], Anuradha Singh[3], Jacqueline Becker[4], Bradley Delman[1], Priti Balchandani[1,2]

[1] Diagnostic, Molecular and Interventional Radiology,
[2] BioMedical Engineering and Imaging Institute
[3] Neurology [4] General Internal Medicine, Icahn School of Medicine at Mount Sinai, New York, NY

Introduction: Since late 2019, the novel coronavirus disease 2019 (COVID-19) has emerged as a global pandemic. It is highly contagious, still ongoing and is confirmed to have infected 200 million and killed 5 million people worldwide. Many COVID-19 patients, after recovery, continue to have persistent neurological sequelae, which are not well understood, including stroke, visual defects, anosmia/dysgeusia, brain fog, among others. Long-haul COVID-19 syndrome is expected to become a serious healthcare burden. Here, we report our preliminary neuroradiological findings from ultrahigh-field 7T MRI in patients with post-COVID neurological symptoms.

Materials and Methods: Eight patients who had recovered from COVID-19 and presented with post-COVID neurological symptoms were enrolled. Patients underwent whole brain MRI on a Siemens Magnetom 7T scanner. The MRI protocol was specifically developed for this COVID-19 study and included MP2RAGE, FLAIR, T2-TSE, and other sequences. Images were evaluated by three neuroradiologists.

Results: The post-COVID neurological symptoms and the heterogeneous neuroradiological findings from 7T MRI are listed in Table-1. Bilateral olfactory bulb thinning was observed in Patient 4 (Figure-1), who presented with dysgeusia and COVID-long-haul syndrome. Brainstem abnormalities were observed in two patients (Figure-2). Chronic microhemorrhage and macrohemorrhage was observed in two patients (Figure-3), who presented with encephalopathy. Moderate FLAIR/T2 hyperintensities were observed in Patient 6 (Figure-4), who presented with several neurological symptoms including COVID long haul syndrome, numbness, headache and blurry vision. Incidental findings of prominent arachnoid granulations were observed in four patients, which may be unrelated to COVID-19. The time between COVID-19 diagnosis and 7T MRI was 12 ± 5 months.

Conclusions: It is interesting that these 7T brain-MRI findings persist even after 12 months post COVID infection. In particular, three of the patients in this study, who presented findings from 7T brain-MRI, did not present any findings from 1.5T brain-MRI during their COVID-related hospitalization. This may be due to lack of high resolution/SNR in the clinical exams, or these findings may be chronic in nature. It is also interesting that 4 patients presented incidental finding of prominent arachnoid granulations. This may indicate lymphatic involvement in the neurotropism of SARS-CoV-2 virus. This study is ongoing and in the early stages. We expect to find meaningful links between 7T neuroradiological findings and neurological symptoms in a larger cohort.

	Neurological Symptoms (post-COVID)	7T T2/FLAIR Hyperintensities (Fazekas scale)	Neuroradiological Findings from 7T MRI	Time between COVID Diagnosis and 7T MRI (months)	Sex	Age
Patient 1	Brain fog Headache	1	Brain volume loss greater than expected for age, Prominent arachnoid granulations	2	M	57
Patient 2	Encephalopathy	1	Brain volume loss greater than expected for age, Prominent arachnoid granulations, Chronic macrohemorrhages in right frontal cortex Brainstem microhemorrhage	11	F	58
Patient 3	Encephalopathy	1	Frontal and subinsular microhemorrhage Prominent arachnoid granulations	12	M	61
Patient 4	Dysgeusia COVID long haul syndrome	1	Thinned olfactory bulbs Hyperintensity of lower medulla tracts in brainstem	13	F	58
Patient 5	Anosmia/dysgeusia Brain fog	1	Incidental arachnoid cyst	14	M	52
Patient 6	COVID long haul syndrome Numbness in left face and thigh Daily headache, blurry vision R-MCA thrombus	2	Prominent arachnoid granulations Prominent perivascular spaces	14	F	60
Patient 7	Brain fog Poor language fluency	0	Incidental arachnoid cyst	18	F	31
Patient 8	Memory issues and brain fog Headaches Photophobia	1	Prominent arachnoid granulations	7	M	51

Table-1: Neuroradiological findings from 7T brain-MRI, post-COVID neurological symptoms and patient details.

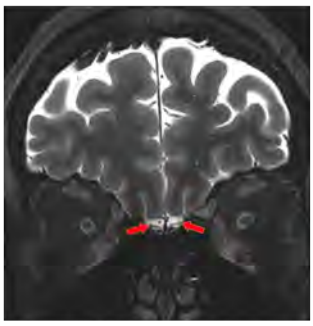

Figure-1: Bilateral thinning of olfactory bulbs (arrows) observed in a patient (Patient 4) with post-COVID symptom of dysgeusia

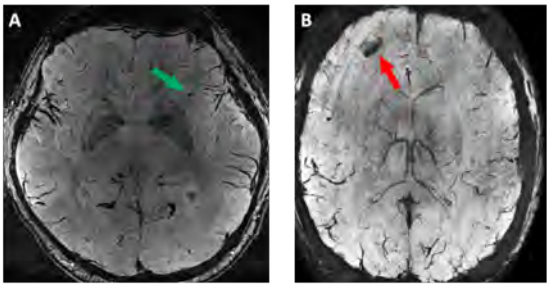

Figure-3: A: Susceptibility in left frontal subinsular region (green arrow) indicating chronic microhemorrhage in Patient 3. **B:** Susceptibility in right frontal cortex (red arrow) indicating chronic macrohemorrhage in Patient 4.

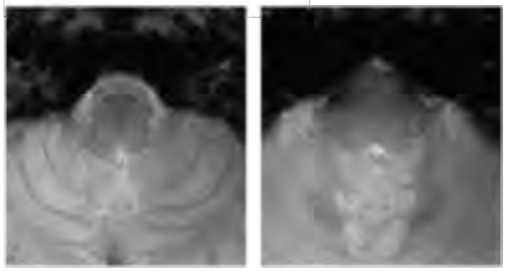

Figure-2: Example of brainstem images from Patient 4 in the lower medulla tracts, acquired with the T2*-weighted multiecho spoiled gradient echo (MEDIC) sequence.

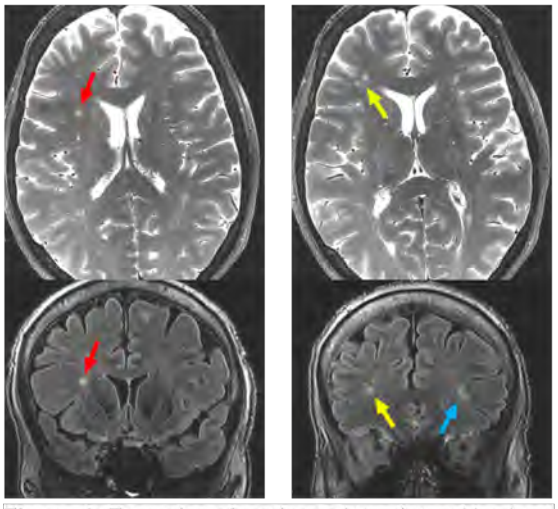

Figure-4: Examples of moderate hyperintensities in T2-weighted TSE (upper row) and FLAIR images (lower row) in Patient 6 (Fazekas scale 2).

Figure 0.1

Comparison of Physiological Noise Models for Thermal Stimulus fMRI in the Cervical Spinal Cord at 7T

Alan C. Seifert[1,2,3] and S. Johanna Vannesjo[4]

[1] D1Biomedical Engineering and Imaging Institute, Icahn School of Medicine at Mount Sinai, New York, NY USA
[2] Department of Radiology, Icahn School of Medicine at Mount Sinai, New York, NY USA
[3] Graduate School of Biomedical Sciences, Icahn School of Medicine at Mount Sinai, New York, NY USA
[4] Department of Physics, Norwegian University of Science and Technology (NTNU), Trondheim, Norway

Introduction: FMRI of the spinal cord is vulnerable to signal fluctuations due to respiration, motion, and pulsatile flow of cerebrospinal fluid (CSF). A suitable physiological noise model (PNM) is crucial for maximizing sensitivity to activation while rejecting non-BOLD signal. We imaged activation in the cervical cord using three 7T BOLD fMRI protocols, calculated correlations among components of a 37-term PNM and task model, and compared the results of analyses using four candidate PNMs.

Materials and Methods: C4-C7 vertebral levels of six healthy volunteers were scanned at 7T using one single-shot and two multi-shot EPI fMRI protocols. Pulse-oximeter and respiratory traces were acquired. Noxious thermal stimulation was applied to the right thumb at 3/10 intensity. GLM analysis was performed using four PNMs: a 37-term "FullPNM" (8 cardiac, 8 respiratory, 16 cardiac-respiratory interaction, heart rate (HR), respiratory volume per time (RVT), CSF signal, and 2 motion), a 35-term "NoRvtHr" (FullPNM minus HR and RVT), a 32-term "CardRespOnly" (8 cardiac, 8 respiratory, 16 cardiac-respiratory interaction), and a 3-term "CsfMcOnly" (CSF signal, and 2 motion correction).

Results: HR and RVT were correlated with task (r2$\sim$5 percent), while CSF and motion were only weakly correlated with task (r2$\sim$1 percent). CSF and motion were correlated with respiration, and CSF was also correlated with the cardiac cycle. Cardiac and respiratory terms are negligibly correlated with task. Relative to FullPNM, NoRvtHr yields slightly higher z-scores. CardRespOnly yields slightly higher z-scores, but z-scores and BOLD percent signal change are more variable than FullPNM or NoRvtHr. CsfMcOnly yields lower z-scores and BOLD percent signal changes.

Discussion and Conclusions: NoRvtHr may outperform FullPNM, although the margin is small, while CardRespOnly is variable and CsfMcOnly underperforms. CsfMcOnly is derived entirely from imaging data, and contains cardiac and respiratory information through their effects on CSF and motion. Generation of regressors directly from imaging data was expected to be particularly useful for multi-shot analyses, where data for a single temporal image frame is acquired in four shots at different phases of the cardiac and respiratory cycles. However, CsfMcOnly performed poorly, suggesting that an aggressively parsimonious PNM that maximizes degrees of freedom unnecessarily sacrifices terms that more fully explain non-BOLD signal contributions even in those additional cardiac and respiratory terms are not linked one-to-one with each temporal image frame. In 7T cervical spinal cord task fMRI, a comprehensive PNM is valuable, although terms that may be correlated with the task should be used with caution.

a)

	Z-Score				BOLD % Signal Change			
	Single-Shot 0.75 mm	4-Shot 0.75 mm	4-Shot 0.60 mm	Combined	Single-Shot 0.75 mm	4-Shot 0.75 mm	4-Shot 0.60 mm	Combined
Full PNM	2.80 ± 0.66	2.17 ± 0.82	2.68 ± 0.52	2.55 ± 0.70	0.81 ± 0.26	1.19 ± 0.49	2.93 ± 1.36	1.64 ± 1.24
No RVT or HR	3.00 ± 0.70	2.24 ± 0.76	2.70 ± 0.58	2.64 ± 0.72	0.87 ± 0.37	1.22 ± 0.44	2.94 ± 1.45	1.67 ± 1.26
Cardiac and Resp. Only	3.05 ± 0.89	2.12 ± 0.69	2.78 ± 1.00	2.65 ± 0.91	0.95 ± 0.44	1.36 ± 0.59	3.37 ± 2.02	1.90 ± 1.60
CSF and Motion Only	2.88 ± 0.61	2.19 ± 0.69	1.95 ± 0.94	2.34 ± 0.82	0.93 ± 0.52	1.13 ± 0.28	1.97 ± 1.25	1.34 ± 0.88

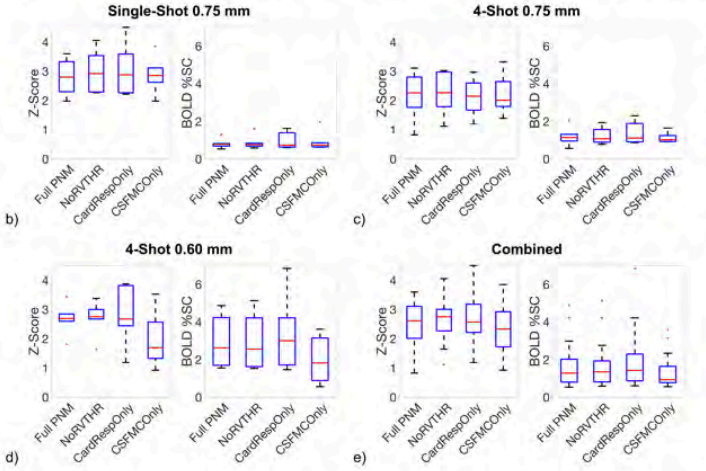

Figure 1: Table of z-scores and BOLD percent signal changes measured at the most significantly activated plausible voxel (i.e., located in the ipsilateral dorsal quadrant at a plausible vertebral level), both separately for each acquisition protocol, and for the combination of all three acquisition protocols (a). The same data are also displayed as boxplots (b-e). FullPNM and NoRvtHr are generally comparable, while CardRespOnly is more variable, and CsfMcOnly performs poorly.

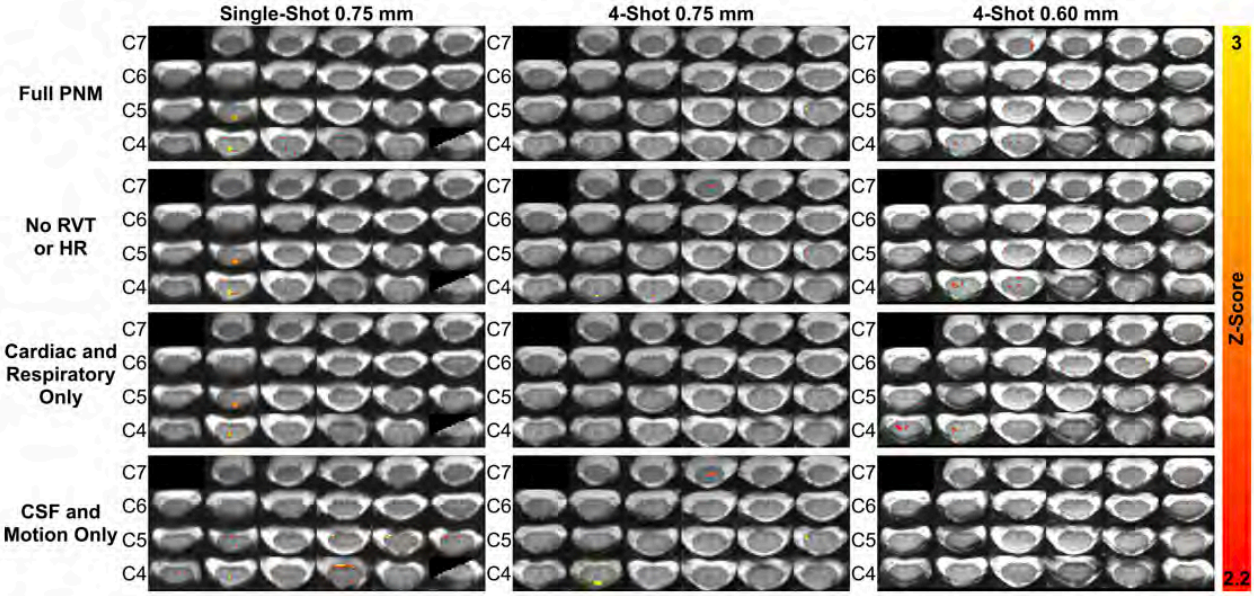

Figure 2: Activation maps for each acquisition protocol and PNM in a single representative subject. Relative to FullPNM, the NoRvtHr PNM slightly boosts significance of activation while introducing a small number of additional false positive voxels. CardRespOnly and CsfMcOnly produce variable changes in significance, but CsfMcOnly contributes a large number of additional false positive voxels.

Figure 0.2

The use of clinical information and CXR radiomics information for the classification of patient's severity

G. Soultanidis[1], V. Fauveau[1], M. Pereanez[1], Y. Yang[1], Z. A. Fayad[1]

[1] 1. BioMedical Engineering and Imaging Institute, Icahn School of Medicine at Mount Sinai, New York, NY, United States

Introduction: The SARS-CoV2 pandemic has strained the health system around the globe. The request for a fast and simple assessment of an infected patient's needs, based on easy to obtain information is crucial. One of the basic exams of a COVID-19 patient is a chest radiography (CXR) and basic physiological measurements with blood work. The purpose of this study is to use radiomics analysis, for the classification of patients into the ones that need to be admitted, intubated or possible to expire from the first CXR they receive when arriving at the hospital.

Materials and Methods: For this study, we used the database created at our hospital and selected the CXR of 467 patients. 252 patients of these were admitted for hospitalization. 77 of the admitted were intubated and 50 of the expired, expired. We performed the segmentation of the lungs manually and by using automated segmentation toolkit. This is the lungVAE, a neural network segmentation tool of the lungs in CXR. We then extracted the regions of interest (ROI) for the radiomics analysis, using PyRadiomics. In the meantime, we collect clinical data from these patients, like age, blood pressure and blood tests. We use two methods to classify the patients: a Multi-layer Perceptron (MLP) classifier and ResNet50 model. To use the ResNet50 model, we have to use a methodology, DeepInsight to convert radiomic features and clinical data into images, importable to ResNet50 model. We then evaluate the predictive capabilities of the clinical data, the radiomic features from CXR and the combination of them. As a metric, we use the Area Under the Curve (AUC). The AUC produced by the manual segmentation and the automated, was not very different, giving us confident that the automated segmentation was accurate.

Results: For the ResNet50 model, the AUC are not significant, with AUC values at 0.55, 0.53 and 0.51 for the prediction of Administration, intubation and expiration. For the MLP on the the AUC from the CXR radiomics analysis alone is 0.71 for the admission prediction, 0.6 for the intubation prediction and 0.52 for the expiration prediction. On the other hand, the clinical data give 0.92 for the admission prediction, 0.91 for the intubation prediction and 0.77 for the expiration prediction. A combined model would give 0.78 for the admission prediction, 0.84 for the intubation prediction and 0.77 for the expiration prediction.

Conclusions: We demonstrate that from the radiomics, we can extract some information about the condition of the patient, by taking into account the entire lung but the results are considerably enhanced when clinical information are included in the model.

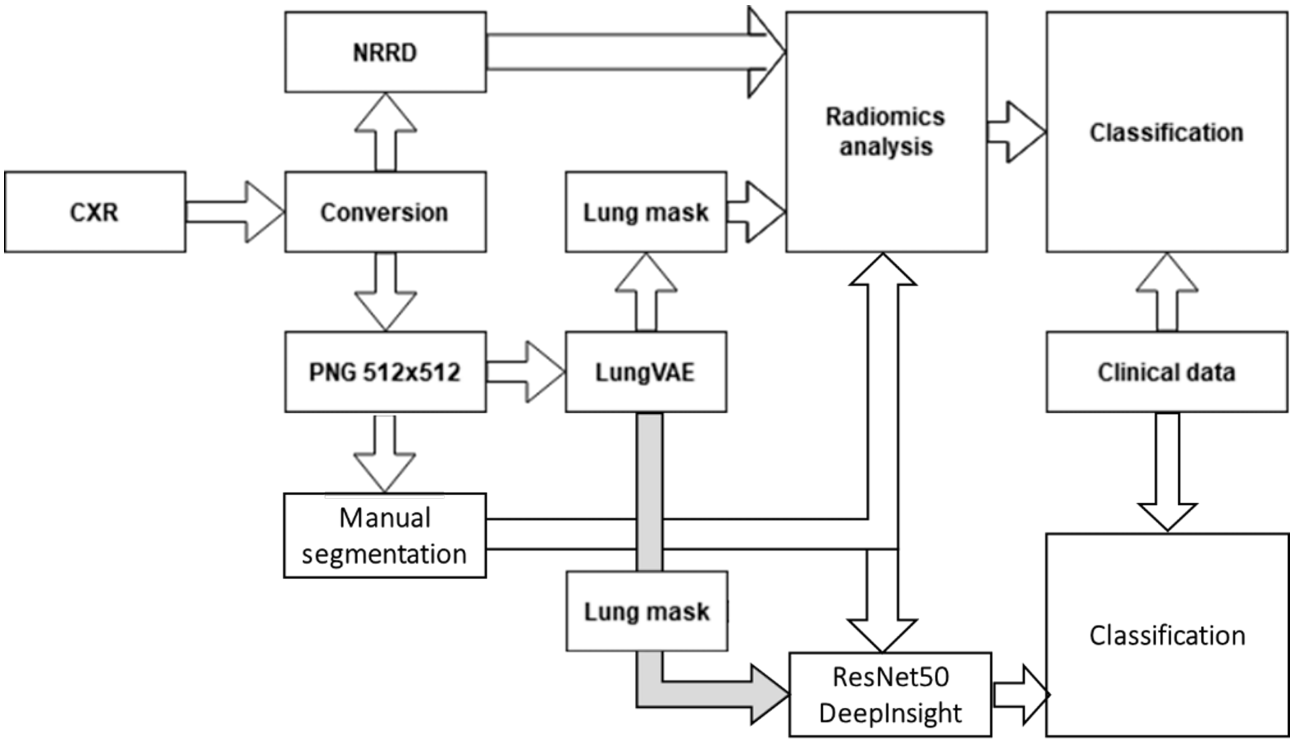

Figure 0.1: Radiomics extraction pipeline.

Table 0.1: AUC scores of manual segmentation

Manual segmentation						
	Clinical data only		CXR radiomics		Clin. dt and CXR radiom	
	MLP class	ResNet50	MLP class	ResNet50	MLP class	ResNet50
Admission	0.973 ± 0.053	0.559 ± 0.14	0.74 ± 0.086	0.564 ± 0.148	0.790 ± 0.097	0.552 ± 0.18
Intubation	0.901 ± 0.095	0.512 ± 0.12	0.587 ± 0.245	0.564 ± 0.24	0.843 ± 0.074	0.513 ± 0.29
Expiration	0.780 ± 0.195	0.487 ± 0.25	0.585 ± 0.494	0.507 ± 3.58	0.763 ± 0.17	0.486 ± 0.21

Table 0.2: AUC scores of automated segmentation

Automated segmentation						
	Clinical data only		CXR radiomics		Clin. dt and CXR radiom	
	MLP class	ResNet50	MLP class	ResNet50	MLP class	ResNet50
Admission	0.973 ± 0.053	0.562 ± 0.14	0.73 ± 0.077	0.557 ± 0.136	0.789 ± 0.053	0.551 ± 0.19
Intubation	0.901 ± 0.095	0.505 ± 0.12	0.589 ± 0.134	0.537 ± 0.14	0.833 ± 0.064	0.514 ± 0.29
Expiration	0.780 ± 0.195	0.498 ± 0.25	0.576 ± 0.207	0.509 ± 2.64	0.764 ± 0.14	0.488 ± 0.21

Systematically evaluating DOTATATE and FDG as PET immuno-imaging tracers of cardiovascular inflammation

Yohana C. Toner[1,2,3], Adam A. Ghotbi[1,2,4], Sonum Naidu[1,2], Ken Sakurai[1,2], Mandy M.T. van Leent[1,2,4], Jazz Munitz[1,2], Willem J.M. Mulder[1,2,3,5], Zahi A. Fayad[1,2], Claudia Calcagno[1,2]

[1] BioMedical Engineering and Imaging Institute, Icahn School of Medicine at Mount Sinai, New York, NY, USA
[2] Diagnostic, Molecular and Interventional Radiology, Icahn School of Medicine at Mount Sinai, New York, NY, USA
[3] Department of Internal Medicine and Radboud Center for Infectious Diseases, Radboud University Medical Center, Nijmegen, the Netherlands
[4] Cardiovascular Research Institute, Icahn School of Medicine at Mount Sinai, New York, NY, USA
[5] Laboratory of Chemical Biology, Department of Biochemical Engineering, Eindhoven University of Technology, Eindhoven, The Netherlands

Introduction: In recent years, cardiovascular immuno-imaging by positron emission tomography (PET) has undergone tremendous progress in preclinical settings. Clinically, two approved PET tracers hold great potential for inflammation imaging in cardiovascular patients, namely FDG and DOTATATE. While the former is a widely applied metabolic tracer, DOTATATE is a relatively new PET tracer targeting the somatostatin receptor 2 (SST2).

Materials and Methods: We performed a detailed, head-to-head comparison of DOTATATE-based radiotracers and [^{18}F]F-FDG in mouse and rabbit models of cardiovascular inflammation. For mouse experiments, we labeled DOTATATE with the long-lived isotope [^{64}Cu]Cu to enable studying the tracer's mode of action by complementing in vivo PET/CT experiments with thorough ex vivo immunological analyses. For translational PET/MRI rabbit studies, we employed the more widely clinically used [68Ga]Ga-labeled DOTATATE. DOTATATE's pharmacokinetics and timed biodistribution were determined in control and atherosclerotic mice and rabbits by ex vivo gamma counting. Additionally, we performed in vivo PET/CT experiments in mice with atherosclerosis, mice subjected to myocardial infarction and control animals, using both [^{64}Cu]Cu-DOTATATE and [^{18}F]F-FDG. To evaluate differences in the tracers' cellular specificity, we performed ensuing ex vivo flow cytometry and gamma counting.

Results: In mice subjected to myocardial infarction, in vivo [^{64}Cu]Cu-DOTATATE PET showed higher differential uptake between infarcted (SUVmax 1.3, IQR, 1.2-1.4, N=4) and remote myocardium (SUVmax 0.7, IQR, 0.5-0.8, N=4, p=0.0286), and with respect to controls (SUVmax 0.6, IQR, 0.5-0.7, N=4, p=0.0286), than [^{18}F]F-FDG PET. In atherosclerotic mice, [^{64}Cu]Cu-DOTATATE PET aortic signal, but not [^{18}F]F-FDG PET, was higher compared to controls (SUVmax 1.1, IQR, 0.9-1.3 and 0.5, IQR, 0.5-0.6, respectively, N=4, p=0.0286). In both models, [^{64}Cu]Cu-DOTATATE demonstrated preferential accumulation in macrophages with respect to other myeloid cells, while [^{18}F]F-FDG was taken up by macrophages and other leukocytes. In a translational PET/MRI study in atherosclerotic rabbits, we then compared [68Ga]Ga-DOTATATE and [^{18}F]F-FDG for the assessment of aortic inflammation, combined with ex vivo radiometric assays and near-infrared imaging of macrophage burden. Rabbit experiments showed significantly higher aortic accumulation of both [68Ga]Ga-DOTATATE and [^{18}F]F-FDG in atherosclerotic (SUVmax 0.415, IQR, 0.338-0.499, N=32 and 0.446, IQR, 0.387-0.536, N=27, respectively) compared to control animals (SUVmax 0.253, IQR, 0.197-0.285, p=0.0002, N=10 and 0.349, IQR, 0.299-0.423, p=0.0159, N=11, respectively).

Conclusions: We present a detailed, head-to-head comparison of the SST2-specific tracer DOTATATE and the metabolic tracer [^{18}F]F-FDG for the evaluation of inflammation in small animal models of cardiovascular disease. Our results support further investigations on the use of DOTATATE to assess cardiovascular inflammation as a complementary readout to [^{18}F]F-FDG.

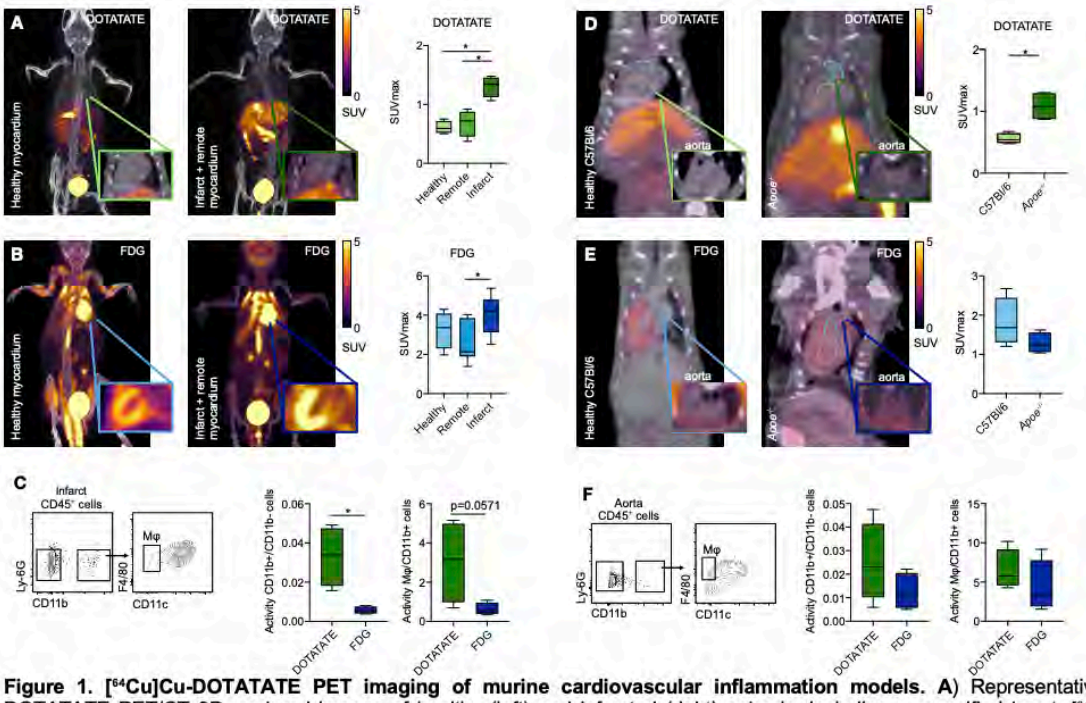

Figure 1. [^{64}Cu]Cu-DOTATATE PET imaging of murine cardiovascular inflammation models. A) Representative fused [^{64}Cu]Cu-DOTATATE PET/CT 3D-rendered images of healthy (left) and infarcted (right) animals, including a magnified heart. [^{64}Cu]Cu-DOTATATE SUV_{max} (*in vivo*) in the heart of C57Bl/6 healthy animals (myocardium) and LAD-ligated mice (remote and infarct). N=4 per group. **B**) Representative fused [^{18}F]F-FDG PET/CT 3D-rendered images of healthy (left) and LAD-ligated (right) animals, including a magnified heart showing myocardium uptake. [^{18}F]F-FDG SUV_{max} (*in vivo*) and %ID/g (*ex vivo*) in the heart of C57Bl/6 healthy animals (myocardium) and LAD-ligated mice (remote and infarct). Controls N=4 and infarcted N=6. **C**) Representative flow cytometry plots identifying $CD11b^-$, $CD11b^+$ and macrophage cell populations in the myocardium. Quantification of activity per cell in the infarcted myocardium. N=4 per group. **D**) Representative fused PET/CT image of [^{64}Cu]Cu-DOTATATE-infused C57Bl/6 (left) and *Apoe*$^{-/-}$ mice after 12 weeks on Western Diet (right). ROIs show left ventricle (orange) and ascending aorta (green). Magnification shows aortic root. *In vivo* [^{64}Cu]Cu-DOTATATE SUV_{max} of the ascending aorta. N=4 per group. **E**) Representative fused PET/CT 3D-rendered image of [^{18}F]F-FDG-infused *Apoe*$^{-/-}$ mice. Magnification shows aortic root. [^{18}F]F-FDG SUV_{max} of ascending aorta. N=4 per group. **F**) Representative flow cytometry plots identifying $CD11b^+$ and macrophage cell populations in the aorta. Quantification of activity per cell in the aorta. N=4 per group. ID: injected dose; Mφ: macrophages; SUV_{max}: maximum standardized uptake value. $CD11b^+$ cells represent $CD11b^+CD11c^{hi}$, excluding macrophage population. *p<0.05. Data are presented as median (IQR).

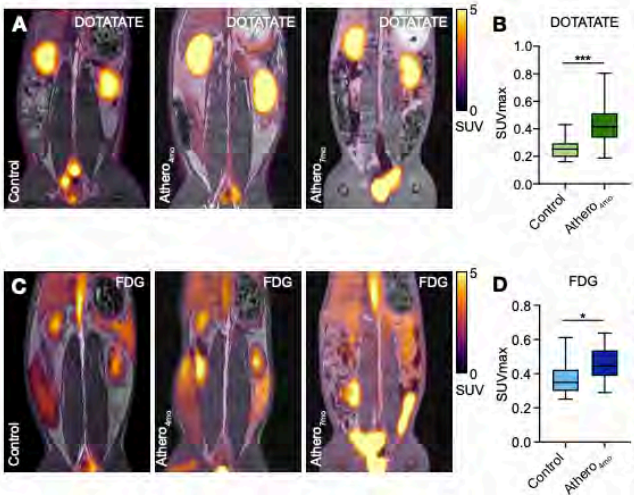

Figure 2. *In vivo* and *ex vivo* imaging of atherosclerosis in rabbits. **A**) Representative fused PET/MR image of [^{68}Ga]Ga-DOTATATE-infused control (left), $athero_{4mo}$ (middle) and $athero_{7mo}$ (right) rabbits. **B**) [^{68}Ga]Ga-DOTATATE SUV_{max} of abdominal aorta in control and $athero_{4mo}$ animals. Controls N=10 and $athero_{4mo}$ N=32. **C**) Representative fused PET/MR image of [^{18}F]F-FDG-infused control (left), $athero_{4mo}$ (middle) and $athero_{7mo}$ (right) rabbits. **D**) [^{18}F]F-FDG SUV_{max} of abdominal aorta in control and $athero_{4mo}$ animals. controls N=11 and $athero_{4mo}$ N=27.

Figure 0.2

Multifrequency Magnetic Resonance Elastography (MRE) at 7T

E.R. Triolo[1], A. Alipour[2], O. Khegai[2], P. Balchandani[2], M. Kurt[1,2]

[1] Department of Mechanical Engineering, University of Washington
[2] BioMedical Engineering and Imaging Institute, Icahn School of Medicine at Mount Sinai

Introduction: Magnetic resonance elastography (MRE) is a technique for determining the mechanical response of tissues using applied harmonic deformation and motion-sensitive MRI[1]. Studies using MRE to investigate the mechanical properties of the human brain are most commonly performed at conventional field strength (3 Tesla (T) or 1.5T), although there have been a few attempts at the ultra-high field strength, 7T[2]. Additionally, most biological tissues, including the human brain, exhibit a frequency-dependent mechanical response[3] which has yet to be explored at 7T. In this study, we investigat the frequency dependence of the mechanical properties of the brain, first validating our methods using a linearly elastic phantom.

Materials and Methods: For validation of the sequence, MRE was performed on a custom MRE phantom (CIRS 049) at 30-80Hz in 10 Hz increments, using a 32-channel head coil (Nova Medical) on a 7T Siemens Magnetom MRI Scanner (see Table 1 for parameters). Full brain coverage MRE was then performed on one healthy human subject at 1.1mm isotropic resolution at 40, 60, and 80Hz. The MRE sequence was a modified single-shot multi-slice spin-echo 2D-EPI sequence with trapezoidal flow-compensated motion encoding gradients (MEGs), synchronized with the acoustic actuator[4] by TTL triggering at the beginning of every TR. Images were masked, denoised using a MP-PCA algorithm[5], and unwrapped[6]. We performed post-processing4 before using Algebraic Inversion to calculate $|G*|$[7].

Results: MRE was successfully performed on the phantom at all frequencies, the wavefield images of which are shown in Figure 1 for each frequency. This data was also used to determine the filter window necessary for quartic smoothing kernel at each frequency, as this must be scaled for wavelength to prevent over-smoothening of short wavelength waves. MRE was also successfully performed on the healthy human subject at the representative frequencies. Elastograms of a representative slice for each frequency are shown in Figure 2.

Conclusions: In the future, this multifrequency MRE protocol can be used to determine region specific frequency-dependent mechanical properties as it has in the past at 3T[3], but at the ultra-high resolution possible at 7T.

Acknowledgements: The authors would also like to acknowledge the support from NSF CMMI 1953323 and NIH funding R21AG071179.

References: [1]Braun, et al., Neuroimage, 2014, [2]Murphy, et al., PloS one, 2013, [3] Kurt, et al. NeuroImage, 2019, [4]Triolo, et al. Proc. BMES, 2021, [5]Veraart, et al. Neuroimage, 2016, [6]Herraez, et al., Applied Optics, 2002, [7]Oliphant, et al., Magn. Reson. Med., 2001

Table 0.3: MRE Parameters for Each Frequency

Frequency (Hz)	Echo Time (TE, ms)	Repetition Time (TR, ms)	Vibration Cycles/TR
30	90	6667	5
40	74	6000	6
50	65	5600	7
60	65	6000	9
70	65	5715	10
80	65	5500	11

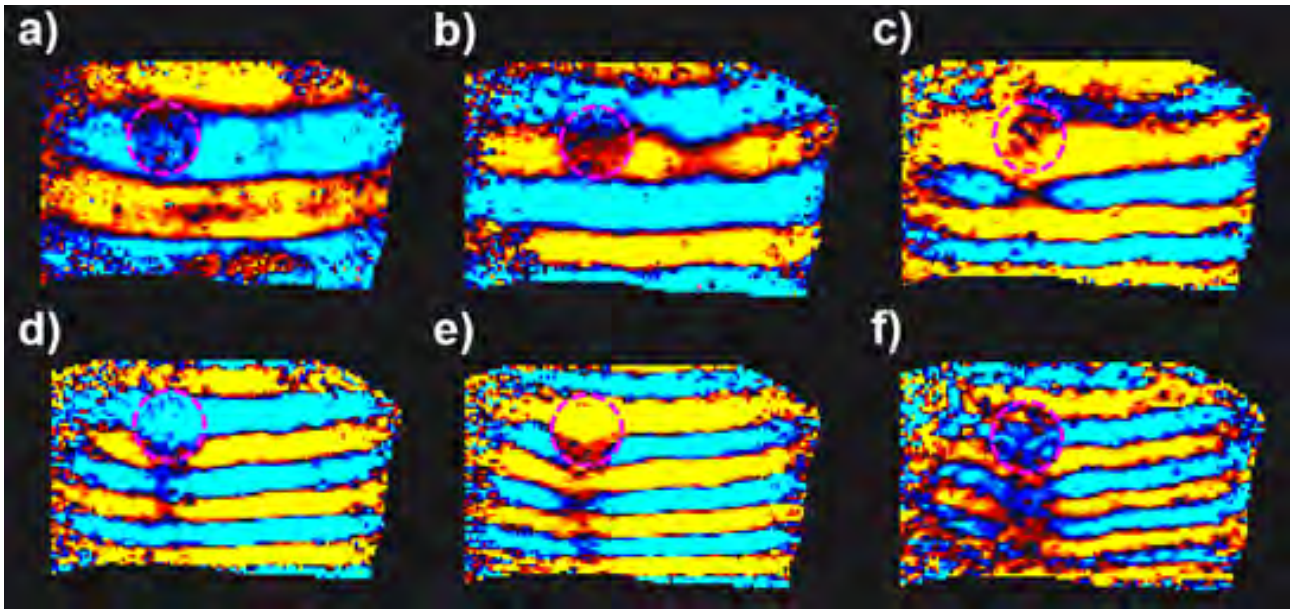

Figure 0.1: Wavefield in the x-Direction in a Central Slice of the Phantom at Each Frequency a)30Hz, b)40Hz, c)50Hz, d)60Hz, e)70Hz, and f)80Hz, Where the Pink Outline is the Location of a Stiff Inclusion

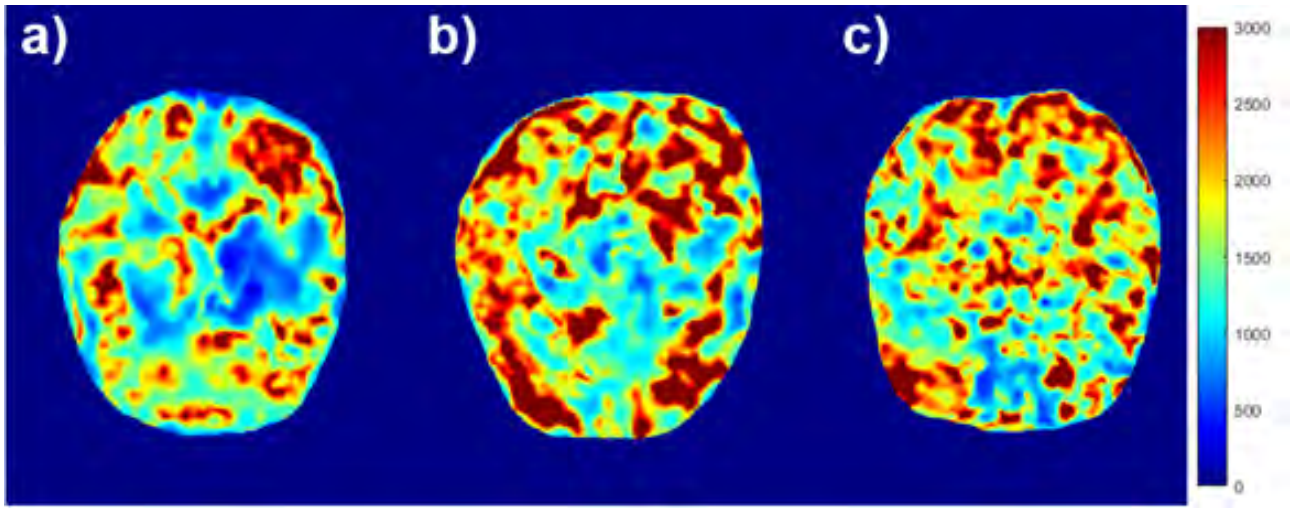

Figure 0.2: The Magnitude of the Complex Shear Modulus Estimate, |G*|, (in Pa) at a Representative Slice for Each Frequency (a) 40Hz, (b) 60Hz, (c) 80Hz

Evaluating the association between hybrid magnetic resonance positron emission tomography and cardiac-related outcomes in cardiac sarcoidosis

Maria Giovanna Trivieri MD PhD[1,2], Philip M. Robson PhD[1], Vittoria Vergani MD[3], Gina LaRocca MD[2], Angelica M. Romero-Daza MD[4], Ronan Abgral MD PhD[5], Nicolas A. Karakatsanis PhD[1,6], Aditya Parikh MD[2], Christia Panagiota MD[2], Anna Palmisano MD[7], Louis DePalo MD[8], Helena L. Chang MS[9], Joseph H. Rothstein MS[9], Rima A. Fayad MPH[1], Marc A. Miller MD[10], Valentin Fuster MD PhD[2], Jagat Narula MD PhD[2], Marc R. Dweck MD PhD[11], Adam Jacobi MD[12], Maria Padilla MD[8], Jason C. Kovacic MD PhD[2,13], Zahi A. Fayad PhD[1]

[1] BioMedical Engineering and Imaging Institute, [2] Cardiovascular Institute, Icahn School of Medicine at Mount Sinai, New York, NY; [3] School of Biomedical Engineering and Imaging Sciences, King's College London, London, UK; [4] Department of Cardiology, Hospital La Luz – Quirón Salud, Madrid, Spain; [5] Department of Nuclear Medicine, University Hospital of Brest, Brest, France; [6] Department of Radiology, Weill Cornell Medical College, New York, NY; [7] Department of Radiology, IRCCS San Raffaele Scientific Institute, Milan, Italy; [8] Division of Pulmonary, Critical Care and Sleep Medicine, Icahn School of Medicine at Mount Sinai, New York, NY; [9] Department of Population Health Science and Policy, Icahn School of Medicine at Mount Sinai, New York, NY; [10] Helmsley Electrophysiology Center, Icahn School of Medicine at Mount Sinai, New York, NY; [11] British Heart Foundation Centre for Cardiovascular Science, University of Edinburgh, Edinburgh, UK; [12] Department of Radiology, Icahn School of Medicine at Mount Sinai, New York, NY; [13] Victor Chang Cardiac Research Institute, Darlinghurst, Australia.

Introduction: Invasive endomyocardial biopsy is the gold standard to diagnose cardiac sarcoidosis (CS), but it has poor sensitivity due to the patchy distribution of disease. Imaging with hybrid late gadolinium enhancement (LGE) MR and ^{18}F-fluorodexyglucose (^{18}F-FDG) PET allows simultaneous assessment of myocardial injury and disease activity and has shown promise for improved diagnosis of active CS based on the combined positive imaging outcome, MR(+)PET(+). In this study our objective was to evaluate an extended hybrid MR/PET imaging strategy in CS employing qualitative and quantitative assessment of PET tracer uptake, and to evaluate its association with cardiac-related outcomes.

Materials and Methods: 148 patients with suspected CS were enrolled for hybrid MR/PET imaging. Patients were classified based on presence/absence of LGE (MR+/MR-), presence/absence of ^{18}F-FDG (PET+/PET-), and pattern of ^{18}F-FDG uptake (focal/diffuse) into the following categories: MR(+)PET(+)$_{\text{FOCAL}}$, MR(+)PET(+)$_{\text{DIFFUSE}}$, MR(+)PET(-), MR(-)PET(+)$_{\text{FOCAL}}$, MR(-)PET(+)$_{\text{DIFFUSE}}$, MR(-)PET(-) (Figure 1). Patients classified as MR(+)PET(+)$_{\text{FOCAL}}$ were designated as having active CS [aCS(+)], while all others were considered as having inactive or absent CS and designated aCS(-). Quantitative values of standard uptake value (SUVmax), target-to-background ratio (TBRmax), target-to-normal-myocardium ratio (TNMRmax) and T2 were measured. Occurrence of a cardiac-related clinical outcome was defined as any of the following during the 6-month period after imaging: cardiac arrest, ventricular arrhythmia, complete heart block, need for cardiac resynchronization/defibrillator/pacemaker/monitoring device (CRT-D, ICD/WCD, or ILR). MR/PET imaging results were compared to the presence of the composite clinical outcome.

Results: Patients designated aCS(+) had more than 4-fold increased odds of meeting the clinical endpoint compared to aCS(-) (unadjusted odds ratio 4.8; 95% CI 2.0-11.4;$p < 0.001$) (Table 1). TNMRmax achieved an area under the receiver operating characteristic curve of 0.90 for separating aCS(+) from aCS(-).

Conclusions: Hybrid MR/PET imaging with an extended image-based classification of CS was statistically associated with clinical outcomes in CS. TNMRmax had high sensitivity and excellent specificity for quantifying the imaging-based classification of active CS.

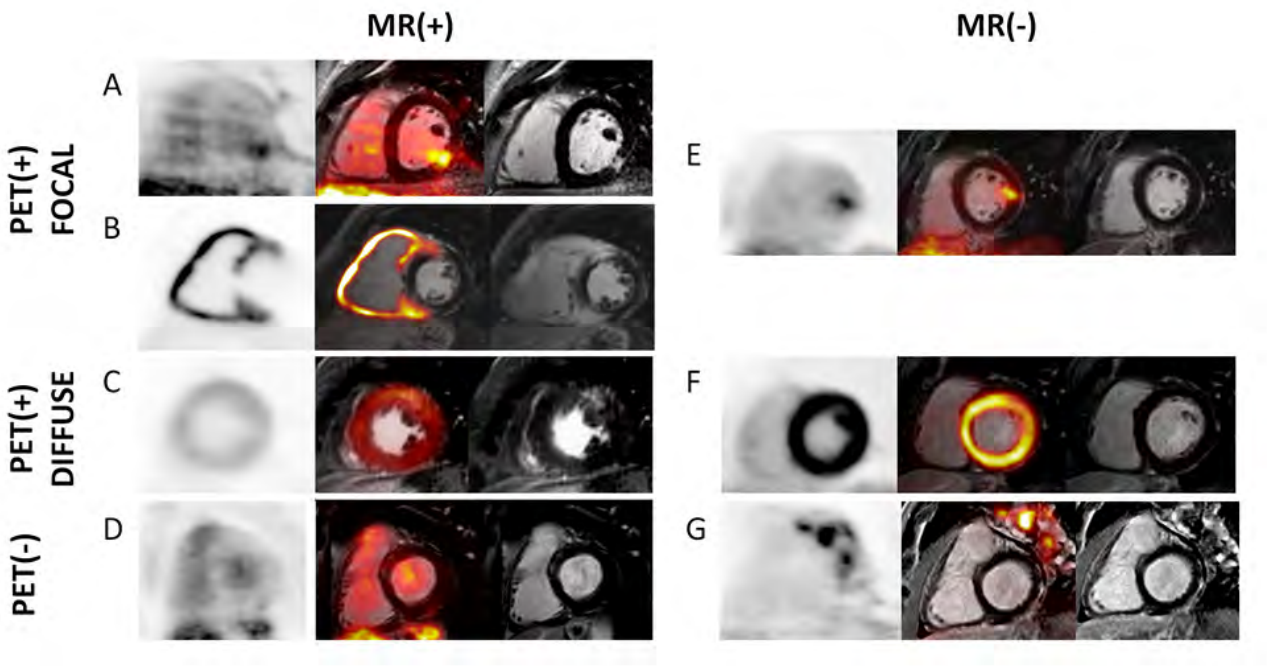

Figure 0.1: Representative short axis 18F-FDG PET (left), LGE MR (right) and fused MR/PET (middle) images for each of the six image-based categories. A: MR(+)PET(+)$_{FOCAL}$, B: MR(+)PET(+)$_{FOCAL}$ with predominantly right ventricular involvement that was subsequently confirmed by cardiac biopsy, C: MR(+)PET(+)$_{DIFFUSE}$] , D: MR(+)PET(-) , E: MR(-)PET(+)$_{FOCAL}$, F: MR(-)PET(+)$_{DIFFUSE}$] , G: MR(-)PET(-) with extra-cardiac 18F-FDG uptake.

Table 0.1: Association of analysis groups with cardiac-related clinical outcomes.

Analysis	Odds of having a cardiac-related clinical outcome/event	OR	CI	P
1	aCS(+) vs. aCS(-)	4.8	2.0 – 11.4	0.00032
2	MR(+)PET(+) vs. non MR(+)PET(+)	2.8	1.3 – 6.4	0.012
3	PET(+) vs. PET(-)	1.6	0.7 – 3.7	0.26
4	MR(+) vs. MR(-)	2.8	1.2 – 6.5	0.015

Analysis 1: aCS(+) [MR(+)PET(+)$_{FOCAL}$] vs. aCS(-) [all others]; analysis 2: MR(+)PET(+) [MR(+)PET(+)$_{FOCAL}$ and MR(+)PET(+)$_{DIFFUSE}$] vs. Non MR(+)PET(+) [all others]; analysis 3: PET(+) [MR(+)PET(+)$_{FOCAL}$, MR(-)PET(+)$_{FOCAL}$, MR(+)PET(+)$_{DIFFUSE}$, and MR(-)PET(+)$_{DIFFUSE}$] vs. PET(-) [all others]; analysis 4: MR(+) [MR(+)PET(+)$_{FOCAL}$, MR(+)PET(+)$_{DIFFUSE}$, MR(+)PET(-)] vs. MR(-) [all others]. OR = odds ratio; CI = 95% confidence interval; p-values are for a two-sided test of significance for the odds ratio.

A modular approach toward producing nanotherapeutics targeting the innate immune system

Mandy M. T. van Leent[1], Anu E. Meerwaldt[1], Alexandre Berchouchi[1], Zahi A. Fayad[1], Carlos Pérez-Medina[1], Willem J. M. Mulder[1], Abraham J. P. Teunissen[1]

[1] Biomedical Engineering and Imaging Institute, Icahn School of Medicine at Mount Sinai, New York, NY, USA

Introduction: Immunotherapy has emerged as a revolutionary cancer treatment. Clinically relevant immunotherapies, such as chimeric antigen receptor T cells, mount a highly specific response by engaging the adaptive immune system. While the value of these therapeutics is indisputable, targeting the innate immune system also holds great promise but remains largely unexplored. Innate immune cells, are activated by pathogen- or damage-associated molecular patterns through pattern recognizing receptors. Upon their activation, they undergo metabolic and epigenetic rewiring, leading to a hypersensitivity toward subsequent encounters with both related and unrelated pathogens. This phenomenon is termed “trained immunity” and can persist for several months. Therapeutically managing trained immunity is a promising treatment paradigm for diseases characterized by excessive inflammation. This can be achieved by treating myeloid cells and their progenitors with drugs that inhibit trained immunity. However, exploiting small-molecule drugs in this manner is hampered by their low myeloid cell specificity.

Results: We report on apolipoprotein A1 (apoA-I)–based nanobiologics that efficiently target myeloid cells and their bone marrow progenitors. To enable nanobiologics’ modular functionalization with small-molecule inhibitors, we established a strategy in which these drugs are derivatized with biocleavable lipophilic promoieties. Using microfluidic formulation technology, we generated differently sized nanobiologics ranging from 20 to 120 nm. Their biodistribution and immune cell specificity were assessed by combining in vivo positron emission tomography (PET) imaging with ex vivo gamma counting with flow cytometry assays. On the basis of this screening, a 35-nm-sized nanobiologic formulation was selected for further studies. Subsequently, we loaded the 35-nm-sized nanobiologics with different small-molecule inhibitors, including the mammalian target of rapamycin (mTOR) inhibitor rapamycin, and found that our prodrug approach resulted in universal and highly efficient drug incorporation and retention. The immunotherapeutic benefits of these drug-loaded nanobiologics were subsequently assessed physicochemically and in vitro. On the basis of these findings, we subjected the mTOR inhibiting nanobiologics (mTORi-NBs) to an optimization and in vivo evaluation process. In addition to experiments in a heart allograft transplantation mouse model, we studied mTORi-NBs’ biodistribution and toxicity profile in non-human primates.

Conclusions: In summary, we developed a robust and modular approach toward producing nanotherapeutics with high propensity to accumulate in the myeloid cell compartment of the hematopoietic organs. This approach facilitates efficiently modulating the innate immune system, which we demonstrated in vitro and in vivo in a heart allograft mouse model. We have demonstrated our nanotherapeutics translatability through safe application in nonhuman primate models.

A spectrally interleaved magnetic resonance spectroscopic imaging sequence incorporating semi-adiabatic pulses at ultrahigh field

Gaurav Verma[1], Seena Dehkharghani[2], Leeor Alon[3], and Priti Balchandani[1]

[1] Biomedical Engineering and Imaging Institute, Icahn School of Medicine at Mount Sinai, New York, NY, United States
[2] Radiology and Neurology, New York University, New York, NY, United States
[3] Radiology, New York University, New York, NY, United States

Introduction: Metabolites at ultrahigh field tend to experience faster t2* relaxation but slower t1 relaxation, such that maximizing signal requires “dead time” between readouts/excitations. Spectral interleaving applies two narrow-band excitations at non-overlapping frequency ranges (like water/metabolites) in one repetition. This provides reference unsuppressed water signals for eddy current correction or absolute quantification through spectral fitting. Moreover, frequency shifts between temperature-insensitive metabolite resonances and temperature-sensitive hydrogen-bound water can facilitate non-invasive thermometry. MR-SASSI applies spectrally-selective spatial-spectral pulses and achieves significantly lower specific absorption rates than other adiabatic approaches. Interleaved spectroscopy is presented implementing low-SAR adiabatic pulses to simultaneously acquire metabolite and partially-excited water signal.

Materials and Methods: The Shinnar-Le Roux-derived pulses (sequence and spatial/spectral profiles shown) had 8ms duration, 660Hz bandwidth (2.2ppm at 7T) with interleaves from 1.9-4.1ppm for metabolites and 4.5-6.7ppm for water (with 5°flip-angle for faster t1-relaxation). Brain phantom and occipital lobe (25Y/F) scans were acquired: TE/TR=31ms/2000ms, two interleaved acquisitions of 4000Hz bandwidth, 2048 complex points and 512ms duration. SVS had 32 averages for 1-minute duration, voxel size=$2.5 \times 2.5 \times 2.5$cm^3. CSI sequence had 4x4 spatial resolution, 8x8 cm^2 field-of-view, 2cm thickness, 8avg, 4-minute duration. Matlab-based reconstruction performed coil combination, averaging, Fourier transform and baseline correction and LCModel prior-knowledge fitting used unsuppressed water signal to perform absolute quantification.

Results: Figure 3 shows CSI interleaved spectra from brain phantom with interleave 1, covering metabolites from 1.9-4.1ppm in red and interleave 2, covering water from 4.5-6.7ppm in blue. Figure 4 shows occipital lobe CSI and metabolite resonances from NAA, creatine (Cr), choline (Cho), myo-Inositol (mI), glutamate and glutamine (Glx) are labeled in accompanying SVS, though comparable resonances are also detectable with CSI. Glx component glutamate/glutamine were partially separable with LCModel fitting showing high-confidence fits for both individual metabolites. Figure 5 shows LCModel processing of occipital lobe study, showing reliable quantification of several metabolites. Chemical shifts for NAA were referenced to 2.02 in phantom and 2.02 in vivo, whereas water chemical shift was 4.85 and 4.70, respectively. Using thermometry formulae derived by Covaciu-2010, [temperature = -97.134*(δWater-δNAA)+296.068], midline temperature estimate was 35.7 °C for human and 21.2 °C for phantom.

Conclusions: Combined with SNR and spectral selectivity advantages at ultrahigh field, this sequence captures subtle chemical shift changes between water and temperature-independent references concurrently and free of potential confounds related to interscan motion or frequency offsets in MR thermometry applications. Future developments will implement echo-planar spectroscopic imaging (EPSI for faster spatial acquisition to enable 3D spectroscopic imaging applications with reasonable durations.

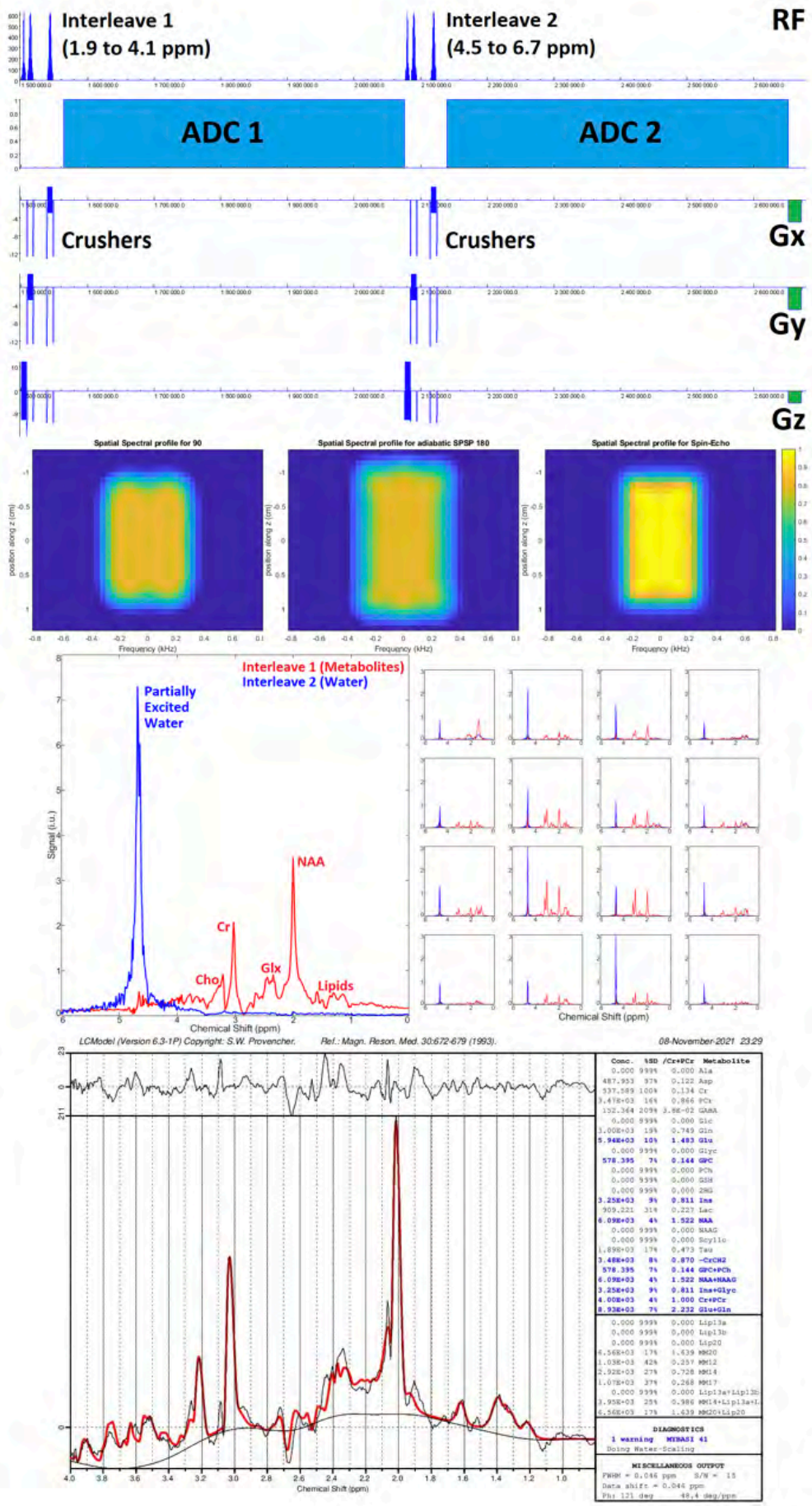
Interleave 1
(1.9 to 4.1 ppm)
Interleave 2
(4.5 to 6.7 ppm)
RF
ADC 1
ADC 2
Crushers
Crushers
Gx
Gy
Gz
Spatial Spectral profile for 90
Spatial Spectral profile for adiabatic SPSP 180
Spatial Spectral profile for Spin-Echo
position along z (cm)
Frequency (kHz)
Interleave 1 (Metabolites)
Interleave 2 (Water)
Partially
Excited
Water
NAA
Cr
Cho
Glx
Lipids
Signal (i.u.)
Chemical Shift (ppm)
LCModel (Version 6.3-1P) Copyright: S.W. Provencher.
Ref.: Magn. Reson. Med. 30:672-679 (1993).
08-November-2021 23:29
Conc. %SD /Cr+PCr Metabolite
0.000 999% 0.000 Ala
487.953 97% 0.122 Asp
537.589 100% 0.134 Cr
3.47E+03 16% 0.866 PCr
152.364 209% 3.8E-02 GABA
0.000 999% 0.000 Glc
3.00E+03 19% 0.749 Gln
5.94E+03 10% 1.483 Glu
0.000 999% 0.000 Glyc
578.395 7% 0.144 GPC
0.000 999% 0.000 PCh
0.000 999% 0.000 GSH
0.000 999% 0.000 2HG
3.25E+03 9% 0.811 Ins
909.221 31% 0.227 Lac
6.09E+03 4% 1.522 NAA
0.000 999% 0.000 NAAG
0.000 999% 0.000 Scyllo
1.89E+03 17% 0.473 Tau
3.48E+03 8% 0.870 -CrCH2
578.395 7% 0.144 GPC+PCh
6.09E+03 4% 1.522 NAA+NAAG
3.25E+03 9% 0.811 Ins+Glyc
4.00E+03 4% 1.000 Cr+PCr
8.93E+03 7% 2.232 Glu+Gln
0.000 999% 0.000 Lip13a
0.000 999% 0.000 Lip13b
0.000 999% 0.000 Lip20
6.56E+03 17% 1.639 MM20
1.03E+03 42% 0.257 MM12
2.92E+03 27% 0.728 MM14
1.07E+03 37% 0.268 MM17
0.000 999% 0.000 Lip13a+Lip13b
3.95E+03 25% 0.986 MM14+Lip13a+L
6.56E+03 17% 1.639 MM20+Lip20
DIAGNOSTICS
1 warning MMBASI 41
Doing Water-Scaling
MISCELLANEOUS OUTPUT
FWHM = 0.046 ppm S/N = 15
Data shift = 0.044 ppm
Phs 121 deg 48.4 deg/ppm

CEST MRI Using Golden-Angle Cartesian Acquisition with Sparse Reconstruction

Ding Xia[1], Rodolphe Leforestier[1], Li Feng[1], Xiang Xu[1]

[1] BioMedical Engineering and Imaging Institute, Icahn School of Medicine at Mount Sinai, New York, USA

Introduction: Chemical exchange saturation transfer (CEST) imaging enables indirect detection of molecules that contain labile protons through their exchange with water. In this study, we proposed a new 3D CEST MRI framework that combines golden-angle rotated variable-density Cartesian acquisition1 and multicoil compressed sensing reconstruction.

Materials and Methods: Our approach employs variable density golden-angle spiral acquisition that is sampled directly on a Cartesian grid. Following the CEST preparation, one “shot”, which include a number of phase-encoding steps predefined by the user in the ky-kz plane, is acquired. Consecutive shots are rotated by the golden angle to allow for a uniform and continuous coverage of k-space.

The experiments were carried out at a Siemens Magnetom 7T scanner. Saturation was achieved by 20 gauss pulses, 50 ms each and 0.5 ms in between, $B1_{rms}$ powers of 0.7 and 2.0 μT. For image readout, 400 k-space lines were acquired per shot after the saturation. 12 shots and 10 shots were acquired for the phantom and human study, respectively. The sampling trajectory was rotated by 137.5° between different shots, including those between each frequency steps (Figure 1).

Results: We tested if reducing the number of shots used in image reconstruction can preserve the spectral features in the CEST spectra in the phantoms. We show that the spectra from images reconstructed using 3 shots showed negligible differences compared to that form images with 10 shots. (Figure 2) For human brain study, no notable image artifacts or visible differences were observed. (Figure 3) We calculated CEST maps using the Lorentzian fitting method 2,3. By using 3 shots with multicoil compressed sensing reconstruction with a spatiotemporal constraint, the CEST map is comparable to the map generated using 10 shots using a spatial constraint only, and potentially less noisy. The acceleration can bring the acquisition time down to approximately 5.5 min for 23 frequency steps with full brain coverage. Further works are needed to optimize the imaging acquisition and reconstruction method to improve the robustness against B0 and B1 inhomogeneities at ultra-high field and to test the method in dynamic CEST imaging studies.

Conclusions: We proposed a 3D CEST imaging using a golden angle rotated and variable density Cartesian acquisition in combination with multicoil compressed sensing reconstruction. We demonstrated that it is possible to obtain whole brain CEST maps within approximately 5.5 min with this method, making it applicable to clinical applications.

References:

1. Cheng, J. Y. et al. Free-breathing pediatric MRI with nonrigid motion correction and acceleration. Journal of magnetic resonance imaging : JMRI 42, 407-420, doi:10.1002/jmri.24785 (2015).
2. Deshmane, A. et al. 3D gradient echo snapshot CEST MRI with low power saturation for human studies at 3T. Magn Reson Med 81, 2412-2423, doi:10.1002/mrm.27569 (2019).
3. Jones, C. K. et al. Nuclear Overhauser enhancement (NOE) imaging in the human brain at 7T. NeuroImage 77, 114-124, doi:http://dx.doi.org/10.1016/j.neuroimage.2013.03.047 (2013).

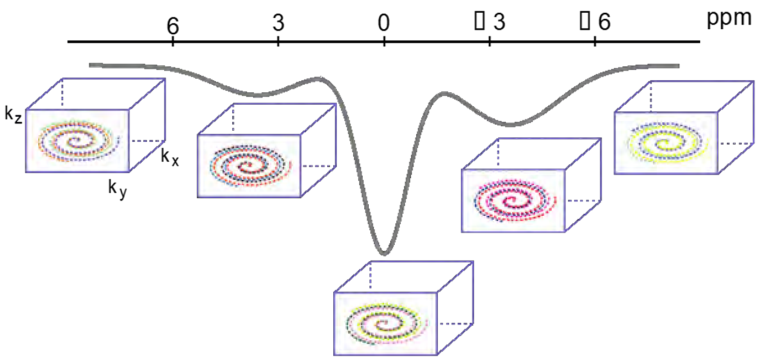

Figure 0.1: Illustration of the acquisition scheme. Consecutive shots are rotated by the golden angle, including shots between frequency steps. Only 3 shots per frequency step are shown here for illustration purpose.

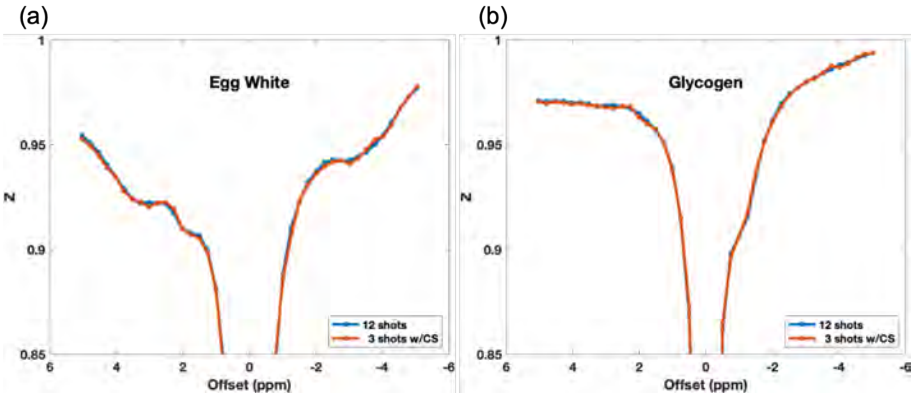

Figure 0.2: Z spectra generated from images reconstructed using 12 shots (blue) and 3 shots (orange) for the egg white (a) and the glycogen (b) phantoms.

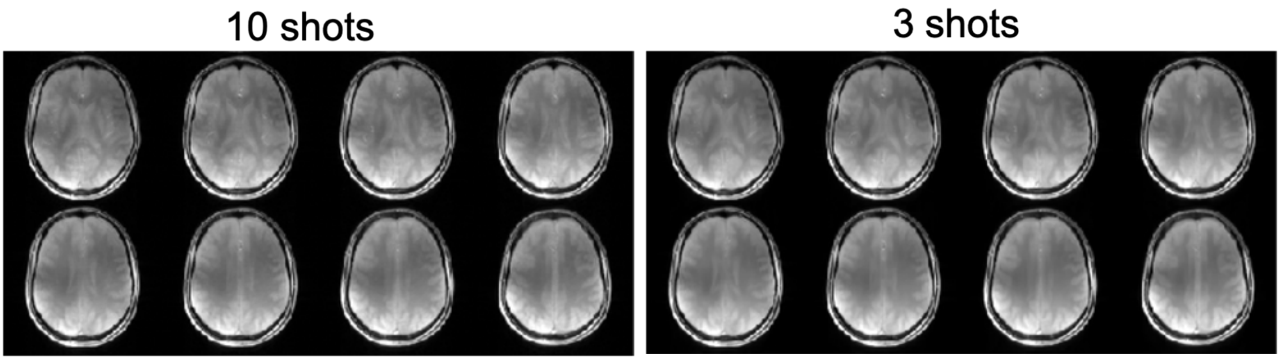

Figure 0.3: 7T Human brain images at -3.5 ppm (magnetization transfer weighted). 30 slices were acquired to cover the whole cerebrum but only 8 slices are shown here. Images are reconstructed using (a) 10 shots and (b) 3 shots.

Deep learning whole breast segmentation enables reproducible quantitative MR-based breast density measurements

Jia Ying[1], Renee Cattell[1,2], Tianyun Zhao[1], Chuan Huang[1,3,4]

[1] Department of Biomedical Engineering, Stony Brook University
[2] Department of Radiation Oncology, Renaissance School of Medicine, Stony Brook University
[3] Department of Radiology, Renaissance School of Medicine, Stony Brook University
[4] Stony Brook Cancer Center, Stony Brook University

Introduction: High breast density (BD) is a risk factor for breast cancer. A quantitatively accurate and reproducible BD measure is desirable. We previously developed a MR-derived quantitative assessment of BD (MagDensity) that relies on precise whole breast segmentation. In this work, we present a highly reproducible and accurate whole breast segmentation algorithm utilizing 3D U-Net to support BD measures using MagDensity.

Materials and Methods: A total of 372 single-sided breast volumes from the Sulindac (NCT01761877) and Metformin (NCT02028221) clinical trials were used to develop the deep learning (DL) algorithm. The data were split randomly into training, validation, and testing sets (222, 74, and 76 volumes, respectively). Fat-water separation was performed as previously described to generate fat-only and water-only images. The Min-Max normalization was applied. The single-sided breast volumes were generated by dividing the breast image in the middle and flipping the left side horizontally to the right. The breast segmentations of the image volumes were generated and manually corrected according to an established protocol based on a previously published automated dynamic programming segmentation method. In this study, a 3D U-Net was developed and used to perform the whole breast segmentation. Its architecture is shown in Figure 1. To evaluate the performance, a test-retest dataset was established, which included 19 pairs of unaffected (single-sided) breast volumes from the Sulindac trial. The data in this set are independent from the DL set. MagDensity for each scan in the test-retest dataset was determined using the three different segmentation methods (manual, dynamic programming, and DL). The test-retest reproducibility was analyzed using the difference between test-retest measures (Δ_{2-1}), mean squared error (MSE), and intraclass correlation coefficient (ICC).

Results: Figure 2 shows a side-by-side comparison of manual, dynamic programming, and DL segmentations. The test-retest reproducibility of MagDensity derived using the three different segmentation methods are summarized in Table 1. MagDensity derived using the DL algorithm showed the smallest MSE (1.140) and achieved the highest ICC (0.976).

Conclusions: The proposed deep learning whole breast segmentation method is accurate and reliable for breast density measurements.

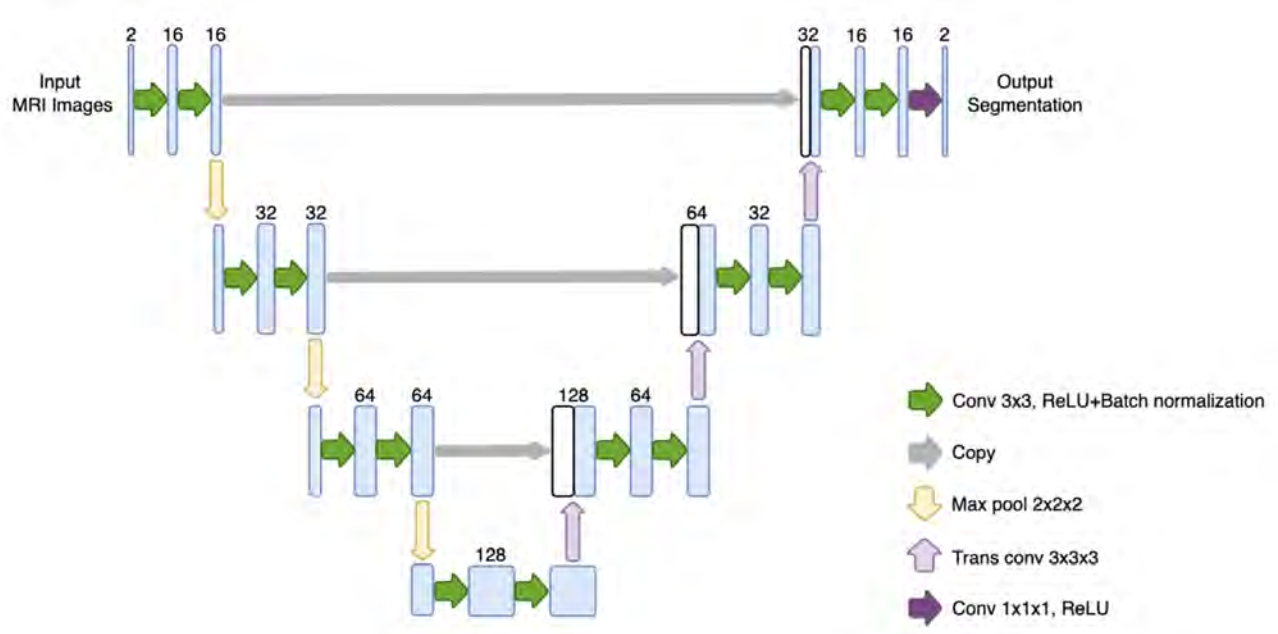

Figure 0.1: Architecture of the 3D U-Net for deep learning breast segmentation.

Figure 0.2: Whole breast segmentation results using manual, dynamic programming, and deep learning methods.

Table 0.1: Comparison of test-retest reproducibility of MagDensity derived using different segmentation methods

	Manual (inter-rater)	Dynamic Programming	Deep Learning
Mean Δ_{2-1}	1.088	0.553	**0.483**
Mean $\lvert\Delta_{2-1}\rvert$	1.115	0.915	**0.859**
Max $\lvert\Delta_{2-1}\rvert$	3.580	2.604	**2.220**
MSE	1.706	1.331	**1.140**
ICC	0.963	0.971	**0.976**
[95% CI]	[0.378 0.911]	[0.912 0.989]	**[0.930, 0.991]**

The Human Smile in Health and Disease: The Neuroimaging Correlates

Lindsey G Zeichner [1,2]

[1] Centre International d'Etudes et de Recherches Vendée/Bas-Poitou, Vouvant, France
[2] Senior Fellow, MFR Research Foundation, New York, USA

Introduction: This study offers a novel interdisciplinary perspective on the human smile, an essential biological process that is central to human survival. Smiling is both the crux of human communication, culture, and socialization as well as linked to physiological processes (e.g., immunity, cardiovascular dynamics, metabolic pathways, neural modulation of affective behavior (mood, emotions, feelings) and to several systemic diseases. Advances in neuroimaging have led to understanding the structure, anatomy, and neural pathways involved in facial expression in general. However, there is a paucity of information relating to the specific facial display known as the "smile". Moreover, to our knowledge, the clinical literature does not speak to the pathophysiology of smiling, nor how the act of smiling is linked to systemic diseases and physiological processes (e.g., immunity, cardiovascular disease, and several neuropsychiatric disorders). The objective of this study was to review the existing contemporary neuroimaging research on smiling (in conjunction with the social and behavioral science literatures), and thereby explain the mechanisms by which the smile mediates health and disease.

Materials and Methods: We conducted a systematic, trimodal literature search of databases encompassing the biomedical, the humanities and social sciences, and the grey literatures. Specifically, we searched materials indexed in PubMed, Web of Science, and Google Scholar spanning the years 1990 until present using relevant MeSH or vocabulary terms.

Results: We found scattered reports in the literature wherein imaging modalities addressed the neurocorrelates of smiling or laughing. The modalities cited were: fMRI, MRI, PET, CT, NIRS, and DTI. These imaging studies supported our conclusions that: smiles are central to mating and proliferation of the human species, are critical to nurturing infants, are essential to communicating kinship or affiliation, and signaling or abating aggression. Smiling mediates the immune response and modulates pain tolerance. Smiling/laughter benefits cardiovascular health, regulates metabolism and even telegraphs the presence of pathogens or toxins. Moreover, we found that neuroimaging studies can be used to explain deficits in smiling or the interpretation of smiling faces in far ranging conditions such as: autism spectrum disorders, major depressive disorders, borderline personality disorder, obsessive compulsive disorder, and Parkinson's disease.

Conclusions: This study brought together diverse and seemingly unconnected findings in the literature. From the imaging literature, we were able to assemble the underlying science to support, explain and illustrate how a select group of facial muscles, that when activated, influence broad systemic processes as well as essential human communication and socialization.

Collecting More Cardiac Structure and Function Information from Vevo Strain Software

Yu Zhou

[1] BioMedical Engineering and Imaging Institute at Icahn School of Medicine at Mount Sinai

Introduction: Cardiac Vevo Strain technology allows for advanced assessment of traditional LV functional parameters as well as global and regional wall motion abnormalities. Speckle-tracking strain can detect these subtle abnormalities, highlighting early myocardial dysfunction [1].

Materials and Methods: The mice were scanned by Vevo 2100 Micro Ultrasound Instrument (FUJIFILMVisualSonics). Transducer MS-550D (40MHz) was used for B model imaging. The ultrasound images were processed with Cardiac Strain on Vevo LAB 3.1.1 software.

Results: Figure 1 shows mouse left ventricular (LV) short axis wall motion points displacements. Figure 2 shows mouse LV short axis wall motion points velocity. Figure 3 shows mouse LV short axis wall segments information. Figure 4 shows mouse LV long axis wall motion points displacements. Figure 5 shows mouse LV long axis wall segments information. Figure 6 shows mouse LV long axis wall motion points velocity. Figure 7 shows mouse LV long axis wall motion strain rate. Figure 8 shows mouse LV long axis anterior and posterior wall strain heat map. Figure 9 shows mouse LV long axis cardiac strain heat map.

Conclusions: Vevo cardiac strain software can detect regional abnormalities and tissue deformation, evaluate cardiac synchrony, and track disease progression or treatment result.

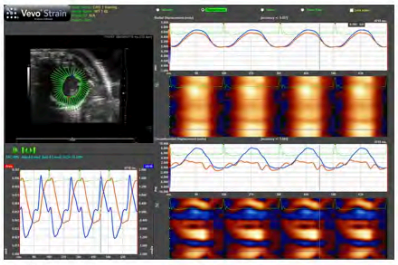

Figure 1 Short axis displacement

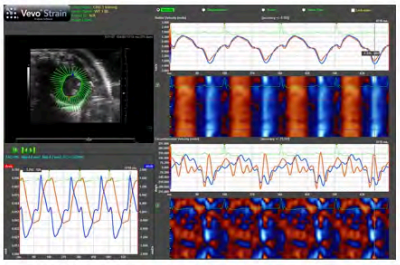

Figure 2 Short axis velocity

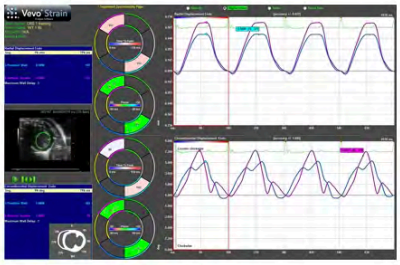

Figure 3 Short axis segments

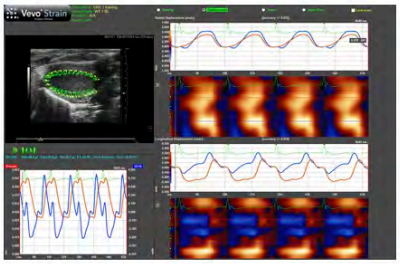

Figure 4 Long axis displacement

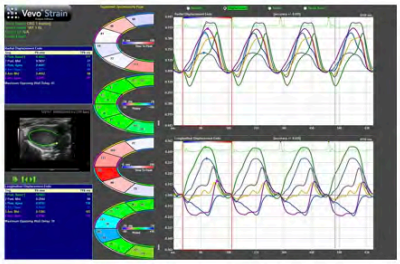

Figure 5 Long axis Segments

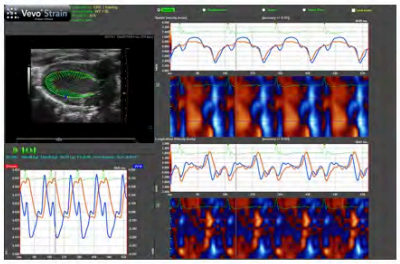

Figure 6 Points velocity

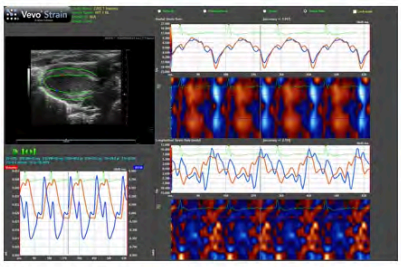

Figure 7 Long axis strain rate

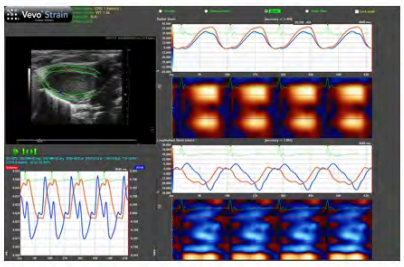

Figure 8 Anterior and posterior strain

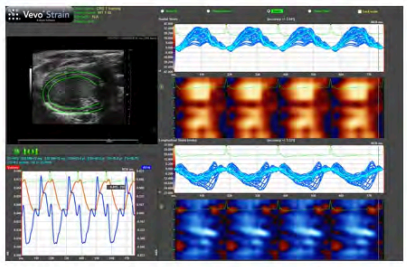

Figure 9 Cardiac strain of LV

Sponsors


MedisoUSA


SA Instruments, Inc.
MR-compatible patient monitors

BMEII highlights 2020-2022

June, 2020 Issue 1

BioMedical Engineering and Imaging Institute

bmeii.mssm.edu

Message from the Director

Zahi Fayad, PhD
Director, BioMedical Engineering
and Imaging Institute
Professor of Radiology and Medicine
zahi.fayad@mssm.edu

Welcome to this special issue of our newsletter where we introduce you to the new formed BioMedical Engineering and Imaging Institute. We have come a long way since the inception of the Imaging Science Laboratories and then Translational Molecular Imaging Institute. Our goal is to continue to invest in the best capital and physical resources in order to produce the best biomedical engineering discoveries to better diagnose and cure diseases. We share the story of our inauguration celebration we had recently. In this issue we introduce our latest faculty recruits (Drs. Yang Yang and Li Feng) that bring further biomedical engineering talent to our Institute. We also introduce the Radiochemistry lab our latest resources expansion that is producing state-of-the-art in radiotracers and immunotherapeutics. Finally, we feature a newly published paper in Nature Medicine by Drs. Yang Yang and Zahi Fayad and our Phd trainee Xueyan Mei on their work using AI to study COVID-19 patients. Finally, we introduce our newly launched website!

BMEII News & Updates

Mount Sinai Establishes BioMedical Engineering and Imaging Institute

Read more at: https://www.mountsinai.org/about/

The Mount Sinai Health System announced the creation of the Biomedical Engineering and Imaging Institute (BMEII), the first of its kind in New York City, and one of a few in the world. The BMEII will leverage Mount Sinai's renowned imaging and nanomedicine programs to establish a broad biomedical engineering research and training programs for its graduate and medical students. It will develop novel medical inventions in the fields of imaging, nanomedicine, artificial intelligence, robotics, sensors, medical devices and computer vision technologies such virtual real, augmented and extended reality. The BMEII is projected to be fully operational by early 2020 and will recruit at least nine prestigious principal investigators and their teams. These researchers will join existing Mount Sinai teams to develop cutting-edge biomedical engineering and imaging technologies to improve the detection, diagnosis, treatment, and prevention of a wide range of human diseases such as cancer, cardiovascular, and neurological diseases. Mount Sinai's Translational and Molecular Imaging Institute, which is at the forefront of brain, heart, and cancer imaging research, along with research in nanomedicine for precision imaging and drug delivery, will be fully incorporated into the BMEII. This will enrich the BMEII's research programs and have a greater impact on biomedical discoveries and patient care.

"Our imaging and nanomedicine programs are leaders in the development and application of these novel technologies to improve patients' diagnosis and treatment," explains Zahi Fayad, PhD, Director of the BMEII. "By integrating artificial intelligence, sensors, robotics, and virtual reality into our programs, the BMEII will take a transformative leap forward in the implementation of next generation medicine and healthcare for our patients and society."

"The creation of Mount Sinai's Biomedical Engineering and Imaging Institute represents a crucial milestone for our medical center," says Eric J. Nestler, MD, PhD, Nash Family Professor of Neuroscience, Director of the Friedman Brain Institute, and Dean for Academic and Scientific Affairs. "Mount Sinai already has established expertise in several areas of imaging and biomedical engineering and we look to further leverage this excellence in creating one of the nation's leading efforts in this exciting area of medical research."

Dennis S. Charney, Anne and Joel Ehrenkranz Dean of the Icahn School of Medicine, and President for Academic Affairs for the Mount Sinai Health System, says, "Mount Sinai has consistently been at the forefront of advancing health care, and the BMEII will revolutionize how we use technology to treat a wide range of conditions. This is a unique endeavor that will create a hub for world-class researchers and innovators, and position us to find groundbreaking solutions for treating disease."

BMEII Human Research Ramp-Up

The BioMedical Engineering and Imaging Institute (BMEII) is open for all imaging services on all modalities. We remain committed to providing the highest quality research, in our state-of-the-art facilities in a SAFE environment for both our subject and our researchers. While BMEIIremained open for approved"For Benefit"studies during the pandemic, following the announcement from the school and PPHS regarding expanding allowable "For Benefit" and "Not For Benefit" human research face-to-face visits, BMEII Human Imaging Core (HIC) has put in place the special guidelines. These guidelines were developed based on guidelines put forth by the FPA, Ambulatory, & the department of Diagnostic, Molecular and Interventional Radiology.

Read more about guidelines on our new website: https://bmeii.mssm.edu

Upcoming Events

- June 18th, 12:30pm. Imaging Research Ramp-up Town Hall. Join Zoom Meeting:https://mssm.zoom.us/j/92693171269?pwd=U1UrTUI3VkhTS3ZIUEdtQi9WRDNsdz09

  Meeting ID: 926 9317 1269
  Password: 388365

Faculty Spotlight

New Faculty & Staff

Yang Yang, PhD

Yang Yang, PhD, is Assistant Professor of Radiology at the BioMedical Engineering and Imaging Institute (BMEII) at the Icahn School of Medicine at Mount Sinai, New York. His research is focused on fast magnetic resonance imaging (MRI) technique development and its translational/clinical applications. Dr. Yang was trained in Biomedical Engineering at University of Virginia on MRI physics, novel pulse sequence development and advanced image reconstruction for fast imaging on cardiac MRI. He worked on interdisciplinary combination of engineering and clinical expertise in cardiovascular imaging to translate new MRI techniques into clinical practice. Specifically, Dr. Yang involved in the projects to develop new spiral pulse sequence to quantify the myocardial perfusion with whole heart coverage to better assess patients with suspected coronary artery disease. He developed techniques for fast imaging to improve resolution and coverage, which includes variable density spiral trajectories design, outer volume suppression (OVS), simultaneous multi-slices (SMS) and iterative constrained image reconstruction with the combination of parallel imaging, compressed sensing and motion compensation. Dr. Yang got his BSE and MSE degrees from Biomedical Engineering at Xi'an Jiaotong University, China on medical device and robotics.

Yang Yang, Ph.D.
Assistant Professor
Dept. of Diagnostic, Molecular and Interventional Radiology
yang.yang@mssm.edu

Li Feng, PhD

Dr. Li Feng is an Assistant Professor at the Biomedical Engineering and Imaging Institute and he joined the Icahn School of Medicine at Mount Sinai in October 2019. He obtained his PhD in Biomedical Imaging from NYU School of Medicine in 2015. Li's research interest has focused on development of novel rapid motion-robust and quantitative MRI techniques combining non-Cartesian acquisition and constrained reconstruction methods. Over the last decade, Li has led the development of several fast and ultrafast MRI techniques, and some of them have been successfully translated into the clinic for a broader spectrum of applications and have resulted in increase in the utility, the simplicity, and the cost-effectiveness of MRI. Li is a Junior Fellow of the International Society for Magnetic Resonance in Medicine (ISMRM) (2015) and was a receiver of the Early Career Award in Basic Science from the Society for Cardiovascular Magnetic Resonance (SCMR) (2014).

Li Feng, Ph.D.
Assistant Professor
Dept. of Diagnostic, Molecular and Interventional Radiology
li.feng@mssm.edu

Newest Additions

BMEII facility is expanding

The new Radiochemistry Lab

With the establishment of the Biomedical Engineering and Imaging Institute, the nanomedicine program has expanded its facilities to include a radiochemistry suite on SC-1 in the dose preparation room. This has been a long-desired vision and goal for the team and facility, as now nano-platform design, synthesis, radioactive labelling, imaging, and biodistribution studies can all take place within the institute. This greatly reduces reliance on other institutions in the creation of new radioactive tracers and immunotherapeutic nanoscale platforms.

Newly purchased equipment, such as an Shimadzu HPLC system (with UV and Radiodetectors), and a radio-TLC system, were placed within the newly shielded bio-safety cabinet. Other new additions include vortexes, thermomixers, microfluidics pumps and chips, a microcentrifuge, and a new computer. These additions complement the dose calibration room, which already included two dose calibrators, a large centrifuge, storage for radioactive isotopes, and a computer dedicated for dose tracking, which will soon be the main hub for NMIS.

SC-1 continues to be a full-stop shop for in vivo imaging and biodistribution studies, and with the addition of the radiochemistry suite, our abilities to create novel therapies and diagnostic tools have been significantly bolstered. For more information on the radiochemistry suite, please reach out to a member of the nanomedicine team lead by Professor Willem Mulder.
Scheduling contacts: Jazz Munitz (jazz.munitz@mssm.edu) and Bram Teunissen (bram.teunissen@mssm.edu).

Willem Mulder, PhD
Director, Nanomedicine
Associate Professor Radiology
willem.mulder@mssm.edu

Mount Sinai First in U.S. to Use Artificial Intelligence to Analyze Coronavirus (COVID-19) Patients

Technology may lead to rapid diagnosis based on CT scans and patient data

Mount Sinai researchers are the first in the country to use artificial intelligence (AI) combined with imaging, and clinical data to analyze patients with coronavirus disease (COVID-19). They have developed a unique algorithm that can rapidly detect COVID-19 based on how lung disease looks in computed tomography (CT scans) of the chest, in combination with patient information including symptoms, age, bloodwork, and possible contact with someone infected with the virus. This study, published in the May 19 issue of Nature Medicine, could help hospitals across the world quickly detect the virus, isolate patients, and prevent it from spreading during this pandemic. "AI has huge potential for analyzing large amounts of data quickly, an attribute that can have a big impact in a situation such as a pandemic. At Mount Sinai, we recognized this early and were able to mobilize the expertise of our faculty and our international collaborations to work on implementing a novel AI model using CT data from coronavirus patients in Chinese medical centers. We were able to show that the AI model was as accurate as an experienced radiologist in diagnosing the disease, and even better in some cases where there was no clear sign of lung disease on CT," says one of the lead authors, Zahi Fayad, PhD, Director of the BioMedical Engineering and Imaging Institute (BMEII) at the Icahn School of Medicine at Mount Sinai."We're now working on how to use this at home and share our findings with others—this toolkit can easily be deployed worldwide to other hospitals, either online or integrated into their own systems." This research expands on a previous Mount Sinai study that identified a characteristic pattern of disease in the lungs of COVID-19 patients and showed how it develops over the course of a week and a half. The new study involved scans of more than 900 patients that Mount Sinai received from institutional collaborators at hospitals in China. The patients were admitted to 18 medical centers in 13 Chinese provinces between January 17 and March 3, 2020. The scans included 419 confirmed COVID-19-positive cases (most either had recently traveled to Wuhan, China, where the outbreak began, or had contact with an infected COVID-19 patient) and 486 COVID-19-negative scans. Researchers also had patients' clinical information, including blood test results showing any abnormalities in white blood cell counts or lymphocyte counts as well as their age, sex, and symptoms (fever, cough, or cough with mucus). They focused on CT scans and blood tests since doctors in China use both of these to diagnose patients with COVID-19 if they come in with fever or have been in contact with an infected patient. The Mount Sinai team integrated data from those CT scans with the clinical information to develop an AI algorithm. It mimics the workflow a physician uses to diagnose COVID-19 and gives a final prediction of positive or negative diagnosis. The AI model produces separate probabilities of being COVID-19-positive based on CT images, clinical data, and both combined. Researchers initially trained and fine-tuned the algorithm on data from 626 out of 905 patients, and then tested the algorithm on the remaining 279 patients in the study group (split between COVID-19-positive and negative cases) to judge the test's sensitivity; higher sensitivity means better detection performance. The algorithm was shown to have statistically significantly higher sensitivity (84 percent) compared to 75 percent for radiologists evaluating the images and clinical data. The AI system also improved the detection of COVID-19-positive patients who had negative CT scans. Specifically, it recognized 68 percent of COVID-19-positive cases, whereas radiologists interpreted all of these cases as negative due to the negative CT appearance. Improved detection is particularly important to keep patients isolated if scans don't show lung disease when patients first present symptoms (since the previous study showed that lung disease doesn't always show up on CT in the first few days) and COVID-19 symptoms are often nonspecific, resembling a flu or common cold, so it can be difficult to diagnose. "This study is important because it shows that an artificial intelligence algorithm can be trained to help with early identification of COVID-19, and this can be used in the clinical setting to triage or prioritize the evaluation of sick patients early in their admission to the emergency room," says Matthew Levin, MD, Director of the Mount Sinai Health System's Clinical Data Science Team, and a member of the Mount Sinai COVID Informatics Center. "This is an early proof concept that we can apply to our own patient data to further develop algorithms that are more specific to our region and diverse populations."

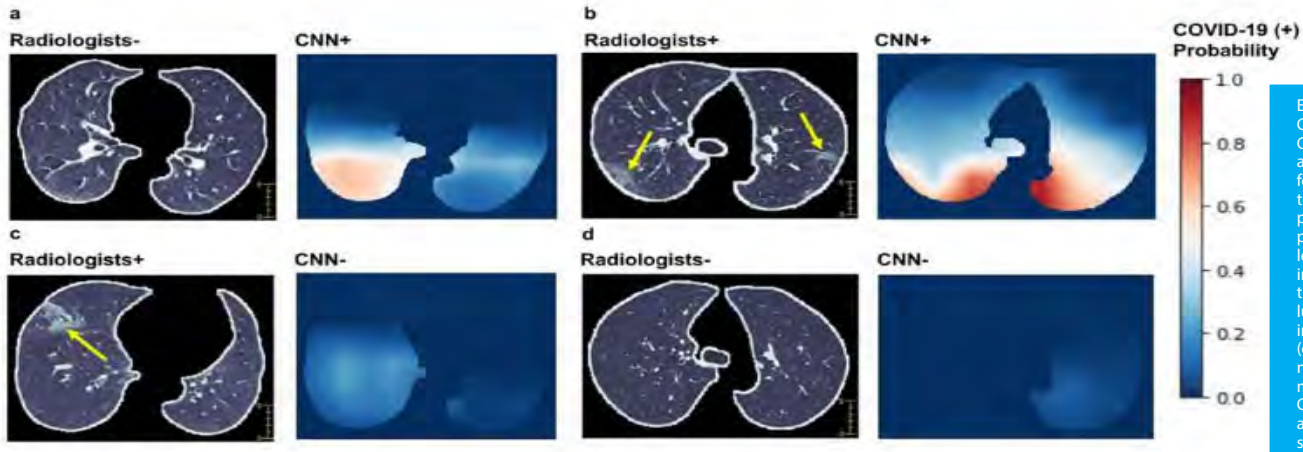

Examples of chest CT images of COVID-19 patients and visualization of features correlated to COVID-19 positivity. For each pair of images, the left image is a CT image showing the segmented lung used as input for the CNN (convolutional neural algorithm) model trained on CT images only, and the right image showe the heatmap of pixels that the

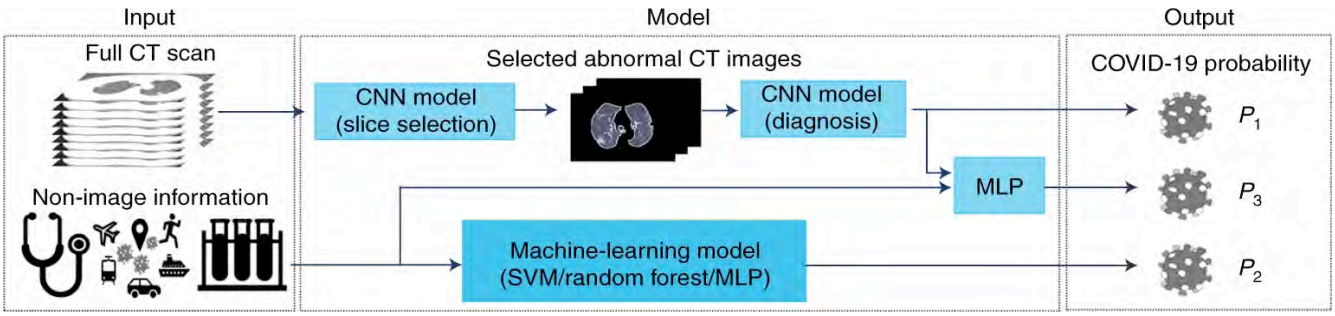

Ilustration of the modeling framework; Three AI models are used to generate the probability of a patient being COVID-19 positive: the first is based on a chest CT scan, the second on clinical information; and the third on a combination of the chest CT scan and clinical information.

Read more in Nature Journal: https://www.nature.com/articles/s41591-020-0931-3

Mount Sinai researchers are now focused on further developing the model to find clues about how well patients will do based on subtleties in their CT data and clinical information. They say this could be important to optimize treatment and improve outcomes.

Xueyan Mei, a trainee in the Graduate School of Biological Sciences at the Icahn School of Medicine at Mount Sinai, and Yang Yang, PhD, Assistant Professor of Radiology at the Icahn School of Medicine at Mount Sinai, also contributed to this work.

Courtesy of Mount Sinai Inside.
https://www.nature.com/articles/s41591-020-0931-3

Zahi Fayad, PhD Director,
BioMedical Engineering
and Imaging Institute
Professor of Radiology and Medicine
zahi.fayad@mssm.edu

Yang Yang, Ph.D.
Assistant Professor
Dept. of Diagnostic, Molecular and
Interventional Radiology
yang.yang@mssm.edu

Xueyan Mei, Graduate Student
Biological Sciences at Icahn School of
Medicine at Mount Sinai
xueyan.mei@icahn.mssm.edu

Cutting edge programs

Research collaborations

Advanced Neuroimaging Research Program (ANRP)

ANRP's scientific mission is to develop advanced imaging technologies and apply them to improve diagnosis, treatment and surgical planning for neurological diseases, ultimately leading to a deeper understanding of the brain in the normal and diseased state. As the director of ANRP, Dr. Balchandani envisions a growing number of ANRP-affiliated laboratories, spanning multiple departments in the Icahn School of Medicine at Mount Sinai (ISMMS), including Neuroscience, Neurosurgery, Psychiatry, Radiology and Neurology. She will be investing in and facilitating the most innovative brain imaging research which also leverages the technical and clinical advantages of ISMMS. This includes developing new acquisition methods, hardware, and analysis tools to provide advanced multi-modal imaging of the brain. She is also working towards ensuring that infrastructure for image acquisition and pre-processing is robust and seamless. Her goal is to increase overall NIH grants submissions and success rates within neuroimaging and to foster a cohesive set of core research projects to optimally position the ANRP for center and program grants.

Here are some ongoing achievements for the Advanced Neuroimaging Research Program (ANRP): building main infrastructure to support innovative and larger scale neuroimaging studies, providing the most advanced imaging sequences for 3T and 7T to support users and enable grants for all PIs in neuroimaging. Working with Siemens to finalize C2Ps for advanced ASL and fMRI sequences, development of new RF pulses and MRI pulse sequences for use by collaborators across multiple departments at ISMMS. Building new MR spectroscopy sequences that will better image metabolites of interest including neurotransmitters, developing new hardware infrastructure such as parallel Transmit capabilities for 7T, setting up multinuclear imaging, starting with sodium imaging at 7T, and developing new pulse sequences for multinuclear work, strengthening PET/MR research in neuro applications. Work closely with Trey Hedden to increase use of PET/MR and 7T for Alzheimer's research, focus on integration of multimodal data and share multimodal analysis methods with other PIs to provide multi-parametric markers for disease, presenting our program to other institutions, and establish collaborative relationships, generate users for our new methods and tools, working with Siemens to ensure quality control of hardware and availability of latest work-in-progress sequences. Secured an on-site Siemens physicist to develop and maintain sequences. Additionally ANRP is involved in guiding new PIs on neuroimaging capabilities and providing templates for IRB submissions for new projects, building research projects and cores for future program grant, strengthening collaborative ties with Psychiatry, Neurosurgery, Neurology and Rehabilitation Medicine, providing neuroimaging support to PIs in all these departments.

Also ANRP is responsible for testing, validating and integrating a data management service with an external vendor, Flywheel, to provide an efficient method for data storage and pre-neuroimaging data for our PIs.

It is a dedicated server to process and store images, Borg Queen, has been purchased, configured and equipped with the appropriate software. ANRP has established a pilot grant program to provide pilot scans contributing to preliminary data for NIH grant applications.

All ANRP recruitments and equipment acquisitions are intrinsically linked to the bioengineering initiative here at Sinai. Neuroimaging recruits will be integral members of BMEII and will contribute to imaging education. The programs will be connected, and their growth will be simultaneous.

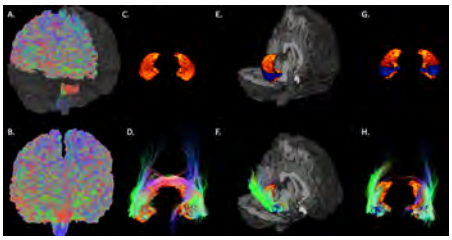

Hippocampal subfield connectivity

Priti Balchandani, PhD, Director, ANRP
High Field Imaging Research
Associate Director
priti.balchandani@mssm.edu

November 2020 Issue 2

Icahn School of Medicine at Mount Sinai

BioMedical Engineering and Imaging Institute

bmeiisinai.org

Zahi Fayad, PhD
Director, BioMedical Engineering and Imaging Institute
Professor of Radiology and Medicine
zahi.fayad@mssm.edu

Message from the Director

In so many ways this year has been unlike any other in recent memory. I am inspired by and grateful for the commitment of our frontline healthcare workers and Mount Sinai's leadership in caring for both patients and the healthcare workforce and in safely restarting research. At BMEII, our work and our institute continue to expand to novel territory, with exciting developments in trained immunity, neuroimaging, COVID-19 research, and our facility offerings. I am pleased to welcome new faculty and staff to BMEII to enhance our research and institutional operations, and to announce our new podcast, ImagingNation. Please enjoy this fall 2020 edition of the BMEII newsletter. Wishing you all continued health and safety.

BMEII News & Updates

Catch Our New Podcast, ImagingNation

This past summer, BMEII launched a podcast called ImagingNation. Hosted by Jazz Munitz, Associate Researcher of Nanoimmunotherapeutics and Manager of Preclinical Nuclear Imaging, the podcast aims to provide insight into imaging, medicine, and bioengineering for a wide variety of audiences. The first episode features Zahi Fayad, PhD and Rob Hirten, MD on the Warrior Watch study and the promise of wearable technology. In the second episode, Drs. Yang Yang, Adam Bernheim, and Michael Chung discuss their pioneering work using clinical data, chest CT images, and artificial intelligence (AI) to rapidly diagnose COVID-19 and the impact of AI on the field of radiology. Stay tuned for new episodes this fall!

You can find ImagingNation on Apple Podcasts, Spotify, and on our website at bmeiisinai.org.

Welcome, New BMEII Staff

Valentin Fauveau, a data scientist and biomedical engineer, joined BMEII as a Programmer Analyst and supports researchers through data management, data analysis, and predictive modeling. Valentin holds a BS in Biomedical Engineering from Universidad de los Andes (Bogota, Colombia) and masters degrees in Medical Imaging and Artificial Intelligence (Télécom Paristech, Paris, France) and Computational Bioengineering (Columbia University, New York, US).

Jenna Korotkin is a Clinical Research Coordinator in the Taouli Lab. She graduated in May 2019 from Cornell University with a BS in Human Biology, Health & Society, and double minors in Human Development, and Policy Analysis & Management. After working at Massachusetts General Hospital, Jenna joined the BMEII team and is responsible for recruitment and regulatory compliance for various imaging studies.

As a Program Manager at BMEII, Mallory Stellato handles patient coordination and operations for Dr. Zahi Fayad's stress and atherosclerosis study and supports communications and business development for the Institute. She completed her MPH in 2020 at Columbia University's Mailman School of Public Health and holds a BS in Biology & Society from Cornell University with a minor in Global Health.

Congratulations to the Radiology Retreat Winners!

Presenter	Talk Title
Shingo Kihira	Association of COVID-19 with Large Vessel Occlusion Strokes: A Case-Control Study
Mark Finkelstein	Value of Chest Radiographs in COVID-19: Analysis of Clinical and Imaging Features in Relation to Patient Outcomes in Young Adults.
Timothy Carlon	Sources of Revenue Loss and Recovery in Radiology Practices During the Coronavirus Disease 2019

Science Spotlight

Scientists Engineer New Cancer Immunotherapy to Train Immune System in Cancer Fight

Nanobiologic immunotherapy uses tiny, bioengineered material to harness immune system

A groundbreaking new type of cancer immunotherapy developed at the Icahn School of Medicine at Mount Sinai trains the innate immune system to help it eliminate tumor cells through the use of nanobiologics, tiny materials bioengineered from natural molecules that are paired with a therapeutic component, according to a study published in *Cell* in October.

This nanobiologic immunotherapy targets the bone marrow, where part of the immune system is formed, and activates a process called trained immunity. This process reprograms bone marrow progenitor cells to produce "trained" innate immune cells that halt the growth of cancer, which is normally able to protect itself from the immune system with the help of other types of cells, called immunosuppressive cells.

This work for the first time demonstrates that trained immunity can be successfully and safely induced for the treatment of cancer. The research was performed in animal models, including a mouse model with melanoma, and the researchers said it is being developed for clinical testing.

Immunotherapies that are already part of standard cancer care, such as the drug that eliminated former President Jimmy Carter's metastatic melanoma, are also able to unmask cancer to the immune system, but they have limitations. The type of immunotherapy used for former President Carter, called a checkpoint inhibitor, fully benefits only a small number of patients and can have severe side effects.

Findings from this research demonstrate that the nanobiologic immunotherapy's trained immunity approach could be used as a stand-alone anti-cancer therapy, potentially with fewer adverse reactions, or in conjunction with checkpoint inhibitor drugs, the scientists say.

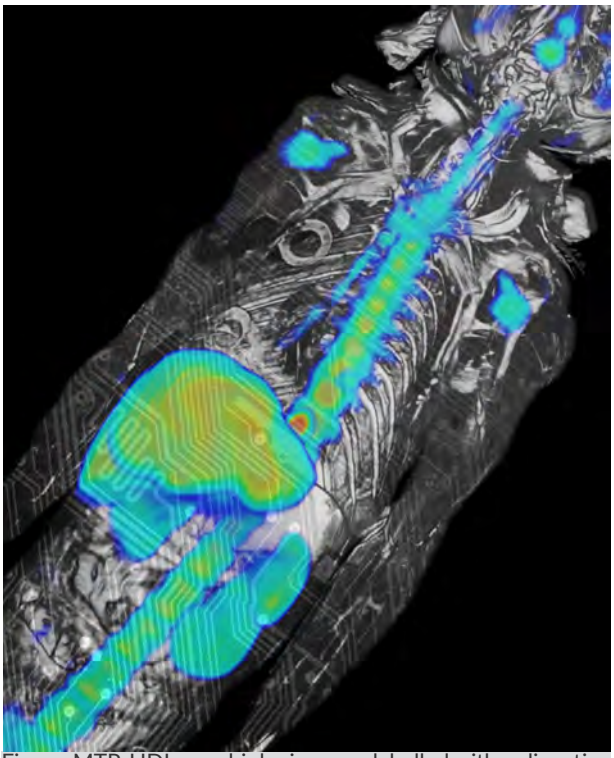

Figure. MTP-HDL nanobiologics were labelled with radioactive 89-Zr, and injected into two nonhuman primates. Using the Biograph Vision PET/MR in the BMEII radiation suite, Mulder and team visualized the biodistribution of the nanobiologics as they accumulated in the hematopoietic organs. This image is also overlaid with graphics of microchip wires to symbolize epigenetic rewiring that is the hallmark of trained immunity.

"Not only have we observed very strong anti-cancer effects of our nanobiologic immunotherapy," said lead author Willem J. Mulder, PhD, Professor of Diagnostic, Molecular and Interventional Radiology and member of the Biomedical Engineering and Imaging Institute at the Icahn School of Medicine at Mount Sinai. "The work involves the development and preclinical evaluation of a novel immunotherapy based on highly biocompatible nanomaterials called nanobiologics. Our study is a significant advancement for both trained immunity and cancer treatment, with real potential to move quickly into use in patients."

This research was part of a large collaboration between the Icahn School of Medicine and multiple other institutes and universities in the United States and Europe.

"This study is a game changer in the field of immunotherapy," said Zahi A. Fayad, PhD, Director of the Biomedical Engineering and Imaging Institute, and another author on the paper. "We are continuing the exploration of the technology at Mount Sinai and with our international collaborators."

The publication is available here.

This article is courtesy of Mount Sinai Media Relations.

Willem Mulder, PhD
Director, Nanomedicine
Professor, Radiology
willem.mulder@mssm.edu

Upcoming Lectures

All lectures will take place virtually. For links, please visit, visit https://bmeiisinai.org/lecture-series/.

Date	Event	Speaker	Title
Mon Nov 9th 1:00-2:00pm	BMEII-Radiology Seminar Series	Dan Ma, PhD Assistant Professor, Department of Biomedical Engineering, Case Western Reserve University, Cleveland, OH	"MR Fingerprinting: A New Path For Clinical Quantitative MR"
Thurs Dec 17th 9:00-10:00am	Lucy G. Moses Lecture in Medical Imaging and Bioengineering	W. Hong Yeo, PhD Assistant Professor, George W. Woodruff School of Mechanical Engineering, Wallace H. Coulter Department of Biomedical Engineering, Director of the IEN Center for Human-Centric Interfaces and Engineering, Georgia Institute of Technology	"Wearable biosensors and biolectronics"

Staff Spotlight

Senior Scientist

Gaurav Verma, PhD

Dr. Gaurav Verma is a senior scientist at the Icahn School of Medicine at Mount Sinai specializing in the development of accelerated and highly-sensitive spectroscopy and imaging sequences for ultra-high field MRI. He has implemented these sequences in the study of human gliomas, psychiatric disorders such as major depression and schizophrenia, and neurological disorders including amyotrophic lateral sclerosis, multiple sclerosis and epilepsy. Dr. Verma's ongoing work explores novel imaging sequences to characterize highly sensitive imaging and metabolic biomarkers for neuropsychiatric disorders, and image processing techniques employing conventional and machine learning-based strategies to glean additional data from the acquired images.

Dr. Verma's ongoing spectroscopy research focuses on the development of very sensitive techniques for the detection of metabolites difficult to detect with conventional methods. This includes neurotransmitters like gamma-aminobutyric acid (GABA) and glutamate whose irregular activity has been implicated in depression. It also includes 2-hydroxyglutarate, an "oncometabolite" only detected in the presence of IDH-mutant tumor. Dr. Verma's imaging work focuses on combining information from multiple imaging modalities. This includes combining structural and connectomic data to perform automated segmentation of brain regions like the thalamus, and developing regression-based algorithms on structural imaging features to model normal and pathological brain aging.

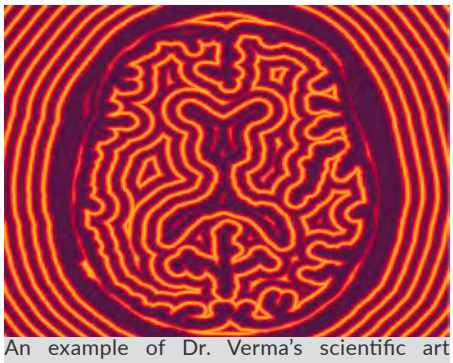

An example of Dr. Verma's scientific art inspired by his work.

Dr. Verma is passionate about sharing his research interests with the general public, including giving lectures and the development of scientific art. An example of this art, generated as a part of applying automated feature detection algorithms to high-resolution brain imaging is shown here.

Gaurav Verma, PhD
Senior Scientist
gaurav.verma@mssm.edu

Faculty Spotlight

New Faculty

Xiang Xu, PhD

Dr. Xiang Xu recently joined the BMEII Neuroimaging Faculty. She holds a PhD in physical chemistry from New York University, with a focus on neuro magnetic resonance (NMR) spectroscopy. Before joining BMEII at Mount Sinai, Dr. Xu completed a postdoctoral fellowship and served as an Assistant Professor at the F. M. Kirby Center for Functional Brain Imaging and the Department of Radiology at Johns Hopkins University.

Her research as a graduate student focused on three major aspects: (1) to enhance NMR sensitivity using para-hydrogen (p-H_2) induced hyperpolarization, (2) to explore unique properties of ^{23}Na NMR and its biological applications, particularly the tensile strength of the cervical connective tissue matrix during pregnancy as well as the diffusion properties of Na^+ in optic nerves, and (3) chemical exchange saturation transfer (CEST). This branch of NMR bridges the chemical exchange properties of functional groups on molecules and enhanced signal detectability via water resonance, making it a suitable method for magnetic resonance imaging (MRI).

Dr. Xu's growing interest in MRI research led her to Dr. Peter van Zijl's research group at Johns Hopkins University, the first to utilize CEST principles for in vivo imaging. During her postdoctoral training, she learned how to perform MRI experiments on both pre-clinical and clinical systems. Building on her background in NMR, Dr. Xu incorporated MRI concepts into CEST spectrum acquisition and developed an ultrafast gradient encoded method to obtain a CEST spectrum with a 10-fold acceleration. As she gained more knowledge in MRI, she extended this method to acquire CEST images in an ultrafast fashion. Dr. Xu has also developed other techniques to improve CEST contrast on both preclinical and clinical scanner platforms. In addition to method development, her research also focuses on the study of the CEST effect of glucose (glucoCEST) in vivo. After observing reproducible glucoCEST enhancement in the tumor region of animal models, she translated the MRI protocol from a preclinical system to 7T and 3T human scanners and studied the glucoCEST effect in human brain tumor patients.

At BMEII, Dr. Xu will continue her efforts in using glucoCEST to study blood brain barrier disruptions in multiple sclerosis, brain tumors and other neurodegenerative diseases. In addition to translational research, she is interested in exploring the exchange properties of other molecules, and improving the sensitivity and reproducibility of CEST MRI. Unlike most conventional MRI, such as T1w or T2w images, where the contrast is generated during the image acquisition period, the contrast in CEST MRI is generated during a preparation period. Therefore, the goal of optimizing a CEST protocol is to prepare more efficient saturation during the preparation period while shortening the readout period. Leveraging the extensive expertise in pulse design and fast imaging at BMEII, Dr. Xu looks forward to many exciting collaborative projects in the coming years.

In her spare time, she enjoys traveling (currently on pause), nature, community gardening and playing with her toddler girls.

Xiang Xu, PhD
Assistant Professor, Radiology
xiang.xu@mssm.edu

Meeting Spotlight

International Society for Magnetic Resonance in Medicine (ISMRM) Presented Abstracts

Session Name	Session Type	Abstract Title (Note: links are only active for registered attendees)	Presenter Name
Pancreas and Hepatobiliary	Digital Poster	Flow quantification with navigator-gated 4D flow MRI in portal hypertension	Octavia Bane, PhD Lab: Taouli
Diffuse Liver & Metabolism	Oral	Splenic T1ρ as a noninvasive biomarker for portal hypertension	Stefanie Hectors, PhD Lab: Taouli
Liver: Methods & Applications	Oral	Fully Automated Prediction of Liver Fibrosis using Deep Learning Analysis of Gadoxetic acid-enhanced MRI	Stefanie Hectors, PhD Lab: Taouli
Junior Fellows Symposium: The Environmental Impact of MRI	Weekday Course	Moderator	Stefanie Hectors, PhD Lab: Taouli
Elastography and Perfusion	Digital Poster	Comparison of multi-platform 2D and 3D MR elastography in vivo and in vitro	Paul Kennedy, PhD Lab: Taouli
Hepatobiliary and Pancreas	Digital Poster	Early Effect of 90Y locoregional therapy on tumor and liver parenchyma stiffness measured with MR elastography: initial experience	Paul Kennedy, PhD Lab: Taouli
Pancreaticohepatobilia	Power Pitch	Utility of magnetic resonance elastography and ultrasound shear wave elastography for assessment of portal hypertension	Paul Kennedy, PhD Lab: Taouli
MRA & Atherosclerosis	Oral	Self-gated dynamic contrast enhanced magnetic resonance imaging of the aortic root in atherosclerotic mice: a natural progression study	Claudia Calcagno, MD, PhD Lab: Fayad
Cardiovascular: Technical	Power Pitch	Moderator	Yang Yang, PhD Lab: Fayad
Novel Acquisitions & Reconstructions	Oral	High Spatiotemporal Resolution Motion-Resolved MRI using XD-GRASP-Pro	Li Feng, PhD Lab: Feng
Quantitative MRI: Reproducibility, Robustness, & New Directions	Power Pitch	Stack-of-Stars Inversion-Recovery MRI for Free-Breathing T1 Mapping and IR-Prepared Fat/Water Separation	Li Feng, PhD Lab: Feng
Machine Learning Reconstruction of Dynamic Acquisitions	Oral	Moderator	Li Feng, PhD Lab: Feng
RF Coils III	Digital Poster	Sensitivity Enhancement at 7T Brain MR imaging Using Wireless Coupled-Split-Ring-Resonators Array	Akbar Alipour, PhD Lab: Balchandani
Neuroimaging at High Field	Digital Poster	An MRI traumatic brain injury case study at 7 Tesla: pre- and post-injury structural network and volumetric reorganization and recovery	Stephanie Brown, PhD Lab: Balchandani
Psychoradiology & AI	Oral	Aberrant Functional Brain Network Topology for Classification between Major Depressive Disorder and Healthy Controls	Yael Jacob, PhD Lab: Balchandani
Image Analysis I	Digital Poster	Quantification of brain age using high-resolution 7T MR imaging and implications in major depressive disorder	Gaurav Verma, PhD Lab: Balchandani
Brain Tumour	Digital Poster	Multiparametric MRI Texture Analysis in Prediction of Genetic Biomarkers in Patients with Brain Glioma	Shingo Kihira, MD Lab: Nael
Beyond the Lumen: Vessel Wall Imaging in Cerebrovascular Diseases	Oral	Vessel Wall MRI in Assessment of Unruptured Intracranial Aneurysms: A Longitudinal Prospective Study	Kambiz Nael, MD Lab: Nael
Emerging Neuro Brain Imaging	Digital Poster	A Container and Detailed Preparation Protocol for Ex Vivo Whole Human Brain MRI	Alan Seifert, PhD Lab: Seifert
Spinal Cord: Cool MR Tools & How to Use Them	Oral	Spatial Specificity of BOLD Signal in the Spinal Cord at 7T Using a Noxious Thermal Stimulus	Alan Seifert, PhD Lab: Seifert
All Things Neurospectroscopy	Digital Poster	Comparison of three tissue sodium concentration quantification methods at 3T and 7T MRI	Lazar Fleysher, PhD Lab: Tang

Imaging Spotlight

Advanced Neuroimaging Research Program (ANRP) Continues to Grow

New areas of research at ANRP include 7T imaging of Alzheimer's Disease, multiple sclerosis, neurological manifestations of COVID-19, anxiety disorders, and Autism Spectrum Disorder. These are projects headed by ANRP PIs as well as investigators across departments, including Psychiatry, Neurology and Neuroscience. Projects have successfully received funding from NIA, NCI, NIMH, NSF and the ADRC core. Technical advancements include building MR elastography at 3T and 7T, development and safety testing of a dual tuned sodium/proton 7T head coil, development of parallel transmit (pTx) imaging protocols, and higher resolution fMRI, spectroscopic and arterial spin labeling (ASL) sequences for use in multi-modal imaging. We have invested in the Flywheel platform, a more secure and robust method to automate neuroimaging processing pipelines, which may be shared between sites to enable collaboration as well as standardization.

ANRP investigators are working on understanding the effects of COVID-19 on the brain. Dr. Balchandani and Dr. Bradley Delman are leading the effort to retrospectively analyze brain imaging data and prospectively study neurological manifestations of the disease at 7T. Close collaboration with Dr. Nathalie Jette in Neurology enables correlation with neurological symptom measures. Dr. Alan Seifert is performing very high-resolution imaging studies of ex vivo brains of COVID-19 decedents and analyzing the imaging features and correlating to histology in collaboration with Dr. Mary Fowkes in Pathology and a team of co-investigators.

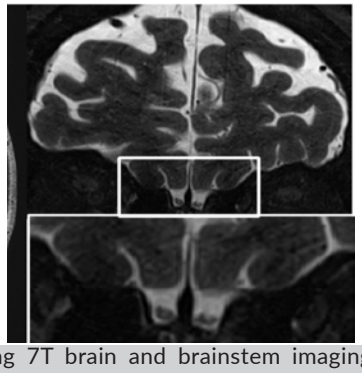

Using 7T brain and brainstem imaging to identify in vivo markers for neurotropism of the SARS-CoV-2 virus.

The ANRP team is growing to include experts that both broaden and strengthen neuroimaging research at BMEII. We recently welcomed a new faculty member, Dr. Xiang Xu, and a new postdoctoral scholar, Dr. Oleksandr (Alex) Khegai. We continue to build strong collaborative ties with neighboring engineering schools. Dr. Mehmet Kurt, who holds an adjunct appointment at BMEII, is MPI on two new funded grants at ANRP from the NIH and NSF.

ANRP continues to provide a mechanism for junior investigators to generate preliminary imaging data for NIH grant submissions, through the ANRP Pilot Grant program. As an example, after receiving the ANRP pilot grant in 2019, Dr. Laurel Morris, Assistant Professor in Psychiatry, has since been awarded a NARSAD Young Investigator Award for the same project, and will be submitting grant applications to external funding agencies using the pilot data generated from the pilot grant.

Core Spotlight

Custom Radiofrequency Hardware Enables Advanced Imaging Methods

A radiofrequency (RF) coil is an essential component of an MRI scanner. An RF coil accomplishes two tasks in an MRI experiment: it excites atomic nuclei within the subject or object being imaged by transmitting a radiofrequency pulse 'on resonance' with the frequency of a given nucleus, and then receives the weak electromagnetic signals emitted by those nuclei. Unlike most scanner hardware components, RF coils can be easily changed between scans and can be custom-designed for optimized performance in specific applications.

The RF Coil Laboratory in BMEII was initially established in 2010, and is available for RF coil building and troubleshooting. The coil lab is equipped with a vector network analyzer, oscilloscopes, a circuit board printer, a 3D printer, a signal generator, DC power supplies, as well as other standard electronics equipment. BMEII core staff, trainees, and faculty have designed, prototyped, and tested numerous custom RF coils and components in this facility for basic and translational research projects.

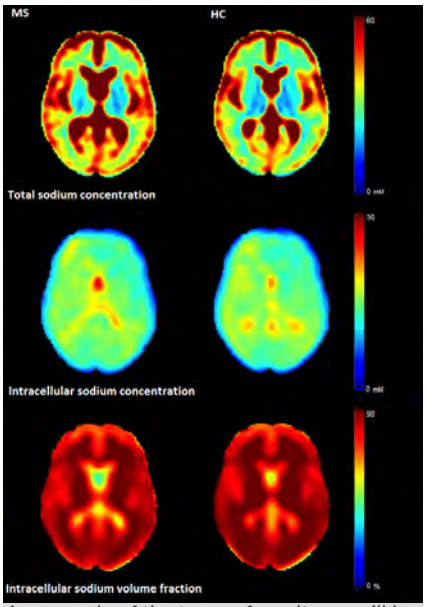

An example of the types of results we will be able to produce with this new sodium coil: maps of mean total sodium concentration, mean intracellular sodium concentration, and mean intracellular sodium volume fraction in subjects with multiple sclerosis and in healthy controls (from Petracca et al., Brain 2016:139;795-806).

These include coils for high resolution 7T MRI of the human cervical spinal cord, brainstem, carotid arteries, and body, as well as a passive wireless resonator array for enhancement of RF fields in the central nervous system and a dedicated coil for rabbit cardiac imaging. In addition to RF hardware, users have also developed mechanical and electronic accessories that are utilized for specific experiments in the high magnetic field environment of the MRI scanners.

BMEII recently partnered with Life Services, LLC to develop a dual-tuned hydrogen and sodium RF head coil for use at 7T. This device is essentially two RF coils, operating at different frequencies, in one housing: a hydrogen RF coil array for producing anatomical images, and a sodium array for mapping important properties of sodium in brain tissue. This 7T sodium head coil will enable new studies of sodium concentration and compartmentalization in diseases such as brain cancer and multiple sclerosis, and may also prove useful for imaging of sodium in skin and skeletal muscle.

For more information about the RF Coil Laboratory, contact Akbar Alipour at akbar.alipour@mssm.edu.
For more information on the sodium coil, contact Alan Seifert at alan.seifert@mssm.edu.

February 2021 Issue 3

BioMedical Engineering and Imaging Institute

bmeiisinai.org

Message from the Director

Zahi Fayad, PhD
Director, BioMedical Engineering and Imaging Institute
Lucy G. Moses Professor in Medical Imaging and Bioengineering
Professor of Radiology and Medicine
zahi.fayad@mssm.edu

It's with a mix of sadness and gratitude that I announce that Willem Mulder, PhD has left his post as Director of Nanomedicine at BMEII. Dr. Mulder's contributions to the growth and success of BMEII since his arrival in 2006 are innumerable, from conducting innovative experiments to training the next generation of leading scientists, and we look forward to continued collaborations with him at his new institutions in the Netherlands. To honor his legacy at BMEII, we have created an endowed annual lectureship in Nanomedicine and an Award for Best Abstract in Nanomedicine at future BMEII annual symposia in his name, made possible by a generous gift from Jean and Nathalie Boulle.

I am delighted to welcome new members to our research and operational staff, as well as to highlight our faculty's and trainee's important work in neuroimaging, and cancer and body imaging. I am pleased to announce a rebranding of our monthly seminar series in partnership with the Department of Diagnostic, Molecular and Interventional Radiology, focusing on Engineering and Medicine, as we continue to expand our research footprint. We hope you enjoy this newsletter and wish everyone health and peace in 2021.

BMEII News & Updates

New Media

BMEII, along with the rest of Mount Sinai, has adapted to the COVID-19 pandemic by implementing extra safety precautions. We created an Imaging Research Walkthrough video to illustrate to our research participants and those who use our facilities what to expect when they arrive for a scan. Take a look at the video here, and subscribe to our YouTube Channel for more video updates from BMEII.

W. Hong Yeo, PhD, Assistant Professor in the George W. Woodruff School of Mechanical Engineering and Wallace H. Coulter Department of Biomedical Engineering and Director of the Center for Human-Centric Interfaces and Engineering at Georgia Tech, delivered the Lucy G. Moses Lecture in Medical Imaging and Bioengineering on December 17, 2020. Dr. Yeo, an expert in nanomembrane electronics and human-machine interfaces discussed "Smart and Connected Soft Bioelectronics for Advancing Human Healthcare and Human-Machine Interfaces." We had a preliminary discussion with Dr. Yeo about the many applications of his work on our podcast, ImagingNation. You can listen and subscribe on Spotify, Apple, or YouTube.

Promotions, Awards, and New Arrival!

Xiang Xu, PhD, Assistant Professor of Diagnostic, Molecular and Interventional Radiology, is a recipient of Second Annual Icahn School of Medicine at Mount Sinai Distinguished Scholar Award for her research proposal entitled, "Simultaneous evaluation of glucose uptake and glymphatic function in Alzheimer's disease using dynamic glucose-enhanced MRI." The prize, sponsored by the Office of Gender Equity in Science and Medicine includes both funding and professional development opportunities.

Priti Balchandani, PhD, Associate Director of BMEII, has been promoted to Professor with Tenure on the Investigator Track in the Department of Diagnostic, Molecular and Interventional Radiology, with secondary appointments in the Departments of Psychiatry and Neuroscience.

Octavia Bane of the Cancer and Body Imaging lab, with husband Max Bane and daughter Livia welcomed their youngest family member. Baby Edward Jonas Bane, weighing 9 lbs 14 oz and measuring 23 1/4 inches was born December 14th, 2020, at 11:40 am at Mount Sinai.

BMEII News & Updates

Welcome, New BMEII Staff

Emre Altinmakas is a post-doctoral fellow in Dr. Taouli 's Cancer and Body Imaging lab, where he works on quantitative MRI applications in various abdominal diseases. He completed his medical training and radiology residency in Istanbul, Turkey, and a postdoctoral fellowship in the Department of Abdominal Radiology at The University of Texas, MD Anderson Cancer Center, followed by abdominal radiology clinical fellowship training in the Department of Medical Imaging at the University of Toronto.

Enamul Bhuiyan is a post-doctoral fellow in the Taouli lab. He received his PhD in Physics from the Sir Peter Mansfield Imaging Centre at the University of Nottingham (U.K.). His thesis focused on developing a novel method for motion correction in MRI, especially in brain imaging. His research focuses on the development of new methods and their applications for biomedical imaging. At BMEII, he is working on body imaging, mostly on liver imaging such as DCE-MRI, DWI, and motion-robust liver imaging. Recently he worked as a post-doc at the Yale School of Medicine.

Oleksandr (Alex) Khegai joined BMEII as a post-doctoral fellow in Dr. Balchandani's Ultrahigh Field MRI group and focuses on development of pulse sequences and methods for 7T MRI. He obtained his PhD degree in Physics from the Technical University of Munich (Germany) and holds an MBA degree from Universidad Carlos III de Madrid (Spain). He completed previous post-doctoral work in Taiwan and at NYU.

As an IT Systems Manager and Dev/Ops technologist, Harry Wong joins BMEII to support researchers through the management of IT systems and pipelines. Harry holds a BS in Computer Science from NYIT (Manhattan) and brings 20+ years of IT experience ranging from IT support, programming, server management, process re-engineering and team management.

Post-Doc Spotlight

Development of a Wireless Radio Frequency Array to Improve MRI

Akbar Alipour, PhD

Dr. Akbar Alipour received his Ph.D. in electrical and electronics engineering from Bilkent University, Ankara, Turkey, in 2017. He was a postdoctoral fellow at the Johns Hopkins School of Medicine and Biomedical Engineering from October 2017 to September 2019. During his Ph.D. research at Bilkent University, he worked on Magnetic Resonance Imaging (MRI) guided interventions through developing new devices and materials, under the supervision of Profs. Ergin Atalar and Hilmi Demir at the National Magnetic Resonance Research Center (UMRAM). During his postdoctoral research at Hopkins, Dr. Alipour worked with Prof. Henry Halperin on cardiac interventional MRI devices. He joined the BioMedical Engineering and Imaging Institute (BMEII) at Icahn School of Medicine at Mount Sinai (ISMMS) to continue his research in ultra-high field (UHF) MRI in the Neuroimaging laboratory led by Prof. Priti Balchandani in August 2019. He started by developing a new method to improve brain MRI at 7T, hypothesizing that it is possible to improve the transmit efficiency of a standard MRI coil using wireless radio frequency array to visualize the whole brain, focusing on the central nervous system.

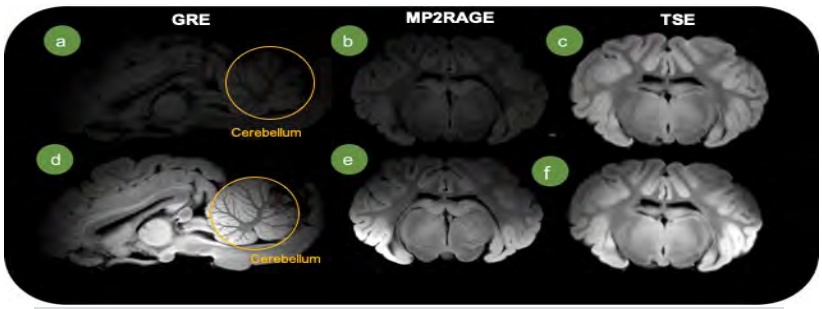

Figure 1. Top row shows MR images obtained without the RF array and bottom row shows MR images obtained in the presence of the RF array. The base of skull and cerebellum are more clearly visible in the presence of the array with about 4-fold SNR improvement.

In recent years, new human magnetic resonance imaging systems operating at static magnetic fields strengths of 7 Tesla or higher have become available, providing better signal sensitivity compared with lower field strengths. However, imaging human-sized objects at such high field strength and associated precession frequencies are limited due to the technical challenges associated with the wavelength effect, which substantially disturbs the transmit field uniformity over the human body when conventional coils are used. In collaboration with other scientists in BMEII, Dr. Alipour developed a novel passive inductively-coupled radiofrequency resonator array design with a simple structure that worked in conjunction with conventional coils and required only to be tuned to the desired operating frequency. We showed that inductive-coupling between the resonator array and the coil improved the transmit efficiency and signal sensitivity in the interested region. The proposed array was independent of the coil type and static magnetic field strength making it an attractive approach

continued on next page

New Faculty

Paul Kennedy, PhD

Dr. Paul Kennedy recently joined the BMEII faculty as an Instructor of Radiology, having initially joined the Institute as a postdoctoral fellow in Dr. Taouli's Cancer and Body Imaging lab in 2016. Dr. Kennedy completed his undergraduate degree in Physics and Astrophysics and master's degree in Medical Imaging physics at Trinity College Dublin, before completing his PhD in Medical Physics at The University of Edinburgh in Scotland. His PhD research was focused on magnetic resonance elastography (MRE), a noninvasive method for measuring tissue mechanical properties. As part of his PhD research, Dr. Kennedy explored the properties of human skeletal muscle with specific emphasis on the impact of intense exercise on quadricep muscle stiffness and highlighted differing engagement patterns associated with quadriceps muscle contraction. Dr. Kennedy also studied the changes in muscle stiffness associated with advanced aging (>80 years old) and found that aged muscles were significantly less stiff than those of younger subjects.

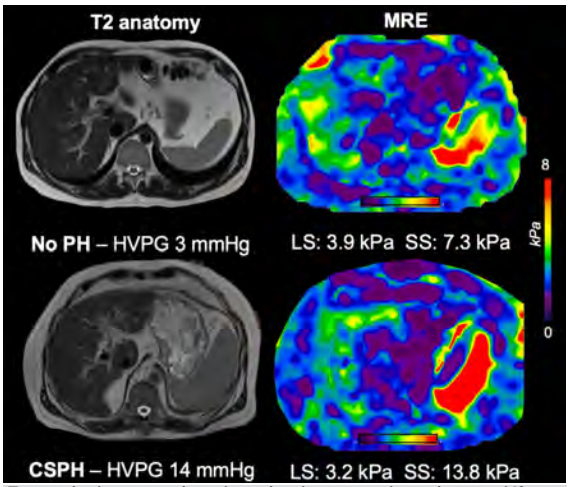

Example images showing the increase in spleen stiffness in the setting of CSPH. Spleen stiffness shows excellent ability for diagnosing CSPH. LS=liver stiffness. SS=spleen stiffness. HVPG=hepatic venous pressure gradient.

Having completed his PhD, Dr. Kennedy joined the Taouli lab to apply his knowledge of MRE to body and cancer imaging. At BMEII he has used multiparametric MRI to non-invasively assess clinically significant portal hypertension (CSPH), a condition associated with advanced liver disease and carries a risk of severe complications such as variceal bleeding and ascites. CSPH is currently diagnosed via an invasive measure of hepatic venous pressure gradient (CSPH=HVPG ≥10 mmHg), a technique which is not widely available. Initial results are very promising, with spleen stiffness (affected by the hemodynamic changes associated with portal hypertension) diagnosing CSPH with excellent accuracy. The impact of CSPH on MRE is shown in Figure 1. Dr. Kennedy has also published work examining the response of liver cancer to locoregional radioembolization therapy with Yttrium 90 and the impact of kidney transplant dysfunction on kidney mechanical properties. More recently Dr. Kennedy worked on an automated method for liver fibrosis diagnosis based on deep learning neural networks. Dr. Kennedy has also authored several review articles on elastography and portal hypertension imaging.

As an instructor Dr. Kennedy will continue his work on MRE and expand his research focus into long term outcome prognostication based on advanced multiparametric MRI and artificial intelligence. His interest in liver cancer therapy is continuing with studies examining tumor response to immunotherapy and non-invasive methods for predicting tumor immunophenotype which can impact therapy response. Dr. Kennedy looks forward to strengthening his existing collaborations within BMEII, Mount Sinai and external institutions and companies to perform impactful research with meaningful patient benefit.

Outside of research, Dr. Kennedy enjoys snowboarding, running, cycling and swimming. These pursuits will be superseded in April when he and his wife are expecting their first child.

Paul Kennedy, PhD
Instructor, Radiology
paul.kennedy@mountsinai.org

continued from previous page

for altering the transmit field distribution specially at high field systems, where the wavelength is comparable with the human size. The array imaging performance in cadaver brain MRI is shown in Figure 1. The preliminary data of this work resulted in one submitted provisional patent, one paper, and two international conference proceedings.

In another study, in collaboration with Drs. Priti Balchandani, Trey Hedden, and Bradley Delman, Dr. Alipour used 7T MRI to investigate baseline and change in brain iron levels in individuals with Alzheimer's disease (AD) compared with healthy control participants. This study aimed to evaluate the correlation between brain iron levels and beta-amyloid aggregation in patients with AD. This study was recently funded by the Alzheimer's Disease Research Center (ADRC) at ISMMS.

Dr. Alipour believes that being a part of BMEII's dynamic environment and being surrounded by hardworking, smart, and kind people built the foundations of his career goal to become a recognized leader and educator in translational neuroimaging.

Akbar Alipour, PhD
Postdoctoral Fellow
akbar.alipour@mssm.edu

Lab Spotlight

Nanoscale Engineering with Massive Impact: Farewell to Prof. Willem Mulder

Jazz Munitz

As the BioMedical Engineering and Imaging Institute continues to rapidly expand, there have been numerous researchers and staff members who have made this institute so exceptional. It is with a grateful and saddened heart that we say goodbye to Prof. Willem Mulder, one of the first members of the original Translational and Molecular Imaging Institute, whose unhindered creativity and stoicism helped build BMEII to its current stature. To honor his impact, we sat down with him for an interview to reflect on where it all started, and how far it's come.

Q: How did you first hear about Mount Sinai?

A: I had heard of Mount Sinai from movies and TV shows like *Law & Order*. Scientifically, Sinai became something mythical to me back when I was a PhD student. Reading the work from Zahi and Dr. Fuster, I was intrigued by both the science and the people behind it.

Q: When did you first meet Zahi?

A: I was working on vessel wall molecular imaging in mice back when I was a PhD student. I reached out to Zahi by email and we arranged to meet in Cologne in, I believe, September of 2005 at the annual Molecular Imaging Conference. Two months later I was on a flight to NYC (for the first time) to spend the tail end of my PhD trajectory in Zahi's lab, from mid-November to mid-December. We were exceptionally productive together, and produced the manuscript "Molecular imaging of macrophages in atherosclerotic plaques using bimodal PEG-micelles" in a month, which was published in *Magnetic Resonance in Medicine*.

Q: How did the Nanomedicine program start?

A: In April 2006 Zahi called me out of the blue, as he had set up meetings with Dr. Drayer and Dr. Charney for my recruitment. I remember spending time in Central Park prior to these meetings where I had sunburnt my head terribly, and went into the meetings looking like a tomato. How could I have known that the NYC sun is burning hard in April? In October 2006, I moved to the US to work on a preclinical molecular imaging program, but I was mostly interested in developing nanomedicine into an immunotherapy modality, which is exactly what BMEII's Nanomedicine Program is internationally renowned for today.

Q: Who was your first student?

A: My first student was a Dutch medical student, Mark Lobatto who got to spend an externship at Mount Sinai. He was introduced through his aunt to Dr. Fuster and then ended up with Zahi. Mark and I have completely different personalities, but hit it off and he set up all of our first nanomedicine studies in atherosclerotic rabbit models. We remained in touch and through the Amsterdam Medical Center, I was able to hire Mark as a PhD student to come to Mount Sinai and work on his research. He was awarded his doctorate cum laude (top 2 percentile in Dutch Academia).

Q: What do you remember of moving into the Hess Center?

A: Since I travelled between NYC and the Netherlands very frequently, I was fortunate to spend the first part of my tenure in a basement where I had no sense of time. We were very productive even with limited means, but our research program really levelled up when we took our lean and mean attitude to Hess. I can't think of a better imaging facility in the world. The infrastructure is unique, particularly in how it's managed by Radiology and BMEII.

Willem Mulder stand up paddleboarding, one of his favorite activities. *Photo credit: Bart van Overbeeke*

Q: What was the first big paper you published, when you really felt that you'd made it?

A: I still don't feel that I've made it, but there have certainly been milestone papers:
1) Lobatto et al. *Nature Reviews Drug Discovery*, the first time that we'd shared with the world our vision of nanomedicine in cardiovascular disease; 2) Raphael Duivenvoorden, Jun Tang et al. *Nature Communications*, which we had worked on for five years, beginning in 2008. It was our first study where we fully integrated immunology and demonstrated the application of nanomedicine for innate immune regulation; 3) Binderup, Duivenvoorden, Fay et al. in *Science Translational Medicine*. As one of the reviewers eloquently stated: "A tour de force." Zahi and I worked on a large NHLBI Program of Excellence in Nanotechnology, which started in 2010. This study is the climax of that program. We pulled of nano-immunotherapy of atherosclerotic inflammation in large animal models, facilitated by clinical PET/MR imaging; 4) Max Senders et al. in *Nature Nanotechnology*, where we demonstrated the use of new nanotech and multimodal imaging methods to study immune cell dynamics in living mice; 5) Bram Priem et al. *Cell*, demonstrating the use of our proprietary nanobiologic technology as an efficacious and safe immunotherapy for cancer.

continued on next page

continued from previous page

Q: What have been some of your favorite memories?

A: I've made a lifetime of memories at Mount Sinai and in NYC. Funniest memory: taking my stand up paddleboard on the Hudson River, and getting pulled off the water by helicopter, boat, firetruck, etc. Most rewarding: Seeing some 15-year-old kid, Jazz Munitz, who sent me an email back in 2012, develop his talents toward becoming a highly versatile individual. I see in him the doctor of the future, with strong a scientific foundation, highly interested in technology and engineering, and exceptional social skills. Most grateful: working with uniquely talented individuals like Bram Teunissen and Mandy van Leent.

Dr. Willem Mulder and Jazz Munitz, circa 2015.

Q: What went into your decision to leave Mount Sinai?

A: This was the hardest decision of my life. I had been struggling with my personal life for years, due to living in NYC, so far away from my wife and daughters in the Netherlands. This is something I discussed with Zahi many times. As a sidebar for the new BMEII folks, Zahi is a great mentor for career advice, because he reads and understands people very well. I intended to remain at Sinai after turning down an awarded ERC Consolidator Grant in 2019. Then 2020 happened and it became increasingly clear last summer that travel would remain compromised for a long time, and I was forced to rethink this decision. Zahi recommended I pursue a nontraditional structure. Together with Mihai Netea, a prolific clinician and infectious disease specialist at Radboud University Medical Center (Radboudumc) and the discoverer of trained immunity, I worked on establishing a program between my alma mater, Eindhoven University of Technology (TU/e) and Radboudumc. I now have positions at Radboudumc and the TU/e to establish a translational immunology program between the institutions. I have also been appointed CSO of our biotech startup Trained Therapeutix Discovery, which is the direct result of the technologies the Nanomedicine Lab generated.

Q: How did the founding of Trained Therapeutix Discovery (TTxD), your biotech startup, come to be?

A: This was truly my dream. When I started working with Jordi Ochando, Mihai Netea and Leo Joosten we knew this was the time. The idea started in November of 2016, had real traction in 2017, and negotiations took place from mid-April 2018 to May 2019, which was an absolutely insane process. We have raised a $6 million seed investment with the support of the Jean Boulle group.

Q: How are you doing now back in the Netherlands?

A: The experience at Mount Sinai overall, and my relationship with Zahi shaped me in many ways. The ties between Radboudumc, TU/e, and Sinai investigators remain very strong, and we're fully involved in two large programs. On a personal level, I finally live full time with my wife, daughters, and dogs, and I finally feel like a fulfilled and happy man.

Q: What does the future of the BMEII Nanomedicine program look like, and who will be directing in your absence?

A: Mandy van Leent, my former PhD student, and Bram Teunissen, former post-doc, have recently been promoted to Instructors. They are for a large extent responsible for some of the Lab's recent successes. They are capable of taking my crazy white board drawings and concepts and solidifying them into tangible realities. They are hyper productive and now they get the opportunity to work on their own concepts, and I am convinced they'll do brilliantly. Bram and Mandy are more advanced in their thinking and science than I was at that stage. Bram and Mandy will continue their independent careers off the lab I built, with Mandy specializing in immunology and in vivo imaging and Bram in radiochemistry and nanotechnology. They will work on their own programs, but collectively they will give immuno-imaging at BMEII a tremendous boost, which will be of interest to the entire institute and will find application in a wide range of conditions. It goes without saying that I plan to maintain collaborations with Sinai/BMEII. We are already working on establishing two large Program Project Grants. We will continue to work together and I will stay formally connected through an adjunct position, which was made possible through an endowment by Jean Boulle.

We are forever grateful for the creativity and brilliance that Dr. Mulder brought to Mount Sinai. His vision formed a unique and productive nanomedicine program, which will continue to churn out new and exciting research into nanotechnology and immunomodulation. We all wish Willem the best of luck in his future endeavors, and his influence here at BMEII will never be forgotten. Willem, you will be missed, and we raise a beaker in cheers towards your bright future!

Willem Mulder, PhD
Former Director,
Nanomedicine
Professor, Radiology

Meeting Spotlight

BMEII 2021 Engineering & Medicine Seminar Series

In December 2020, we launched our inaugural Engineering and Medicine seminar, a new series focused on the innovation and opportunity at the intersection of engineering and medicine. In partnership with the Department of Diagnostic, Molectular and Interventional Radiology, this series invites experts in the fields of neuroimaging, cardiovascular imaging, cancer/body imaging, nanomedicine, and artificial intelligence, including lectures from some of our newest faculty members at BMEII. Save the dates for this year's seminars, which will be delivered via Zoom. Click here to join.

Speaker Name	Date and Time	Seminar Title
Twan Lammers, DSc, PhD RWTH Aachen University Clinic, Germany	January 11 1-2 PM	Smart Strategies to Improve Cancer Nanomedicine
Olivia Viessmann, PhD Massachusetts General Hospital, Harvard Medical School	January 20 12-1 PM	Anatomical and Physiological Biases in Modern High-resolution fMRI
Jessica Zhang, PhD Carnegie Mellon University	February 8 1-2 PM	Material Transport Simulation in Complex Neurite Networks Using Isogeometric Analysis and Machine Learning Techniques
Jinghua Wang, PhD Deep MRI Imaging Inc.	February 17 12-1 PM	Novel Techniques to Improve MR Image Quality
Mandy van Leent, MD BMEII, Icahn School of Medicine at Mount Sinai	February 22 1-2 PM	Regulation of Innate Immunity through Nanotherapeutics
Dustin Scheinost, PhD Yale University School of Medicine	February 25 12-1 PM	Developing Connectome-Based Predictive Models of Behavior
Hugo Aerts, PhD Brigham and Women's Hospital, Harvard Medical School	March 8 1-2 PM	Artificial Intelligence in Cancer Imaging
Daniel A. Heller, PhD Memorial Sloan Kettering Cancer Center	March 15 2-3 PM	Nanomedicines for the Resarch, Detection, and Treatment of Cancer and Allied Diseases
Bram Teunissen, PhD BMEII, Icahn School of Medicine at Mount Sinai	March 22 1-2 PM	Chemistry in Nanomedicine: Developing New Nanotherapeutics and Imaging Probes
Jon Lovell, PhD, MS State University of New York at Buffalo	April 12 1-2 PM	Drug and Antigen Delivery Applications Using Porphyrin-Based Particles
Octavia Bane, PhD BMEII, Icahn School of Medicine at Mount Sinai	April 26 1-2 PM	Multiparametric MRI of the Kidney
Dan Ennis, PhD Stanford University	May 10 1-2 PM	Novel MRI Techniques to Measure Cardiac Structure and Function
Hayit Greenspan, PhD BMEII, Icahn School of Medicine at Mount Sinai	May 24 1-2 PM	AI in Medical Imaging: Deep Learning Challenges and Solutions for Detection, Segmentation, and Characertization, with Applications to Automated COVID-19 Tools for Severity Analysis Over Time
Jurgen Futterer, MD, PhD Radboud University Nijmegen Medical Centre, The Netherlands	June 14 1-2 PM	Interventional MRI in Oncology
Robin de Graaf, PhD Yale University School of Medicine	June 28 1-2 PM	Recent Advances in In Vivo MR Spectroscopy – Deuterium Metabolic Imaging
William Grissom, PhD, MSE Vanderbilt University	July 12 1-2 PM	New Encoding Approaches in Low-Field MRI
Xiang Xu, PhD BMEII, Icahn School of Medicine at Mount Sinai	September 13 1-2 PM	CEST MRI: APT, glucoCEST and Beyond
Peng Hu, PhD UCLA	October 11 1-2 PM	Ferumoxytol-enhanced Cardiovascular MRI: Opportunities and Challenges
James Duncan, PhD Yale University	October 25 1-2 PM	Neuroimage Analysis in Autism: from Model-Based Estimation to Data-driven Learning
Paul Kennedy, PhD BMEII, Icahn School of Medicine at Mount Sinai	November 8 1-2 PM	Magnetic Resonance Elastography - Applications and Advancements
TBN: Lucy G. Moses Lecture in Medical Imaging and Bioengineering	December 16	TBD

Imaging Spotlight

Congratulations to the 2021 ANRP Pilot Grant Winners

The ANRP pilot grant mechanism is designed to provide junior investigators with the opportunity to develop and implement new neuroimaging related research projects. These grants enable pilot scans on the research MRI scanners at the BioMedical Engineering and Imaging Institute (BMEII) to facilitate the acquisition of preliminary data for NIH applications. All innovative neuroimaging related projects are considered. The objective of the grant program is to stimulate new neuroimaging NIH grants and provide the resources for new investigators to obtain critical pilot data and achieve independence. We convened a committee of experts across many departments involved in brain research to review grants and select our winners.




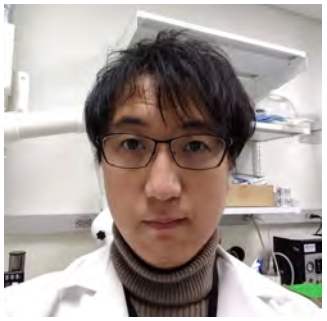

Winners top row: Catherine Elorette, PhD, "Role of face selective patches within macaque frontal cortex in valuation of face stimuli"; Rui Feng, MD, MS, "Complex imaging of the facial nerve in skull base surgical planning and resection of vestibular schwannoma: techno-logical development in 7T ultra-high field MRI"; Yael Jacob, PhD, "Network based real-time neurofeedback using 7-Tesla MRI for treatment of depression"; Kazuya Okamura, MD, "Chemo-fMRI: Coupling chemogenetic circuit manipulation and fMRI in mice for translation."

Winners bottom row: Philip Robson, PhD, "Development of Arterial Spin Labeling Cerebral Perfusion Measurements at 7T "; Alan Seifert, PhD, "Functional MRI of Visual-Vestibular-Cerebellar Interaction"; Genevieve Yang, MD, PhD, "Emotion and cognition as a therapeutic target for real-time fMRI neurofeedback in addiction."



Core Spotlight

BMEII and ANRP Introduce New Imaging Processing Platform

ANRP is now supporting Flywheel, a new platform for data management, automated image processing and pipelining. The Flywheel platform allows for groups to implement standardize processing routines across an entire study and manage data access for collaborations.

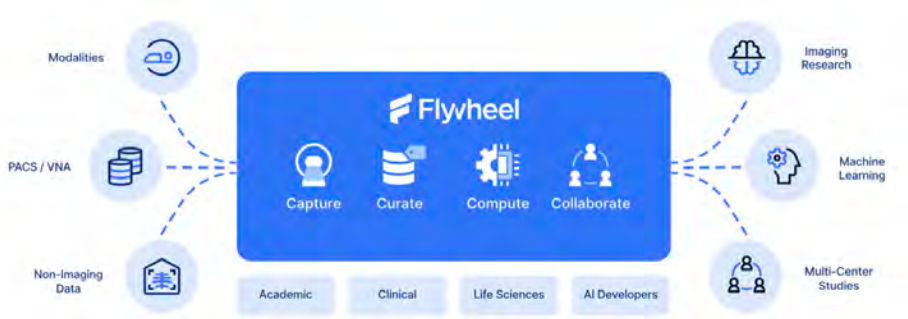

Through Flywheel gear exchange, the platform will host a number of standard image processing routines that include; FreeSurfer segmentation, fMRI and diffusion preprocessing, and much more. In addition to the standard processing we have worked with Flywheel to implement customizable anonymization, multi-echo processing, and MRS automated quantification with LC Model.

ANRP will help the groups set up projects on the platform by uploading archived data, setting up auto send for new acquisitions and, setting up processing pipelines. While many of the gears have been developed for neuroimaging, many can be applied to any MRI datasets and other acquisition modalities. Additionally, support can be provided to create new, customized gears for specific processing needs.

For additional information and costs, please reach out to Dr. Priti Balchandani at priti.balchandani@mssm.edu or Chris Cannistraci at christopher.cannistraci@mssm.edu.

June 2021 Issue 4

Icahn School of Medicine at Mount Sinai

BioMedical Engineering and Imaging Institute

bmeiisinai.org

Zahi Fayad, PhD
Director, BioMedical Engineering and Imaging Institute
Lucy G. Moses Professor in Medical Imaging and Bioengineering
Professor of Radiology & Medicine (Cardiology)
zahi.fayad@mssm.edu

Message from the Director

With summer upon us, COVID-19 restrictions lifting, and vaccinations rising, there is much to celebrate. I am grateful to my team for their persistence and strength throughout the uncertainty of the last sixteen months. While we all take time to enjoy the summer sunshine and re-opening of borders, we will not relent in our efforts to understand this disease and its long-term effects, alongside collaborators across the health system. BMEII is full of so many talented and dedicated people, and it is a joy to see several faculty, staff, and post-docs recognized for their service and innovation through recent awards. We continue to expand and hire across our research programs and welcome applications from under-represented groups. I hope you enjoy this edition of the BMEII newsletter, and I wish you all an enjoyable and healthy summer. Thank you for your support.

BMEII News & Updates

BMEII in the News

COVID-19 research conducted at BMEII has gained national attention in recent months. Both NBC Today and NBC News covered our imaging research investigating cardiac inflammation in post-acute sequelae of SARS Co-V- 2 (PASC) patients. These features follow patients who have experienced persisting symptoms of COVID and important research happening across the country and here at Mount Sinai to understand what the longterm effects of COVID are and why some patients experience extended illness.

Congratulations Corner

Yael Jacob, PhD, a postdoctoral fellow in the Balchandani Lab, is a recipient of the inaugural Friedman Brain Institute Postdoc Innovator Award. The award will provide $25,000 to support innovative research by a postdoctoral fellow in any laboratory affiliated with the Friedman Brain Institute. Dr. Jacob will apply the funding towards her project entitled "Network based real-time neurofeedback using ultra-high field MRI to reduce rumination levels in depression."

ImagingNation Podcast

Join us on ImagingNation, a podcast where we discuss all things imaging science, research, innovation, and society. Listen to our latest episodes on Apple and Spotify.

BMEII is hiring!

We are looking for innovative, motivated faculty, postdocs, researchers, and support staff to join our team. Visit our website for all open positions and instructions on how to apply.

BMEII News & Updates

Welcome, New BMEII Staff

Ghadi Abboud is a post-doctoral fellow in Dr. Taouli 's Cancer and Body Imaging lab, where he works on quantitative MRI applications in various abdominal diseases. He completed his medical training and radiology residency in Beirut, Lebanon. He also holds an EMBA from the University of Balamand, Lebanon.

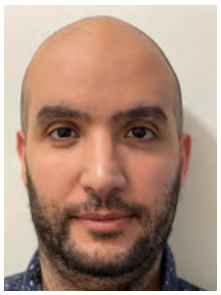

Jessica Fernandes joined BMEII as a Senior Associate Researcher and manages the Nanomedicine lab. Originally from Brazil, Jessica completed a BS in Biomedical Science at UFPR (Federal University of Paraná) and MS in Biosciences and Biotechnology at Fiocruz (Carlos Chagas Institute). She has developed expertise in monoclonal and bi-specific antibodies production and cellular and molecular biology.

Chendi Cao joined BMEII as a post-doctoral fellow in Dr. Yang's Cardiovascular Imaging group and focuses on novel imaging techniques for comprehensive cardiovascular magnetic resonance (CMR) imaging using non-Cartesian trajectories and motion-correction techniques. His research will consist of pulse sequence programming and development, acquisition of image data on patients and healthy volunteers, image reconstruction with Gadgetron. He obtained his PhD in Computer Science and MS, BS in Statistics from Kansas State University.

Patrick Tanella is a Program Coordinator for Dr. Taouli's Cancer and Body Imaging lab, where he assists with RECIST requests, the annual research retreat, and general lab support. Prior to joining BMEII, Patrick completed his BA in Psychology and Art History at Vassar College in addition to spending a semester at University College London. He is interested in connecting art and public health, and hopes to merge the two disciplines by using painting as a holistic form of therapy for cancer patients.

Staff Spotlight

Our STAR Clinical Research Managers

Two of our clinical research staff were recently honored by Dr. David Reich, President of The Mount Sinai Hospital with the STAR Award for the exceptional compassion and care they have shown throughout the COVID-19 pandemic. These awards are given to employees who exemplify the Mount Sinai values and service standards of empathy, equity, teamwork, creativity, agility, safety, compassion, and excellence.

On May 26, Dr. David Reich surprised Renata Pyzik (left) and Rima Fayad (right) with the Mount Sinai STAR Award.

Renata Pyzik, MS, MA, is a Project Manager who has worked on cardiovascular imaging studies at BMEII for six years. Renata plays an instrumental role in managing Dr. Fayad's clinical research studies, including maintaining local and FDA/NIH compliance, establishing new projects, managing databases, analyzing data, and coordinating recruitment. Renata says, "Improving diagnostics and searching for new technologies, like imaging techniques, has always been a driving force for me. I am inspired by Dr. Zahi Fayad and the BMEII staff to advance educationally and professionally." One memorable experience from the last year involved the early detection of lung cancer in a patient participating in COVID-19 imaging research. Catching the disease early is potentially lifesaving, and the patient was extremely grateful for the discovery. Beyond BMEII, Renata is very active and enjoys competitive skating, tour guiding, crocheting and needlepoint. She is also passionate about fundraising for families with children with special needs.

Rima Fayad, MPH, is a Clinical Research Manager and has been with BMEII for 14 years. She recruits and consents patients participating in cardiac imaging studies and ensures adherence to safety measures, regulatory compliance, and study protocols. Despite the challenges of maintaining a safe environment for patients and staff during the pandemic, Rima loves being able to meet and form relationships with research participants, and always keeps safety in mind. Recently, a patient wrote a letter in gratitude for Rima's courteous and professional attitude and for how well she and our research techs were able to put him at ease. For Rima, the STAR award inspires her to keep doing better. She emphasizes the importance of teamwork and is grateful to be part of BMEII. Outside of work, Rima enjoys running, traveling, hosting friends, and spending time with family.

If you would like to nominate STAR employees for embodying Mount Sinai values, visit: https://sinaicentral.mssm.edu/star/

Faculty Spotlight

Rising Star

Li Feng, PhD

Dr. Li Feng is an Assistant Professor of Radiology at the Icahn School of Medicine at Mount Sinai. Dr. Feng obtained his PhD in Biomedical Imaging from NYU School of Medicine in 2015. His research has primarily focused on development of novel rapid motion-robust and quantitative MRI techniques combining advanced acquisition schemes (e.g. golden-angle radial sampling) and image reconstruction strategies (e.g. compressed sensing and deep learning). These new methods can enable acquisition of diverse and comprehensive information in a single, rapid and continuous stream. Over the last decade, Dr. Feng has led the development of several fast and ultrafast MRI techniques. One of them, called Golden-angle RAdial Sparse Parallel (GRASP) MRI, has been successfully translated into the clinic for a broad spectrum of applications and has resulted in increase of the utility, the simplicity, and the cost-effectiveness of MRI. Dr. Feng was named as a Junior Fellow of the International Society for Magnetic Resonance in Medicine (ISMRM) in 2015 and was a winner of the Early Career Award in Basic Science from the Society for Cardiovascular Magnetic Resonance (SCMR) in 2014. Dr. Feng is also a recipient of the 2021 Junior Faculty Council Award for Academic Excellence at Mount Sinai.

Dr. Feng was recently awarded a 4-year R01 grant by the NIH/NIBIB to develop and optimize new dynamic MRI techniques based on GRASP MRI for rapid free-breathing and easy-to-use perfusion quantification in the liver. The proposed new methods are expected to achieve improved imaging performance, reduced reconstruction time and substantially simplified perfusion analysis compared to existing MRI methods. These new technical developments will be integrated into the clinical setting to generate a new liver MR perfusion framework, which would enable significant progress towards improved characterization and management of many liver diseases with high clinical impact, such as hepatocellular carcinoma (HCC). It could also change the entire experience of MR imaging for physicians, for patients and for technologists.

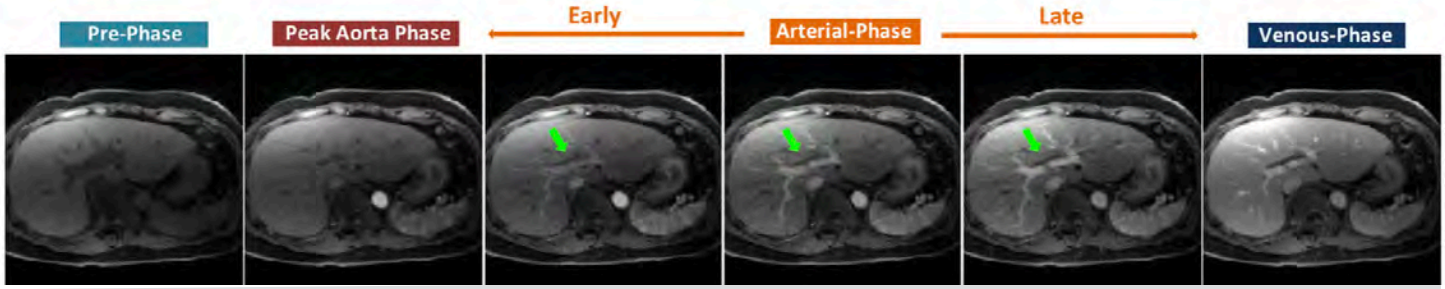

Figure 1: Fast free-breathing 3D dynamic contrast-enhanced MRI (DCE-MRI) of the liver using the GRASP technique. High resolution contrast-enhanced liver images at multiple time points can be obtained for clinical use.

Dr. Feng has received a fundable score on another recent NIH R01 submission, which is now being considered for funding. Building on Dr. Feng's expertise in GRASP MRI and its variant, called XD-GRASP (GRASP with eXtra Dimensions) MRI, this grant proposal aims to evaluate the long-term consequences of COVID-19 on the lungs. Tracking damage in the lungs is important for early identification of COVID-19-induced pulmonary diseases such as lung fibrosis or lung function reduction. However, existing clinical methods are insufficient for simultaneous structure and regional function evaluation of the lung, and therefore there is a pressing clinical need to develop new imaging methods for this purpose. This project aims to develop a novel MRI technique for non-invasive and radiation-free imaging of pulmonary anatomy and function with improved motion robustness, which will enable a 10-minute free-breathing "one-stop-shop" examination of the lung. As a scientific community, we are still learning the long-term effects of COVID-19. Thus, this new method proposed by Dr. Feng holds great potential to improve management of any lingering effects of this disease, and it can also be applied to evaluate other pulmonary diseases.

In addition, together with Mingqian Huang, MD, Musculoskeletal Chief, Dr. Feng recently initiated a project in collaboration with a company called Hyperfine, which develops and builds bedside portable low-field MRI scanners with a mission of making MRI machines for every place and everyone. The main purpose of this project is to investigate the performance of the Hyperfine MRI scanner in musculoskeletal applications and to evaluate whether a low-field portable MRI scanner could achieve sufficient diagnostic image quality in assessing different diseases in the knee joint compared to routine clinical MRI scanner.

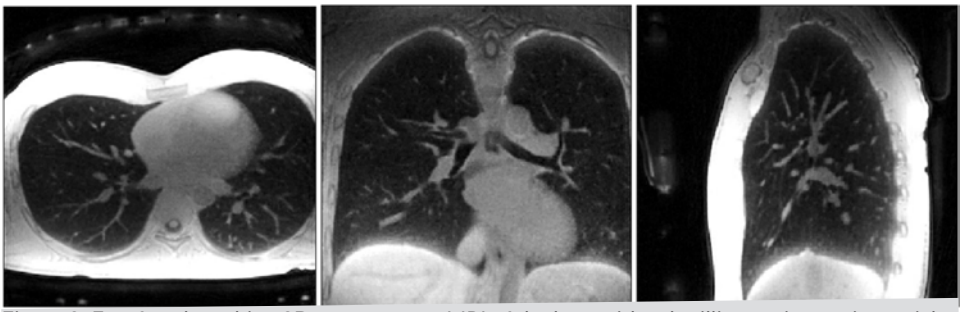

Figure 2: Fast free-breathing 3D non-contrast MRI of the lung with submillimeter isotropic spatial resolution using the XD-GRASP technique. Good delineation of lung structure can be obtained without radiation exposure and without the need for breath holding.

Conflict of interest disclosure: Dr. Feng is one of the named inventors in a patent on the GRASP and XD-GRASP MRI techniques.

Li Feng, PhD
Assistant Professor, Radiology
li.feng@mssm.edu

Meeting Spotlight

International Society for Magnetic Resonance in Medicine (ISMRM) Presented Abstracts

Several BMEII and Radiology faculty presented scientific and educational talks and posters at the May 2021 ISMRM virtual conference. The sessions are available at this link (login required).

Section Name	Session Type	Abstract Title (Note: links are only active for registered attendees)	Presenter Name
Elastography	Scientific Talk	Tumor stiffness and stiffness change using 3D MR elastography are markers of tumor lymphocyte infiltration and immunotherapy response in HCC.	Paul Kennedy, PhD* Lab: Taouli
Simultaneous Multiparameter & Multidimensional Cardiovascular MRI	Educational Talk	Basics of Multidimensional Imaging	Li Feng, PhD* Lab: Feng
RF Design I	Scientific Talk	Enhanced Ultra-High Field Brain MRI Using a Wireless Radiofrequency Sheet	Akbar Alipour, PhD* Lab: Balchandani
Spectroscopy: ACQ/ Recon/Analysis	Scientific Poster	Ultrahigh-field echo-planar spectroscopic imaging with semi-adiabatic spatial-spectral pulses	Gaurav Verma, PhD* Lab: Balchandani
Safety	Scientific Talk	RF safety and image quality testing of deep brain stimulation electrodes with 3T MRI	Gaurav Verma, PhD* Lab: Balchandani
Multiple Sclerosis	Scientific Talk	Prediction of multiple sclerosis clinical progression using whole brain adiabatic T1rho and Relaxation Along a Fictitious Field imaging	Ivan Jambor, MD* Radiology
Artificial Intelligence (Machine Learning & Deep Learning) Applications to Neuroradiology	Scientific Poster	Classification Between Epilepsy Patients and Healthy Controls Using Multi-Modal Structure-Function Brain Network	Yael Jacob, PhD* Lab: Balchandani
MRI in Stroke: Vessels, Flow & Tissue Structure	Scientific Talk	GraspMRA: High Temporal Resolution, Non-Contrast Enhanced, Time-Resolved 4D MR Angiography Using Golden-angle Radial Sparse Parallel Imaging	Li Feng, PhD* Lab: Feng
Fat & Metabolism	Scientific Talk	MP-Dixon-GRASP: Magnetization-Prepared Multiecho GRASP MRI for Free-Breathing Fat/Water-Separated 3D T1 Mapping	Li Feng, PhD* Lab: Feng
Cancer: Contrast Agents & MRS	Scientific Poster	Estimation of capillary level input function for abbreviated breast Dynamic Contrast-Enhanced MRI using deep learning approach	Li Feng, PhD Lab: Feng
Imaging of Heart Failure	Scientific Talk	Cardiovascular magnetic resonance T1rho endogenous contrast can detect early myocardial fibrosis in hypertrophic cardiomyopathy	Yang Yang, PhD Lab: Fayad
CEST, MT &T1P	Scientific Poster	Whole-brain amide CEST at 3T with a steady-state radial MRI acquisition	Xiang Xu, PhD Lab: Xu
Quantitative Cardiovascular Tissue Characterization	Scientific Talk	Comparison of free-breathing self-gated continuous IR spiral T1 mapping: dual flip angle versus Bloch-Siegert B1-corrected techniques	Yang Yang, PhD Lab: Fayad
Imaging Metabolites: CEST, MR & MRS	Scientific Talk	A digital human head phantom for validation of retrospective motion correction in glucoCEST MRI	Xiang Xu, PhD Lab: Xu
Prostate	Scientific Poster	Machine learning challenge using uniform prostate MRI scans from 4 centers (PRORAD)	Ivan Jambor, MD Radiology
Machine Learning for Quantitative Imaging	Scientific Talk	Self-supervised Deep Learning for Rapid Quantitative Imaging	Li Feng, PhD Lab: Feng

*Indicates presenting author

Engineering & Medicine Seminar Series

For an updated schedule of lectures, check out our webpage. The series will take place on Zoom for the remainder of the year. Interested in presenting? Contact Mallory Stellato at mallory.stellato@mssm.edu.

Grant Spotlight

Exciting New Grants

Sara Lewis, MD, Associate Professor, and **Octavia Bane, PhD**, Instructor of Diagnostic, Molecular and Interventional Radiology, are co-recipients of an R01 award from the NIDDK, for their project proposal "Characterization of Renal Allograft Fibrosis and Prediction of Outcome Using a Quantitative MRI Approach". The purpose of the project is to validate a robust, quantitative multiparametric (mp)MRI approach based on diffusion-weighted and relaxometry (T1 and T1rho) MRI to accurately and non-invasively measure renal transplant fibrosis and clinical outcome. Concomitantly with detecting and staging renal transplant fibrosis, the study aims to detect and stage other histopathological diagnoses of inflammation, and to assess the added values of urinary biomarkers of fibrosis. mpMRI in combination with urinary biomarkers will then be used to predict renal transplant outcome over 2 years. The bi-center, prospective study is based on the collaboration of imaging scientists, transplant nephrologists and renal pathologists at Mount Sinai and Weill Cornell Medical Center (WCMC). The study aims to recruit 120 patients with renal transplant scheduled to undergo indication biopsy at Mount Sinai, and 120 patients scheduled to undergo indication or surveillance biopsy at WCMC. Patients will be imaged at 3T with mpMRI protocols harmonized between the two centers.

Akbar Alipour, PhD, a post-doctoral fellow in the Balchandani Lab received funding for his project "Quantifying beta amyloid plaques aggregation in Alzheimer's diseases using 7T MRI" from the Alzheimer's Disease Research Center Developmental Projects (Mount Sinai ADRC/NIA) for funding. Alzheimer's disease (AD) is definitively diagnosed with conformity only by detecting biomarkers as seen under microscopy and only on postmortem neuropathology. Since definitive diagnosis comes too late to effect management, there is need for an accurate noninvasive technique to characterize AD onset. Higher regional brain iron concentrations in patients with AD are associated with beta amyloid plaques and neurofibrillary tangles. Iron accumulation was found to increase the production of amyloid precursor protein and thus might be directly involved in the formation of beta amyloid plaques. The detection of amyloid plaques on MRI relies on precise co-localization of these deposits with iron, which allows them to appear more conspicuous on high-field MRI. MRI at ultra-high field strength, such as 7T, increases sensitivity by offering improved signal-to-noise ratio and MR contrast. High-field MRI is one technique by which AD has been increasingly studied non-invasively and in vivo. Therefore, the magnetic susceptibility at 7T MRI is increased in the amyloid plaque-containing regions of AD tissue compared with brains of healthy controls, features that may elucidate pathology underlying susceptibility changes over time in AD patients."

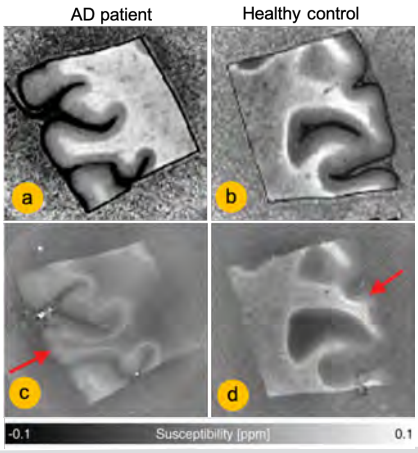

T1-weighted morphological MRI (a,b) and quantitative susceptibility maps (c,d) of frontal cortex postmortem brain tissue of an AD patient (a,c) and healthy control (b,d). Higher susceptibility values in the gray matter of the AD tissue (arrows) are likely due to higher amyloid plaque burden.

Core Spotlight

BMEII Expands Artificial Intelligence Technology

As BMEII continues to increase our artificial intelligence (AI) and deep-learning capabilities, we have acquired an NVIDIA DGX-A100 server, one of the latest instruments developed by NVIDIA to accelerate AI development. From training to inference, this third-generation supercomputer was built to support the largest AI datasets and to optimize and accelerate the computing power of multiple workloads. With six times the training performance of its predecessor and eight GPUs, the DGX-A100 (BMEII-HPC-2) server will boost efficiency and allow for parallel computing. Now, our researchers can train more innovative and comprehensive neural networks within a shorter turnaround time, processing millions of images in one day. BMEII-HPC-2 provides BMEII with the performance of 5 petaFLOPS AI and 10 petaFLOPS INT8. The server runs NVIDIADGX Server 5 based on Ubuntu 20.04 and can support other OS through either Linux containers or virtual machines.

The NVIDIA DGX-A100, or BMEII-HPC-2 server.

For additional information, please reach out to Chris Cannistraci at christopher.cannistraci@mssm.edu.

October 2021 Issue 5

Icahn School of Medicine at Mount Sinai

BioMedical Engineering and Imaging Institute

bmeiisinai.org

Zahi Fayad, PhD
Director, BioMedical Engineering and Imaging Institute
Lucy G. Moses Professor in Medical Imaging and Bioengineering
Professor of Radiology & Medicine (Cardiology)
zahi.fayad@mssm.edu

Message from the Director

Welcome and welcome back! With the start of a new academic year, there is much to look forward to. I am thrilled to announce that the BMEII Symposium will be back as an in-person event in 2022 after a two-year hiatus due to the pandemic. We look forward to gathering experts across imaging modalities, nanotechnology, machine learning, data science, and digital health to learn from one another and advance our collective understanding of how these tools can promote health and wellbeing. More information on our events can be found in this issue and will be distributed over the coming months. In the meantime, please enjoy the Fall issue of the BMEII newsletter.

BMEII News & Updates

Congratulations Corner

Yael Jacob, PhD, who started as a postdoctoral Fellow at BMEII in April 2018, joined the Depression and Anxiety Center for Discovery and Treatment in the Department of Psychiatry as Assistant Professor with a secondary appointment in BMEII this fall. Her research uses advanced neuroimaging to study structural and functional neural networks across different mood and anxiety disorders to understand how brain networks communicate and influence each other during different cognitive states.

Bradley Delman, MD has worked with Priti Balchandani, PhD since 2016 and has been formally BMEII-affiliated faculty since 2018. This fall, he has been promoted to Full Professor. He provides clinical and diagnostic expertise for many of the 7T neuroimaging protocols under Dr. Balchandani. This work complements his administrative, quality and clinical roles in the Department of Radiology. Dr. Delman is honored to contribute to such a well-organized and productive team.

BMEII is hiring!

We are looking for innovative, motivated faculty, postdocs, researchers, and support staff to join our team. Visit our website for all open positions and instructions on how to apply.

Welcome, New BMEII Staff

Jamel A. Hicks recently joined BMEII as an Administrative Assistant. In his 5 years at Mount Sinai, Jamel has been a Patient Service Representative at Mount Sinai Union Square and a Senior Secretary in the Department of Orthopedics. Jamel completed his MBA in financial services at the Metropolitan College of New York. He is honored to join BMEII and looks forward to working with the diverse staff here.

Liliana Hopkins, a high school senior at Secaucus High School, joined BMEII in June 2021 as a volunteer. Her primary responsibilities included the redesigning and rewriting of the neuroimaging webpage. In addition to her work for BMEII, Liliana completed an internship at the Metropolitan Museum of Art and a mentorship for The Incandescent Review's Summer Studio. She plans to pursue a career in science communication and degrees in both the sciences and humanities.

Shams Rashid completed his undergraduate studies in Electrical Engineering at the City College of New York and received his PhD in Biomedical Engineering from Stony Brook University. He trained as a postdoctoral scholar at UCLA, specializing in Cardiac MRI. Prior to joining Mount Sinai, he was an Associate Scientist in St. Francis Hospital (Roslyn, NY). As an Instructor in BMEII, Shams plans to focus on Translational Neuroimaging with Ultrahigh Field MRI in the ANRP as well as contribute collaboratively to Cardiovascular and Body MRI.

Sera Saju is a research coordinator for multiple projects in ANRP looking at post-COVID symptoms. Before working at Mount Sinai, Sera was a research assistant for 2 years at NYU Langone for a study investigating predictive markers for bariatric surgery outcomes. She is currently working toward a Master's in Biomedical Science at Rutgers University while applying to medical schools.

Postdoc Spotlight

Bram Priem, MD

Bram Priem is a post-doctoral fellow in BMEII's Nanomedicine Laboratory. He received his medical degree at the University of Amsterdam in the Netherlands in 2016. After working in the medical field for a year, he started a PhD in nanotechnology with Dr. Willem Mulder as a supervisor and visited Mount Sinai several times for experiments. Dr. Priem's doctoral work focused on the development of a nanoparticle that induces trained immunity as a novel immunotherapy in cancer treatment. For this project he used BMEII's extensive facilities. Using imaging probes and the micro PET/CT, Dr. Priem and his team were able to image shifts of myeloid cell populations and increases in metabolism in the bone marrow and confirm the biodistribution of their novel particle in mice and non-human primates. This project has resulted in a publication in Cell titled: 'Trained Immunity-Promoting Nanobiologic Therapy Suppresses Tumor Growth and Potentiates Checkpoint Inhibition'.

Currently Dr. Priem is performing a follow up project that has a deeper focus on the changes happening in the tumor microenvironment after treatment with their trained immunity inducing nanobiologic.

While his work primarily focuses on cancer treatment, Dr. Priem also aims to contribute to the fast and early detection of cancer and to identify the translational characteristics of nanoparticles in other diseases. To this end, he is currently investigating the results of treatment on the immune system inside the tumor microenvironment. The Nanomedicine Lab, now run by Drs. Bram Teunnissen and Mandy van Leent, combines both chemistry and translational research for the fast and efficient development of new treatments. This provides a creative and collaborative working environment. Outside of research, Dr. Priem enjoys running, snowboarding and cooking. In the future he hopes to start a residency in Internal Medicine and become an Oncologist.

Bram Priem, MD
Postdoctoral Fellow,
Nanomedicine
bram.priem@mssm.edu

Meeting Spotlight

Save the Date!

BMEII Symposium & Radiology Retreat

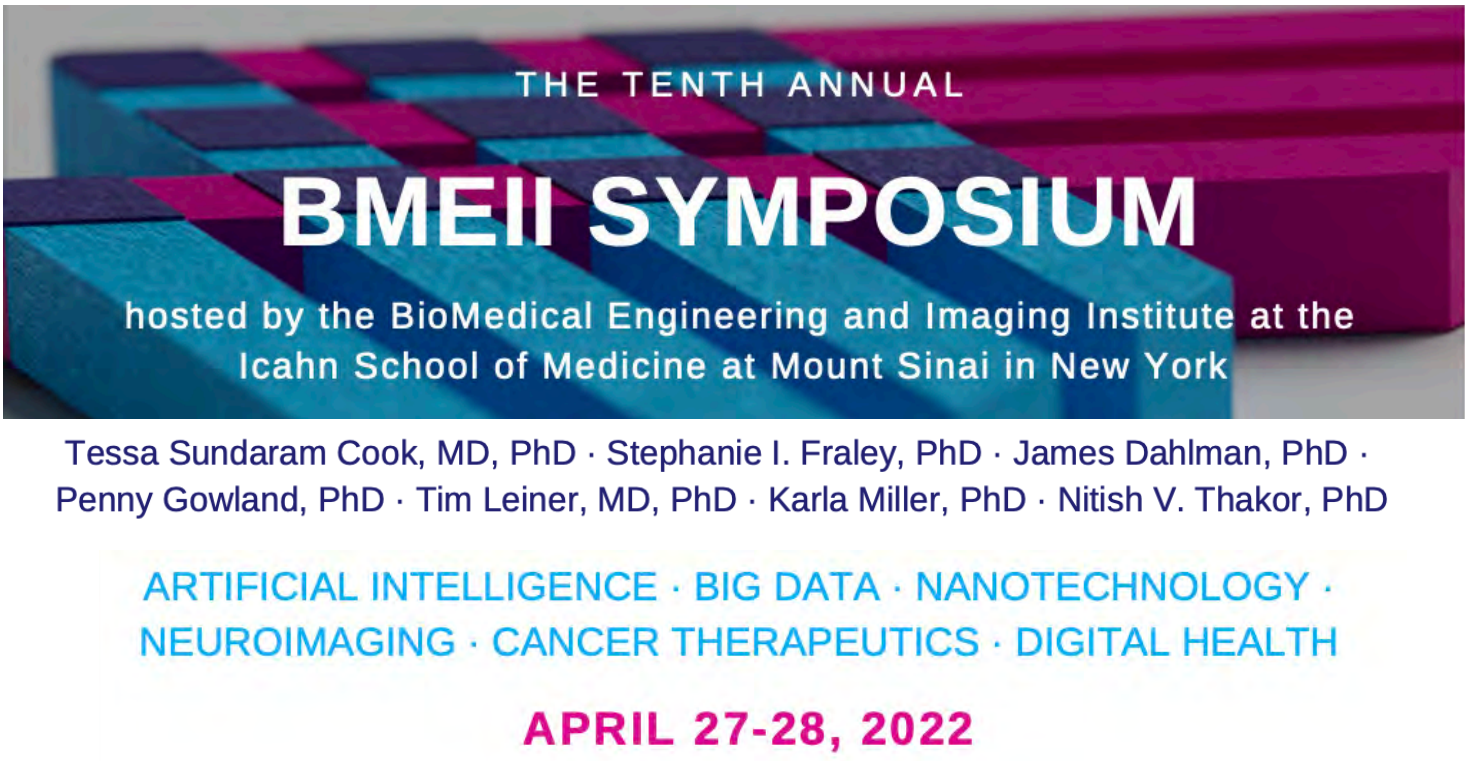

Engineering & Medicine Seminar Series

For an updated schedule of lectures, check out our webpage. The series will take place on Zoom for the remainder of the year. Interested in presenting? Contact Mallory Stellato at mallory.stellato@mssm.edu.

Faculty Spotlight

The Intersection of Neurosurgery, Psychiatry, and Imaging

Ki Sueng Choi, PhD

Ki Sueng Choi, PhD, is an Assistant Professor of Radiology and Neurosurgery at the Icahn School of Medicine at Mount Sinai and joined the BMEII Neuroimaging faculty in 2018. He heads a multimodal imaging core at the Nash Family Center for Advanced Circuit Therapeutics (CACT), specializing in advanced precision surgical treatments for neuropsychiatric disorders. Dr. Choi earned his PhD in bioengineering from the Georgia Institute of Technology, focusing on functional and structural neuroimaging in various psychiatric disorders. He completed a postdoctoral fellowship and served as an Assistant Professor in the Department of Psychiatry and Behavioral Science at Emory University.

Dr. Choi is the Imaging Core lead scientist at CACT. His research focuses on connectome-based deep brain stimulation (DBS) strategies for various neurological and psychiatric disorders. The Choi lab is developing a precision surgical targeting approach based on brain connectivity analyses, "Connectome DBS," that integrates multimodal structural (diffusion tractography) and functional (resting-state fMRI and PET) imaging strategies. Over the past decades, DBS has demonstrated remarkable clinical benefits for people with neuropsychiatric conditions. Though current DBS targets are still predominantly based on the historical efficacy of stereotactic lesions, accumulating evidence suggests that DBS primarily works by rebalancing and remodeling diseased brain circuits. Therefore, the field of DBS is currently experiencing a paradigm shift away from the focal effects of stimulation on the target anatomical structure toward impacting distributed brain networks. This development is paralleled by the maturation of the "connectome" in the field of neuroimaging. Significantly, the recent implementation of computational neural field models to DBS leads and diffusion tractography images allows us to estimate activation white matter pathways in an individual patient with given stimulation parameters (i.e. location, amplitude, pulse width). This novel connectome approach has been applied to subcallosal cingulate DBS for treatment-resistant depression, and it shows an 80% response rate compared to 41% anatomy-based targeting. Currently, this approach is being tested in OCD patients treated with DBS of the Anterior Limb of Internal Capsule (ALIC), a recently funded R01 project (Drs. Choi and Figee, MPI). In addition, a newly developed toolbox that enables real-time visualization of activation white matter pathways with given stimulation settings, now allows for a patient-specific tractography-based determination of the optimal target location in the operating room and programming tractography-informed stimulation settings during follow-up.

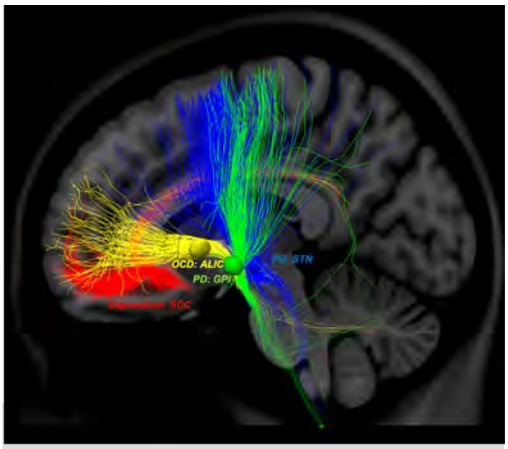

Figure 1. Connectome Deep Brain Stimulation and white matter activation pathway in Subcallosal Cingulate Cortex (SCC) for treatment-resistant depression (Red), Anterior Limb of Internal Capsule (ALIC) for OCD (Yellow), STN and GPi for Parkinson's Disease (GPi: Green and STN: Blue).

In addition to DBS research, Dr. Choi and his team are studying brain mechanisms mediating depression pathogenesis and antidepressant treatment response using multimodal neuroimaging strategies, including resting-state fMRI, PET, and structural techniques. Current projects emphasize developing novel imaging biomarkers predictive of disease progression, treatment response, and optimal treatment selection for individual depressed patients at all stages of illness.

Ki Sueng Choi, PhD
Assistant Professor, Radiology, Neurosurgery
kisueng.choi@mssm.edu

Core Spotlight

Core Staff

While this feature has mostly focused on Core hardware, we all know that the hardware would be largely useless without the dedication and tireless efforts of our Core staff. This month we'd like to profile the MRI and Nuclear Medicine research technologists who work in the Human Imaging Center in BMEII. We'd also like to recognize all the clinical technologist (too numerous to mention) that assist with research on other systems around the medical center.

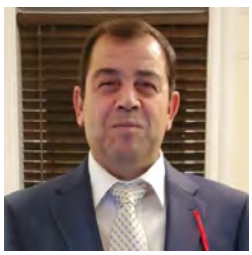

From left to right: Kamil Banibaker, Dewey Chu, Kimberly Jackson. Not pictured: Clayton Reid.

Kamil Banibaker, RT (R) (MR) (ARRT), has been working in radiologic technology for 40 years doing MRI, CT, interventions, and research. He has a Bachelor of Science from Long Island University and has been with BMEII since 2013. Outside of work, he enjoys walking, soccer, swimming, and tennis.

Dewey Chu, RT (R) (MR) (ARRT), has been in MRI since 2009 and started working at BMEII in 2013. Dewey works with the Skyra 3T, Magnetom 7T, and the PET/MRI scanners. His hobby is traveling to different countries for site seeing.

Kimberly Jackson, BS, LNMT, RT (N), (MR), started as a licensed nuclear medicine technologist in 2010 and went on to obtain her MRI license in 2015. Kim joined BMEII in 2019 but has been involved in PET/MR as a Lead Technologist since 2012 when the first ever simultaneous PET/MR study was performed in New York. She is skilled in PET/MRI, Clinical Research, Physics, Science, Fine Arts, and Public Speaking.

Clayton Reid, RT (R) (MR) (ARRT), has been scanning in MRI since 1993 and has been in the BMEII as a per diem technologist for the past 4 years. He enjoys spending time with his family and car customization.

March 2022 Issue 6

Icahn School of Medicine at Mount Sinai

BioMedical Engineering and Imaging Institute

bmeiisinai.org

Zahi Fayad, PhD
Director, BioMedical Engineering and Imaging Institute
Lucy G. Moses Professor in Medical Imaging and Bioengineering
Professor of Radiology; Medicine (Cardiology); AI & Human Health
zahi.fayad@mssm.edu

Message from the Director

Our faculty, trainees, and staff continue to impress with their many accomplishments, awards, and innovative, boundary-pushing research. We are excited to continue expanding our facilities and operations this year through a new Siemens MAGNETOM Prisma 3T MRI and through key hires to broaden our research scope in neuroimaging and wearable devices.

We look forward to convening in April for the 10th Annual BMEII Symposium, the first time since 2019, and the first symposium under our new name. With renowned speakers ranging from nanomedicine to cancer imaging to healthcare leadership, this event will be an exciting chance to reconnect and exchange ideas with colleagues in the metropolitan area.

We wish all of our readers a happy and healthy 2022.

BMEII News & Updates

Congratulations Corner

Please join us in congratulating the following BMEII members on their well-deserved achievements:

Award Recipients: BMEII Faculty and Affiliated Faculty received pilot grant awards from the Friedman Brain Institute, which were also named Mount Sinai Alzheimer's Disease Research Center (ADRC) Scholarship. Lazar Fleysher, PhD aims to develop and apply novel ultrahigh field (7T) sodium brain imaging to detect cell distress at an earlier stage of Alzheimer's Disease. Xiang Xu, PhD and Trey Hedden, PhD will apply saturation transfer based MRI methods to study pathological aggregates related to Alzheimer's Disease.

ANRP Pilot Grant Awardees Selected: The Advanced Neuroimaging Research Program (ANRP) awarded pilot grants to the following individuals: Erin Beck, MD, Ho Wing Chan, MD, Xiang Xu, PhD, Nilsson Holguin, PhD, Benjamin Rapoport, MD PhD, and Shams Rashid, PhD.

New Grants: Li Feng, PhD recently received a new NIH/NIBIB R21 grant for his study "3D Free-Breathing Fat and Iron Corrected T1 Mapping." Xiang Xu, PhD was awarded an R21 from NINDS for her study "Structural and metabolic neuroimaging of ME/CFS occurring with and without COVID-19 infection."

Promotions: Li Feng, PhD has been promoted to Associate Professor. Octavia Bane, PhD has been promoted to Assistant Professor.

Educational Milestones: Mandy van Leent, MD PhD successfully defended her PhD thesis (cum laude) "Employing nanomedicine in inflammatory diseases" from the University of Amsterdam. Xueyan Mei, PhD earned her PhD after defending her dissertation "Cats to CATs with RadImageNet: A Transformative Platform for Medical Imaging AI Research," and will stay at BMEII as a post-doctoral fellow to continue her important research in AI and imaging. Mackenzie Langan, a current MS student, has been accepted to the PhD program at the Graduate School of Biomedical Sciences at Mount Sinai.

Expanding BMEII Family: On December 10, 2021, Shams Rashid and his wife welcomed their daughter Naba. Li Feng and his wife welcomed a new baby girl, Scarlett, on December 24, 2021. On January 12, 2022, Dewey Chu and his wife welcomed baby Adrian.

BMEII is hiring!

We are looking for innovative, motivated faculty, postdocs, researchers, and support staff to join our team. Visit our website for all open positions and instructions on how to apply.

Media Spotlight

Researchers across Mount Sinai, including Dr. Zahi Fayad and several of our collaborators, were featured in a recent supplement to *Science* magazine entitled "The Frontiers of Medical Research". To read the supplement, click here.

New podcast episodes! Tune in to our podcast "ImagingNation" to catch up on the latest research in kidney imaging (Dr. Octavia Bane and Dr. Sara Lewis) and MRI applications to neuroimaging (Dr. Gaurav Verma) on Apple or Spotify.

Welcome, New BMEII Staff

Barbara (Babs) Chacon is a Program Coordinator II for Dr. Taouli's lab. She graduated from Rutgers University with Bachelor's degree in Psychology. Her focus in the lab is coordinating research related meetings and events, assisting with the completion of RECIST (Response Evaluation Criteria in Solid Tumors) requests from various research teams, and handling any administrative tasks necessary to keep the lab running smoothly.

Raina Ghai-Mehta, MSN, RN, CRN is a registered nurse with 10 years of experience and joined BMEII as a Licensed Clinical Research Manger. She previously worked at Memorial Sloan Kettering Cancer Center as Clinical Research Nurse IV in Diagnostic Radiology. Over her career there, she transitioned into research nursing and worked with interdisciplinary teams in the development of clinical trials/research, data collection, safety, and medical information programs.

Anthony Kaplan RT (N) (CT), LNMT graduated from Molloy College and has been working as a Nuclear Medicine Technologist since 2009, specializing in nuclear cardiology and PET/CT. He joined the BMEII PET/MR team in late 2021. Anthony earned his CT license in 2017 and is currently earning his MRI license through Molloy College. He lives on Long Island with his wife, 9-year-old son and 6-year-old daughter. When not at work, Anthony enjoys playing the drums and going on bike rides with the family's golden retriever.

Rodolphe LeForestier is a Postdoctoral Fellow in the Neuroimaging Lab at BMEII. He obtained a PhD in Physics and MS in Medical Physics at the University of Rennes 1, France. He works with Dr. Xiang Xu to develop and improve MRI techniques in CEST imaging, and is particularly interested in the possible use of glucose as a contrast agent at 7T.

Judit Morla-Folch is a post-doctoral fellow in the Nanomedicine Lab, where she works on the development and characterization of novel nanoimmunotherapeutics. Prior to joining Mount Sinai, she trained as a postdoctoral scholar at the University Autonoma of Barcelona (UAB) and New Jersey Institute of Technology (NJIT), working on the development of fluorescent nanoparticles for bioimaging and theragnostic. Her current research in the Nanomedicine Lab focuses on fighting cancer using photodynamic and targeted radiotherapies combined with immunotherapies.

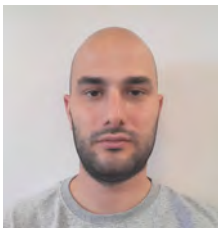

Efe Ozkaya is a post-doctoral fellow in Dr. Taouli's Cancer and Body Imaging lab, where he works on the assessment of liver stiffness through Magnetic Resonance Elastography. He completed his PhD studies in the Mechanical Engineering Department at Stevens Institute of Technology, Hoboken, NJ.

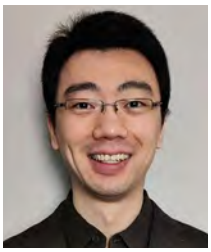

As a Senior Research Scientist, **Ding Xia** works with Dr. Li Feng and Dr. Xiang Xu on developing advanced MRI sequences and image reconstruction methods for rapid quantitative MRI and CEST MRI. Ding came to BMEII with experience in pulse sequence programming and quantitative imaging. He previously worked as a Research Scientist at the Center for Biomedical Imaging at the NYU School of Medicine, where he specialized in MR fingerprinting, quantitative imaging, multi-nuclear imaging and CEST MRI.

Postdoc Spotlight

Chendi Cao, PhD

Dr. Chendi Cao received his PhD in computer science from Kansas State University in 2021. He joined BMEII as a post-doctoral fellow in Dr. Yang's cardiovascular imaging group and focuses on novel imaging techniques for comprehensive CMR imaging using non-Cartesian trajectories and motion-correction techniques and deep learning image classification methods. His research mainly focuses on two aspects: (1) Constructing novel image reconstruction methods using Matlab by sorting self-extracted signal and ECG-gated cardiac signal; and (2) Developing deep learning image classification framework for interstitial lung disease (ILD) disease.

Dr. Yang and Dr. Cao are developing a multidimensional dual-echo free-breathing MRI for the cardiac exam with the ability for simultaneous assessment of lung structure in the same scan for patients who have recovered from COVID-19. The research group has been at the forefront of using non-Cartesian pulse sequence acquisitions and advanced image reconstruction for fast motion-robust MRI. Based on these prior developments, they are developing and evaluating a free-breathing lung and heart MRI framework that will enable one-stop-shop characterization of whole lung and heart function together. Their dual-echo MRI techniques can provide comprehensive assessments of heart function and tissue with simultaneous evaluation of lung structure with sufficient diagnostic performance.

Dr. Yang and Dr. Cao are also working on an ongoing deep learning project on image classification for ILD, a disease that consists of a diverse group of conditions categorized by alveolar inflammation and interstitial fibrosis. The diagnosis of ILD requires holistic reviews of clinical, radiological, and pathological results. In addition, it usually takes years to train a specialist to recognize this disease and the level of clinical experience also plays a significant role in making decisions. The lack of experienced physicians and accurate diagnoses for ILD might limit the availability of credible medical resources to patients. To expand the accessibility of ILD diagnosis, we are developing an artificial intelligence (AI) approach to learning from definitive ILD cases diagnosed by experienced experts with their consensus to classify 5 types of fibrosing idiopathic interstitial pneumonia (IIPs) based on chest CT images and patient clinical history.

Chendi Cao, PhD
Postdoctoral Fellow,
Cardiovascular Imaging
chendi.cao@mssm.edu

Faculty Spotlight

Expanding Multiparametric Kidney Imaging

Octavia Bane, PhD

Dr. Octavia Bane was recently appointed to the position of Assistant Professor of Radiology, after having worked as an Instructor in BMEII for the past three years. Dr. Bane initially joined the Body/Cancer MRI lab of Professor Bachir Taouli as a postdoctoral research fellow in Spring 2013. After successfully defending her PhD on quantification of myocardial blood volume with blood pool contrast agents in the departments of Biomedical Engineering and Radiology at Northwestern University, she was recruited to work on multiparametric MRI of hepatocellular carcinoma. Dr. Bane held an NCI T32 Institutional Training Grant fellowship from the Department of Oncology at Mount Sinai in 2014-2015.

Dr. Bane's current research focuses on the development of multiparametric MRI protocols and techniques for assessment of renal dysfunction in transplanted and native kidneys, as well as in renal cancer. With mentors Dr. Taouli and Dr. Sara Lewis, Dr. Bane advanced the Body MRI's lab expansion into renal imaging, helping to successfully obtain initial funding in the form of an NRSA F32 individual postdoctoral fellowship (2016-2018) with the National Institute of Diabetes, Digestive and Kidney Diseases (NIDDK). Dr. Lewis and Dr. Bane are the recent recipients of an R01 from the NIDDK (2021-2026) that will fund a bi-center study at Mount Sinai and Weill Cornell Medical Center of renal transplant dysfunction and outcomes in patients with renal transplantation using mpMRI and urinary biomarkers.

Multiparametric (mp)MRI has the unique potential to identify intrinsic causes of renal transplant dysfunction. Previous work has shown that functional MRI can provide insight into renal function using DCE-MRI (with low dose gadolinium contrast agent, to estimate single kidney filtration rate and perfusion), intravoxel incoherent motion diffusion-weighted imaging (IVIM-DWI, to provide information on flow and diffusion), diffusion tensor imaging (DTI), T1 (which has been shown to reflect tissue inflammation and edema), T1 rho (which reflects the interactions of protons with macromolecules such as collagen) and T2* relaxometry (influenced by the BOLD effect, which reflects oxygen bioavailability). Dr. Bane's preliminary results in 28 initial patients (Fig. 1) with renal transplantation studied with mpMRI show that IVIM-DWI, T1 and T1rho parameters are sensitive to the presence of allograft fibrosis. To advance mpMRI in the kidney, Dr. Bane has co-authored several consensus review papers and has served as a panelist and panel co-chair (2018-2019) with the EU COST Action PARENCHIMA, an international collaboration which aims to develop non-invasive renal MRI biomarkers that are sensitive to chronic kidney disease (CKD) pathophysiology, can predict CKD progression or response to treatment.

During the last three years, Dr. Bane and Dr. Lewis have expanded their renal mpMRI research efforts to study renal cancer, and progressive and de novo CKD in patients undergoing partial nephrectomy (PN). They found that IVIM-DWI parameters in the kidney correlated with inflammatory proteomic markers from urine with differential expression between ccRCC and non-ccRCC tumors. Their collaboration with the groups of Dr. Ketan Badani in Urology, and Dr. Amir Horowitz in Oncological Sciences/ Human Immune Monitoring Center on this project has led to the development of the multidisciplinary Kidney Cancer Research Group within Mount Sinai.

Outside of kidney imaging, Dr. Bane studies 4D flow MRI and relaxometry (T1, T2, T1rho) applications in portal hypertension and mpMRI in Crohn's disease. Dr. Bane looks forward to strengthening her existing collaborations and to establishing new collaborations in BMEII, within Mount Sinai and with external academic centers and medical technology companies.

Outside of research, Dr. Bane enjoys traveling, socializing with friends, gardening and spending time with her young family (husband Max, daughter Livia, 5 years old, son Edward, 1 year old, and pet cat Annie, 15 years old).

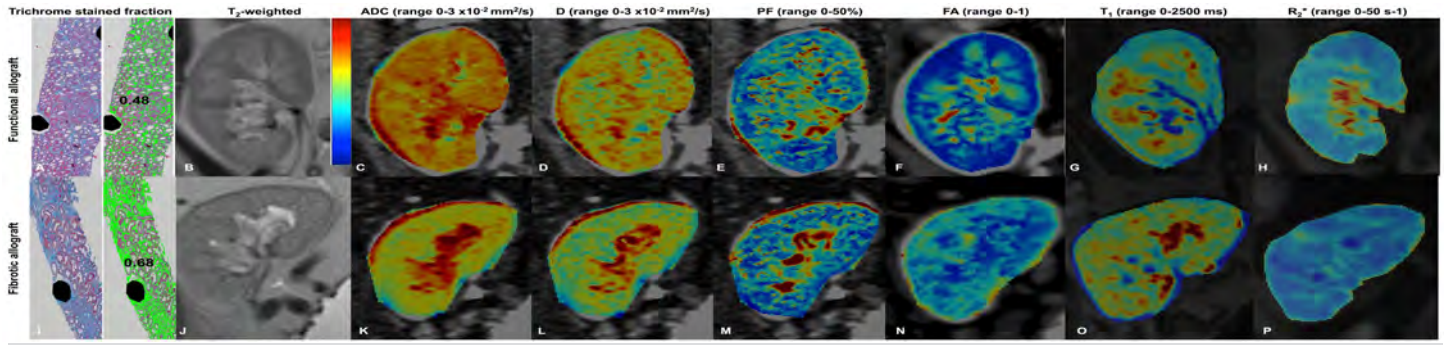

Fig.1. Advanced diffusion maps show overall lower values, and T1 maps show elevated values in a patient with moderate renal allograft fibrosis (I-P) compared to a patient with functional allograft (A-H).

Octavia Bane, PhD
Assistant Professor, Radiology
octavia.bane@mountsinai.org

Engineering & Medicine Seminar Series

For an updated schedule of lectures, check out our webpage. The series will take place on Zoom for the remainder of the year. Interested in presenting? Contact Mallory Stellato at mallory.stellato@mssm.edu.

Community Spotlight

Neuroimaging Stars on the Rise

Last summer, two students from Staten Island Technical High School reached out to the neuroimaging team at BMEII, expressing interest in our research on major depression and other neuropsychiatric diseases. The students, Tara Lago and Mariella Reynoso, contacted Priti Balchandani, PhD and Gaurav Verma, PhD hoping to collaborate on their student research project after discovering their studies on 7T MRI applications in epilepsy and depression. "This was the first time we encountered the idea of using neuroimaging to better understand and diagnose neurological diseases, and right away, we were intrigued," say Mariella and Tara.

After an initial virtual meeting, the student team and BMEII research collaborators began a project investigating differences in cortical curvature among major depression patients compared to healthy controls. The students received training on data handling and research ethics, and were provided de-identified data to investigate these differences. The BMEII team has developed image processing pipelines for data anonymization to facilitate this type of collaborative research.

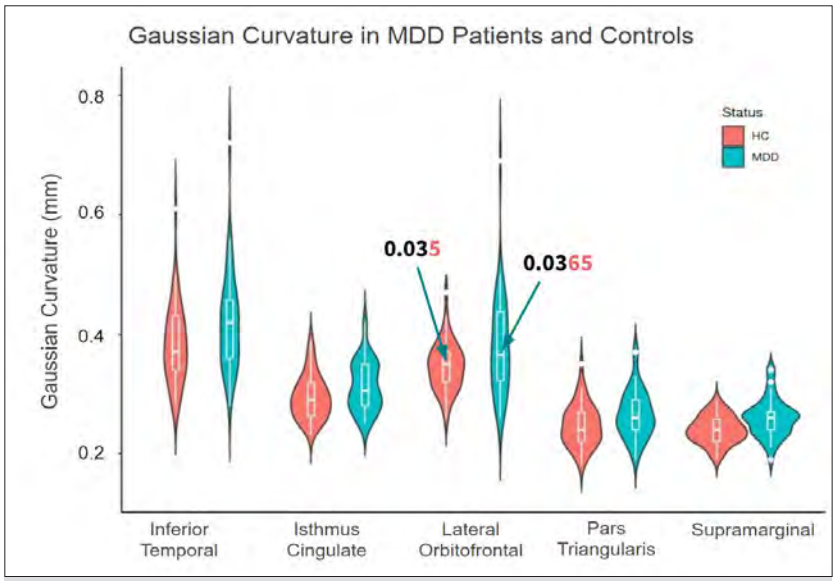

Top left: Mariella Reynoso. Top right: Tara Lago. Fig. 1. In all regions where differences were significant, curvature was higher in patients with major depression (MDD) compared to healthy controls (HC).

Throughout the fall, the team performed literature review and presentations, investigated appropriate statistical methods and performed this analysis using a general linear model in the statistical software R. With help from collaborator Yael Jacob, PhD, the students performed covariance for age and gender, and corrections for multiple comparisons. The results of the study were compiled and submitted to the Terra NYC STEM Fair, where Tara and Mariella were selected as finalists, and written up and prepared as a scientific paper. The student team recently learned that their abstract was accepted for an online pitch at the 2022 meeting of the International Society for Magnetic Resonance in Medicine (ISMRM).

Mariella and Tara plan to continue exploring their curiosity about the brain and their growing interest in genetics, including mosaicism and epigenetics. Mariella plans to get involved in undergraduate research and pursue a PhD to become a biologist, and Tara plans to study neuroscience and become a physician-scientist.

Of their experience, Tara and Mariella shared, "While working with BMEII, we gained many unexpected but wonderful opportunities. We presented our findings to a research team and submitted an abstract to a conference! We improved our statistical analysis and background research skills. Before this project, we were unaware about what working at a lab entailed. We realized that research is an intensely collaborative process that involves a diverse group of professionals contributing their expertise. We also learned that research takes time and dedication, and that insignificant results are still important because they enhance our knowledge about a topic."

Dr. Verma and Dr. Balchandani have been highly impressed with Tara and Mariella's initiative and enthusiasm throughout the collaboration, and are pleased to have opportunities to work with motivated students in the community doing incredible work.

Core Spotlight

New State-of-the-Art Prisma 3T Coming Later this Year

BMEII is excited to announce to our imaging community that we will be installing a new Siemens Prisma 3 Tesla MRI later this spring/summer 2022. This multimillion-dollar investment, jointly funded by a NYFIRST state grant, the Icahn School of Medicine, and the Department of Radiology, will provide BMEII with this state-of-the-art MRI to significantly expand the capabilities of our imaging institute.

With an 80 mT/m @ 200 T/m/s XR gradients, the Prisma will have the ability, amongst many other capabilities, to acquire high-resolution isotropic DTI up to 256 directions and unparalleled angiography with the sensitivity to detect small vessels without contrast.

The Prisma is the preferred, and often sole, imaging system approved for many multi-site neuroimaging studies. Additionally, BMEII and Mount Sinai will now be equipped to better align with many standardized neuroimaging protocols such as The Human Connectome Project.

The system will come with the Numaris X software platform which hosts features and benefits that will improve workflow. Along with a suite of coils (64 channel head/neck coil, 15 ch knee, and 18 ch and 30 ch body array coils), the system will have the software and hardware wear to perform MR

continued on next page

Meeting Spotlight

International Society for Magnetic Resonance in Medicine (ISMRM) Accepted Abstracts

Name	Session Day	Session Type	Session Time	Group/Affiliation
Akbar Alipour	5/11/22	Digital Poster	14:30-15:30	Neuroimaging
Akbar Alipour	5/9/22	Power Pitch	17:00-18:00	Neuroimaging
Octavia Bane	5/11/22	Digital Poster	9:15-10:15	Cancer/Body Imaging
Octavia Bane	5/11/22	Digital Poster	10:15-11:15	Cancer/Body Imaging
Ki Sueng Choi	5/11/22	Digital Poster	14:30-15:30	Neuroimaging
Valentin Fauveau	5/10/22	Digital Poster	14:30-15:30	AI & Imaging
Yael Jacob	5/12/22	Oral	17:00-19:00	Neuroimaging
Yael Jacob	5/11/22	Digital Poster	14:30-15:30	Neuroimaging
Mackenzie Langan	5/11/22	Digital Poster	9:15-10:15	Neuroimaging (student)
Mackenzie Langan	5/11/22	Power Pitch	14:30-16:30	Neuroimaging (student)
Lily McCarthy	5/12/22	Oral	17:00-19:00	Neuroimaging (student)
Shams Rashid	5/11/22	Digital Poster	15:30-16:30	Neuroimaging
Alan Seifert	5/10/22	Digital Poster	10:15-11:15	Neuroimaging
Gaurav Verma	5/9/22	Digital Poster	15:45-16:45	Neuroimaging
Gaurav Verma	5/10/22	Digital Poster	10:15-11:15	Neuroimaging
Ding Xia	5/11/22	Online Pitch	14:30-16:30	Cardiovascular Imaging
Xiang Xu	5/9/22	Power Pitch	14:45-15:45	Neuroimaging
Tara Lago & Mariella Reynoso	5/10/22	Online Pitch	16:45-18:45	Neuroimaging (high school students)
Emily Triolo	5/11/22	Digital Poster	9:15-10:15	Stevens Institute, BMEII affiliated
Enamul Bhuiyan	5/11/22	Digital Poster	9:15-10:15	Cancer/Body Imaging
Enamul Bhuiyan	5/11/22	Digital Poster	9:15-10:15	Cancer/Body Imaging
Jennifer Watchmaker, Ding Xia, Li Feng, et al.	5/10/22	Digital Poster	15:30-16:20	Cardiovascular Imaging

continued from previous page

Elastography of the abdomen.

Many will notice that the construction for the system has already begun on the SC-2 level of the Hess Center for Science and Medicine. Along with the Prisma, Radiology Associates will install a new Siemens Biograph Vision PET/CT in the adjacent bay. While the Vision will be prioritized to clinical care, time will be available to continue and grow our PET research program.

We expect both systems to be installed in the spring and be available for use in the summer of 2022. Please feel free to reach out to us with any questions or details necessary for future grant submissions.

The Icahn School of Medicine at Mount Sinai gratefully acknowledges Empire State Development, which helped support this project.